FLUKA SIMULATION OF THE RADIATION ENVIRONMENT ON THE SURFACE OF MARS

A Dissertation

by

JEREMY DELL NORTHUM

Submitted to the Office of Graduate Studies of
Texas A&M University
in partial fulfillment of the requirements for the degree of

DOCTOR OF PHILOSOPHY

Chair of Committee,	Stephen B. Guetersloh
Committee Members,	Leslie A. Braby
	John R. Ford
	John M. Lawler
Head of Department,	Yassin A. Hassan

August 2013

Major Subject: Nuclear Engineering

ABSTRACT

Uncertainties persist regarding the assessment of the carcinogenic risk associated with galactic cosmic ray (GCR) exposure. The GCR spectrum peaks in the range of 300 MeV/n to 700 MeV/n and is comprised of elemental ions from H to Ni. While Fe ions represent only 0.03% of the GCR spectrum in terms of particle abundance, they are responsible for nearly 30% of the dose equivalent in free space. Because of this, radiation biology studies focusing on understanding the biological effects of GCR exposure generally use Fe ions. Acting as a thin shield, the Martian atmosphere alters the GCR spectrum in a manner that significantly reduces the importance of Fe ions. Additionally, albedo particles emanating from the regolith complicate the radiation environment.

The present study uses the Monte Carlo code FLUKA to simulate the response of a tissue-equivalent proportional counter on the surface of Mars to produce dosimetry quantities and microdosimetry distributions. The dose equivalent rate on the surface of Mars was found to be 0.18 Sv/y with an average quality factor of 2.9 and a dose mean lineal energy of 18.4 keV/μm. Albedo neutrons accounted for 25% of the dose equivalent. Additionally, differential energy spectra were generated in order to determine the fractional contribution to frequency, dose, and dose equivalent for each elemental ion from H to Ni on the surface of Mars. Fe ions were found to account for just 1.3% of the dose equivalent while H and He ions were found to account for 32% and 17%, respectively. It is anticipated that these data will provide relevant benchmarks for use in future risk assessment and mission planning studies.

ACKNOWLEDGMENTS

This work would not have been possible without the guidance and support of my adviser Dr. Stephen Guetersloh and my committee members Dr. Leslie Braby, Dr. John Ford, and Dr. John Lawler. I am thankful for their efforts.

This work was supported by the U.S. Nuclear Regulatory Commission, Faculty Development Program, grant number NRC-38-10-923, contract number C11-00494.

NOMENCLATURE

ACE	Advanced Composition Explorer
ARS	Acute radiation syndrome
AU	Astronomical unit
BFO	Blood-forming organ
BO	Badhwar–O'Neill
CRIS	Cosmic Ray Isotope Spectrometer
CSDA	Continuous slowing down approximation
DES	Differential energy spectra
EMMREM	Earth-Moon-Mars Radiation Environment Module
EVA	Extravehicular activity
GCR	Galactic cosmic ray
HZE	High z and energy
ICRP	International Commission on Radiological Protection
ICRU	International Commission on Radiation Units & Measurements
ISS	International Space Station
LEO	Low-Earth orbit
LET	Linear energy transfer
MARIE	Martian Radiation Environment Experiment
Mars-GRAM	Mars Global Reference Atmospheric Model
MER	Mars Exploration Rover
MSL	Mars Science Laboratory
NASA	National Aeronautics and Space Administration
NCRP	National Council on Radiation Protection & Measurements

NIST	National Institute of Standards and Technology
NOAA	National Oceanic and Atmospheric Administration
RAD	Radiation Assessment Detector
RTG	Radioisotope thermal generator
SI	International System of Units
SP	Stopping power
SPE	Solar particle event
TE	Tissue equivalent
TEPC	Tissue-equivalent proportional counter
UTC	Coordinated Universal Time

TABLE OF CONTENTS

LIST OF FIGURES

FIGURE Page

LIST OF TABLES

TABLE Page

1. INTRODUCTION

1.1 Purpose

The successful landing (*1*) of the *Curiosity* rover of NASA's Mars Science Laboratory (MSL) mission (*2*) on 6 August 2012 sparked a renewed interest in the exploration of Mars. As with every NASA mission to Mars, the goal of MSL is to study the habitability of the planet. Specifically, it will investigate whether conditions have been favorable for microbial life and for preserving clues in the rocks about possible past life.

Consistent with assessing the habitability of Mars is the need to understand the radiation environment on the surface. To that end, MSL has been equipped with a sophisticated radiation detection instrument, Radiation Assessment Detector (RAD) (*3*), to characterize the radiation environment. This information is necessary for planning the human exploration of Mars and is relevant to assessing the planet's ability to harbor life.

Ionizing radiation is one of the most well-proven carcinogens. While knowledge of the carcinogenic nature of ionizing radiation dates back to the early twentieth century, the vast majority of data comes from the survivors of the atomic bomb attacks against the Japanese cities of Hiroshima and Nagasaki (*4*–*9*). These data, however, have rather significant limitations for applicability to estimating the risk of exposure to space radiation. The composition of the radiation produced by the atomic bombs was almost exclusively a gamma and neutron mixture. The charged particle component was nearly negligible and a high z and energy (HZE) component was altogether nonexistent. A reliable method for extrapolating risk values from high-dose-rate γ exposures to the low-dose-rate exposures to protons, heavy ions, and

secondary radiations encountered in space dose not currently exist (*10*). Because of the lack of data, uncertainties abound regarding the biological effects of space radiation, especially HZE particles.

The purpose of this study is to investigate the composition and quality of the radiation environment on the surface of Mars in an attempt to reduce the uncertainties of risk assessments for human exposure.

1.2 Galactic Cosmic Rays

A galactic cosmic ray (GCR) is a high-energy charged particle originating from outside the solar system (*11*). Discovered by Victor Hess (*12*) in 1912, they are comprised mostly of ions of every element from H to Ni. Ions above Ni do contribute to the GCR spectrum albeit at a much lower intensity; relative abundances (*11*) of ions heavier than Fe decrease by factors of $10^2 - 10^6$. Ascertaining the exact source of these charged particles is complicated by the numerous magnetic fields dispersed throughout space. These magnetic fields alter the trajectories of GCRs which result in arrival directions that do not usually point back to the sources (*13*).

The kinetic energies (*14*) of these ions span from approximately 10 MeV/n to 10^{12} MeV/n with a peak around 300 MeV/n to 700 MeV/n. Providing sufficient shielding against such a large energy range remains a difficult task. Additionally, the low fluence rate of GCRs results in a chronic, low-dose-rate exposure that contributes to stochastic effects typical of ionizing radiation (*14*, *15*).

The intensity of the GCR spectrum is not constant in time and a significant negative correlation exists between GCR fluence rate and solar activity. Incoming cosmic rays are "modulated" (*14*, *16*) by the solar wind which consists of a stream of charged particles emanating from the sun. A typical solar wind at solar minimum consists of a proton velocity of 400 km/s and an electron density of 7×10^6 m^{-3}

which corresponds to a mass-loss rate of $\sim 10^9$ kg/s (*17*).

Periods of high solar activity result in lower GCR intensities and vice versa. A recent example of this phenomenon is the relatively high GCR intensity that was persistent during the extended solar minimum of 2008–2010 (*18*). Typical GCR abundance in free space at solar minimum (*14*, *19–21*) is approximately 4 cm^{-2} s^{-1} for all ions and energies.

The modulation of cosmic rays through the heliosphere is complicated by the various forces influencing their trajectories including: outward convection by the solar wind, inward diffusion due to scattering by magnetic field irregularities, adiabatic cooling, field gradient, particle curvature and heliospheric neutral sheet drifts, and at lower energies, shock acceleration (*14*).

While the heliosphere has little to no effect on particles with kinetic energies > 10 GeV/n, the influence to particles with kinetic energies less than ~ 1 GeV/n can be quite pronounced (*14*). Since the peak of the GCR spectrum is in the range of 300 MeV/n to 700 MeV/n, solar modulation has a direct impact on the radiation doses humans would receive during interplanetary travel (*14*, *22*). Additionally, the charge-to-mass ratio (Z/A) of an incident ion plays an important role in determining how much it is modulated by the solar wind. Therefore, protons with $Z/A = 1$ are modulated more than other ions with $Z/A \sim \frac{1}{2}$.

Active measurement of the GCR spectrum is ongoing with the Cosmic Ray Isotope Spectrometer (CRIS) on board NASA's Advanced Composition Explorer (ACE) spacecraft. ACE, positioned at the Sun-Earth L_1 Lagrange point 1.5×10^6 km sunward of Earth, has provided detailed measurements of the properties of GCRs since its launch in August 1997 (*23*).

1.2.1 Composition

The GCR spectrum is comprised mostly of H and He ions which, taken together, constitute $\sim 99\%$ of the total spectrum. The remaining $< 1\%$ of the spectrum is comprised of HZE particles – that is, high energy charged particles with $z > 2$. The GCR spectrum follows the general trend of decreasing abundance with increasing z with the exception of Fe ions at $z = 26$.

Fe ions stand out because of their unique relationship with the other ions of the GCR spectrum. The stopping power of an ion is proportional to z^2 where z is the charge of the ion. Therefore, while Fe ions comprise approximately 0.03% of the total GCR spectrum at solar minimum, they are responsible for at least 8% of the dose and, factoring in quality factors, 28% of the dose equivalent – a characteristic that leads to a large number of Fe-ion-based research studies (*24*).

Space radiation protection studies often present the fractional contribution to frequency, dose, and dose equivalent of each ion in the GCR spectrum. These distributions are obtained by integrating the differential energy spectra for each ion. The frequency distribution is produced by a simple integration; the dose distribution is produced by integrating the spectra with each bin weighted by the corresponding stopping power; the dose equivalent distribution is produced by integrating the spectra with each bin weighted by the corresponding stopping power and quality factor.

Applying this technique to the 2010 version (*21*) of the Badhwar–O'Neill GCR model (*19–21*) yields the fractional contribution to frequency, dose, and dose equivalent of each elemental ion in free space at solar minimum ($\Phi = 450$ MV) as presented in Table 1.1.

Table 1.1
Free Space Frequency, Dose, and Dose Equivalent Distributions

z	Frequency	Dose	Dose Equivalent
1	8.98E-01	3.87E-01	6.25E-02
2	9.36E-02	1.94E-01	3.47E-02
3	3.37E-04	1.51E-03	3.23E-04
4	2.10E-04	1.49E-03	3.47E-04
5	6.98E-04	8.51E-03	3.26E-03
6	2.56E-03	4.74E-02	2.97E-02
7	6.79E-04	1.65E-02	1.30E-02
8	2.42E-03	8.13E-02	9.69E-02
9	4.37E-05	1.65E-03	2.03E-03
10	3.71E-04	1.89E-02	3.23E-02
11	7.47E-05	4.39E-03	8.30E-03
12	4.86E-04	3.63E-02	8.41E-02
13	8.00E-05	6.64E-03	1.64E-02
14	3.66E-04	3.69E-02	1.03E-01
15	1.31E-05	1.32E-03	3.69E-03
16	6.90E-05	8.52E-03	2.67E-02
17	1.33E-05	1.69E-03	5.60E-03
18	2.65E-05	4.02E-03	1.41E-02
19	2.01E-05	3.48E-03	1.28E-02
20	5.34E-05	1.09E-02	4.01E-02
21	1.01E-05	2.21E-03	8.34E-03
22	3.67E-05	9.47E-03	3.42E-02
23	1.71E-05	4.69E-03	1.66E-02
24	3.57E-05	1.07E-02	3.62E-02
25	2.24E-05	7.12E-03	2.34E-02
26	2.52E-04	8.91E-02	2.77E-01
27	1.23E-06	4.55E-04	1.38E-03
28	1.17E-05	4.56E-03	1.36E-02

While H and He ions together constitute 99% of the GCR spectrum in terms of particle abundance, they account for only 58% of the dose and 10% of the dose equivalent. The z^2 nature of the energy loss by ions passing through matter makes the seemingly irrelevant heavy ions quite relevant for the purposes of dosimetry and radiation protection. These distributions are plotted in Figure 1.1.

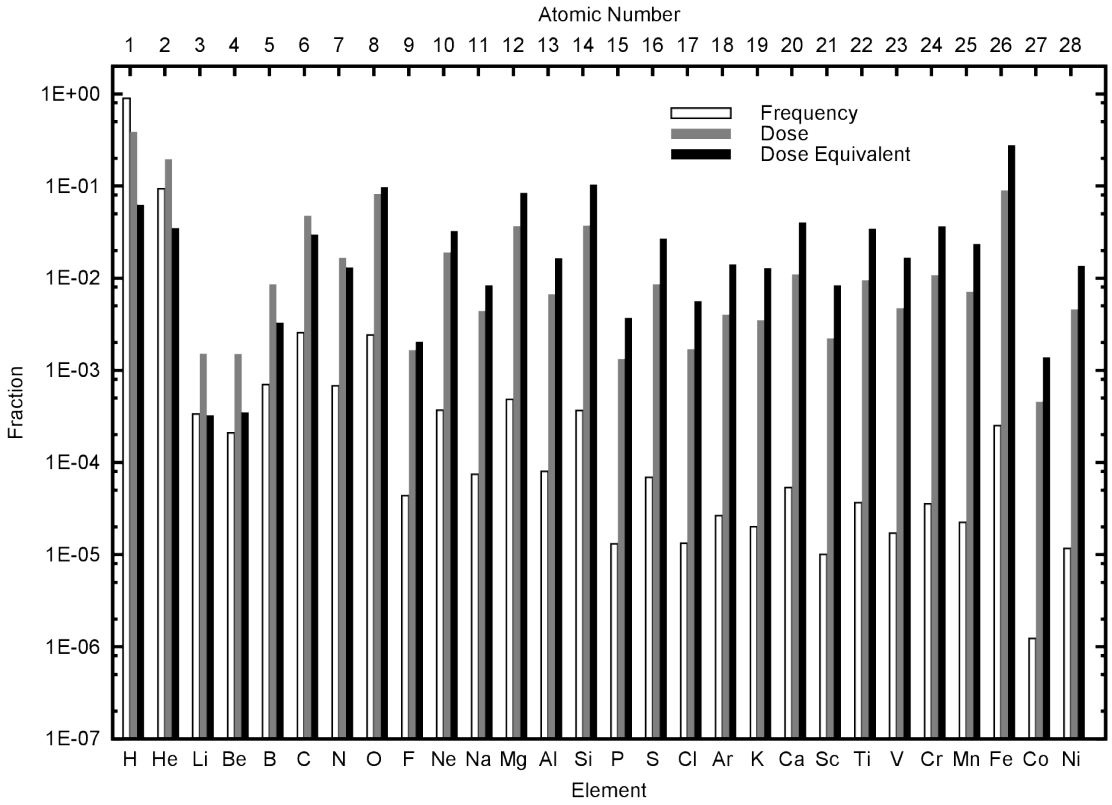

Figure 1.1. Fractional contributions to frequency, dose, and dose equivalent of each elemental ion in free space. These distributions were generated from the Badhwar–O'Neill model with a solar modulation parameter of $\Phi = 450$ MV.

Differential energy spectra of the 11 most abundant GCR ions are presented in Figure 1.2. These fluence rate profiles were generated from the 2010 version of the Badhwar–O'Neill model (*21*) with a solar modulation parameter of $\Phi = 450$ MV.

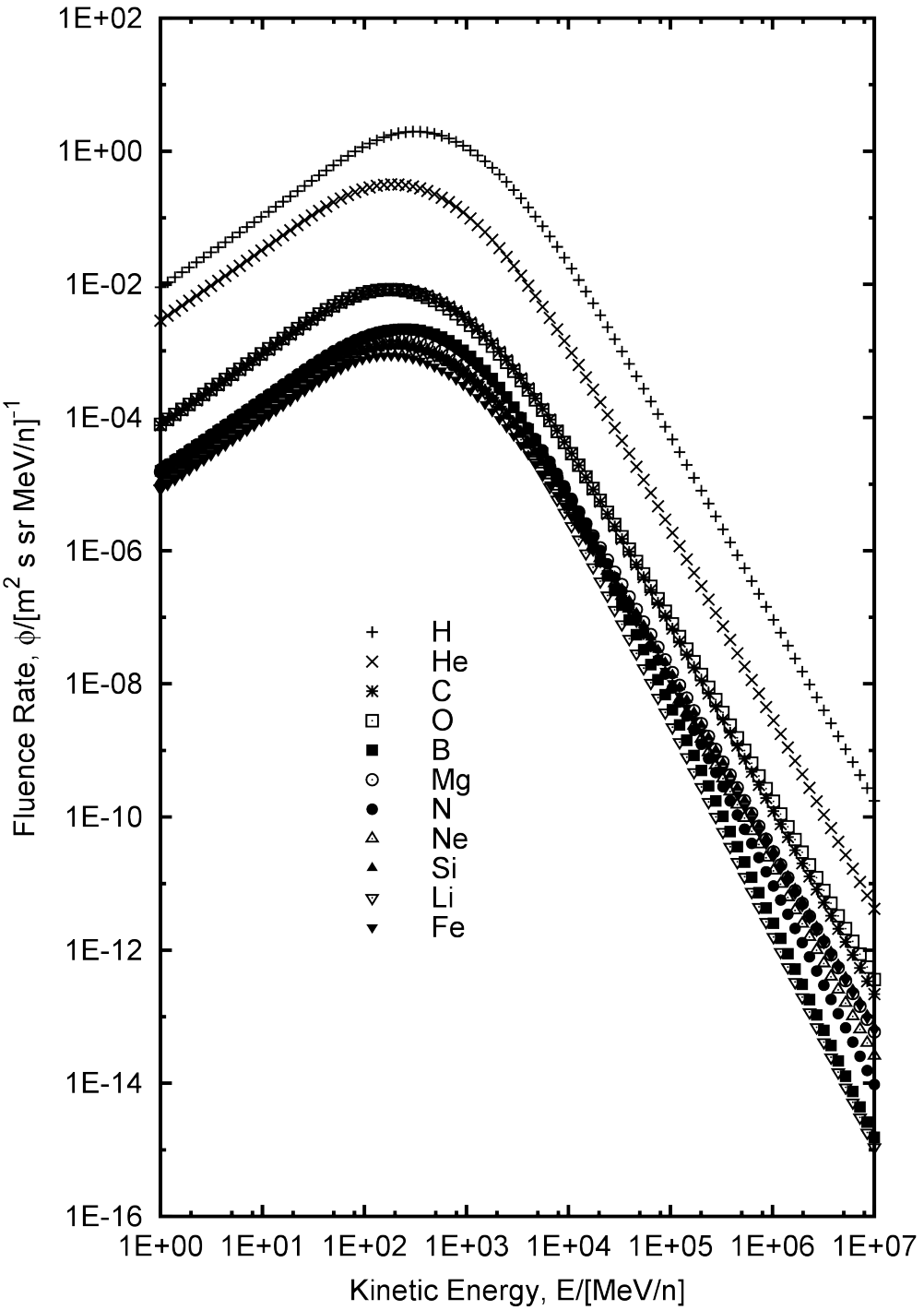

Figure 1.2. Differential energy spectra for the eleven most abundant GCR ions in free space. These curves were produced from the Badhwar–O'Neill model with a solar modulation parameter of $\Phi = 450$ MV.

1.2.2 Dosimetry

Dose equivalent rates resulting from exposure to cosmic rays in free space have been estimated in many studies. Blood-forming organ (BFO) dose equivalent rates have been estimated at 0.4 Sv/y (*25*), 0.6 Sv/y (*26*), 0.9 Sv/y (*27*), and 0.5 Sv/y (*28*). Skin dose rates have been estimated at 0.7 Sv/y (*25*), 0.9 Sv/y (*26*), and 0.8 Sv/y (*28*). These estimates for BFO and skin dose equivalent rates assume little (< 1 g/cm^2) or no shielding. Similarly, estimates for free space, unshielded, dose equivalent rates are 1.2 Sv/y (*25*) and 1.3 Sv/y (*26*).

The influence of the solar cycle on GCR dose equivalent rates has been studied in unshielded free space. The 1977 solar minimum GCR spectrum has been reported to have resulted in 0.73 Sv/y to BFO and 0.96 Sv/y to the skin. Likewise, the 1970 solar maximum GCR spectrum resulted in 0.28 Sv/y to BFO and 0.33 Sv/y to the skin (*29*).

Similar calculations have been made (*25*) but with a greater emphasis placed on the influence of Al shielding thickness. Calculation of GCR dose rates, including depth-dose characteristics (*27*) and the influence of solar cycles (*26*) as a function of Al shielding thickness, have been performed as well.

A comparison of NASA's HZETRN code and data collected by the Martian Radiation Environment Experiment (MARIE) (*30*) has been made with model and measurements agreeing on a dose rate of ~ 0.02 cGy/day during August 2003 (*31*).

1.3 Solar Particle Events

A solar particle event (SPE) is characterized by a large release of energetic charged particles from the sun. While most SPEs are largely dominated by protons, reflecting the composition of the sun, He and heavier ions can be present in lower abundances. SPEs are characterized by large fluence rates over relatively short periods of time

(hours or days). During such an event, it is possible for the fluence rate of protons with energy ≥ 10 MeV to increase by a factor of $10^4 - 10^5$ over background rates (*32*). For example, the large SPEs of November 1960, August 1972, and October 1989 all had proton fluences of $\sim 5 \times 10^9$ cm^{-2} with energies ≥ 30 MeV (*14*). Because of the potential for large fluences, SPEs pose the greatest radiation risk to humans in interplanetary space outside the protection of earth's magnetic field (*14*). SPEs are troublesome for mission planners because it is not inconceivable for doses received from large events to lead to deterministic effects, namely Acute Radiation Syndrome (ARS) (*32*).

The unpredictability of large SPEs has lead to the inclusion of "storm shelters" in future interplanetary vehicle designs. Such shelters would need to be easily and quickly ($<$ 1 hour) accessible and should reduce BFO dose to below the nausea threshold (*14*) which corresponds to 1–3 Gy (*33*).

As previously stated, one of the key problems with SPEs is their seemingly unpredictable nature. A recent article (*34*) illustrates this problem as it relates to the electric grid. It is stated that critical components of the electrical grid are designed to withstand SPEs typical of the past few decades. It is argued that the worst-case scenario SPE is very much an unknown and making preparations for such an event is exceedingly difficult. The March 2011 earthquake and resulting tsunami in Japan that lead to the Fukushima Daiichi accident serves an example of what is known as a beyond design-basis accident – that is, sequences of events that are possible but were not fully considered in the design process because they were judged to be too unlikely. While this article is limited to protecting the electrical grid, this logic applies equally as well to the problem of providing adequate shielding against large, unpredictable SPEs.

1.3.1 Dosimetry

Table 1.2 shows interplanetary space estimates (*32*) of skin dose D_{skin} and effective dose E using NASA's BRYNTRN code for three historically large events: August 1972, October 1989, and September 1989. Each entry contains total event doses as well as the maximum hourly rates. The spacecraft scenario assumes 5 g/cm^2 of Al shielding while the extravehicular activity (EVA) scenario assumes 0.3 g/cm^2 of Al shielding. As these data clearly demonstrate, unshielded exposure to SPEs has the potential to lead to severe short- and long-term health effects.

Table 1.2
Dose Estimates for Historical SPEs

	August 1972		October 1989		September 1989	
Doses (*32*)	EVA	Spacecraft	EVA	Spacecraft	EVA	Spacecraft
Total						
D_{skin} [Gy]	32.2	2.70	26.0	1.45	7.68	0.53
E [Sv]	3.02	0.61	2.00	0.49	0.69	0.20
Maximum Rate						
$\dot{D}_{\text{skin}}$ [Gy/h]	9.81	0.28	2.60	0.15	0.77	0.05
$\dot{E}$ [Sv/h]	0.47	0.12	0.20	0.05	0.07	0.02

A similar study used the BRYNTRN code to estimate skin and bone marrow doses for a selection of SPEs (*28*).

1.3.2 Carrington Event

The Carrington Event (*35*) of 1 September 1859 is the largest SPE of the past 500 years (*36*) and is often regarded as the worst-case scenario SPE. Estimates (*37*) of the possible doses received from > 30 MeV protons in LEO during such an event are based on an integral fluence of 1.88×10^{10} cm^{-2}, a quantity derived from an assessment of ice core samples (*36*).

Doses behind 1 g/cm^2 of Al shielding, slightly thicker than a space suit, were reported as 2.1 Gy-Eq whole body, 51 Gy-Eq for skin, and 36 Gy-Eq for the eye. Behind 10 g/cm^2 of Al, a typical spacecraft shielding thickness, the doses were 0.21 Gy-Eq for BFO, 1.8 Gy-Eq for the skin, and 1.6 Gy-Eq for the eye (*37*).

A recent paper has called into question the practice of using ice core samples to estimate proton fluences from SPEs (*38*), suggesting large uncertainties in the above estimates.

1.4 Mars

Radiation levels are much higher on Mars than they are on Earth for two main reasons. First, it has been known for some time (*39*) that Mars does not possess a global magnetic field capable of providing any significant shielding from space radiation. Particles incident on Mars will see at most a 40 nT interplanetary magnetic field strength which is too weak to cause any significant deflection in trajectories. A discussion (*39*) of the gyroradii of 1 MeV protons near Mars reveals the insignificance of these magnetic fields: the typical interplanetary field strength of 3 nT results in a $\sim$ 10-Mars-radii gyroradius and the strongest field strength of 40 nT results in a gyroradius equal to $\sim$ 1 Mars radius.

Secondly, the atmosphere of Mars is quite thin (*40*) representing 2% of Earth's atmosphere: a mass thickness of $\sim$ 20 g/cm^2 for Mars compared to the $\sim$ 1000

g/cm^2 mass thickness of Earth's atmosphere. For these reasons, many more charged particles reach the surface of Mars than on Earth.

Because of the atmosphere, the charged particle fluence rate is actually *greater* on the surface of Mars than would be on another planet or moon with no atmosphere (*3*). The Martian atmosphere is thick enough to result in significant secondary particle production but not thick enough to stop nearly all particles as is the case for Earth. Despite this, the dose rate on the surface of Mars is generally accepted to be less than in free space because of the fragmentation of heavy ions incident on the top of the atmosphere (*3*). This reduction in the effective z of the incident spectrum can drastically reduce doses because of the z^2 nature of the energy loss of charged particles passing through matter.

Additionally, the interaction of incident particles with the Martian regolith complicates the radiation environment near the surface. Such interactions can lead to the production of albedo neutrons and γ rays (*3*, *10*, *41*).

Finally, if the effects of the atmosphere and regolith are ignored, the GCR dose rate on the surface of Mars should be half that of interplanetary space. For any sufficiently large planet or moon, the field of view for incident GCRs is reduced to 2π sr because the celestial body functions as a shield to the normally isotropic GCR spectrum. Despite the reduction in the dose rate provided by the atmosphere and planet geometry, multi-year missions to Mars will require adequate shielding to avoid deterministic effects of radiation and minimize the risk for stochastic effects (*42*).

As previously stated, the MSL rover has been equipped with the RAD instrument in an attempt to characterize this exceptionally complex radiation environment and has five primary science objectives (*3*):

- To measure energetic particle spectra at the surface of Mars;
- To measure dose and determine dose equivalent rates for human explorers on the surface of Mars;
- To use these measurements to enable the validation of Mars atmospheric transmission models and radiation transport codes;
- To provide input to the determination of the radiation hazard and potential mutagenic influences to life at or just below the Martian surface;
- To provide input to the determination of the chemical and isotopic effects of energetic particles on the Martian surface and atmosphere.

The RAD instrument has a few limitations/issues that will affect its ability to achieve its science objectives. The first limitation is the relatively narrow field of view of its charged-particle telescope. The charged-particle telescope has a view cone of 60° full opening angle (*3*). In addition to limiting the count rate, and therefore increasing the counting time necessary to achieve statistically significant results, this relatively narrow field of view does not allow for the detection of charged particles that traverse the Martian atmosphere at angles greater than 30° from normal incidence. Such particles would presumably have a higher stopping power because they had passed through more of the atmosphere, and, as a result, could contribute significantly to the dose.

Another limitation of RAD is the use of non-tissue-equivalent material for dosimetry calculations. This can become an issue when scaling $\frac{\mathrm{d}E}{\mathrm{d}x}$ between Si and water as mentioned in the technical description (*3*). A comparison between proton stopping powers from NIST's PSTAR database (*43*) shows that such scaling can introduce inaccuracies on the order of 10% over the dynamic range of RAD.

Any data collected by RAD will be directly influenced by the rover itself. To begin with, MSL is powered by a neutron-emitting radioisotope thermal generator (RTG) (*2*, *3*). Properly measuring low energy neutrons will be difficult because of the presence of this artificial neutron source. Secondly, the RAD detector is located inside the rover which provides distorted, artificial shielding. Such shielding may lead to an underestimate of the neutron and γ dose rates.

Finally, the RAD instrument has a limited sensitivity to very high energy ions. As the technical description of the project points out, the $\frac{\mathrm{d}E}{\mathrm{d}x}$ resolution of RAD is sufficient to distinguish between major particle species. However, differential fluences are provided for only a limited energy range, about 10 Mev/n to 100 MeV/n for protons and He ions, and integral fluences for ions with higher energies (*3*).

Taken together, these limitations and issues will need to be considered when analyzing raw data from the RAD instrument in order to provide an accurate description of the radiation environment on the surface of Mars. That said, the RAD instrument is still a very capable detector, especially considering the mass (1.56 kg), volume (240 cm^3), power (4.2 W), and data rate (400 kB/day) restrictions imposed by interplanetary space travel (*3*).

1.5 Previous Work

Dose estimates for missions to Mars have been calculated based on various scenarios. One such study utilizes the 1977 solar minimum and 1970 solar maximum GCR spectra (*44*). An assumption is made that the GCR fluence rate is 10% greater at Mars (at 1.5 AU from the Sun) compared to Earth due to the decreased solar modulation. Despite the announcement of this assumption, it was not taken into account during dose calculations. Dose equivalent rates on the surface of approximately 9 cSv/y were reported at solar maximum with very little difference seen over varying

atmosphere thicknesses (*44*).

An estimated dose rate of 63 mGy/y at solar minimum has been made with the GEANT4 code using a GCR spectrum from the SPENVIS database (*45*).

A description of the influence of the Martian atmosphere on the GCR spectrum using a modified version of the GEANT4-based ATMOCOSMICS code (*46*) has been performed. Differential energy spectra for neutrons, photons, protons, and electrons at the surface are presented along with fluence vs. depth profiles in the Martian atmosphere. This study only considers protons and does not consider heavier ions.

A separate study (*47*) estimates the dose rate on the surface at 65 mGy/y at solar minimum and 30 mGy/y at solar maximum using a code based on the GEANT4 toolkit and also only considers incident protons.

In a different approach, the expected number of hits per cell per year are presented for solar minimum and maximum conditions. Dose equivalent rates as a function of position on Mars are presented with a range of 10 cSv/y to 20 cSv/y at solar maximum ($\Phi = 1075$ MV) (*48*). Data are presented as a function of altitude in the atmosphere (that is, elevation). While cell hit and dose equivalent rates do increase with elevation, the increase is not significant.

GEANT4 and CREME96 have been used to generate secondary particle fluence rates at the surface (*49*). A GCR proton dose rate of 2.00 rad/y (SiO_2), 20 mGy/y, is reported. This study only considers protons and makes no mention of the transport of heavy ions through the Martian atmosphere.

GCR-induced neutron fluence rates have been estimated with HZETRN (*50*). Low-energy-neutron fluence rates on the surface were reported as being greater than previously thought due to the large number of neutrons produced in the Martian regolith. The authors note that any habitat designed for the Martian surface must be designed to shield against neutrons.

Dose equivalent rates as a function of shield type and thickness have been calculated with the HZETRN code and NASA's Mars Global Reference Atmospheric Model (Mars-GRAM). Unshielded dose equivalent rates are reported as approximately 23 cSv/y for solar minimum and approximately 8 cSv/y for solar maximum (*51*).

A paper (*52*) discussing NASA's Earth-Moon-Mars Radiation Environment Module (EMMREM) presents detailed, tabulated organ and effective dose values behind 5 g/cm^2 and 20 g/cm^2 of Al shielding in interplanetary space. Cumulative effective doses for the August 1972 SPE of 0.612 Sv and 0.046 Sv were reported with 5 g/cm^2 and 20 g/cm^2 of Al shielding, respectively. Effective dose rates from the GCR spectrum of 0.611 Sv/y and 0.492 Sv/y were reported behind 5 g/cm^2 and 20 g/cm^2 of Al shielding, respectively. Effective dose rates on the surface of Mars are presented as a function of particle type and charge (*52*).

Townsend *et al.* present perhaps the most detailed dosimetric assessment of the radiation environment on the surface of Mars. Skin, eye, bone marrow, central nervous system (brain), and heart absorbed dose rates are presented along with effective dose rates as a function of atmosphere and Al shielding thickness at solar minimum (Φ = 417 MV) (*53*). The data are presented as a series of lookup tables with 150 combinations of atmosphere thicknesses (0 to 300 g/cm^2) and Al shielding thicknesses (0 to 100 g/cm^2). These data were calculated with HZETRN as part of EMMREM. An unshielded free space dose rate of 0.044 cGy/d to the skin was presented along with an effective dose rate of 0.204 cSv/d. Unshielded dose rates on the surface of Mars, those values corresponding to an atmosphere thickness of 15 g/cm^2, were reported as 0.031 cGy/d to the skin and an effective dose rate of 0.076 cSv/d (*53*).

Microdosimetry distributions have been presented for a selection of ions that

comprise the GCR spectrum. These distributions are included with a discussion of how they relate to evaluating the hazards to astronauts that result from exposure to GCRs during space travel (*54*).

1.6 Statement of the Problem

As the preceding section demonstrates, a fair amount of work has been performed to estimate the radiation environment humans may encounter on the surface of Mars. What is not entirely clear, however, is the quality of the radiation environment. Uncertainties persist regarding the carcinogenic risk associated with exposure to space radiation (*55*). The uncertainties are so great that the National Council on Radiation Protection & Measurements (NCRP) dedicated an entire report to the problem. NCRP Report No. 153, *Information Needed to Make Radiation Protection Recommendations for Space Missions Beyond Low-Earth Orbit*, details research that needs to be performed to properly assess the risks associated with exposure to space radiation (*14*).

One of the largest uncertainties concerns the determination of the quality factor Q for the GCR spectrum. What is proposed in the present study is the production of microdosimetry distributions for the radiation environment on the surface of Mars with the goal of providing relevant benchmarks for use in further radiation biology and mission planning studies. Fe-ion beams are often used for radiation biology studies geared towards understanding the biological effects of exposure to GCRs. It is anticipated that Fe ions may not be the most appropriate beam for radiation biology studies focused on Mars. The atmosphere of Mars is thick enough to produce a significant amount of fragmentation products and ionization losses will be great enough to significantly slow down incident ions. At the same time, the atmosphere is thin enough to allow a significant fraction of the incident ions to reach the surface.

Additionally, many secondary and recoil particles can be produced from the interaction of the incident GCRs with the Martian regolith. The radiation environment in free space is complex enough; the radiation environment on the surface of Mars is expected to be equally, if not more, complex.

The quantity of interest in the present study will be lineal energy y because of its relative ease of measurement. y will be determined by recording energy deposition in the gas volume of tissue-equivalent proportional counter (TEPC) with a solid, tissue-equivalent (TE) wall simulating a 1-μm site of unit density. $f(y)$ and $d(y)$ distributions will be produced from the TEPC along with their averages, $\bar{y}_{\mathrm{F}}$ and $\bar{y}_{\mathrm{D}}$, respectively.

The International Commission on Radiation Units and Measurements (ICRU) recently recommended the use of the energy distribution of particle radiance as a function of particle type and time for analyzing the risks from exposure to low-dose and heterogeneous exposures. In the same report, it was stated that the $f(y)$ distribution and event rate as a function of time might be satisfactory when a differential energy distribution is either unknown or difficult to measure (*56*). Since the present study will involve the simulation of the radiation environment, particle type and energy can be readily obtained.

All calculations will be performed with the FLUKA code (*57*, *58*) which is a mature and well-developed Monte Carlo transport code that specializes in the simulation of ions at energies typical of the GCR spectrum. FLUKA's ability to simulate the response of a TEPC has been well documented. Comparisons with experimental data have been performed for TEPCs exposed to photons (*59*–*61*), neutrons (*59*), protons (*62*, *63*), He ions (*63*), C ions (*63*, *64*), N ions (*63*), O ions (*63*), Ne ions (*63*), Si ions (*63*), and Fe ions (*63*, *65*). Additionally, FLUKA has been used to successfully simulate the response of a TEPC to cosmic rays on board commercial aircraft (*66*).

In all cases, the FLUKA- and experimentally-generated microdosimetric responses were compared and found to be in good agreement.

While FLUKA will be used to generate y distributions, it can, at the same time, be used to score particle type and energy – a task not possible with a real TEPC. y distributions are helpful for quantifying dose in a mixed radiation environment along with providing insight into the quality but they do not allow for the identification of incident particles. The desire to measure particle spectra, along with the TEPC's limitation for such a task, lead to the decision to equip the RAD instrument with a charged-particle telescope instead of a TEPC (*3*).

FLUKA's ability to score particle type and energy on the surface of Mars translates into the ability to generate differential energy spectra. These spectra, similar to the free space spectra presented in Figure 1.2, and the response of a TEPC, can be generated in the same FLUKA simulation. From these differential energy spectra the frequency, dose, and dose equivalent fractions of each ion can be produced for the surface of Mars, similar to the free space fractions presented in Figure 1.1.

Radiation risks to humans in space depend in part on the microscopic distributions of energy deposition events in tissues. While these distributions depend on the space radiation environment, they are also influenced by the astronaut's surroundings and any shielding that may be present (*67*). The atmosphere and regolith of Mars both undoubtedly influence these microdosimetry distributions as compared to free space measurements. Characterization and quantification of these distributions will serve as an addition to the body of knowledge of the radiation environment on the surface of Mars. Such an advancement may, however indirectly, aid in putting the first human on Mars.

It is anticipated that the results of the present study will be helpful for future detector and shielding designs and radiation biology experiments. Generated data

could perhaps lead to the development of a benchmark ion species and energy for the surface of Mars in the same manner that Fe ions serve as a free space benchmark. Finally, such calculations may prove beneficial for comparison with the data collected by the RAD instrument.

2. THEORY

2.1 Stopping Power

Charged-particle Coulomb-force interactions (*68*) can be classified by the relationship between the classical impact parameter b and the atomic radius a. This classification system results in three general groups: "soft" collisions ($b \gg a$), hard (or "knock-on") collisions ($b \sim a$), and Coulomb-force interactions with the external nuclear field ($b \ll a$). The soft collisions represent interactions between the atom as a whole and the incident ion while hard collisions represent interactions between individual electrons of the atom and the incident ion. Taken together, these soft and hard collisions serve as the two phenomena constituting the electronic stopping power of charged particles slowing down in matter. Interactions with the external nuclear field, as the name implies, represents interactions between a nucleus in the stopping medium and the incident ion. Elastic recoil reactions and inelastic fragment-producing reactions can result when an incident ion interacts with the nucleus.

2.1.1 Basic Quantities

The rate of energy loss per unit path length by the incident particle is known as the stopping power or linear energy transfer (LET) and denoted as $\frac{\mathrm{d}T}{\mathrm{d}x}$ which has SI units of J/m and common units of keV/μm. If stopping power is divided by density (thereby normalizing it for all densities), it is known as the mass stopping power. Ignoring radiative stopping power, the collision stopping power becomes the total stopping power

$$\left(\frac{\mathrm{d}T}{\rho \mathrm{d}x}\right)_c = \left(\frac{\mathrm{d}T_s}{\rho \mathrm{d}x}\right)_c + \left(\frac{\mathrm{d}T_h}{\rho \mathrm{d}x}\right)_c \tag{2.1}$$

where the subscript s denotes soft collisions, h denotes hard collisions, and c denotes collision (as opposed to radiative).

The maximum energy that can be transferred to an atomic electron (*16*, *33*, *69*) in a hard collision (and therefore the maximum energy of a delta ray) is

$$T'_{\max} = \frac{2m_0c^2\left(\frac{\beta^2}{1-\beta^2}\right)}{\left(1 + \frac{2(m/M)}{\sqrt{1-\beta^2}} + (m/M)^2\right)} \tag{2.2}$$

where m/M is the ratio of the electron mass to the mass of the incident particle, m_0c^2 is the rest mass energy of an electron (~ 0.511 MeV), and β is the ratio of the incident particle velocity v to the speed of light c:

$$\beta = \frac{v}{c}. \tag{2.3}$$

Equation 2.2 can be simplified (*16*, *68*, *69*) by eliminating the denominator giving

$$T'_{\max} \approx 2m_0c^2\left(\frac{\beta^2}{1-\beta^2}\right) = 1.022\left(\frac{\beta^2}{1-\beta^2}\right)\text{MeV} \tag{2.4}$$

which overestimates $T'_{\max}$ for protons by only 0.1% at 1.0 MeV and 0.23% at 1000 MeV (*69*).

$T'_{\max}$ for incident positrons is

$$T'_{\max} = T \tag{2.5}$$

assuming annihilation does not occur. $T'_{\max}$ for incident electrons is

$$T'_{\max} \equiv \frac{T}{2} \tag{2.6}$$

because incident and struck electrons are indistinguishable after the collision and, by convention, the electron with the greater energy is always referred to as the primary (*68*).

The relationship (*68*, *70*) between kinetic energy T and β is described by

$$T = M_0c^2\left[\frac{1}{\sqrt{1-\beta^2}} - 1\right] \tag{2.7}$$

where M_0c^2 is the rest mass energy of the incident particle. As Equation 2.7 demonstrates, the kinetic energy required by any particle to reach a given velocity is proportional to its rest mass energy. Rearranging Equation 2.7 to present β as a function of T gives

$$\beta = \left[1 - \left(\frac{1}{(T/M_0c^2)+1}\right)^2\right]. \tag{2.8}$$

2.1.2 Charged Particles

Equation 2.1 can be expanded (*16*, *33*, *68*, *69*, *71–74*) for charged particles to give

$$\left(\frac{\mathrm{d}T}{\rho \mathrm{d}x}\right)_c = \frac{2Cm_0c^2z^2}{\beta^2}\left[\ln\left(\frac{2m_0c^2\beta^2T'_{\max}}{I^2(1-\beta^2)}\right) - 2\beta^2\right] \tag{2.9}$$

where

$$C \equiv \frac{\pi N_\mathrm{A} Z r_0^2}{A} = 0.1502\,\frac{Z}{A}\,\frac{\mathrm{cm}^2}{\mathrm{g}} \tag{2.10}$$

given that N_A is Avogadro's number, Z and A are the atomic number and mass number of the stopping medium, respectively, and, therefore, $\frac{N_\mathrm{A}Z}{A}$ is the number of electrons per gram of the stopping medium where

$$r_0 = \frac{e^2}{m_0c^2} = 2.818 \times 10^{-13}\mathrm{cm} \tag{2.11}$$

is the classical electron radius. In addition, z is the charge of the incident particle and I is the mean excitation potential of the struck atom.

Equation 2.9 can be simplified by combining the terms before the bracket and declaring a constant k such that

$$k \equiv \frac{2Cm_0c^2z^2}{\beta^2} = 0.1535\frac{Zz^2}{A\beta^2}\frac{\text{MeV}}{\text{g/cm}^2} \tag{2.12}$$

to give

$$\left(\frac{\text{d}T}{\rho\text{d}x}\right)_c = 0.1535\,\frac{Zz^2}{A\beta^2}\left[\ln\left(\frac{2m_0c^2\beta^2T'_{\text{max}}}{I^2(1-\beta^2)}\right) - 2\beta^2\right]\,\frac{\text{MeV cm}^2}{\text{g}} \tag{2.13}$$

which can be simplified even further by substituting T'_{max} from Equation 2.4 to yield

$$\left(\frac{\text{d}T}{\rho\text{d}x}\right)_c = 0.3071\,\frac{Zz^2}{A\beta^2}\left[\ln\left(\frac{2m_0c^2\beta^2}{(1-\beta^2)}\right) - \beta^2 - \ln I\right]\,\frac{\text{MeV cm}^2}{\text{g}}. \tag{2.14}$$

The notation varies from reference to reference but Equation 2.14 is commonly referred to as the *Bethe formula*.

Several correction terms can be introduced to the general Bethe formula to increase its accuracy. The first is the shell correction which takes into account the relative participation of atomic electrons in the slowing down process at low energies. This correction term is important only when the velocity of the charged particle is no longer much greater than that of the atomic electrons in the stopping medium.

A second correction term, known as the density correction, can be included to account for the polarization or density effect in condensed media. Additional correction factors can be included that compensate for departures from the first Born approximation. The literature (*16*, *68*, *69*, *75*, *76*) contains a detailed discussion of these correction factors.

2.1.3 Electrons and Positrons

Similarly, Equation 2.1 can be expanded (*33*,*68*,*73*,*75*) for electrons and positrons such that

$$\left(\frac{\mathrm{d}T}{\rho \mathrm{d}x}\right)_c = 0.1535\,\frac{Z}{A\beta^2}\left[\ln\left(\frac{T}{I}\right)^2 + \ln\left(1+\frac{\tau}{2}\right) + F^{\pm}(\tau) - \delta\right]\,\frac{\mathrm{MeV\,cm^2}}{\mathrm{g}} \tag{2.15}$$

where δ is the previously mentioned density correction,

$$\tau \equiv \frac{T}{m_0 c^2}, \tag{2.16}$$

for electrons

$$F^{-}(\tau) = (1-\beta^2)\big[1+\tau^2/8-(2\tau+1)\ln 2\big], \tag{2.17}$$

and for positrons

$$F^{+}(\tau) = 2\ln 2 - \frac{\beta^2}{12}\left(23+\frac{14}{\tau+2}+\frac{10}{(\tau+2)^2}+\frac{4}{(\tau+2)^3}\right). \tag{2.18}$$

2.1.4 Restricted Stopping Power

Another quantity of interest is the restricted stopping power (*68*,*69*,*75*) which is the fraction of the collision stopping power that includes all soft collisions and those hard collisions resulting in delta rays with energies less than the cutoff value Δ. If Δ is increased to equal T'_{max} (given in Equations 2.4, 2.5, and 2.6), then

$$\left(\frac{\mathrm{d}T}{\rho \mathrm{d}x}\right)_{\Delta} = \left(\frac{\mathrm{d}T}{\rho \mathrm{d}x}\right)_c. \tag{2.19}$$

For heavy ions (*68*, *69*, *75*) this quantity is

$$\left(\frac{\mathrm{d}T}{\rho \mathrm{d}x}\right)_{\Delta} = 0.1535\,\frac{Zz^2}{A\beta^2}\left[\ln\left(\frac{2m_0c^2\beta^2\Delta}{I^2(1-\beta^2)}\right) - 2\beta^2 - \frac{2C}{Z}\right]\,\frac{\mathrm{MeV\,cm^2}}{\mathrm{g}}. \tag{2.20}$$

For electrons and positrons (*68*, *75*) this quantity is

$$\left(\frac{\mathrm{d}T}{\rho \mathrm{d}x}\right)_{\Delta} = 0.1535\,\frac{Z}{A\beta^2}\left[\ln\left(\frac{T}{I}\right)^2 + \ln\left(1+\frac{\tau}{2}\right) + G^{\pm}(\tau,\eta) - \delta\right]\,\frac{\mathrm{MeV\,cm^2}}{\mathrm{g}} \tag{2.21}$$

where

$$\eta = \frac{\Delta}{T}, \tag{2.22}$$

for electrons

$$\begin{aligned} G^{-}(\tau,\eta) = &-1-\beta^2+\ln\left[4(1-\eta)\eta\right]+(1-\eta)^{-1} \\ &+(1-\beta^2)\left[\tau^2\eta^2/2+(2\tau+1)ln(1-\eta)\right], \end{aligned} \tag{2.23}$$

and for positrons

$$G^{+}(\tau,\eta) = \ln 4\eta - \beta^2\left[\begin{array}{l} 1+(2-\xi^2)\eta-(3+\xi^2)(\xi\tau/2)\eta^2 \\ +(1+\xi\tau)(\xi^2\tau^2/3)\eta^3-(\xi^3\tau^3/4)\eta^4 \end{array}\right] \tag{2.24}$$

given that

$$\xi \equiv (\tau+2)^{-1}. \tag{2.25}$$

It should be noted that $G^{-}(\tau,1/2) = F^{-}(\tau)$ and $G^{+}(\tau,1) = F^{+}(\tau)$ meaning the restricted stopping power equals the stopping power when $\Delta = T/2$ for electrons and $\Delta = T$ for positrons (*75*). This relationship confirms the spacial condition described by Equation 2.19.

2.1.5 Dependencies of the Bethe Formula

The Bethe formula described in Equation 2.14 warrants special attention because of the pivotal role it plays in describing the behavior of heavy ions slowing down and losing energy in matter. Of specific interest is the role that some of the variables play in influencing the stopping power. An understanding of these dependencies allows for the exploitation of certain physical phenomena for the benefit of simulations, experiments, and real world radiation protection applications.

The factor Z/A outside the bracket makes the formula proportional to the number of electrons per unit mass of the medium. Therefore, the ideal shielding material for charged particles, despite its impracticality, is H with $Z/A = 1$. The stopping power decreases as Z increases due to a decrease in the Z/A ratio. Additionally, the stopping power decreases as Z increases due to the term $-\ln I$ in the bracket.

The strongest dependence on velocity comes from the inverse β^2 outside of the bracket which rapidly decreases the stopping power as β increases. This inverse relationship between particle velocity and stopping power accounts for the Bragg Peak that is the hallmark of charged particle depth-dose curves. It should be noted, however, that the Bethe formula is neither appropriate nor accurate for very low energies. The stopping power does not increase without limit as β decreases as the formula implies. As a charged particle slows down, the stopping power reaches a maximum and then decreases as β approaches zero.

There is a *very* strong dependence of the stopping power on particle charge z since it is proportional to z^2. To illustrate this strong dependence, consider the stopping power of a proton and α particle of the same velocity in the same stopping medium. The α particle has a charge of $z = 2$ and the proton has a charge of $z = 1$. Because of this difference, the α particle has a stopping power $2^2 = 4$ times greater than that

of the proton. Likewise, and demonstrating a much more extreme case, the stopping power of an Fe ion with $z = 26$ is a factor of $26^2 = 676$ greater than a proton of the same velocity in the same stopping medium.

There is no dependence of the stopping power on the particle mass. The mass of the incident particles does not appear in the stopping power formula.

Attix (*68*) offers a detailed discussion of these dependencies.

2.1.6 Continuous Slowing Down Approximation

The range of a charged particle is the expectation value of the path length p that it follows until it comes to rest which is defined as

$$\mathfrak{R}_{\mathrm{CSDA}} = \int_0^{T_0} \left(\frac{\mathrm{d}T}{\rho \mathrm{d}x} \right)^{-1} \mathrm{d}T \tag{2.26}$$

where T_0 is the starting energy of the particle. If $\mathrm{d}T/\rho\mathrm{d}x$ is in MeV cm^2/g and $\mathrm{d}T$ in MeV, then $\mathfrak{R}_{\mathrm{CSDA}}$ is thus given in terms of the area density with units of g/cm^2 (*68*). Because of the complexity of the stopping power equations, they and $\mathfrak{R}_{\mathrm{CSDA}}$ are often found in tabulated references. $\mathfrak{R}_{\mathrm{CSDA}}$ for a heavy ion of charge z and rest mass M_0 can be found via tabulated proton data by the relationship

$$\mathfrak{R}_{\mathrm{CSDA}} = \frac{\mathfrak{R}^P_{\mathrm{CSDA}} M_0}{M_0^P z^2} \tag{2.27}$$

where $\mathfrak{R}^P_{\mathrm{CSDA}}$ is the range of a proton of rest mass M_0^P. Because of the differences between z and the charge of an ion at low velocities, the relationship described by Equation 2.27 should only be used as an approximation tool and tabulated data should be used whenever possible. ICRU Report 49 (*69*) contains stopping power and range tables for protons and α particles, and ICRU Report 73 (*76*) contains stopping power and range tables for heavy ions. Additionally, ICRU Report 37 (*75*)

contains stopping power and range tables for electrons and positrons.

2.1.7 General Considerations

Up to this point the stopping power has been presented with units of $\frac{\text{MeV cm}^2}{\text{g}}$. In the fields of microdosimetry and radiological protection, however, the units of keV/μm are more commonly used where

$$10\,\frac{\text{MeV cm}^2}{\text{g}} = 1\,\frac{\text{keV}}{\mu\text{m}} \tag{2.28}$$

at unit density ($\rho = 1$ g/cm^3).

In the case where the stopping medium is a mixture of elements, the stopping power is represented by the weighted sum of the stopping powers of the composing materials according to Bragg's Rule (*68*, *75*):

$$\left(\frac{\text{d}T}{\rho \text{d}x}\right)_{mix} = f_{z_1}\left(\frac{\text{d}T}{\rho \text{d}x}\right)_{z_1} + f_{z_2}\left(\frac{\text{d}T}{\rho \text{d}x}\right)_{z_2} + \ldots \tag{2.29}$$

Similarly, δ for a mixture is

$$\delta = \frac{\sum_i f_{z_i}(Z/A)_i \delta_i}{Z/A}. \tag{2.30}$$

2.2 Fragmentation

A discussion of particles slowing down in matter would not be complete without including nuclear fragmentation. As mentioned in the beginning of the last section, inelastic nuclear reactions are a pathway for charged particles to lose energy as they slow down in matter. Although sometimes only briefly mentioned or even completely ignored in the discussion of charged particles slowing down in matter, nuclear fragmentation can play a significant role in influencing the spatial dependence and quan-

tity of energy deposition events. A large amount of work has been done to measure charge-changing cross sections (*77–85*) for use in radiation protection (*86–93*) and for general physics research (*94*). Additionally, the study of nuclear fragmentation has been a focus of study for researchers at Lawrence Berkeley National Laboratory for nearly twenty years (*82*).

Nuclear interactions are of great importance when analyzing space radiation because they can result in the fragmentation of incident ions. Fragmentation of heavy ions produces lighter ions which have a lower nuclear charge z. The production of these lighter ions reduces the dose because of the z^2 dependence of the electronic stopping power. When fragmentation occurs, the sum of the squares of fragment charges will be smaller than the square of the charge of the incident heavy ion. At the same time, light ions can cause fragmentation of target nuclei resulting in ions with lower velocity and higher charge than the primary thereby increasing the dose.

Low Z shielding materials attenuate a very broad range of incident ions at the expense of producing many low stopping power ions, fragments, that deliver a lower dose. At the same time, high Z shielding materials attenuate those segments of the GCR spectrum with the highest stopping power at the expense of producing a broad range of LET components for which biological response may be enhanced relative to free space exposures (*67*). Additionally, the use of high Z shielding materials can lead to high Z fragments, even under light ion irradiation.

The dose from GCRs can be reduced by incident ions losing energy from electronic interactions and stopping in shielding material. However, this technique cannot be relied upon to provide adequate shielding against some of the more energetic particles typical of the GCR spectrum because of relatively thin shielding that results from payload restrictions (*82*).

Therefore, a trade off exists in determining the type and thickness of shielding

material for protection from space radiation. This trade off was addressed in a study (*95*) that investigated different shielding configurations aboard the ISS. For the 1.0 GeV/n Fe ions investigated in the study, a net decrease in the average dose per incident ion was reported to result from the introduction of shielding. Miller *et al.* determined it was advantageous to add material to fragment the incident ions, even at the expense of slowing the fragments and surviving primaries. Despite the fact that this slowing made the ions more ionizing, this increase in stopping power was negated by the much larger decrease in stopping power resulting from the reduction of ion charge caused by fragmentation (*95*).

2.3 Dosimetry

ICRU Report 85, *Fundamental Quantities and Units for Ionizing Radiation (Revised)* (*96*), gives a detailed presentation of the Commission's recommendations for quantities and units specifically intended for radiation protection. A complete discussion of the contents of this report would be neither appropriate nor necessary for the scope of this work. However, a brief synopsis highlighting the quantities and units relevant to this work are presented to ensure a proper understanding of the these fundamental concepts.

2.3.1 Average Values

Perhaps the most common quantity in radiation protection is linear energy transfer (LET). LET, or electronic stopping power, is quite simply the average energy loss of a charged particle per unit distance traveled. The LET of charged particles of a given type and energy in a specific material can be denoted as the restricted LET

$$L_{\Delta} = \frac{\mathrm{d}E_{\Delta}}{\mathrm{d}l} \tag{2.31}$$

where $\mathrm{d}E_\Delta$ is the mean energy lost by the charged particles due to electronic interactions in traversing a distance $\mathrm{d}l$, minus the mean sum of the kinetic energies in excess of Δ of all the electrons released by the charged particles (*96*). If no energy cutoff is imposed, the unrestricted LET is equal to the electronic stopping power, and may be denoted as L_∞ or simply as L. In that case,

$$L = L_\infty = \frac{\mathrm{d}E}{\mathrm{d}l}. \tag{2.32}$$

LET has SI units of J/m; however, these units are rarely used in radiation protection. Instead, a conversion factor is introduced to convert J/m to the much more meaningful and widely used units of keV/μm where $1\,\mathrm{keV}/\mu\mathrm{m} = 1.602 \times 10^{-10}\,\mathrm{J/m}$.

There are two stochastic quantities of interest in dosimetry. The first is energy deposition

$$\epsilon_i = \epsilon_{in} - \epsilon_{out} + Q \tag{2.33}$$

where ϵ_{in} is the energy of the incident ionizing particle (excluding rest energy), ϵ_{out} is the sum of the energies of all ionizing particles leaving the interaction (excluding rest energy), and Q is the change in rest energies of the nucleus and of all particles involved in the interaction (*96*). $Q > 0$ corresponds to a decrease of rest mass energy and $Q < 0$ corresponds to an increase in rest mass energy.

The second quantity of interest is the energy imparted ϵ to the matter in a given volume which is the sum of all energy depositions in the volume, thus

$$\epsilon = \sum_i \epsilon_i \tag{2.34}$$

where the summation is performed over all energy depositions ϵ_i in that volume (*96*).

Energy imparted is a stochastic quantity. However, its mean, denoted by $\bar{\epsilon}$ is the

foundation of one of the most fundamental quantities in radiation protection. The absorbed dose D is a measure of the energy imparted per unit mass given that

$$D = \frac{\mathrm{d}\bar{\epsilon}}{\mathrm{d}m} \tag{2.35}$$

where $\mathrm{d}\bar{\epsilon}$ is the mean energy imparted by ionizing radiation to matter of mass $\mathrm{d}m$. The absorbed dose is the mean energy imparted per unit mass *at a point*. It should be noted that the process of ionization losses is not valid as $\mathrm{d}m$ approaches zero (*68*, *96*). Absorbed dose has SI units of J/kg with the special name gray (Gy).

If temporal resolution is required, the absorbed-dose rate (*68*, *96*) is

$$\dot{D} = \frac{\mathrm{d}D}{\mathrm{d}t} = \frac{\mathrm{d}}{\mathrm{d}t}\left(\frac{\mathrm{d}\bar{\epsilon}}{\mathrm{d}m}\right) \tag{2.36}$$

where $\mathrm{d}D$ is the increment of absorbed does in the time interval $\mathrm{d}t$ which has SI units of Gy/s.

2.3.2 Radiation Quality

All radiation types are not created equal. Photons, electrons, neutrons, protons, α particles, and heavy ions produce ionizations with different spatial distributions. This fundamental difference results in interactions that can lead to large, orders-of-magnitude differences in energy deposition in small sites. Many types of ionizing radiation can be described as sparsely ionizing, that is, they deposit very little energy along their path of travel. Examples include X rays, γ rays, electrons, and positrons. Many other types of radiation, however, can be described a densely ionizing because they deposit large amounts of energy along their path. Examples include high energy neutrons, α particles, fission fragments, and the heavy ions found in the GCR spectrum. These densely ionizing particles can be energetic enough to produce delta

rays capable of producing ionizations as well.

Absorbed dose, despite its simplicity, rigor, and reliability as a basic physical quantity, is simply not an adequate metric for quantifying detriment from exposure to ionizing radiation (*97*). The same absorbed dose from different types of radiation results in different rates of stochastic effects, most notably radiation-induced cancer (*97*). Meaning, a dose of 1 Gy of photons does not carry the same increased risk of cancer as 1 Gy of α particles, for example.

To address this issue, the dose equivalent is calculated in an attempt to normalize the measurement of risk such that

$$H = D \times Q \tag{2.37}$$

where D is the absorbed dose at the point of interest in tissue and Q the corresponding dimensionless quality factor at this point. The dose equivalent has units of J/kg with the special name sievert (Sv). While 1 Gy of photons does not carry the same increased risk of cancer as 1 Gy of α particles, as previously mentioned, 1 Sv of photons *does* carry the same increased risk of cancer as 1 Sv of α particles, assuming the quality factor accurately quantifies the stochastic differences of the two particle types.

The value of the quality factor is determined by the type and energy of charged particles passing a small volume. It is well known that the biological effectiveness of a radiation is correlated with the ionization density along the track of charged particles in tissue (*97*). Therefore, Q is defined as a function of L of charged particles in water. The relation between L and Q that was proposed by the International Commission on Radiological Protection (ICRP) in *Publication 60* in 1991 appears in Table 2.1.

Table 2.1
ICRP 60 $Q(L)$ Function

L [keV/μm]	$Q(L)$
$L \leq 10$	1
$10 < L \leq 100$	$0.32L - 2.2$
$L > 100$	$300/\sqrt{L}$

This $Q(L)$ function attempts to account for the results of radiobiological investigations on cellular and molecular systems as well as on the results of animal experiments. At the time of the release of the Commission's most current recommendations, *Publication 103* in 2007, no new radiobiological findings were presented that prompted changing the $Q(L)$ function. Therefore, the $Q(L)$ relationship first presented in *Publication 60* remains unchanged in *Publication 103* (*97*). The $Q(L)$ function is presented graphically in Figure 2.1. $Q(L)$ reaches a maximum value of approximately 30 at $L = 100$ keV/μm.

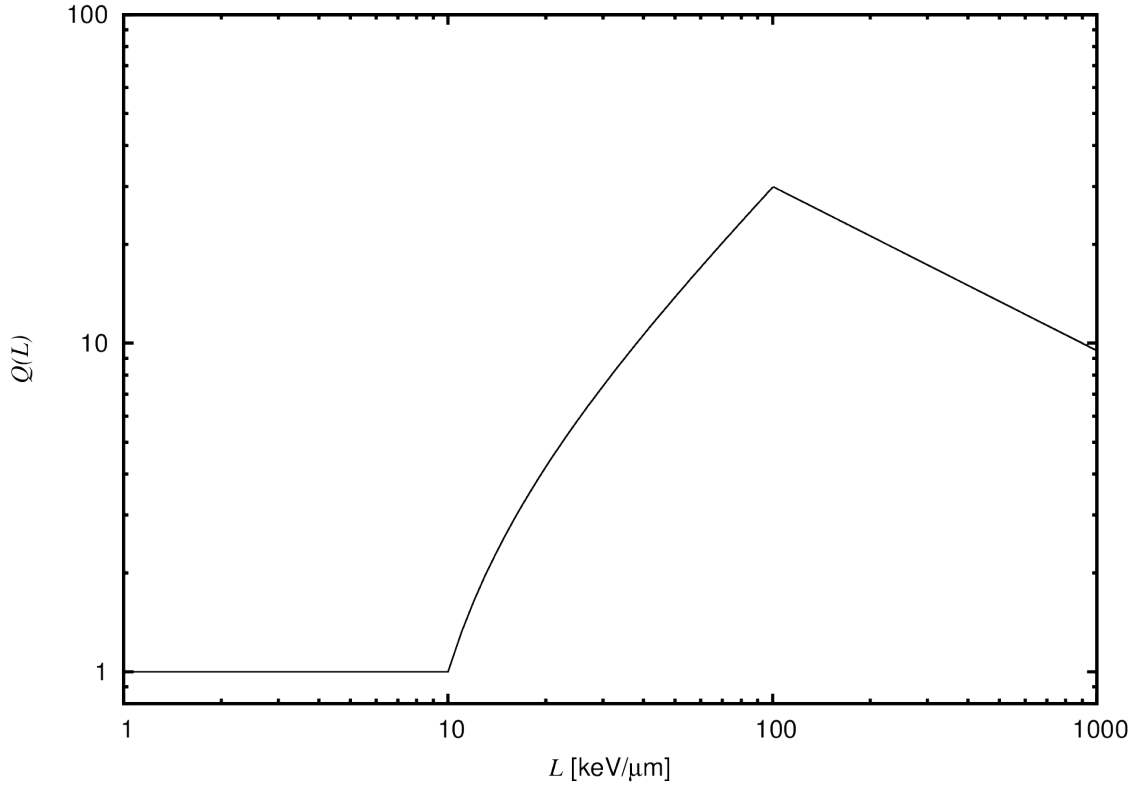

Figure 2.1. ICRP 60 quality factor as a function of L.

The average quality factor (*33*, *97–99*) of a mixed field of ionizing radiation can be determined by

$$\bar{Q} = \frac{1}{D} \int_0^\infty Q(L) D(L) \mathrm{d}L \tag{2.38}$$

where $Q(L)$ is the quality factor for a given value of L and $D(L)\mathrm{d}L$ is the absorbed dose at LET between L and $L + \mathrm{d}L$. It should be noted that $\bar{Q}$ represents a dose average, not an event average.

Dose equivalent H and quality factor Q are classified as *operational quantities* by the ICRP. The equivalent dose H_T and effective dose E presented in the Commission's recommendations (*97*, *98*) are not directly measurable in tissue and as a result, cannot be used in radiation monitoring. This is due to the conceptual differences

between dose equivalent and equivalent dose: equivalent dose is the average dose weighted by a radiation weighting factor w_{R} and dose equivalent is a point function of the absorbed dose weighted by a quality factor Q (*33*, *97–99*).

To overcome these conceptual differences, radiation protection systems employ operational quantities that can be measured and from which the equivalent dose H_{T} and the effective dose E can be assessed. Operational quantities are intended to serve as an estimate, preferably conservative upper limits, for the value of the protection quantities related to an exposure to most types of radiation. For external exposures, operational dose equivalent quantities have been defined for area and individual monitoring. Equivalent dose H_{T} and organ doses can be calculated from operational dose equivalent quantities by utilizing dose conversion coefficients for external exposure (*97*).

Quantifying risk from exposure to heavy ions in the GCR spectrum has proven to be an exceedingly difficult task (*55*). NASA has undertaken work to develop a risk projection model for space radiation cancer risks (*52*, *100*) that addresses the large uncertainties in the quality of GCRs.

2.4 Microdosimetric Quantities

Microdosimetry is the study of the patterns of energy deposition from ionizing radiation interacting with microscopic volumes much smaller than the range of secondary particles generated by the incident particle. Since its inception less than 50 years ago it has been very important in the field of radiobiology (*101*).

LET is an expectation value at a point of the energy lost by the incident radiation in the direction of traversal (*68*), but it is a one-dimensional concept that does not describe the radial extent of energy transfer (*102*, *103*). At the macroscopic level, different incident particles may have the same LET at some point along their path

but due to the dependence of secondary delta-ray energy as a function of velocity, the local energy deposited may be very different due to energy escaping the volume of interest. This radial energy loss is a factor of both the incident ion velocity and the target geometry. Therefore, microscopic energy measurements are commonly presented in terms of the stochastic energy deposition or dose distributions in the volume and geometry relevant to the study (*104*).

In the field of microdosimetry, care must be taken to ensure energy deposition events are characterized properly. The common health physics values of absorbed dose and dose equivalent, while perfectly applicable and widely used for large site sizes, do not carry the same relevance when applied to small volumes (i.e. 1 μm site sizes). On the large scale, these average values are sufficient for most applications. On the small scale, however, they do not accurately describe energy deposition. The stochastic nature of energy deposition events becomes increasingly evident as the site size is reduced until a point is reached where the average values no longer accurately describe the physical phenomena. At this point, energy deposition events are best described by a probability distribution (*104*).

Since microdosimetry is the study of energy deposition in very small volumes, a practical method for measurements needed to be developed. Measuring the energy deposition in sites on the order of 1 μm can be quite impractical if not impossible in some situations. To aid in this study, small volumes are simulated by much larger physical volumes. Therefore, a 1 μm site size of unit density (1 g/cm^3) can be simulated by a volume orders of magnitude greater in physical dimension, to a size that is much easier to work with. This is done by maintaining the same mass thickness or area density, measured in units of g/cm^2, in the simulated volume. This simple relationship is

$$(\rho \mathrm{d}x)_1 = (\rho \mathrm{d}x)_2 \tag{2.39}$$

where ρ_1 and $\mathrm{d}x_1$ are the density and simulated site size, respectively, and ρ_2 and $\mathrm{d}x_2$ are the density and size of physical site, respectively. For the common site size of 1 μm, ρ_1 would be equal to 1 g/cm^3 and $\mathrm{d}x_1$ would be equal to 1 μm. Therefore, ρ_2 and $\mathrm{d}x_2$ are chosen such that their product equals the product of ρ_1 and $\mathrm{d}x_1$, 1×10^{-4} g/cm^2.

2.4.1 Lineal Energy

The most common stochastic value used in microdosimetry measurements and simulations is lineal energy. The lineal energy y is

$$y = \frac{\epsilon}{\bar{l}} \tag{2.40}$$

where ϵ is the energy imparted to the matter in a given volume by a single energy-deposition event and $\bar{l}$ is the mean chord length of the volume (*104–106*). Lineal energy is most commonly expressed in units of keV/μm. The mean chord length $\bar{l}$ of a convex body is equal to

$$\bar{l} = \frac{4V}{S} \tag{2.41}$$

by Cauchy's theorem (*107*) where V and S are the volume and surface area of the site, respectively. Applying this to a sphere, Equation 2.41 becomes

$$\bar{l} = \frac{4V}{S} = \frac{4\left(\frac{4}{3}\right)\pi r^3}{4\pi r^2} = \frac{4r}{3} = \frac{2(2r)}{3} = \frac{2D}{3} \tag{2.42}$$

where r and D are the radius and diameter of the sphere, respectively. Likewise, Equation 2.41 applied to a right circular cylinder becomes

$$\bar{l} = \frac{4V}{S} = \frac{4\pi r^2 H}{2\pi r^2 + 2\pi r H} = \frac{4rH}{2r + 2H} = \frac{2DH}{D + 2H} \tag{2.43}$$

where r is the radius, D is the diameter, and H is the height.

2.4.2 Specific Energy

Experimental data are usually expressed as a function of y (*104*). However, the use of specific energy is useful in certain situations. The specific energy z is

$$z = \frac{\epsilon}{m} \tag{2.44}$$

where ϵ is the energy imparted by ionizing radiation to matter in a volume of mass m. Specific energy has units of J/kg which is termed gray (Gy) (*96*).

The relationship between z (in a single event) and y is

$$z = \frac{4y}{\rho S} \tag{2.45}$$

where ρ is the density and S is the surface area of the site. This relationship follows from the fact that, according to Cauchy (*107*), the mean chord length in a convex site is given by $4V/S$. In the case of a spherical site, $S = 4\pi r^2$ and

$$z = \frac{y}{\pi r^2 \rho}. \tag{2.46}$$

In most applications of microdosimetry ρ is taken to be equal to 1 g/cm^3, z is given the unit gray (1 Gy = 1 J/kg), y is expressed in keV/μm, and r is in μm (*104*). With these units, z can be presented as a function of y and r such that

$$z = \frac{0.204y}{(2r)^2}. \tag{2.47}$$

2.4.3 Microdosimetry Distributions

When analyzing microdosimetry data it is customary to consider the probability distribution of y. The value of the distribution function $F(y)$ is the probability that the lineal energy due to a single energy-deposition event is equal to or less than y. The probability density $f(y)$ is the derivative of $F(y)$ with respect to y such that

$$f(y) = \frac{\mathrm{d}F(y)}{\mathrm{d}y}. \tag{2.48}$$

$F(y)$ and $f(y)$ are independent of absorbed dose and absorbed-dose rate, but are dependent on the size and shape of the volume (*96*).

The mean of the $f(y)$ distribution $\bar{y}_\mathrm{F}$ is the frequency mean lineal energy which is equal to

$$\bar{y}_\mathrm{F} = \int_0^\infty y f(y)\,\mathrm{d}y. \tag{2.49}$$

The dose distribution, reflecting the fact that higher lineal energies deposit a higher dose (*108*), is also often considered where

$$d(y) = \frac{y f(y)}{\bar{y}_\mathrm{F}} \tag{2.50}$$

and the mean of this distribution, the dose mean lineal energy, is

$$\bar{y}_\mathrm{D} = \frac{1}{\bar{y}_\mathrm{F}} \int_0^\infty y^2 f(y)\,\mathrm{d}y \tag{2.51}$$

where $\bar{y}_\mathrm{F}$ is the frequency mean lineal energy from Equation 2.49. The frequency mean lineal energy $\bar{y}_\mathrm{F}$ is the first moment of the $f(y)$ distribution and the dose mean lineal energy $\bar{y}_\mathrm{D}$ is the ratio of the second and first moments of the $f(y)$ distribution (*104*). $\bar{y}_\mathrm{F}$ and $\bar{y}_\mathrm{D}$ are both non-stochastic quantities (*105*) and typically

have units of keV/μm.

The quantity z is also a stochastic quantity and can result from one or more energy-deposition events. The distribution function $F(z)$ is the probability that the specific energy is equal to or less than z. The probability density $f(z)$ is the derivative of $F(z)$ with respect to z such that

$$f(z) = \frac{\mathrm{d}F(z)}{\mathrm{d}z}. \tag{2.52}$$

$F(z)$ and $f(z)$ depend on absorbed dose in the mass m from Equation 2.44.

Likewise, the distribution function of the specific energy deposited in a single energy-deposition event, denoted by $F_1(z)$, is the conditional probability that a specific energy less than or equal to z is deposited if one energy-deposition event has occurred (*96*, *105*). The probability density $f_1(z)$ is the derivative of $F_1(z)$ with respect to z such that

$$f_1(z) = \frac{\mathrm{d}F_1(z)}{\mathrm{d}z}. \tag{2.53}$$

The mean of the $f_1(z)$ distribution, denoted by $\bar{z}_\mathrm{F}$, is the frequency mean specific energy per event which is equal to

$$\bar{z}_\mathrm{F} = \int_0^\infty z f_1(z)\,\mathrm{d}z. \tag{2.54}$$

The dose distribution of z per energy deposition event is also often considered. If $D_1(z)$ is taken to be the fraction of absorbed dose per event delivered by energy deposition events of specific energy less than or equal to z then the dose probability density $d_1(z)$ is the derivative of $D_1(z)$ with respect to z such that

$$d_1(z) = \frac{\mathrm{d}D_1(z)}{\mathrm{d}z} \tag{2.55}$$

and the mean of this distribution, the dose mean specific energy per event, is

$$\bar{z}_{\mathrm{D}} = \int_0^\infty z d_1(z)\,\mathrm{d}z \tag{2.56}$$

where $f_1(z)$ is the frequency distribution of z from Equation 2.53. The relationship between $d_1(z)$ and $f_1(z)$ is

$$d_1(z) = \frac{z}{\bar{z}_{\mathrm{F}}} f_1(z) \tag{2.57}$$

where $\bar{z}_{\mathrm{F}}$ is the frequency mean specific energy per event from Equation 2.54.

Substituting Equation 2.57 in Equation 2.56 gives $\bar{z}_{\mathrm{D}}$ as a function of $f_1(z)$ such that

$$\bar{z}_{\mathrm{D}} = \frac{1}{\bar{z}_{\mathrm{F}}} \int_0^\infty z^2 f_1(z)\,\mathrm{d}z. \tag{2.58}$$

$\bar{z}_{\mathrm{F}}$ and $\bar{z}_{\mathrm{D}}$ are both non-stochastic quantities (*105*) and typically have units of Gy.

It must be re-emphasized that $f_1(z)$ denotes a *single-event* quantity while $f(z)$ represents a general (multi-event) quantity (*104*, *105*).

2.5 Tissue-Equivalent Proportional Counters

A tissue-equivalent proportional counter (TEPC) is a specialized type of proportional counter whose wall and fill gas mimic the elemental composition of biological tissue (*73*). It is a versatile dosimeter because it can measure both absorbed dose and dose equivalent in a mixed radiation field and serves as the principal instrument of microdosimetry (*104*). For walls that are sufficiently thick compared to the range of delta rays produced in the wall, an equilibrium exists whereby the fluence of delta rays entering the gas volume becomes independent of the wall thickness. In the case of a low pressure TEPC, direct measurement of energy imparted, from Equation 2.34, is possible on an event-by-event basis.

From this measurement of energy imparted, and, therefore, absorbed dose in the

gas, the absorbed dose in the wall can be found according to the Bragg-Gray Cavity Theory which addresses a field of charged particles that crosses a gas/wall interface. The Bragg-Gray Cavity Theory assumes the thickness of the gas layer is so small in comparison with the range of the charged particles striking it that its presence does not perturb the charged-particle field (*68*).

Under this assumption, the dose in the gas is

$$D_g = \Phi \left[\left(\frac{\mathrm{d}T}{\rho \mathrm{d}x} \right)_{c,g} \right]_T \tag{2.59}$$

and the dose in the wall is

$$D_w = \Phi \left[\left(\frac{\mathrm{d}T}{\rho \mathrm{d}x} \right)_{c,w} \right]_T \tag{2.60}$$

where $[(\mathrm{d}T/\rho \mathrm{d}x)_{c,g}]$ and $[(\mathrm{d}T/\rho \mathrm{d}x)_{c,w}]$ are the mass collision stopping powers of the gas and wall regions, respectively, at energy T.

If Φ is assumed to be continuous across the gas/wall interface then the ratio of the absorbed doses in the two media is

$$\frac{D_w}{D_g} = \frac{(\mathrm{d}T/\rho \mathrm{d}x)_{c,w}}{(\mathrm{d}T/\rho \mathrm{d}x)_{c,g}}. \tag{2.61}$$

This relationship can be simplified (*68*) to

$$\frac{D_w}{D_g} = \frac{{}_m\bar{S}_w}{{}_m\bar{S}_g} = {}_m\bar{S}_g^w \tag{2.62}$$

where ${}_m\bar{S}_w$ and ${}_m\bar{S}_g$ are the average mass collision stopping powers in the wall and gas, respectively, for a differential energy distribution. As a result, the absorbed dose in the wall can be described as a function of the absorbed dose in the gas. If

both the gas and wall material are tissue-equivalent, meaning ${}_m\bar{S}_w = {}_m\bar{S}_g$, then the relationship is simplified to

$$\frac{D_w}{D_g} = \frac{{}_m\bar{S}_w}{{}_m\bar{S}_g} = \frac{{}_m\bar{S}_g}{{}_m\bar{S}_g} = 1 \tag{2.63}$$

where the dose in the wall is equal to the dose in the gas.

This relationship, along with the knowledge of the quality of the radiation provided by the y distribution and the tissue-equivalence of the wall material and gas, allows a TEPC to provide a measurement of absorbed dose and dose equivalent in tissue exposed to a mixed radiation field.

In theory, making an assessment of radiation quality with a TEPC is not a straightforward task. Radiation quality Q is presented as a function of L as detailed in Table 2.1. A TEPC, however, measures lineal energy y, not L. L is the average energy *lost* per unit path length while y is a stochastic measure of the energy *imparted* per unit path length. Energy lost and energy imparted cannot be assumed to be the same and are often different due to energy loss straggling and delta rays escaping the site. That said, L and y are similar and their difference can be largely disregarded for densely ionizing radiation. For sparsely ionizing radiation, however, the differences can be quite pronounced and y can have smaller values than L (*99*).

In practice, L is taken to be equal to y for the purposes of determining Q from a TEPC. The difference between the L and y is outweighed by the ease of measuring y and the difficulty of measuring L. Despite the contrast in the ease of measurability of the two quantities, L has been retained as the reference parameter in the current system of radiation protection quantities because it is more convenient in computations (*99*).

2.6 Convolution

Convolution describes the action of an observing instrument when it takes a weighted mean of a physical quantity over a narrow range of a variable (*109*). In other words, convolution describes how much two functions overlap as one function is translated over the other.

The idea of convolution is relevant to microdosimetry when discussing multiple-event spectra. $f_1(z)$ distributions represent *single-event* spectra. These spectra show what a z distribution would look like assuming the site was subject to only one event. If the site is subject to more than one event, as would be possible during a very high-fluence SPE, then the concept of convolution would need to be applied to the z distribution to produce multi-event spectra from a single-event spectrum. The measured or simulated z distribution would need to be self-convolved (to be defined later in this section) as many times as needed to correspond to the appropriate number of events and absorbed dose. The result would still be a frequency distribution, but the corresponding number of events would be dependent on the absorbed dose. The 1^{st} self-convolution would produce a frequency distribution for two events, the 2^{nd} self-convolution would produce a frequency distribution for three events, and so on.

The convolution (*110*) of two functions $f(x)$ and $g(x)$, provided that $f(x)$ and $g(x)$ are integrable functions, is denoted as $h(x)$ such that

$$h(x) = f(x) * g(x) = \int_{-\infty}^{\infty} f(u)g(x-u)\,\mathrm{d}u. \tag{2.64}$$

For the purposes of radiation protection, the convolution will be taken over a finite

interval $[0, T]$ where

$$h(x) = f(x) * g(x) = \int_0^T f(u)g(x-u)\,\mathrm{d}u \tag{2.65}$$

given that the function $h(x)$ is the convolution of functions $f(x)$ and $g(x)$ and, again, provided that $f(x)$ and $g(x)$ are integrable over the finite interval.

It should be noted (*110*) that each particular value of x is treated as a constant with respect to the variable u in the integrand. For every x, $h(x)$ computes the area curve of the point-wise product of $f(u)$ and $g(x-u)$. Since the curve of $g(x-u)$ continues to shift along the u-axis, when x takes on each different value, the curve of the product changes with x; hence, the area computed by the convolution integral is a function of x.

2.6.1 Fourier Transforms

A discussion of convolution would not be complete without a mention of Fourier transforms because of the unique link between the two. The Fourier transform of a function $f(x)$ is given as

$$\mathcal{F}\{f(x)\} = \int_{-\infty}^{\infty} f(x)e^{-j2\pi ft}\,\mathrm{d}t. \tag{2.66}$$

If the Fourier transforms of $f(x)$ and $g(x)$ are denoted as $\mathcal{F}\{f(x)\} = F(x)$ and $\mathcal{F}\{g(x)\} = G(x)$, respectively, then the following equation (*109*, *110*), known as the *convolution theorem*, can be used to find the convolution of the two functions where

$$\mathcal{F}\{f(x) * g(x)\} = F(x)G(x). \tag{2.67}$$

The convolution theorem is heavily utilized by the electrical engineering community for signal processing (*110*).

2.6.2 Linear Discrete Convolution

For the purposes of radiation protection, it is convenient to utilize linear discrete convolution. Because of the close connection to the continuous convolution, the *linear* discrete convolution is also referred to as the *regular* or *conventional* discrete convolution in signal processing literature (*110*).

Chu (*110*) presents an excellent discussion and step-by-step algorithm describing discrete convolution which is summarized as

$$h(n) = \sum_{i=0}^{n} f(i)g(n-i) \tag{2.68}$$

where n is the index of the discrete convolution result h. If f and g both have a length of N then the length of h is $2N-1$. Therefore, to generate the complete linear discrete convolution result, Equation 2.68 must be used to calculate every value of $h(n)$ on the interval $[0, 2N-1]$.

To this point it has been assumed that f and g are non-identical functions. However, for the purposes of producing multi-event spectra, they will in fact be identical functions (that is, $f = g$). So, the convolution, at least for the first step, will be a self convolution of f. In this case, Equation 2.68 becomes

$$h(n) = \sum_{i=0}^{n} f(i)f(n-i). \tag{2.69}$$

If we denote h_1 as the 1^{st} convolution, h_2 as the 2^{nd} convolution, and so on, then the

self-convolution chain of f can be described by

$$\begin{aligned}
1^{\text{st}} \text{ convolution: } & h_1(n) = \sum_{i=0}^{n} f(i) f(n-i) \\
2^{\text{nd}} \text{ convolution: } & h_2(n) = \sum_{i=0}^{n} f(i) h_1(n-i) \\
3^{\text{rd}} \text{ convolution: } & h_3(n) = \sum_{i=0}^{n} f(i) h_2(n-i) \\
& \vdots \\
N^{\text{th}} \text{ convolution: } & h_N(n) = \sum_{i=0}^{n} f(i) h_{N-1}(n-i)
\end{aligned} \tag{2.70}$$

which can be repeated as many times as necessary.

Applied to microdosimetry, Equation 2.70 becomes

$$\begin{aligned}
1^{\text{st}} \text{ convolution: } & f_2(z) = \sum_{i=0}^{z} f_1(i) f_1(z-i) \\
2^{\text{nd}} \text{ convolution: } & f_3(z) = \sum_{i=0}^{z} f_1(i) f_2(z-i) \\
3^{\text{rd}} \text{ convolution: } & f_4(z) = \sum_{i=0}^{z} f_1(i) f_3(z-i) \\
& \vdots \\
N^{\text{th}} \text{ convolution: } & f_N(z) = \sum_{i=0}^{z} f_1(i) f_{N-1}(z-i)
\end{aligned} \tag{2.71}$$

where $f_1(z)$ is the single-event distribution.

An example of the linear discrete self-convolution methodology described in Equation 2.70 is presented in Figure 2.2. This plot contains the 1^{st}, 2^{nd}, and 3^{rd} self convolutions of a uniform distribution 40 bins wide with all areas under the curve normalized to 1. As Figure 2.2 demonstrates, the convolved distribution approaches

a Gaussian distribution as N increases.

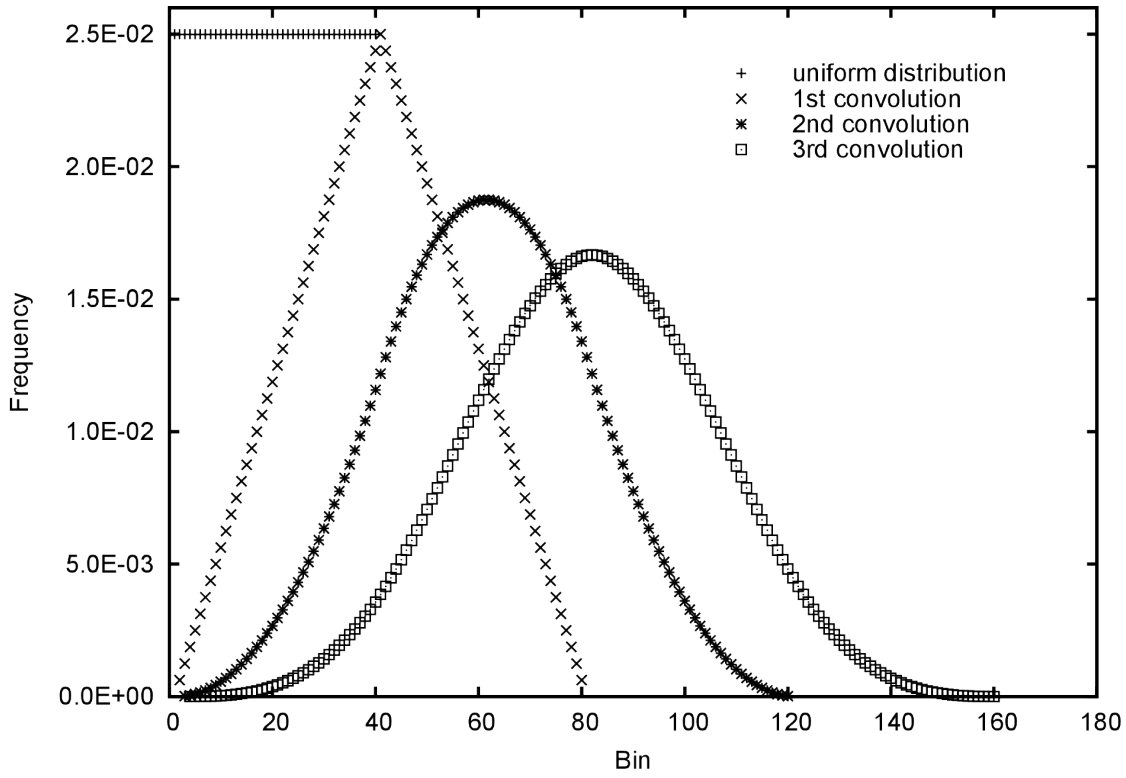

Figure 2.2. Self convolution of a uniform distribution.

As this convolution example illustrates, the patterns of energy deposition characteristic to (single-event) y distributions do not exist for high dose irradiations or, depending on the situation, exposure to high dose rates. In either case, a site can experience multiple events and the once insightful y distribution becomes a featureless Gaussian distribution.

2.7 Multiple Events

The discussion in the previous section on convolving z distributions to produce multi-event spectra intentionally omitted mention of how many times a distribution must be self convolved. This is because the number of self convolutions is determined by the absorbed dose D that was received by the site. As was mentioned earlier in this chapter, $f(y)$ does not depend on dose or dose rate. That is, it represents a *single-event* spectrum. While it is customary (*104*) to represent single-event distributions as a function of lineal energy y rather than specific energy z, $\bar{z}_{\mathrm{F}}$ must be considered to calculate the number of events. The relationship presented in Equation 2.47 allows for z to be expressed as a function of y.

Rossi (*104*) defines the event frequency as

$$\Phi^* = \frac{1}{\bar{z}_{\mathrm{F}}} \tag{2.72}$$

which represents the average number of events per unit dose. Combining this relationship with the fact that $\bar{z}_{\mathrm{F}}$ represents the dose to the site (*105*) yields the average number of events corresponding to an absorbed dose D as

$$\Phi^* D = \frac{D}{\bar{z}_{\mathrm{F}}}. \tag{2.73}$$

Therefore, the number of events corresponding to an absorbed dose D with a known y distribution can be calculated by combining Equations 2.47 and 2.73 to produce

$$\Phi^* D = \frac{D(2r)^2}{0.204\,\bar{y}_{\mathrm{F}}} \tag{2.74}$$

where r is the radius of the site in μm, $\bar{y}_{\mathrm{F}}$ is in units of keV/μm, and D is in Gy.

2.8 Random Sampling

Simulating the radiation environment in space requires the random sampling of differential energy spectra. For the case of GCRs in the present study, this requires randomly sampling the differential energy spectra from the Badhwar–O'Neill model (*19–21*).

Sampling from this discrete probability distribution requires the calculation of the cumulative distribution. If the probability distribution is presented as a series of kinetic energies $E_1, E_2, \ldots, E_n$ with corresponding fluence rates of $\phi_1, \phi_2, \ldots, \phi_n$, then the cumulative distribution is built by calculating the cumulative fluence rate according to

$$\begin{aligned} \Phi_0 &= 0 \\ \Phi_1 &= \phi_1 * E_1 \\ \Phi_2 &= \Phi_1 + [\phi_2 * (E_2 - E_1)] \\ &\vdots \\ \Phi_n &= \Phi_{n-1} + [\phi_n * (E_n - E_{n-1})] \end{aligned} \tag{2.75}$$

where E is the kinetic energy in units of MeV/n and ϕ is the differential energy fluence rate expressed in units of $[\mathrm{m^2\,s\,sr\,MeV/n}]^{-1}$.

If Φ is normalized where $\Phi_0 = 0$ and $\Phi_n = 1$, then a Φ interval can be found such that $\Phi_{i-1} \leq r < \Phi_i$ where r is a random number on the interval [0,1). A random energy inside the interval can be found according to

$$E = E_{i-1} + (E_i - E_{i-1}) * r \tag{2.76}$$

where, again, r is a random number and E is kinetic energy.

3. METHODS

The objective of this study is to use the Monte Carlo transport code FLUKA (*57*, *58*) to simulate the response of a TEPC on the surface of Mars. That is, to simulate a phenomenon that has never before occurred and, as a result, no experimental data exists for comparison. While simulation data are often generated in an attempt to verify and sometimes offer an explanation of certain features of experimental data, such a sequence of events will not take place for these data. It is anticipated that the opposite will occur: the data produced by the present study will be compared with experimental data once they are recorded.

3.1 FLUKA Description

The FLUKA code was originally developed in 1962 by J. Ranft and H. Geibel who initiated the code for hadron beams. The name FLUKA (from FLUktuierende KAscade) came in 1970. Between 1970 and 1987 the development of the code was carried out in the framework of a collaboration between CERN and the groups of Leipzig and Helsinki. That version was essentially for shielding calculations. Since 1989 FLUKA has been developed within INFN (National Institute of Nuclear Physics) with the personal collaboration of A. Fassò (CERN) and J. Ranft (Leipzig). Since 2002, FLUKA is an INFN project and is carried on in collaboration with CERN and the University of Houston (*57*).

FLUKA is a general purpose Monte Carlo code for the interaction and transport of hadrons, heavy ions, and electromagnetic particles from a few keV (or thermal energies for neutrons) to cosmic ray energies in various materials (*58*).

As in most simulation codes that adopt a "condensed history" approach, in FLUKA "continuous" processes such as energy loss and angular deflections due to

Coulomb interactions and "discrete" processes (delta-ray production, nuclear interactions, decays, bremsstrahlung and photon interaction) are treated separately (*57*).

According to the FLUKA manual, delta-ray production is controlled via Bhabha and Møller scattering (*57*). As observed in previous work (*65*), delta-ray production greatly influences the response of a TEPC. Specifically, the two phenomena of interest are delta-ray production in the wall and delta-ray escape from the gas to the wall. Simulating the response of a TEPC would be very difficult if not impossible without an accurate model for delta-ray production.

FLUKA is the code of choice for the present study because of its ability to simulate about 60 different particles, including electrons from 1 keV to thousands of TeV and hadrons of energies up to 20 TeV (*57*). For this application, FLUKA is a very flexible code. FLUKA's most current transport limits (*57*) appear in Table 3.1.

Table 3.1
FLUKA Transport Limits

	Secondary Particles	Primary Particles
charged hadrons	1 keV–20 TeV$^{(*)}$	100 keV–20 TeV$^{(*)(\dagger)}$
neutrons	thermal–20 TeV$^{(*)}$	thermal–20 TeV$^{(*)}$
antineutrons	1 keV–20 TeV$^{(*)}$	10 MeV–20 TeV$^{(*)}$
muons	1 keV–1 PeV	100 keV–1 PeV$^{(\dagger)}$
electrons	1 keV–1 PeV	70 keV–1 PeV (low-Z materials)$^{(\dagger)}$
		150 keV–1 PeV (high-Z materials)$^{(\dagger)}$
photons	100 eV–10 PeV	1 keV–10 PeV
heavy ions	$<$ 10 PeV/n	$<$ 10 PeV/n

$^{(*)}$ upper limit 10 PeV with the DPMJET interface
$^{(\dagger)}$ lower limit 10 keV in single scattering mode

3.2 Benchmarking for this Study

FLUKA is a mature and well-developed Monte Carlo transport code. Like many other transport codes, it calculates the stopping power of ions passing through matter with the Bethe Formula (*57*) which was discussed in Chapter 2 and presented in Equation 2.14.

The following tables present a comparison between FLUKA and tabulated stopping powers for a selection of ions and kinetic energies. Table 3.2 contains a comparison for H and He ions while Table 3.3 contains a comparison for C, O, Ne, Si, and Fe ions. The sources of the "tabulated" stopping power (SP) values are the NIST PSTAR and ASTAR databases (*43*) for H and He ions, respectively, and ICRU Report 73 (*76*) for the heavy ions.

The tabulated data from all three sources have been normalized to unit density. Since A-150 tissue-equivalent (TE) plastic has a density of 1.127 g/cm^3, any reference made to a 1 μm slab is in fact referring to a slab of with a physical dimension of 0.887 μm. This reflects a normalization to unit density according to Equation 2.39. Therefore, the keV/μm units in Tables 3.2 and 3.3 are in fact keV/μm *at unit density*.

It should be noted that both the tabulated and FLUKA SP values are based on the Bethe Formula. Therefore, the comparison between the two sources is a test to ensure both sources are implementing the formula correctly. Any differences between the two can most likely be attributed to the use of different correction factors. As the tables show, the differences between the two models in the peak GCR energy range of 300 MeV/n to 700 MeV/n is quite small.

Table 3.2
Stopping Power Comparison for H and He Ions in A-150 TE Plastic

Ion	Energy [MeV]	FLUKA SP [keV/μm]	Tabulated SP [keV/μm]	Difference [%]
H	10	5.230E+00	5.226E+00	0.07
	20	2.982E+00	2.973E+00	0.31
	30	2.148E+00	2.136E+00	0.59
	40	1.700E+00	1.693E+00	0.40
	50	1.415E+00	1.416E+00	-0.04
	60	1.224E+00	1.225E+00	-0.05
	70	1.092E+00	1.086E+00	0.53
	80	9.810E-01	9.795E-01	0.16
	90	9.036E-01	8.954E-01	0.91
	100	8.300E-01	8.273E-01	0.33
	200	5.046E-01	5.092E-01	-0.91
	300	4.026E-01	3.987E-01	0.97
	400	3.496E-01	3.433E-01	1.83
	500	3.097E-01	3.105E-01	-0.26
	600	2.879E-01	2.892E-01	-0.44
	700	2.668E-01	2.742E-01	-2.68
	800	2.579E-01	2.632E-01	-1.98
	900	2.491E-01	2.548E-01	-2.23
	1000	2.423E-01	2.485E-01	-2.49
He	50	1.744E+01	1.734E+01	0.57
	100	9.901E+00	9.854E+00	0.47
	500	2.815E+00	2.796E+00	0.69
	1000	1.760E+00	1.765E+00	-0.28

Table 3.3
Stopping Power Comparison for a Selection of Heavy Ions in A-150 TE Plastic

Ion	Energy [MeV/n]	FLUKA SP [keV/μm]	Tabulated SP [keV/μm]	Difference [%]
C	100	2.998E+01	2.999E+01	-0.05
	500	1.113E+01	1.130E+01	-1.58
	1000	8.729E+00	9.126E+00	-4.36
O	100	5.325E+01	5.333E+01	-0.15
	500	1.984E+01	2.014E+01	-1.47
	1000	1.555E+01	1.625E+01	-4.30
Ne	100	8.317E+01	8.332E+01	-0.18
	500	3.103E+01	3.152E+01	-1.55
	1000	2.430E+01	2.545E+01	-4.52
Si	100	1.631E+02	1.632E+02	-0.09
	500	6.095E+01	6.199E+01	-1.67
	1000	4.786E+01	5.007E+01	-4.41
Fe[(1)]	100	5.565E+02	5.647E+02	-1.44
	500	2.125E+02	2.149E+02	-1.11
	1000	1.663E+02	1.740E+02	-4.41

It should be noted that the SP values listed in Tables 3.2 and 3.3, and similarly the values provided by the Bethe Formula, represent *average* quantities. In reality, the

[(1)]ICRU 73 only provides stopping power data for Fe ions in elemental targets. Therefore, the FLUKA SP was compared to a weighted sum of elemental stopping powers according to Equation 2.29. Because ICRU 73 does not contain SP values for Fe ions in F or Ca elemental targets, the values presented above were calculated based on the weighted sum of H, C, N, and O elemental targets. Taken together, H, C, N, and O account for 96.4% of A-150 TE plastic by weight.

energy lost by an ion passing through matter fluctuates in the manner described by Landau (*111*) and Vavilov (*112*). The most probable energy loss can be considerably less than the mean given by the Bethe equation. Figure 3.1 shows the energy loss distribution produced by FLUKA for 500 MeV/n C ions passing through A-150 TE plastic. The resulting distribution is the characteristic Landau/Vavilov distribution.

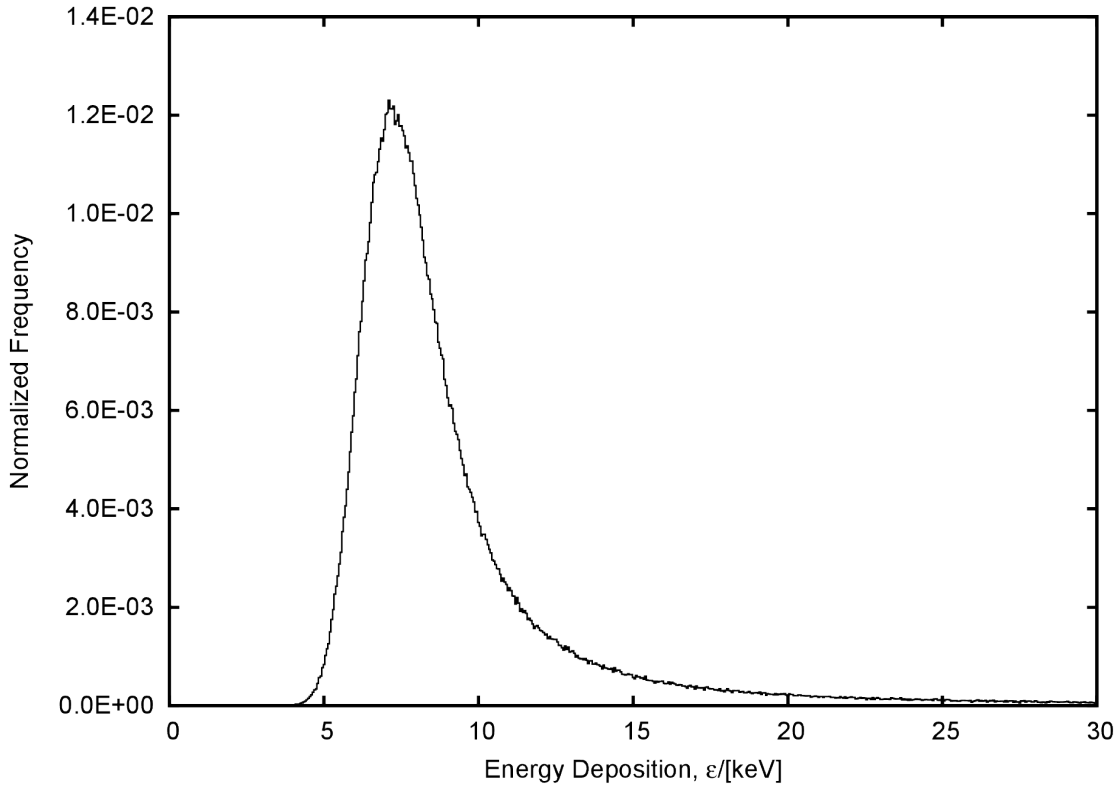

Figure 3.1. Landau/Vavilov distribution generated by FLUKA for 500 MeV/n ^{12}C ions passing through a 1 μm slab of A-150 TE plastic.

A careful observation of this distribution reveals a significant difference between the most probable value, 7.1 keV, and the average value, 11.1 keV. It must be

emphasized that this distribution represents the energy deposited by the ion as it passed through a 1 μm slab of A-150 TE plastic with delta-ray transport turned off. The Landau/Vavilov distribution describes the energy *loss* by an ion as it passes through matter. Since delta-ray transport was turned off, and, therefore, all delta-ray energy was deposited locally, this energy deposition distribution is also the energy loss spectrum. If delta-ray transport had been turned on, however, the energy deposited in the thin slab would not necessarily have been the same as the energy lost by the C ion. Many of the delta rays produced by the C ions would be reasonably expected to escape the thin slab.

Figure 3.2 illustrates FLUKA's ability to correctly account for the influence of a proton's energy on its range.

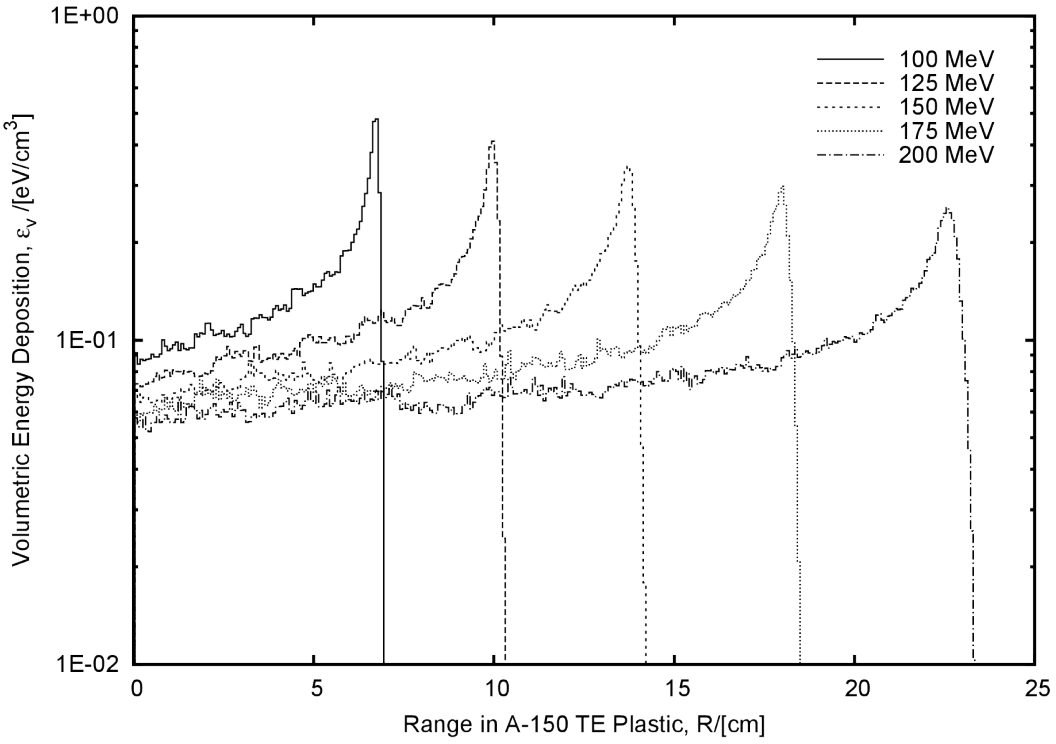

Figure 3.2. Depth dose curves generated by FLUKA for 100 MeV to 200 MeV protons in A-150 TE plastic.

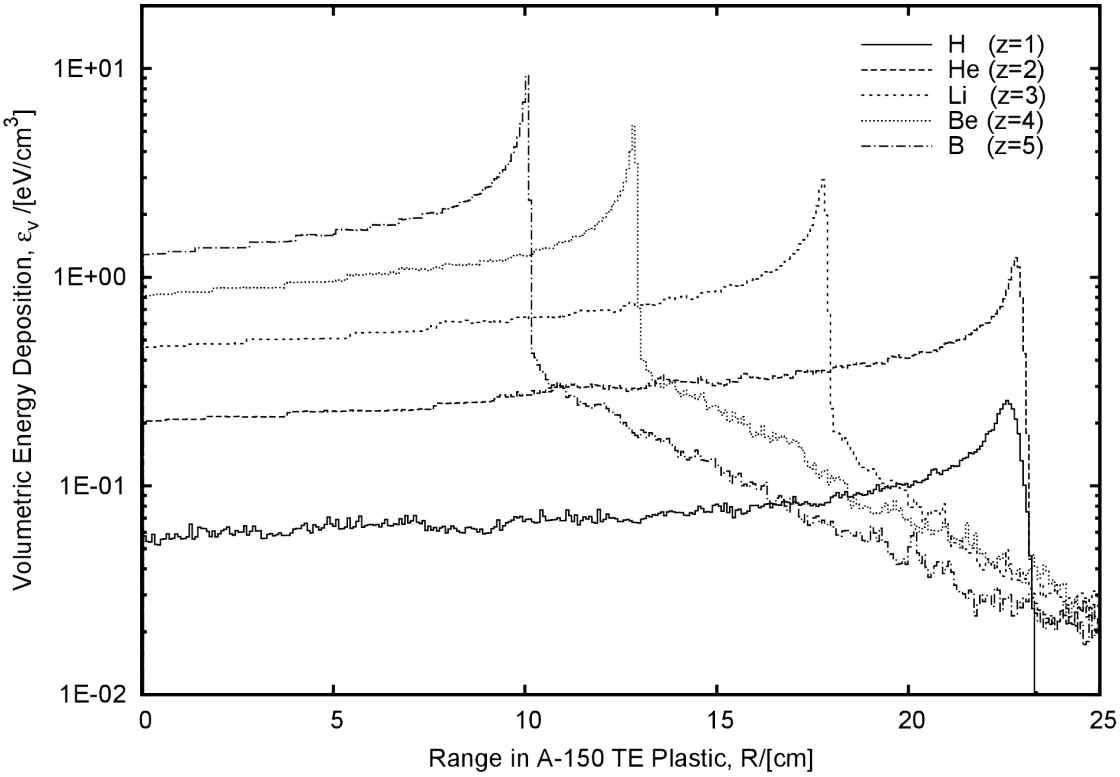

Figure 3.3. Depth dose curves generated by FLUKA for 200 MeV/n H, He, Li, Be, and B ions in A-150 TE plastic.

Likewise, Figure 3.3 illustrates FLUKA's ability to correctly account for the z^2 dependence of stopping power. Because of the increased stopping power that accompanies increased z, the range of an ion is inversely related to its charge. Thus, an ion's range decreases as z increases with the exception of protons and alpha particles which have the same range at the same velocity.

3.3 Prefatory Comments

The data presented in the present study were produced with FLUKA version 2011.2 using DPMJET version II.5 and involved the preparation of standard input files according to the manual (*57*). Since an isotropic GCR source is not standard

in FLUKA, a custom SOURCE[2] subroutine was utilized.

The global PRECISIOn[3] default, utilizing fully analogue absorption for low-energy neutrons, low-energy neutron transport to thermal energies, and a particle transport threshold of 100 keV for all other particles, was used in all simulations. Lower delta-ray production and transport thresholds were implemented for the TEPC to properly account for the influence of delta-ray effects. The manual contains a full description of the defaults (*57*).

Random numbers were generated with the built-in FLRNDM subroutine which returns a 64-bit random number on the interval [0,1). The FLUKA random number generator was used exclusively to preserve history reproducibility. (No external random number generators were used.)

3.4 Free Space Model

A spherical TEPC was modeled in a FLUKA input file that simulated a 1-μm site size of unit density. The gas volume was 1.27 cm in diameter with a wall thickness of 0.254 cm.

A simple calculation was performed using Equation 2.39 that gave the necessary gas density to produce a 1-μm site of 7.87×10^{-5} g/cm^3. Propane (C_3H_8) was used as the fill gas. A-150 TE plastic (*43*), which has a density of 1.127 g/cm^3 and a mean excitation energy of 65.1 eV, was used as the TEPC wall material for the present study.

[2] FLUKA input file options are presented in all caps and are truncated to eight characters. This document will use the same format.

[3] An example of the eight-character truncation.

The elemental composition of A-150 TE plastic appears in Table 3.4.

Table 3.4
Elemental Composition of A-150 Tissue-Equivalent Plastic

Atomic Number	Weight Fraction
1	0.1013
6	0.7755
7	0.0351
8	0.0523
9	0.0174
20	0.0184

Delta-ray transport was enabled to simulate wall effects and the influence of delta rays stopping and starting in the gas volume. The minimum delta-ray production and transport limit in FLUKA is 1 keV. To ensure maximum accuracy, the delta-ray production and transport limits for these TEPC simulations were set to this 1 keV minimum in the gas volume. Any electron that reaches this 1 keV transport limit locally deposits its kinetic energy.

The delta-ray production and transport thresholds in the wall were set according to a zone system, similar to the method used by Böhlen *et al.* (*63*). In this scheme, the delta-ray production and transport limits increase as the distance from the gas volume increases. Doing so results in expending CPU time on only those delta rays that have a reasonable chance of reaching the gas volume, and thereby contributing to the recorded energy deposition. Transporting delta rays down to the minimum threshold of 1 keV many hundreds of micrometers away from the gas volume is

unnecessary if there is a very low probability of these delta rays reaching the gas volume.

Böhlen *et al.* (*63*) implemented a scheme that set delta-ray production and transport limits as follows: 1 keV from the gas/wall interface to 3 μm inside the wall, 10 keV for the region of the wall 3 μm to 200 μm from the gas/wall interface, and 100 keV in the rest of the wall. These ranges were set under the assumption that delta rays would not penetrate further than their CSDA ranges (*43*) of 2.2 μm for 10 keV electrons and 126 μm for 100 keV electrons.

The limits used in the present study were 5 μm and 250 μm for the 10 keV and 100 keV thresholds, respectively, where the minimum distance to the gas was no less than twice the CSDA range of an electron with kinetic energy equal to the threshold energy. Implementing such a layering scheme strikes a balance between computational efficiency and accuracy.

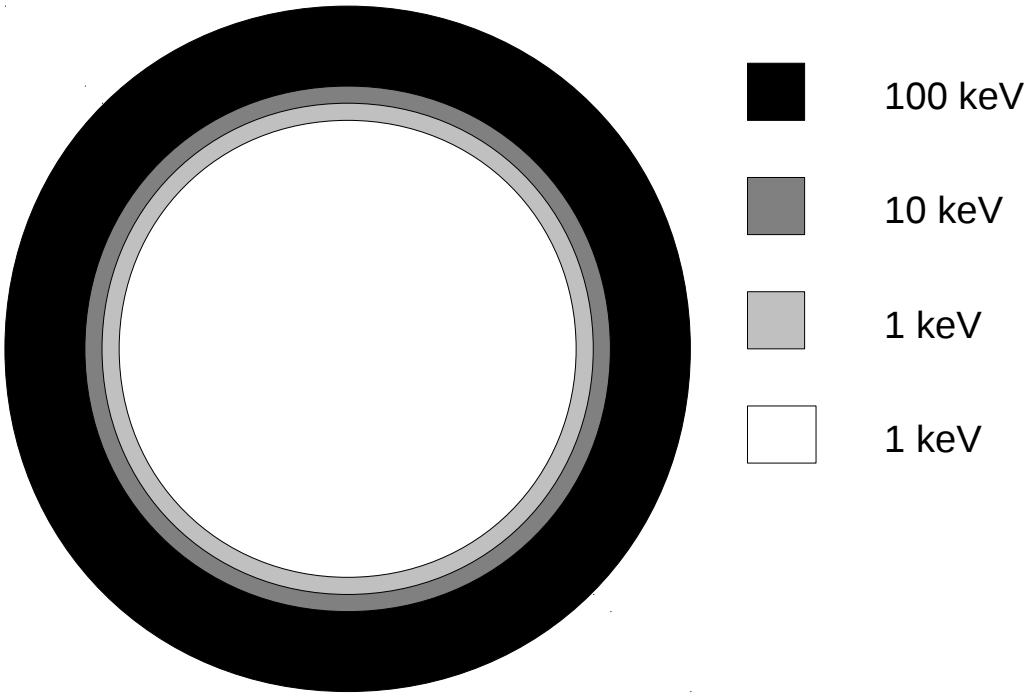

Figure 3.4. Schematic of delta-ray thresholds in the TEPC (not to scale). The interior cavity is filled with propane at a reduced pressure to simulate a 1-μm site. All three regions of the wall are A-150 TE plastic. The minimum distance from the 10-keV-threshold region to the gas volume is twice the CSDA range of a 10 keV electron. Likewise, the minimum distance from the 100-keV-threshold region to the gas volume is twice the CSDA range of a 100 keV electron.

Figure 3.4 contains a cross-sectional view (not to scale) of the TEPC showing the delta-ray threshold scheme in the wall. Delta-ray production and transport thresholds were set to 1 keV in the gas volume.

3.5 Mars Model

Care was taken to ensure that Mars was accurately modeled in all respects. This includes modeling the regolith, atmosphere, and the entire planet at its proper size. As previously mentioned, Mars does not posses a global magnetic field capable of

providing any significant shielding from space radiation.

3.5.1 Regolith

Regolith composition information was taken from Mars Exploration Rover (MER) A and B mission data. These data are presented as wt. % of specific oxides (*113*) and appear in Table 3.5.

Table 3.5
Chemical Composition of Martian Regolith

Oxide	MER-A [wt. %]	MER-B [wt. %]
Na_2O	3.02	2.17
MgO	8.49	7.64
Al_2O_3	10.20	9.39
SiO_2	46.20	46.20
P_2O_5	1.01	0.85
SO_3	6.32	5.57
Cl	0.76	0.67
K_2O	0.46	0.48
CaO	6.37	7.15
TiO_2	0.95	0.97
Cr_2O_3	0.29	0.41
MnO	0.31	0.37
FeO	15.60	18.00
NiO	0.06	0.05

The chemical composition percentages in Table 3.5 were converted to mass fractions of specific elements for the FLUKA input file. Table 3.6 presents the elemental composition of the Martian regolith, in mass fraction of each element, along with the average. While MER-A and MER-B reported different elemental compositions, the differences were slight and the averages were used in the input file.

Table 3.6
Elemental Composition of Martian Regolith

Element	MER-A	MER-B	Average
O	0.4382	0.4321	0.4352
Si	0.2159	0.2161	0.2160
Fe	0.1212	0.1400	0.1306
Al	0.0540	0.0497	0.0518
Mg	0.0512	0.0461	0.0486
Ca	0.0455	0.0511	0.0483
S	0.0253	0.0223	0.0238
Na	0.0224	0.0161	0.0193
Cl	0.0076	0.0067	0.0072
Ti	0.0057	0.0058	0.0058
P	0.0044	0.0037	0.0041
K	0.0038	0.0040	0.0039
Mn	0.0024	0.0029	0.0026
Cr	0.0020	0.0028	0.0024
Ni	0.0005	0.0004	0.0004

An exact value for regolith density was not readily found in the literature. Only a range of $\rho = 1$–2 g/cm^3 could be found (*114*, *115*). An average value of $\rho = 1.5$ g/cm^3 was used in the input file. This lack of a more specific value for the regolith density should have minimal impact on the results, assuming the regolith region of the model is sufficiently thick.

3.5.2 Atmosphere

Compared to Earth, the atmosphere of Mars is considerably thinner, which corresponds to much less shielding from GCRs. Records from the Viking missions (*40*) report an atmosphere mass thickness in the range of 16–22 g/cm^2 and a surface pressure in the range of 6–8 mbar. Additionally, NASA's Mars Fact Sheet (*116*) reports a surface pressure of 6.36 mbar, a surface density of ~ 0.020 kg/m^3, and that the atmosphere is largely comprised of CO_2.

NASA maintains the Mars-GRAM code (*117*), obtainable upon written request, which presents information on density, temperature, pressure, winds, and selected atmospheric constituents as a function of geographic position and time. The chemical composition of the Martian atmosphere, as reported by Mars-GRAM, appears in Table 3.7.

Table 3.7
Chemical Composition of the Martian Atmosphere

Compound	Volume [%]
CO_2	94.92
N_2	2.88
Ar	1.73
O_2	0.14
CO	0.10
H_2O	0.23

For the purposes of building an input file, the composition of the atmosphere needs to be known in terms of the mass fraction of each element. To that end, the percent volume values in Table 3.7 were converted to mass fractions via the molar mass of each component element. The mass fraction of each element in the Martian atmosphere appears in Table 3.8.

Table 3.8
Elemental Composition of the Martian Atmosphere

Element	Mass Fraction
O	0.6961
C	0.2608
N	0.0270
Ar	0.0160

In addition to elemental composition, it is important to know the physical properties of the Martian atmosphere, specifically density and pressure, as a function of altitude. Mars-GRAM was used to generate density and pressure profiles presented in 35 discrete layers at Gale Crater, the landing site (*2*) of MSL. This layering scheme approximates the Martian atmosphere with regions of decreasing density and pressure with increasing altitude. A layer-by-layer description of the density profile is presented in Table 3.9.

Table 3.9
Martian Atmosphere Layer Model

Layer No.	Height [km]	Density [g/cm^3]	Thickness [g/cm^2]
1	0.000E+00	1.992E-05	4.868E+00
2	2.444E+00	1.409E-05	7.080E+00
3	7.469E+00	9.028E-06	4.302E+00
4	1.223E+01	6.003E-06	2.902E+00
5	1.707E+01	3.901E-06	2.041E+00
6	2.230E+01	2.469E-06	1.201E+00
7	2.717E+01	1.528E-06	7.723E-01
8	3.222E+01	9.223E-07	4.713E-01
9	3.733E+01	5.390E-07	2.678E-01
10	4.230E+01	2.981E-07	1.503E-01
11	4.734E+01	1.672E-07	8.106E-02
12	5.219E+01	9.570E-08	4.646E-02
13	5.704E+01	5.494E-08	2.660E-02
14	6.189E+01	3.280E-08	1.640E-02
15	6.688E+01	2.021E-08	1.012E-02

Table 3.9 Continued

Layer No.	Height [km]	Density [g/cm^3]	Thickness [g/cm^2]
16	7.189E+01	1.090E-08	5.576E-03
17	7.701E+01	5.441E-09	2.705E-03
18	8.198E+01	2.636E-09	1.303E-03
19	8.692E+01	1.158E-09	5.923E-04
20	9.204E+01	5.019E-10	2.624E-04
21	9.727E+01	2.190E-10	1.093E-04
22	1.023E+02	9.845E-11	4.883E-05
23	1.072E+02	4.515E-11	2.276E-05
24	1.123E+02	2.126E-11	1.067E-05
25	1.173E+02	1.061E-11	5.443E-06
26	1.224E+02	5.558E-12	2.801E-06
27	1.275E+02	3.076E-12	1.544E-06
28	1.325E+02	1.797E-12	9.129E-07
29	1.376E+02	1.071E-12	5.398E-07
30	1.426E+02	5.959E-13	2.974E-07
31	1.476E+02	3.407E-13	1.707E-07
32	1.526E+02	1.992E-13	1.012E-07
33	1.577E+02	1.187E-13	6.018E-08
34	1.627E+02	7.199E-14	3.729E-08
35	1.679E+02	4.452E-14	2.226E-08

The top layer of the atmosphere is bounded by an additional boundary 5 km above the last boundary in Table 3.9 which corresponds to a height of 172.92 km above the surface. Combined, these 35 layers simulate an atmosphere thickness of

24.2 g/cm^2. This value is higher than the average atmosphere thickness due to the low elevation of Gale Crater, 3.788 km below mean radius (*117*). The Mars-GRAM code requires the user to specify a date, time, latitude, and longitude for the generation of an atmosphere model. As a result, the layer scheme presented in Table 3.9 is specific to latitude 4.49° S and longitude 137.42° E which corresponds to Gale Crater. Additionally, the time and date were set to 12:00 UTC on 1 March 2013 which corresponds to a time when MSL was in active operation. It should be noted that daily averages of atmospheric density and pressure were used so the fluctuations in these values that occur throughout each sol can largely be ignored.

3.5.3 Planet

With sufficient detail about the regolith and atmosphere known, an accurate model of the planet itself can be constructed. For the purposes of this study, Mars was assumed to be a sphere with a mean radius of 3396 km (*118*).

The model for the input file consists of concentric spheres, centered on the origin, used to describe the regolith region, surface, and atmosphere layers. The first two spheres of the model have radii of 3395.970 km and 3396 km which correspond to the bottom of the regolith and the surface of Mars, respectively. The region inside the bottom of the regolith was filled with a blackhole, the material used to terminate particle trajectories. The region between the bottom of the regolith layer and the surface layer was filled with the regolith material as detailed in Table 3.6 at a density of $\rho = 1.5$ g/cm^3. The mass thickness of this 30 m regolith region is 4500 g/cm^2.

The atmosphere regions were constructed by implementing spheres with radii equal to the planetary radius, 3396 km, plus the height of each layer from Table 3.9. The regions between the spheres were filled with the Martian atmosphere gas with the elemental composition from Table 3.8 and the corresponding density and

pressure from Table 3.9.

The last remaining sphere has a radius of 3396.001 km and represents an arbitrary boundary 1 m above the surface. It exists solely for the purpose of data analysis and does not influence particle transport. The region between the surface sphere and this boundary sphere as well as the region between the boundary sphere and the top of the first atmosphere layer are both filled with gas at the same density and pressure.

3.6 Simulation Overview

The complex nature of the radiation environment in space required the use of custom, non-default FLUKA sources. This was accomplished by modifying the default SOURCE subroutine to describe the specific problem. Afterwords, FLUKA was recompiled to generate a new executable utilizing the new SOURCE subroutine.

3.6.1 Sampling the Badhwar–O'Neill Spectra

The Badhwar–O'Neill (BO) model (*19–21*) was used to generate the GCR source incident on both the TEPC in free space and the upper atmosphere of Mars. Table 3.10 presents the results of a comparison between the Badhwar–O'Neill model and 1.0×10^8 iterations of the random-sampling technique described in Equation 2.75. The presented data are fractional abundances of each ion at a solar modulation parameter of $\Phi = 450$ MV.

Table 3.10
Badhwar–O'Neill Model Random Sample Test

	BO	Randomly			BO	Randomly	
z	Model	Sampled	Ratio	z	Model	Sampled	Ratio
1	8.976E-01	8.976E-01	1.0000	15	1.314E-05	1.341E-05	1.0203
2	9.350E-02	9.345E-02	0.9995	16	6.896E-05	6.978E-05	1.0119
3	3.365E-04	3.336E-04	0.9911	17	1.324E-05	1.333E-05	1.0067
4	2.096E-04	2.104E-04	1.0040	18	2.652E-05	2.626E-05	0.9902
5	6.978E-04	6.933E-04	0.9935	19	2.005E-05	1.948E-05	0.9715
6	2.560E-03	2.559E-03	0.9995	20	5.333E-05	5.337E-05	1.0008
7	6.784E-04	6.820E-04	1.0052	21	1.007E-05	1.011E-05	1.0042
8	2.422E-03	2.429E-03	1.0031	22	3.664E-05	3.728E-05	1.0175
9	4.365E-05	4.230E-05	0.9690	23	1.711E-05	1.771E-05	1.0351
10	3.709E-04	3.755E-04	1.0123	24	3.570E-05	3.591E-05	1.0058
11	7.465E-05	7.411E-05	0.9927	25	2.243E-05	2.197E-05	0.9795
12	4.863E-04	4.887E-04	1.0050	26	2.524E-04	2.542E-04	1.0071
13	7.998E-05	8.026E-05	1.0035	27	1.227E-06	1.050E-06	0.8561
14	3.660E-04	3.653E-04	0.9982	28	1.174E-05	1.120E-05	0.9539

As this comparison demonstrates, the random-sampling technique is properly sampling the Badhwar–O'Neill spectrum with small, expected variation present between the summed and randomly-sampled fractional abundances.

For each call of the SOURCE subroutine, once for each Monte Carlo iteration, the charge and kinetic energy of the primary ion is randomly sampled from the Badhwar–O'Neill model. The Badhwar–O'Neill model does not specify an atomic mass for any

of the ions present in the spectrum. As a result, the isotope with the highest natural abundance was chosen. The influence of the non-uniformity of isotopes on the results of this study is expected to be slight and quite negligible for the heavier ions.

3.6.2 Free Space

With the particle type and kinetic energy known, the starting coordinates (x, y, z) and direction cosines (u, v, w) were randomly sampled as well. SFLOOD is an auxiliary subroutine in FLUKA that returns in (x, y, z) a random position on the surface of a unit sphere, centered on the origin, and random cosines (u, v, w) distributed to generate a uniform and isotropic fluence inside the sphere. For the case of the TEPC in free space, (x, y, z) were multiplied by 0.8891 cm to generate a source sphere with a radius 1 μm greater than the TEPC.

This source was implemented in the SOURCE subroutine with the following code where SOURCERADIUS = 0.8891 cm.

```
CALL SFLOOD ( XXX, YYY, ZZZ, UXXX, VYYY, WZZZ )

XBEAM = XXX*SOURCERADIUS
YBEAM = YYY*SOURCERADIUS
ZBEAM = ZZZ*SOURCERADIUS

UBEAM = UXXX
VBEAM = VYYY
WBEAM = WZZZ
```

y distributions were obtained by using FLUKA's EVENTDAT command to record energy deposition on an event-by-event basis in the gas volume of the TEPC. In this manner, the FLUKA output is similar to the output of a multi-channel analyzer. A simple algorithm was implemented in a small C++ program to histogram the data and calculate $\bar{y}_{\mathrm{F}}$ and $\bar{y}_{\mathrm{D}}$. Additionally, the histogramming program calculated absorbed dose and dose equivalent along with average quality factor for each simulated

irradiation of the TEPC.

3.6.3 Mars: Part One, Downward Component

A considerably more complicated approach was required to determine y distributions and dosimetry quantities on the surface of Mars. To accomplish this task, a two-step method was chosen as the most efficient means of accurately characterizing the radiation environment on the surface of Mars. The most straightforward approach would be to model a TEPC, at proper dimensions, on the surface of Mars, at proper dimensions. While this approach is quite simple, it is prohibitively inefficient from a computational point of view. A 1.27 cm diameter TEPC is so small compared to Mars that an unreasonable run time would be necessary to generate any meaningful results with FLUKA.

The two-step method solves this problem. The first part of the two-step method involves modeling the planet and atmosphere at proper dimensions. The process of sampling the Badhwar–O'Neill spectrum to determine incident particle type and energy for the Mars model was identical to the method used for the TEPC in free space. The sampling of (x, y, z) and (u, v, w) was the same except (x, y, z) were multiplied by 3.59600001×10^8 cm which places the source sphere 1 cm above the top layer of the atmosphere.

The USERDUMP command was used to generate a separate output describing the type and kinetic energy of any particle that crossed the boundary 1 m above the surface. This was achieved by using a modified version of the MGDRAW subroutine, specifically, the BXDRAW command which is called at each boundary crossing.

Any particle crossing this boundary, directed towards the surface, initiated a call of BXDRAW which resulted in writing particle type, charge, mass, kinetic energy, (x, y, z), and (u, v, w) using the following code segment.

```
      WRITE(DOWNWARDOUTPUT,100) JTRACK,ICHRGE(JTRACK),
     & IBARCH(JTRACK),ETRACK-AM(JTRACK),XSCO,YSCO,ZSCO,
     & CXTRCK,CYTRCK,CZTRCK
  100 FORMAT(I4,I4,I4,E15.6,E18.10,E18.10,E18.10,E15.6,E15.6,E15.6)
```

The manual (*57*) notes that user-written scoring via MGDRAW must be avoided in all runs where biasing is present to avoid errors in properly accounting for particle weights. Because these simulations were fully-analogue, meaning no biasing was employed, recording particle weight was not necessary since they were all equal to 1.

To rule out the possibility of counting particles crossing this boundary multiple times, the regolith region, along with the atmosphere region between the surface and the boundary 1 m above the surface, was filled with a blackhole. Any particle that crossed the boundary 1 m above the surface would have its relevant descriptive information recorded via MGDRAW and then it would be terminated upon entering the adjacent region filled with the blackhole. In this manner, only the downward component of particle fluence 1 m above the surface can be considered.

In addition to the detailed information written to file for all particle types, particle type, charge, mass, and kinetic energy were written to five additional, separate files for use in part two of the two-step method.

The elemental ion component of the downward particle fluence was written to file with the following code.

```
IF(((JTRACK .GT. -7) .AND. (JTRACK .LT. -1)) .OR.
     & (JTRACK .EQ. 1)) THEN
WRITE(DOWNWARD_CP,"(I4,I4,I4,E15.6,F15.6)") JTRACK,
     & ICHRGE(JTRACK), IBARCH(JTRACK), ETRACK-AM(JTRACK)
END IF
```

The electron (including positron) component of the downward particle fluence was written to file with the following code.

```
IF((JTRACK .EQ. 3) .OR. (JTRACK .EQ. 4)) THEN
WRITE(DOWNWARD_EL,"(I4,I4,I4,E15.6,F15.6)") JTRACK,
     & ICHRGE(JTRACK), IBARCH(JTRACK), ETRACK-AM(JTRACK)
END IF
```

The photon component of the downward particle fluence was written to file with the following code.

```
IF(JTRACK .EQ. 7) THEN
WRITE(DOWNWARD_PH,"(I4,I4,I4,E15.6,F15.6)") JTRACK,
     & ICHRGE(JTRACK), IBARCH(JTRACK), ETRACK-AM(JTRACK)
END IF
```

The neutron component of the downward particle fluence was written to file with the following code.

```
IF(JTRACK .EQ. 8) THEN
WRITE(DOWNWARD_NE,"(I4,I4,I4,E15.6,F15.6)") JTRACK,
     & ICHRGE(JTRACK), IBARCH(JTRACK), ETRACK-AM(JTRACK)
END IF
```

Finally, the Boolean logic used to separate out the four previously mentioned categories of particles was inverted to include all other particles transported by FLUKA. This "other" component of the downward particle fluence was written to file with the following code.

```
IF(((JTRACK .GT. 8) .AND. (JTRACK .LT. 63)) .OR.
     & (JTRACK .EQ. 2) .OR. (JTRACK .EQ. 5) .OR. (JTRACK .EQ. 6)) THEN
WRITE(DOWNWARD_OT,"(I4,I4,I4,E15.6,F15.6)") JTRACK,
     & ICHRGE(JTRACK), IBARCH(JTRACK), ETRACK-AM(JTRACK)
END IF
```

To summarize, six separate outputs were generated from the downward component simulation. The first output was a full description of the particle spectrum at 1 m above the surface. This output included particle type, charge, mass, kinetic

energy, (x, y, z), and (u, v, w) and was later used as the input for the continuation of part one of the two-step method – producing the albedo component.

The other five outputs serve as the input for the downward component simulations of part two of the two-step method. These files contain the particle type and kinetic energy of the fluence spectrum at 1 m above the surface, sorted into five categories: elemental ions (specifically, ions from $z = 1$ to $z = 28$), electrons (and positrons), photons, neutrons, and all other particles transported by FLUKA. Sorting the downward spectrum in this manner allows for the generation of y distributions and dosimetry value for each particle type.

The electron component output includes *all* electrons and positrons produced in the atmosphere that reached the boundary 1 m above the surface. The BXDRAW entry of the MGDRAW subroutine does not distinguish between delta rays, photoelectrons, or electrons produced in nuclear fragmentation reactions.

3.6.4 Mars: Part One, Albedo Component

With the downward component properly accounted for, the next step was to address the albedo component. To accomplish this task, the assignment of the blackhole regions was reversed: the regolith region was filled with Martian regolith and the region between the surface and the boundary 1 m above the surface was filled with the Martian atmosphere at the appropriate density and pressure. The regions above the boundary 1 m above the surface, previously filled with the atmosphere layers, were filled with a blackhole.

Given that 99 is the unit number of the data file, the particle information written to a file in the simulation of the downward component of the particle fluence was read into a custom SOURCE subroutine with the following code.

```
READ (99, '(A)') LINE
READ (LINE, *) IJBEAM, IPROZ, IPROA, ENERGY, XBEAM, YBEAM, ZBEAM,
     & U, V, W
```

Additionally, the vector (u, v, w) was renormalized to avoid numerical precision errors with the following code.

```
UVW = SQRT(U**2 + V**2 + W**2)
UBEAM = U / UVW
VBEAM = V / UVW
WBEAM = W / UVW
```

With the particle information and the regolith and planet model up to 1 m above the surface in place, the albedo component of the particle fluence could be generated by transporting the particles from the USERDUMP data file through the last meter of atmosphere and into the regolith. Any particle that scattered back up to the boundary 1 m above the surface initiated a call to BXDRAW and its type, charge, mass, kinetic energy, and (x, y, z) and (u, v, w) vectors were written to file with the following code.

```
      WRITE(ALBEDOOUTPUT,100) JTRACK,ICHRGE(JTRACK),
     & IBARCH(JTRACK),ETRACK-AM(JTRACK),XSCO,YSCO,ZSCO,
     & CXTRCK,CYTRCK,CZTRCK
100 FORMAT(I4,I4,I4,E15.6,E18.10,E18.10,E18.10,E15.6,E15.6,E15.6)
```

In addition, particle type, charge, mass, and kinetic energy were written to five additional, separate files for use in part two of the two-step method.

The elemental ion component of the albedo particle fluence was written to file with the following code.

```
IF(((JTRACK .GT. -7) .AND. (JTRACK .LT. -1)) .OR.
     & (JTRACK .EQ. 1)) THEN
WRITE(ALBEDO_CP,"(I4,I4,I4,E15.6,F15.6)") JTRACK,
     & ICHRGE(JTRACK), IBARCH(JTRACK), ETRACK-AM(JTRACK)
END IF
```

The electron (including positron) component of the albedo particle fluence was written to file with the following code.

```
IF((JTRACK .EQ. 3) .OR. (JTRACK .EQ. 4)) THEN
WRITE(ALBEDO_EL,"(I4,I4,I4,E15.6,F15.6)") JTRACK,
     & ICHRGE(JTRACK), IBARCH(JTRACK), ETRACK-AM(JTRACK)
END IF
```

The photon component of the albedo particle fluence was written to file with the following code.

```
IF(JTRACK .EQ. 7) THEN
WRITE(ALBEDO_PH,"(I4,I4,I4,E15.6,F15.6)") JTRACK,
     & ICHRGE(JTRACK), IBARCH(JTRACK), ETRACK-AM(JTRACK)
END IF
```

The neutron component of the albedo particle fluence was written to file with the following code.

```
IF(JTRACK .EQ. 8) THEN
WRITE(ALBEDO_NE,"(I4,I4,I4,E15.6,F15.6)") JTRACK,
     & ICHRGE(JTRACK), IBARCH(JTRACK), ETRACK-AM(JTRACK)
END IF
```

Finally, the "other" component of the albedo particle fluence was written to file with the following code.

```
IF(((JTRACK .GT. 8) .AND. (JTRACK .LT. 63)) .OR.
     & (JTRACK .EQ. 2) .OR. (JTRACK .EQ. 5) .OR. (JTRACK .EQ. 6)) THEN
WRITE(ALBEDO_OT,"(I4,I4,I4,E15.6,F15.6)") JTRACK,
     & ICHRGE(JTRACK), IBARCH(JTRACK), ETRACK-AM(JTRACK)
END IF
```

This is the same methodology used to record the downward component of the particle fluence for part two of the two-step method.

3.6.5 Mars: Part Two

The second part of the two-step method is very similar to the free space simulation. The geometry and materials for the free space and part two simulations are identical. The only difference is the source: the free space simulation sampled the Badhwar–O'Neill spectrum while the part two simulations read particle type and kinetic energy from the output files from part one. That is, the free space simulation used the Badhwar–O'Neill model as the source while part two simulations use a modified spectrum created by passing the Badhwar–O'Neill model through the Martian atmosphere.

The elemental ion, electron, photon, neutron, and "other" responses were produced for both the downward and albedo components resulting in ten unique simulations. (Characterization of a TEPC in free space required only one simulation.) Each part two simulation implemented a simple Fortran READ statement to obtain particle type and energy from the information that was written to file in part one.

```
READ (99, '(A)') LINE
READ (LINE, *) IJBEAM, IPROZ, IPROA, ENERGY
```

SFLOOD was again used to determine (x, y, z) and (u, v, w) for the TEPC and (x, y, z) were again multiplied by SOURCERADIUS = 0.8891 cm.

3.7 Processing the Results

The EVENTDAT command used for the TEPC simulations records energy deposition on an event-by-event basis for each region specified in the input file. A C++ program was used to extract and histogram all non-zero energy deposition values

recorded for the TEPC gas volume. These data were used to generate y distributions; $\bar{y}_{\mathrm{F}}$ and $\bar{y}_{\mathrm{D}}$ were calculated according to Equations 2.49 and 2.51, respectively.

A linear extrapolation in the $f(y)$ distribution was performed from 0.3 keV/μm down to 0.1 keV/μm. This was done to mimic the data processing technique utilized with experimental microdosimetry data. A more detailed explanation of the linear extrapolation technique is presented in Appendix A.

To obtain a proper assessment of absorbed dose and dose equivalent rates the irradiation time must be known. Such an assessment can be made from simulation data according to

$$t = \frac{N}{\phi \Omega A} \tag{3.1}$$

where N is the number of primary particle histories, ϕ is the incident particle fluence rate, Ω is the solid angle, and A is the projected area of the region of interest.

3.7.1 TEPC Response

Equation 3.1 can be modified for the specific case of the TEPC in free space. In this case, the free space irradiation time can be found according to

$$t_{\mathrm{FS}} = \frac{N}{\phi_{\mathrm{FS}}\, \Omega_{\mathrm{FS}}\, A_{\mathrm{TEPC}}} \tag{3.2}$$

where N is the number of primary particle histories, ϕ_{FS} is the integral fluence rate from the Badhwar–O'Neill model, A_{TEPC} is the projected area of the TEPC, and, because the GCR spectrum is assumed to be isotropic in free space, $\Omega_{\mathrm{FS}} = 4\pi$ sr.

The integral fluence rate of the Badhwar–O'Neill spectrum at $\Phi = 450$ MV is $\phi = 3.37 \times 10^{-1}$ [cm^2 s sr]$^{-1}$. Given this fluence rate, and the projected area of the

TEPC, $A_{\mathrm{TEPC}} = \pi(0.889\ \mathrm{cm})^2 = 2.48\ \mathrm{cm}^2$, the free space irradiation time is

$$t_{\mathrm{FS}} = \frac{N}{(0.337\,[\mathrm{cm}^2\ \mathrm{s}\ \mathrm{sr}]^{-1})\,(4\pi\ \mathrm{sr})\,(2.48\,\mathrm{cm}^2)} = \frac{N}{10.5}\ \ [\mathrm{s}]. \tag{3.3}$$

Equation 3.3 allows for a quick calculation of irradiation time as a function of the number of histories simulated in FLUKA. Since all simulations in the present study were for 1.0×10^8 primary particle histories, the corresponding free space irradiation time is 0.301 y.

Determining the irradiation time is more complicated for the TEPC on the surface of Mars because of the methodology employed – every particle simulated to reach the surface of Mars was later treated as incident on the TEPC.

Equation 3.1 can be modified for the specific case of the TEPC on the surface of Mars. In this case, the surface of Mars irradiation time can be found according to

$$t_{\mathrm{M}} = \frac{N}{\phi_{\mathrm{FS}}\Omega_{\mathrm{M}}A_{\mathrm{Atmo}}} \tag{3.4}$$

where N is the number of primary particle histories, ϕ_{FS} is the integral fluence rate from the Badhwar–O'Neill model, A_{Atmo} is the projected area of the top of the atmosphere of Mars, the location of the GCR source for the surface of Mars simulation, and, because the planet acts as a shield against half of the incident GCRs, $\Omega_{\mathrm{M}} = 2\pi$ sr.

Given that $\phi_{\mathrm{FS}} = 3.37 \times 10^{-1}\ [\mathrm{cm}^2\ \mathrm{s}\ \mathrm{sr}]^{-1}$ and $A_{\mathrm{Atmo}} = \pi(3.56892 \times 10^8\ \mathrm{cm})^2 = 4.00 \times 10^{17}\ \mathrm{cm}^2$, Equation 3.4 becomes

$$t_{\mathrm{M}} = \frac{N}{(0.337\,[\mathrm{cm}^2\ \mathrm{s}\ \mathrm{sr}]^{-1})\,(2\pi\ \mathrm{sr})\,(4.00 \times 10^{17}\,\mathrm{cm}^2)} = \frac{N}{8.48 \times 10^{17}}\ \ [\mathrm{s}] \tag{3.5}$$

which presents the surface of Mars irradiation time as a function of N. Given that

$N = 1.0 \times 10^8$, the surface of Mars irradiation time is $t_{\mathrm{M}} = 3.74 \times 10^{-18}$ y. This unnormalized value of t_{M} does not consider the treatment of every particle that reached the surface of Mars as incident on the TEPC. Doing so requires the introduction of the normalization factor $\frac{A_{\mathrm{TEPC}}}{A_{\mathrm{Surface}}}$ where A_{Surface} is the projected area of the boundary 1 m above the surface and is equal to $\pi(3.396001 \times 10^8 \text{ cm})^2 = 3.62 \times 10^{17} \text{ cm}^2$. Dividing Equation 3.5 by $\frac{A_{\mathrm{TEPC}}}{A_{\mathrm{Surface}}}$ gives

$$t_{\mathrm{M}} = \frac{N}{8.48 \times 10^{17}} \frac{A_{\mathrm{Surface}}}{A_{\mathrm{TEPC}}} \text{ [s]} = \frac{N}{8.48 \times 10^{17}} \frac{3.62 \times 10^{17} \text{ cm}^2}{2.48 \text{ cm}^2} \text{ [s]} = \frac{N}{5.81} \text{ [s]}. \quad (3.6)$$

Since $N = 1.0 \times 10^8$, the corresponding normalized surface of Mars irradiation time is 0.545 y. To test this normalization technique, a comparison was made between the dose rate of a TEPC in free space and on the surface of Mars *with no atmosphere or regolith present*. Elimination of the influence of the atmosphere and regolith on the radiation environment should result in a 50% reduction of the absorbed dose rate from planetary shielding alone. With the atmosphere and regolith both replaced with a vacuum, the surface of Mars dose rate was found to be 49.9% of the free space dose rate in this simple test, confirming the normalization technique.

In addition to generating the $f(y)$ and $d(y)$ distributions and the $\bar{y}_{\mathrm{F}}$ and $\bar{y}_{\mathrm{D}}$ values, the C++ program also calculated the integral absorbed dose D and dose equivalent H for each simulated irradiation. From these values, the absorbed dose rate and dose equivalent rate in the TEPC were found according to

$$\dot{D} = \frac{D}{t} \quad (3.7)$$

and

$$\dot{H} = \frac{H}{t}, \quad (3.8)$$

respectively, where D is the integral absorbed dose and H is the integral dose equivalent from the histogramming program and t is the irradiation time from Equation 3.3 for the free space scenario or Equation 3.6 for the surface of Mars scenario. It should be noted that absorbed dose and dose equivalent rates are normalized to Earth years, not Martian years.

The average quality factor of an irradiation was found according to

$$\bar{Q} = \frac{H}{D} = \frac{\dot{H}}{\dot{D}} \tag{3.9}$$

which is simply a restatement of Equation 2.38.

3.7.2 Differential Energy Spectra

Equation 3.1 can also be used for the normalization of the differential energy spectra (DES) produced from the combined downward and albedo elemental ions outputs from part one. The corresponding irradiation time can be found according to

$$t_{\mathrm{DES}} = \frac{N}{\phi_{\mathrm{FS}}\,\Omega_{\mathrm{FS}}\,A_{\mathrm{Atmo}}}. \tag{3.10}$$

Likewise, Equation 3.1 can be rewritten for the surface of Mars according to

$$\phi_{\mathrm{Surface}} = \frac{N_{\mathrm{Surface}}}{A_{\mathrm{Surface}}\,\Omega_{\mathrm{M}}\,t_{\mathrm{DES}}} \tag{3.11}$$

where ϕ_{Surface} is the particle fluence rate 1 m above the surface, N_{Surface} is the number of particles that cross the boundary 1 m above the surface (written to file in part one of the two-step method), A_{Surface} is the projected area of the boundary 1 m above the surface, and t_{DES} is the irradiation time from Equation 3.10. Substituting Equation

3.10 into Equation 3.11 gives

$$\phi_{\text{Surface}} = \frac{N_{\text{Surface}}}{A_{\text{Surface}}\,\Omega_{\text{M}}\left(\frac{N}{\phi_{\text{FS}}\,\Omega_{\text{FS}}\,A_{\text{Atmo}}}\right)} \tag{3.12}$$

and, with $A_{\text{Surface}} = 3.62 \times 10^{17}$ cm^2, $\Omega_{\text{M}} = 2\pi$ sr, $N = 1.0 \times 10^8$, $\Omega_{\text{FS}} = 2\pi$ sr, and $A_{\text{Atmo}} = 4.00 \times 10^{17}$ cm^2,

$$\phi_{\text{Surface}} = N_{\text{Surface}}\left(7.45 \times 10^{-5}\,[\text{m}^2\ \text{s sr}]^{-1}\right) \tag{3.13}$$

which gives the fluence rate 1 m above the surface as a function of the number of particles incident on the surface.

The quantity 7.45×10^{-5} [m^2 s sr]$^{-1}$ from Equation 3.13 is employed to normalize the number of elemental ions incident on the surface N_{Surface} in a given energy bin to area, time, and solid angle. This is equivalent to normalizing with an exposure factor $F = A\Omega t$. For comparison to the Badhwar–O'Neill model, the differential energy spectra must undergo a further normalization of dividing by bin width, in units of MeV/n, to yield a final fluence rate with units of [m^2 s sr MeV/n]$^{-1}$.

3.7.3 Frequency, Dose, and Dose Equivalent Fractions

The combined downward and albedo differential energy spectra were used to generate the fractional contribution to frequency, dose, and dose equivalent of each elemental ion on the surface of Mars.

The frequency distribution was obtained by integrating the differential energy spectrum for each elemental ion. The dose distribution was obtained by integrating the differential energy spectrum of each elemental ion with each bin weighted by the ion- and kinetic-energy-specific stopping power. Finally, the dose equivalent distribution was obtained by integrating the differential energy spectrum of each

elemental ion with each bin weighted by the ion- and kinetic-energy-specific stopping power and the stopping-power-specific quality factor. All three distributions were normalized to unity.

4. RESULTS AND DISCUSSION

The lineal energy distributions presented in this chapter are condensed to six figures to allow for a relatively easy comparison between various components of the particle fluence spectrum in free space and on the surface of Mars. Additionally, and for the sake of brevity, the differential energy spectra presented in this chapter represent a small sampling. The entire data set for both the lineal energy distributions and the differential energy spectra are presented in a series of appendices as detailed in Table 4.1.

Table 4.1
Description of Appendices

Description	Appendix
Free space y distribution and tabulated data	B
Surface of Mars y distributions and tabulated data	C
Surface of Mars downward y distributions and tabulated data	D
Surface of Mars albedo y distributions and tabulated data	E
Surface of Mars differential energy spectra figures	F
Surface of Mars differential energy spectra tabulated data	G
Surface of Mars neutron spectra figures and tabulated data	H

Appendix B contains the lineal energy distribution for a TEPC in free space along with the tabulated values for $yd(y)$ as a function of y used to generate the figure. Likewise, Appendices C, D, and E contain the lineal energy distributions along with

the corresponding tabulated data for a TEPC on the surface of Mars, surface of Mars downward component, and surface of Mars albedo component, respectively.

It is not uncommon for the values of both $d(y)$ and y of microdosimetric spectra to span many orders of magnitude. Because of this, plotting $d(y)$ as a function of y on a linear scale rarely provides any meaningful information. To address this problem, the lineal energy distributions in the present study are presented as $yd(y)$ as a function of y on a semi-log axis. In this manner, regarded as the standard representation of microdosimetric spectra, the area between any two values of y indicates the dose delivered in that range (*104*). Therefore, a quick assessment can be made of the relative contribution to the dose from a specific value of y. It should be noted that each $yd(y)$ vs. y distribution has been normalized to unit area, not dose. Normalizing to unit area allows for an easy comparison between y distributions from different simulated irradiations and/or particle types.

No distinction has been made on the source of electrons for scoring particles outside the TEPC. Any electron, regardless of its origin (including delta rays produced in the atmosphere) was sorted into the electron file. Furthermore, any mention of particle type in regards to y distributions or dosimetry values describes particles present at the boundary 1 m above the surface and, therefore, incident on the detector. So, "elemental ions" describes elemental-ion-induced events and "electrons" describes electron-induced events. Delta rays produced *in the detector* are included in "elemental ions."

Appendix F contains the differential energy spectra for elemental ions with $z = 1$ to $z = 28$. Appendix G contains the tabulated data used to generate the figures in Appendix F. Finally, Appendix H contains the downward and albedo neutron spectra along with the corresponding tabulated data.

4.1 Free Space

The first data set of interest is the response of the TEPC in free space. These data were generated by simulating the response of a TEPC exposed to the Badhwar–O'Neill spectrum at $\Phi = 450$ MV. The TEPC response includes lineal energy distributions and dosimetry values. Additionally, knowledge of the differential energy spectra, obtained from the Badhwar–O'Neill model, allowed for the calculation of the fractional contribution to frequency, dose, and dose equivalent of each elemental ion from $z = 1$ to $z = 28$. No shielding was present.

4.1.1 Lineal Energy Distribution

The y distribution for the TEPC in free space appears in Figure 4.1.

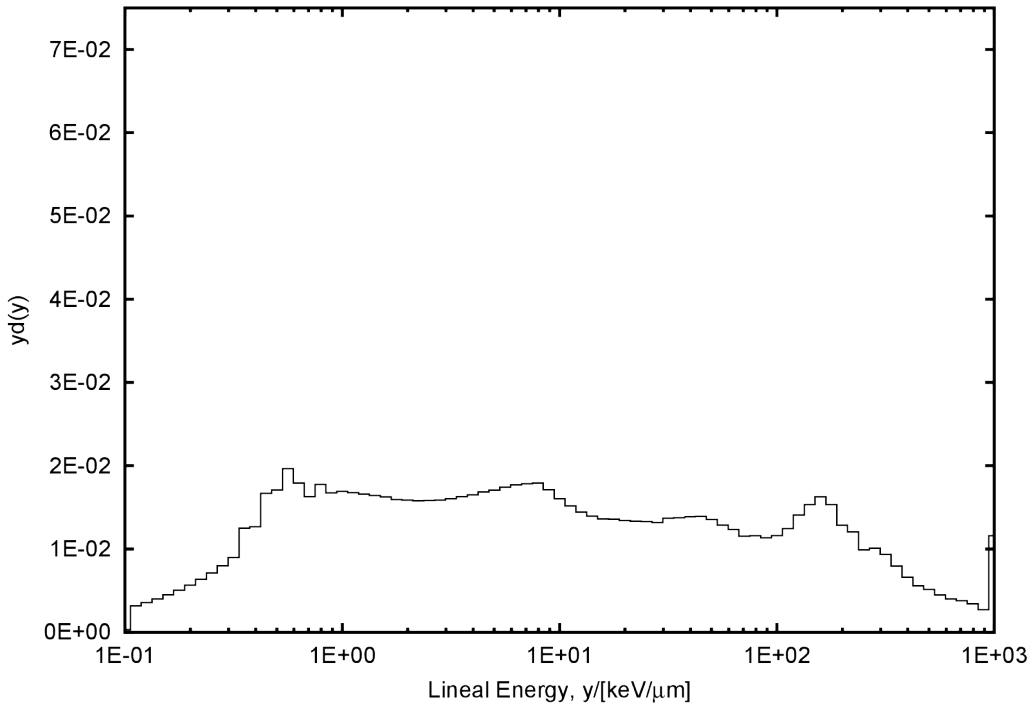

Figure 4.1. Lineal energy distribution for all elemental ions in free space. The source for this simulation was the Badhwar–O'Neill model at $\Phi = 450$ MV. This distribution has been normalized to unit area.

The peak at 0.5 keV/μm is typical of minimally ionizing electrons and protons and the characteristic shoulder at approximately 10 keV/μm indicates the presence of electrons at their maximum stopping power. A point of interest is the peak between 100 keV/μm and 200 keV/μm which corresponds to the influence of Fe ions. For the most part, the y distribution in Figure 4.1 is rather flat across value of y ranging from 0.1 keV/μm to 1000 keV/μm meaning the dose to the gas volume was delivered by a wide range of lineal energies.

The last bin represents all events greater than or equal to 1000 keV/μm.

4.1.2 Dosimetry

The dosimetry values recorded from the unshielded TEPC in free space appear in Table 4.2. The values are normalized to Earth years, not Martian years. A value of $\dot{H} = 1.0$ Sv/y is comparable to the range 0.7 Sv/y to 1.3 Sv/y found in the literature (*25*, *26*, *28*). The influence of heavy ions, specifically Fe, is seen in the large value of $\bar{y}_{\mathrm{D}}$, relative to $\bar{y}_{\mathrm{F}}$, and the high average quality factor.

Table 4.2
TEPC Dosimetry in Free Space

	$\dot{D}$ [Gy/y]	$\dot{H}$ [Sv/y]	$\bar{Q}$	$\bar{y}_{\mathrm{F}}$ [keV/μm]	$\bar{y}_{\mathrm{D}}$ [keV/μm]
Free Space	1.5E-1	1.0E0	6.9	1.4	71.1

Since a solar modulation parameter of $\Phi = 450$ MV was chosen, representing a deep solar minimum, these free space dosimetry values represent a worst-case scenario. Any increase in the solar modulation parameter will result in a decrease in

the absorbed dose rate.

Furthermore, the addition of shielding material will influence these dosimetry rates as well. The exact influence, however, cannot be easily predicted due to the complexities involved. As the amount of shielding increases, the thin-target approximation breaks down and extrapolating dose rates from thin to thick targets becomes unreliable. Because of this, the decision was made for the present study to simulate the response of a TEPC in unshielded free space with the acknowledgment that properly analyzing the influence of shielding requires detailed knowledge of the proposed shielding configuration. In this manner, the present study can serve as a starting point for future studies investigating shielding designs for various space radiation applications.

4.1.3 Frequency, Dose, and Dose Equivalent Distributions

The fractional contributions to frequency, dose, and dose equivalent for each ion in free space were presented in Table 1.1 and plotted in Figure 1.1. The frequency, dose, and dose equivalent distributions are obtained by integrating the fluence rate of each ion, with each bin weighted with its corresponding stopping power to produce the dose distribution, and with each bin weighted with the corresponding stopping power and quality factor to produce the dose equivalent distribution. The dose equivalent distribution is comparable to those found in the literature (*15*, *27*, *55*). Such a favorable comparison serves as a benchmark for comparison to frequency, dose, and dose equivalent distributions on the surface of Mars.

While representing 90% of the total fluence and 39% of the dose, H ions account for just over 6% of the dose equivalent. For comparison, while Fe ions comprise approximately 0.03% of the total GCR spectrum, they are responsible for nearly 9% of the dose and 28% of the dose equivalent. For this reason, and as previously stated,

Fe ions are of interest in unshielded free space.

4.2 Surface of Mars

The first data set of interest is the response of the TEPC on the surface of Mars. These data were generated by recording the response of the TEPC 1 m above the surface with the Badhwar–O'Neill spectrum at $\Phi = 450$ MV incident on the top of the atmosphere. The TEPC response includes lineal energy distributions and dosimetry values for the downward component, albedo component, and combined (downward plus albedo) component of the particle fluence at 1 m above the surface.

Additionally, knowledge of the particle fluence spectrum, obtained from the USERDUMP files, allowed for the generation of differential energy spectra at 1 m above the surface. From these differential energy spectra the fractional contributions to frequency, dose, and dose equivalent of each elemental ion from $z = 1$ to $z = 28$ were calculated.

For the same reasons as the free space simulation, no shielding was present.

4.2.1 Lineal Energy Distributions

Lineal energy distributions for the downward component of the particle fluence on the surface of Mars appear in Figure 4.2. This figure includes y distributions for elemental ions (from $z = 1$ to $z = 28$), electrons (plus positrons), photons, neutrons, and all other particles. The "other" category includes every other particle transported by FLUKA except for those included in the previous four categories. These "other" particles were included for completeness and constitute a small fraction of the total dose and dose equivalent rates.

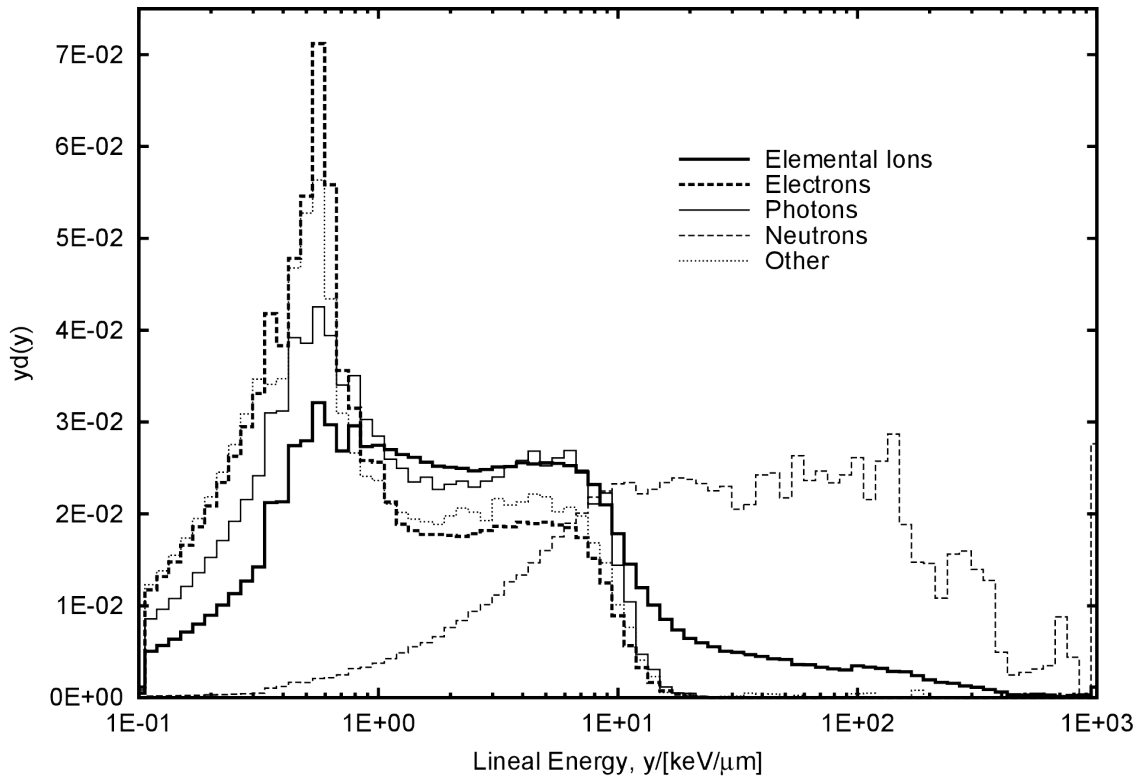

Figure 4.2. Lineal energy distributions for downward elemental ions ($z = 1$ to $z = 28$), electrons (including positrons), photons, neutrons, and all other particles transported by FLUKA on the surface of Mars. Each distribution has been normalized to unit area.

The photon and electron y distributions both have a $y_{\max}$ equal to ≈ 15 keV/μm which is characteristic of the maximum stopping power of an electron (*56*, *104*). The peak in both spectra at approximately 0.5 keV/μm is caused by higher energy (> 100 keV) minimally ionizing electrons.

The majority of the kinetic energy transfer to biological tissue from neutrons is via recoil protons (*56*) where larger values of y indicate a lower neutron energy and vice versa. The peak at 150 keV/μm is the characteristic "proton drop point" which corresponds to the maximum energy deposition possible given that protons have a

maximum L_∞ of $\approx$ 100 keV/μm and $y_{\max} = 3L_\infty/2$ for a spherical site. Events with y less than the proton drop point are produced from recoil protons from higher energy neutrons. Additionally, events with y greater than the proton drop point are evidence of neutron-induced heavy ion recoils.

For values of y less than $\sim$ 10 keV/μm, the elemental ion y distribution appears largely unchanged compared to the free space y distribution. The same cannot be said, however, for values of y greater than 10 keV/μm. The addition of the Martian atmosphere greatly reduced the influence of these events on the total dose rate. Such a change can be expected to result in a significant reduction in $\bar{Q}$ as compared to free space.

Finally, the y distribution for "other" particles, dominated by muons and pions, is quite similar to the electron and photon y distributions.

Lineal energy distributions for the albedo component of the particle fluence on the surface of Mars appear in Figure 4.3.

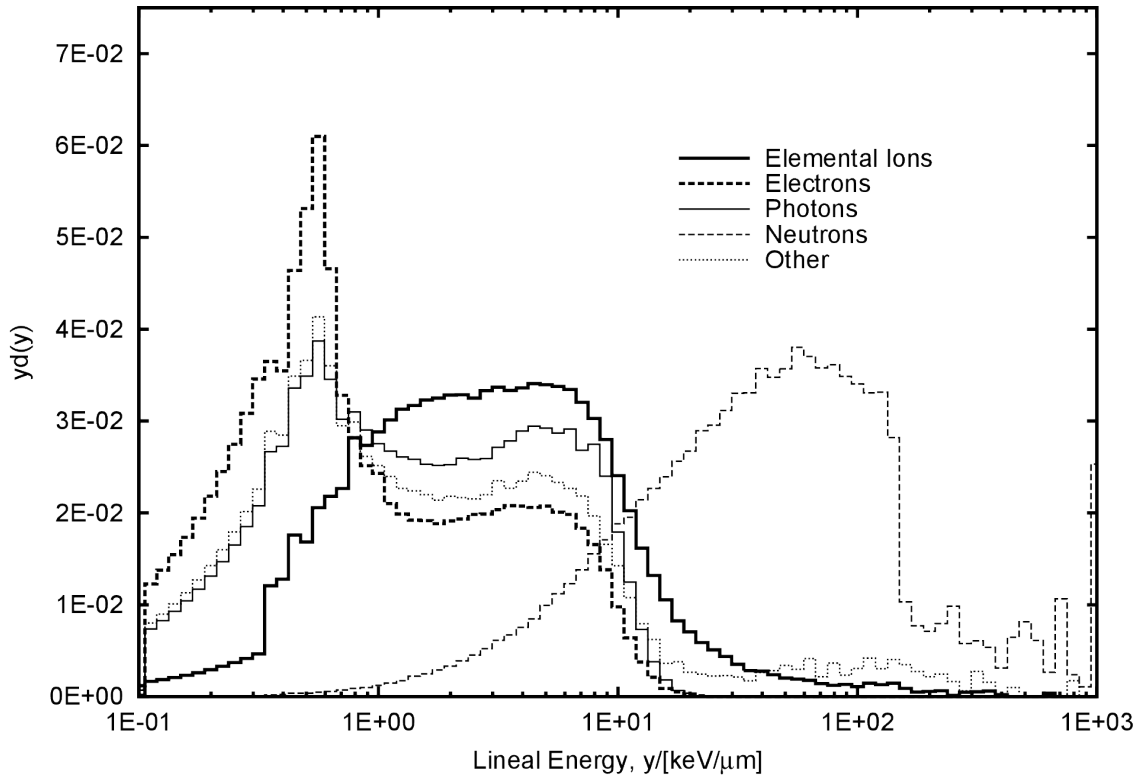

Figure 4.3. Lineal energy distributions for albedo elemental ions ($z = 1$ to $z = 28$), electrons (including positrons), photons, neutrons, and all other particles transported by FLUKA on the surface of Mars. Each distribution has been normalized to unit area.

Little difference is seen in the albedo electron, photon, and "other" y distributions as compared to the same downward distributions. The narrower peak in the albedo neutron y distribution indicates the dose is dominated by lower energy neutrons as compared to the downward neutron y distribution. Albedo elemental ions are almost exclusively protons, comprising 99.8% of the particle spectrum, with ions of $z > 2$

being negligible. Such a simple particle spectrum, relative to the downward elemental ion spectrum which contains ions from $z = 1$ to $z = 28$, leads to the more uniform distribution.

Lineal energy distributions for the combined (downward plus albedo) particle fluence on the surface of Mars appear in Figure 4.4.

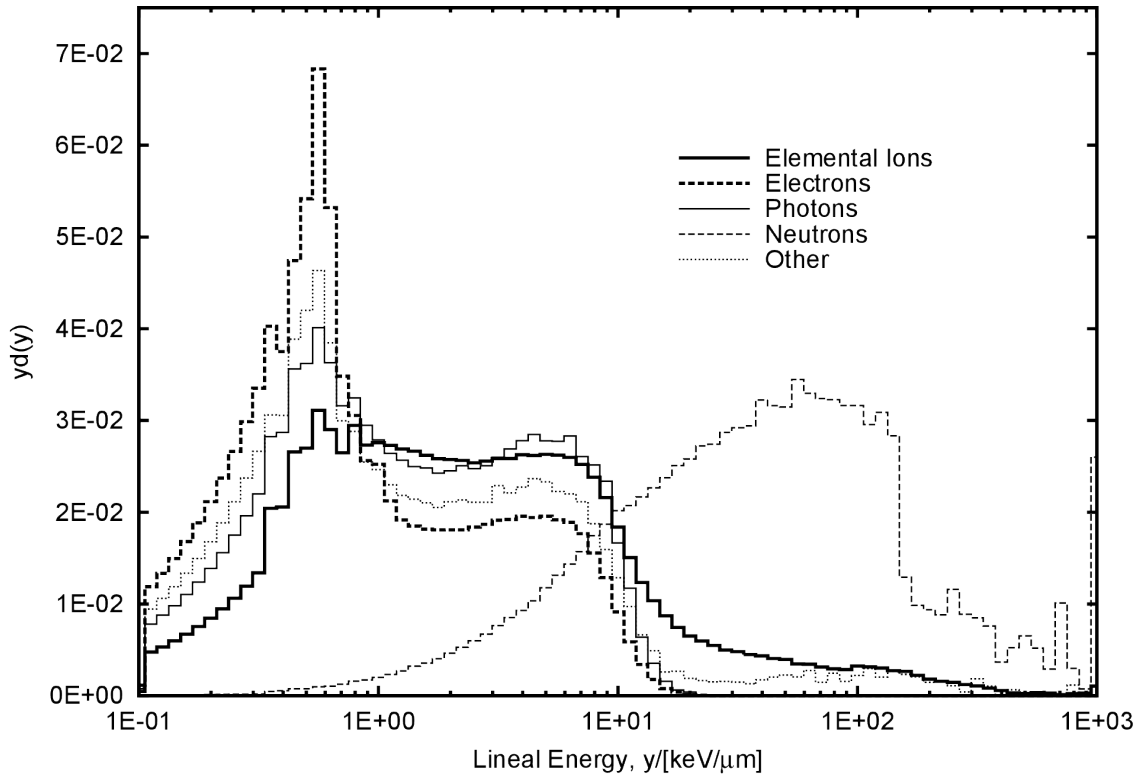

Figure 4.4. Lineal energy distributions for combined (downward plus albedo) elemental ions ($z = 1$ to $z = 28$), electrons (including positrons), photons, neutrons, and all other particles transported by FLUKA on the surface of Mars. Each distribution has been normalized to unit area.

Each distribution in Figure 4.4 represents a dose-weighted sum of corresponding downward and albedo distributions. The negligible difference between the downward

and combined elemental ion y distributions is evidence that albedo elemental ions make a small contribution to the total elemental ion dose. A similar statement, yet to a lesser degree, can be made regarding the relationship between downward and albedo neutrons with albedo neutrons resulting in the majority of the neutron dose.

A comparison of the downward, albedo, and combined (downward plus albedo) y distributions appears in Figure 4.5.

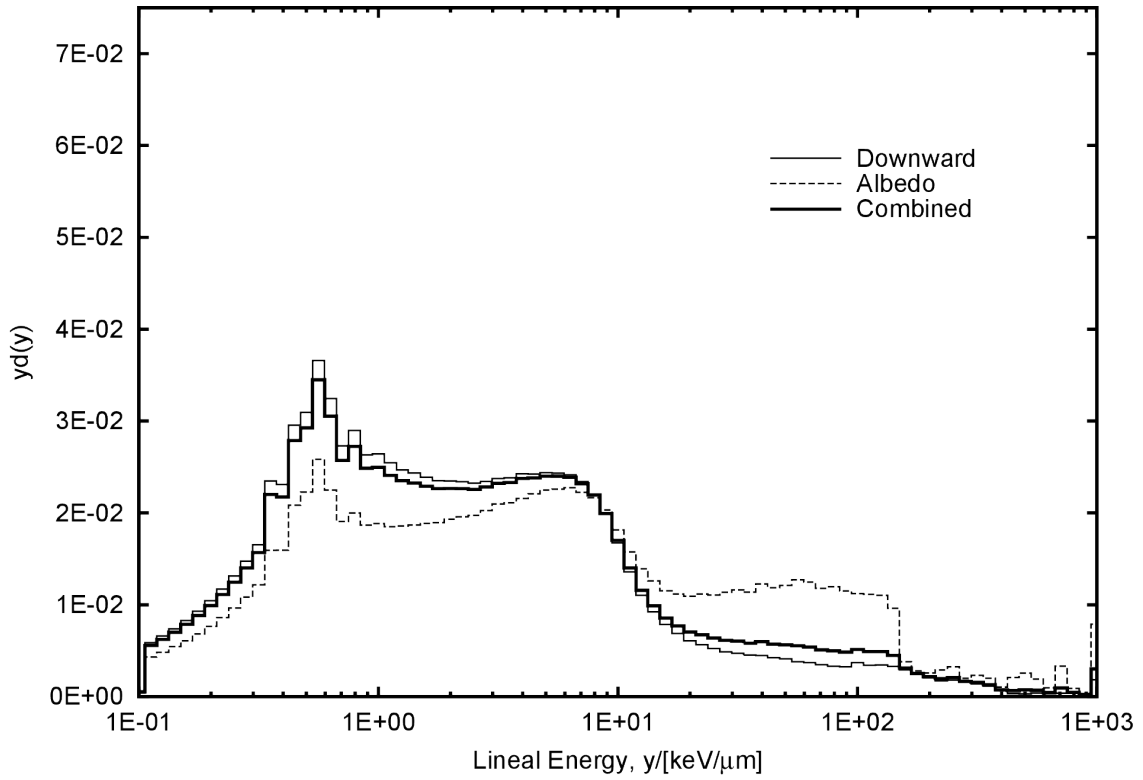

Figure 4.5. Lineal energy distributions for the downward, albedo, and combined (downward plus albedo) components of the particle fluence on the surface of Mars. Each distribution includes all particles transported by FLUKA and is normalized to unit area.

The downward distribution is a dose-weighted sum of the five y distributions

from Figure 4.2. Likewise, the albedo distribution is a dose-weighted sum of the five y distributions from Figure 4.3 and the combined distribution is a dose-weighted sum of the downward and albedo distributions. The combined distribution is what a TEPC on the surface of Mars would measure, assuming no directional shielding was in place to distinguish between the downward and albedo components.

Figure 4.5 demonstrates that while the majority of the dose is delivered with events less than 10 keV/μm, and therefore, with $Q = 1$, events with $y > 10$ keV/μm, and, therefore, with $Q > 1$, still occur and represent a non-negligible contribution to the total dose.

4.2.2 Dosimetry

The dosimetry values for a TEPC on the surface of Mars appear in Table 4.3. Using FLUKA, or, in theory, any Monte Carlo code, allows for the classification of the absorbed dose and dose equivalent rate by particle type. It is recognized that no such classification can be made from experimental TEPC data. That said, this level of detail can be helpful for designing shielding or interpreting TEPC measurements from the surface of Mars, should they exist sometime in the future.

Additionally, dose rate and dose equivalent rate fractions represent the dose rate or dose equivalent rate for the specific particle divided by the combined (albedo plus downward), all-particle dose or dose equivalent rate.

Table 4.3
TEPC Dosimetry by Particle Type on the Surface of Mars

	$\dot{D}$ [Gy/y]	$\dot{D}$ [fraction]	$\dot{H}$ [Sv/y]	$\dot{H}$ [fraction]	$\bar{Q}$	$\bar{y}_{\mathrm{F}}$ [keV/μm]	$\bar{y}_{\mathrm{D}}$ [keV/μm]
Downward							
Elemental Ions[(1)]	4.2E-2	66.0%	9.9E-2	53.8%	2.3	0.9	12.7
Electrons[(2)]	6.8E-3	10.6%	6.9E-3	3.7%	1.0	0.5	1.8
Photons	4.2E-4	0.7%	4.3E-4	0.2%	1.0	0.6	2.4
Neutrons	1.7E-3	2.6%	1.8E-2	9.6%	10.6	7.3	104.9
Other[(3)]	5.4E-4	0.8%	5.7E-4	0.3%	1.1	0.5	2.3
Total	5.2E-2	80.7%	1.3E-1	67.7%	2.4	0.8	14.1
Albedo							
Elemental Ions[(1)]	4.1E-3	6.3%	6.8E-3	3.7%	1.7	1.4	7.3
Electrons[(2)]	2.7E-3	4.2%	2.7E-3	1.5%	1.0	0.5	1.9
Photons	7.3E-4	1.1%	7.5E-4	0.4%	1.0	0.7	2.7
Neutrons	3.9E-3	6.0%	4.7E-2	25.4%	12.2	14.6	103.8
Other[(3)]	1.1E-3	1.7%	2.4E-3	1.3%	2.2	0.7	11.8
Total	1.2E-2	19.3%	6.0E-2	32.3%	4.8	1.1	36.3
Total	6.4E-2	100.0%	1.8E-1	100.0%	2.9	0.9	18.4

The values presented in Table 4.3 reveal that, as expected, downward elemental ions dominate the dose and dose equivalent. Despite this, the shielding offered by the Martian atmosphere resulted in a relatively low $\bar{y}_{\mathrm{D}}$ and $\bar{Q}$.

[(1)]Includes ions from $z = 1$ to $z = 28$.
[(2)]Includes both electrons and positrons.
[(3)]Includes muons, pions, kaons, antiprotons, and antineutrons.

The downward electron dose rate represents 11% of the total dose rate from all particles. This value can be expected to become quite negligible with the addition of any significant amount of shielding. The photon and "other" components offer an insignificant contribution to the overall dose and dose equivalent. Taken together, downward particles are responsible for 81% of the total dose and 68% of the total dose equivalent.

Albedo elemental ions (almost exclusively protons), electrons, photons, and "other" particles account for 13% of the total dose yet only 7% of the total dose equivalent. Of these four particle categories, the "other" component has the highest quality factor with $\bar{Q} = 2.2$. By contrast, albedo neutrons, with $\bar{y}_{\mathrm{D}} = 103.8$, have an average quality factor of $\bar{Q} = 12.2$.

Accounting for 35% of the total dose equivalent, neutrons are of significant interest from a radiation protection point of view with such a high $\bar{y}_{\mathrm{D}}$ and $\bar{Q}$.

4.2.3 Frequency, Dose, and Dose Equivalent Distributions

The generation of differential energy spectra on the surface of Mars (compared to the free space spectra in Section 4.3.3) allowed for the calculation of the fractional contributions to frequency, dose, and dose equivalent for each elemental ion as presented in Table 4.4..

A key feature of these data is that H and He ions account for the majority of the elemental ion dose *and* dose equivalent. In space radiation studies it is common to see spectra comprised largely of H and He ions. That said, having H account for 80% of the elemental ion dose and 40% of the elemental ion dose equivalent, along with He accounting for 13% of the elemental ion dose and 32% of the elemental ion dose equivalent, could impact future Mars-related shielding designs and radiation protection standards.

Table 4.4
Surface of Mars Frequency, Dose, and Dose Equivalent Distributions

z	Frequency	Dose	Dose Equivalent
1	9.57E-01	8.01E-01	4.00E-01
2	4.07E-02	1.33E-01	3.18E-01
3	2.95E-04	2.05E-03	5.36E-03
4	1.57E-04	1.64E-03	2.39E-03
5	2.62E-04	3.97E-03	4.92E-03
6	5.95E-04	1.27E-02	2.02E-02
7	1.85E-04	5.29E-03	1.11E-02
8	3.72E-04	1.38E-02	3.87E-02
9	2.10E-05	9.49E-04	3.30E-03
10	6.26E-05	3.55E-03	1.48E-02
11	2.33E-05	1.53E-03	7.36E-03
12	5.68E-05	4.57E-03	2.54E-02
13	1.56E-05	1.42E-03	8.93E-03
14	3.41E-05	3.64E-03	2.55E-02
15	5.36E-06	6.39E-04	4.93E-03
16	8.70E-06	1.22E-03	9.79E-03
17	4.03E-06	5.97E-04	5.44E-03
18	4.51E-06	8.37E-04	7.71E-03
19	3.45E-06	6.63E-04	6.56E-03
20	5.14E-06	1.04E-03	1.14E-02
21	2.07E-06	4.71E-04	5.28E-03
22	3.86E-06	9.81E-04	1.09E-02
23	2.36E-06	6.80E-04	7.05E-03
24	3.22E-06	9.70E-04	1.00E-02
25	2.59E-06	8.58E-04	8.43E-03
26	7.28E-06	2.52E-03	2.45E-02
27	1.18E-07	5.91E-05	4.58E-04
28	4.02E-07	1.57E-04	1.44E-03

It should be noted that the dose and dose equivalent distributions are normalized to only other elemental ions. This means that H ions account for 80% of the *elemental ion* dose and 40% of the *elemental ion* dose equivalent from Table 4.3, not the total values.

These frequency, dose, and dose equivalent distributions for the surface of Mars are plotted in Figure 4.6. For every ion, with the exception of H where the trend is reversed, the dose equivalent fraction is greater than the dose fraction and both are greater than the frequency fraction.

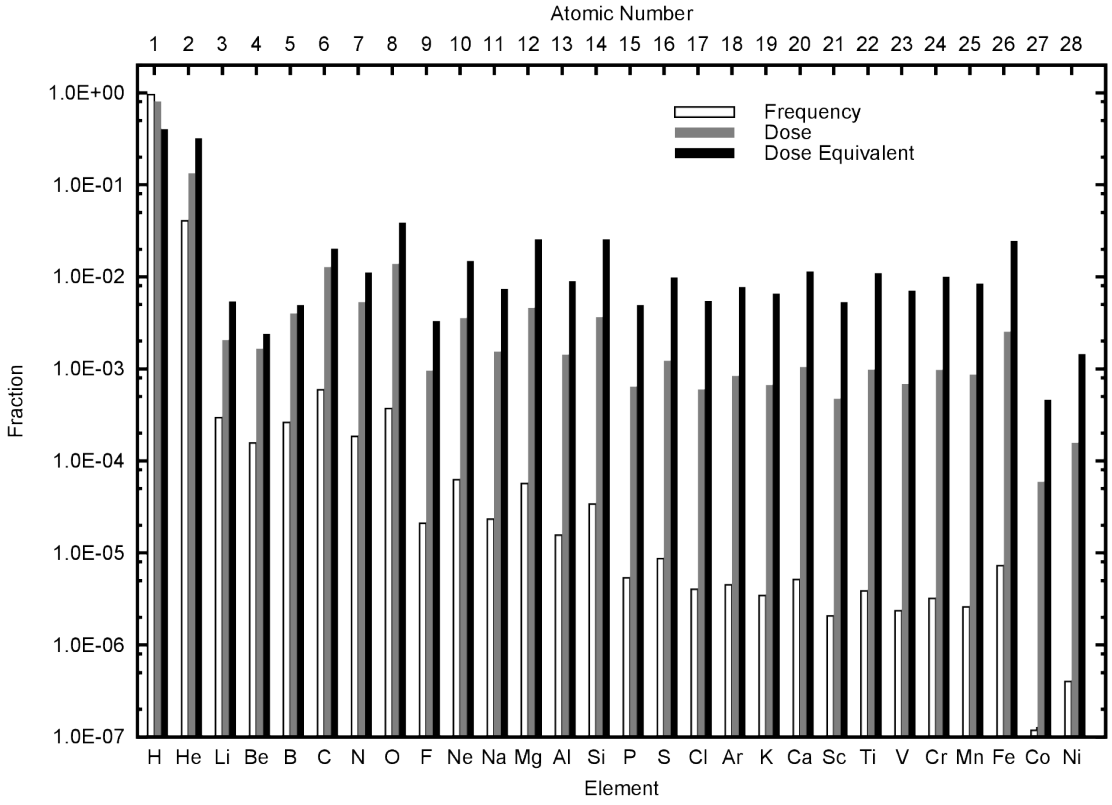

Figure 4.6. Fractional contributions to frequency, dose, and dose equivalent of each elemental ion on the surface of Mars. The dose distribution represents each ion's contribution to the elemental ion dose, not the total (all-particle) dose. Likewise, the dose equivalent distribution represents each ion's contribution to the elemental ion dose equivalent, not the total (all-particle) dose equivalent.

4.3 Free Space/Surface of Mars Comparison

With the free space and surface of Mars y distributions, dosimetry values, differential energy spectra, and the frequency, dose, and dose equivalent distributions presented, a comparison between the two can now take place.

4.3.1 Lineal Energy Distributions

A comparison of the y distributions for a TEPC in free space and on the surface of Mars appears in Figure 4.7.

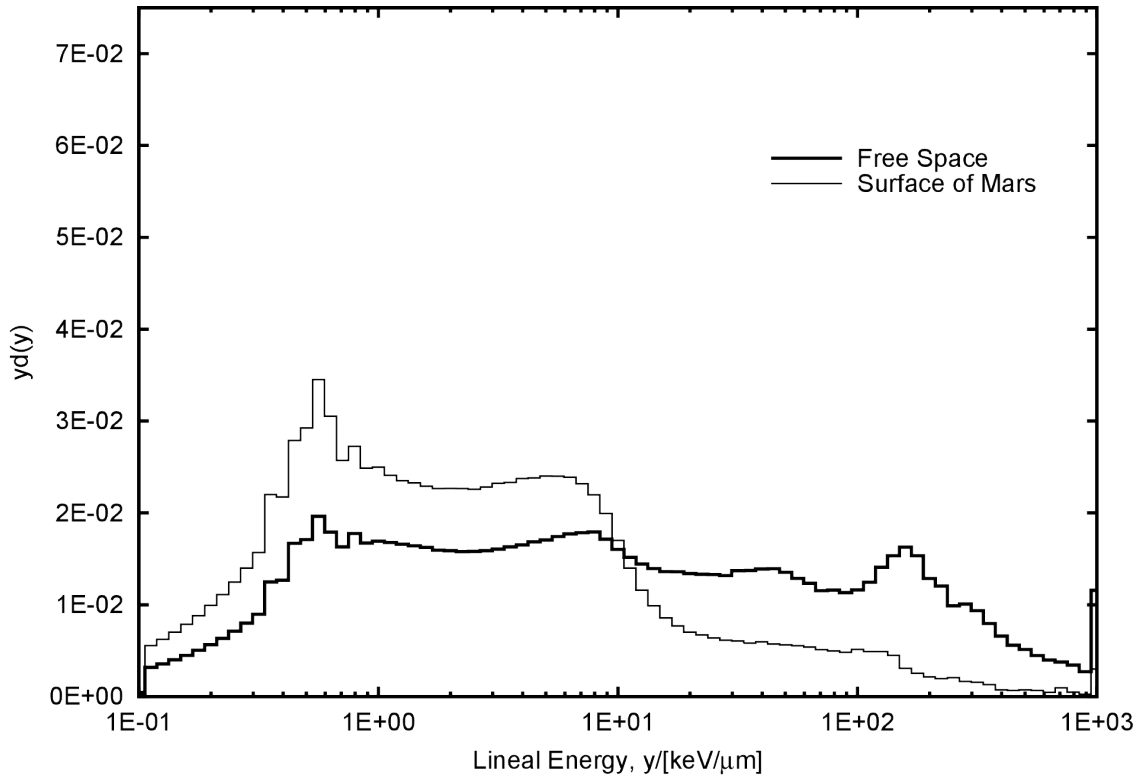

Figure 4.7. Lineal energy distributions for a TEPC in free space and on the surface of Mars. Each distribution includes all particles transported by FLUKA and is normalized to unit area.

As expected, the Martian atmosphere provided some but not complete shielding from the heavy ions present in free space which resulted in a large reduction in the number of events with y greater than 10 keV/μm. The prominent Fe feature in the region from 100 keV/μm to 200 keV/μm has been replaced with a less-significant, neutron-induced proton drop point at 150 keV/μm.

4.3.2 Dosimetry

A comparison of the dosimetry values for free space and the surface of Mars appears in Table 4.5.

Table 4.5
Free Space/Surface of Mars TEPC Dosimetry Comparison

	$\dot{D}$	$\dot{H}$	$\bar{Q}$	$\bar{y}_{\mathrm{F}}$	$\bar{y}_{\mathrm{D}}$
	[Gy/y]	[Sv/y]		[keV/μm]	[keV/μm]
Free Space	1.5E-1	1.0E0	6.9	1.4	71.1
Surface of Mars	6.4E-2	1.8E-1	2.9	0.9	18.4

The dose rate decreases from 0.15 Gy/y in free space to 0.064 Gy/y on the surface of Mars. While the presence of an atmosphere does lead to a reduction in the dose rate, offset by the influence of albedo radiation, the 57% reduction can be largely attributed to the shielding provided by the planet itself. This is assuming the absorbed dose rate would be equal to 0.075 Gy/y in the absence of the Martian atmosphere or albedo radiation.

As expected, the shift in the y distribution on the surface as compared to free space resulted in a reduced average quality factor. This decrease in $\bar{Q}$, coupled with

the 57% decrease in the absorbed dose rate, resulted in a dose equivalent rate of 0.18 Sv/y – a decrease of 82% from 1.0 Sv/y in free space.

A striking feature of the surface of Mars dosimetry values is their comparability to the same quantities measured on board ISS and Space Shuttle missions. In LEO $\dot{D}$ varies from 0.058 Gy/y to 0.12 Gy/y, $\dot{H}$ varies from 0.17 Sv/y to 0.30 Sv/y, and $\bar{Q}$ varies from 2.5 to 3.1 (*119–121*). Such a similarity means operational radiation procedures currently in place may only need minor revision to be applicable to the radiation environment on the surface of Mars.

4.3.3 Differential Energy Spectra

A comparison between the free space and surface of Mars differential energy spectra for elemental ions with $z = 1$ (isotopes combined) appears in Figure 4.8. The free space data were taken from the 2010 version (*21*) of the Badhwar–O'Neill model (*19–21*). The surface of Mars data were generated from the particle fluence 1 m above the surface, including albedo ions, with the Badhwar–O'Neill model from $z = 1$ to $z = 28$ incident on the top of the Martian atmosphere. All differential energy spectra are presented as fluence rate $[\text{m}^2 \text{ s sr MeV/n}]^{-1}$ as a function of kinetic energy [MeV/n].

Two features in Figure 4.8 show evidence of the presence of the thin Martian atmosphere. First, the increase in the number of ions with kinetic energies less than 1 GeV/n is evidence of nuclear fragmentation occurring in the atmosphere which is to be expected in heavy ion shielding problems. Additionally, the spectrum shows no visible change above 10 GeV/n which indicates that 24 g/cm^2 of CO_2 had a negligible effect on these very high energy ions, as expected.

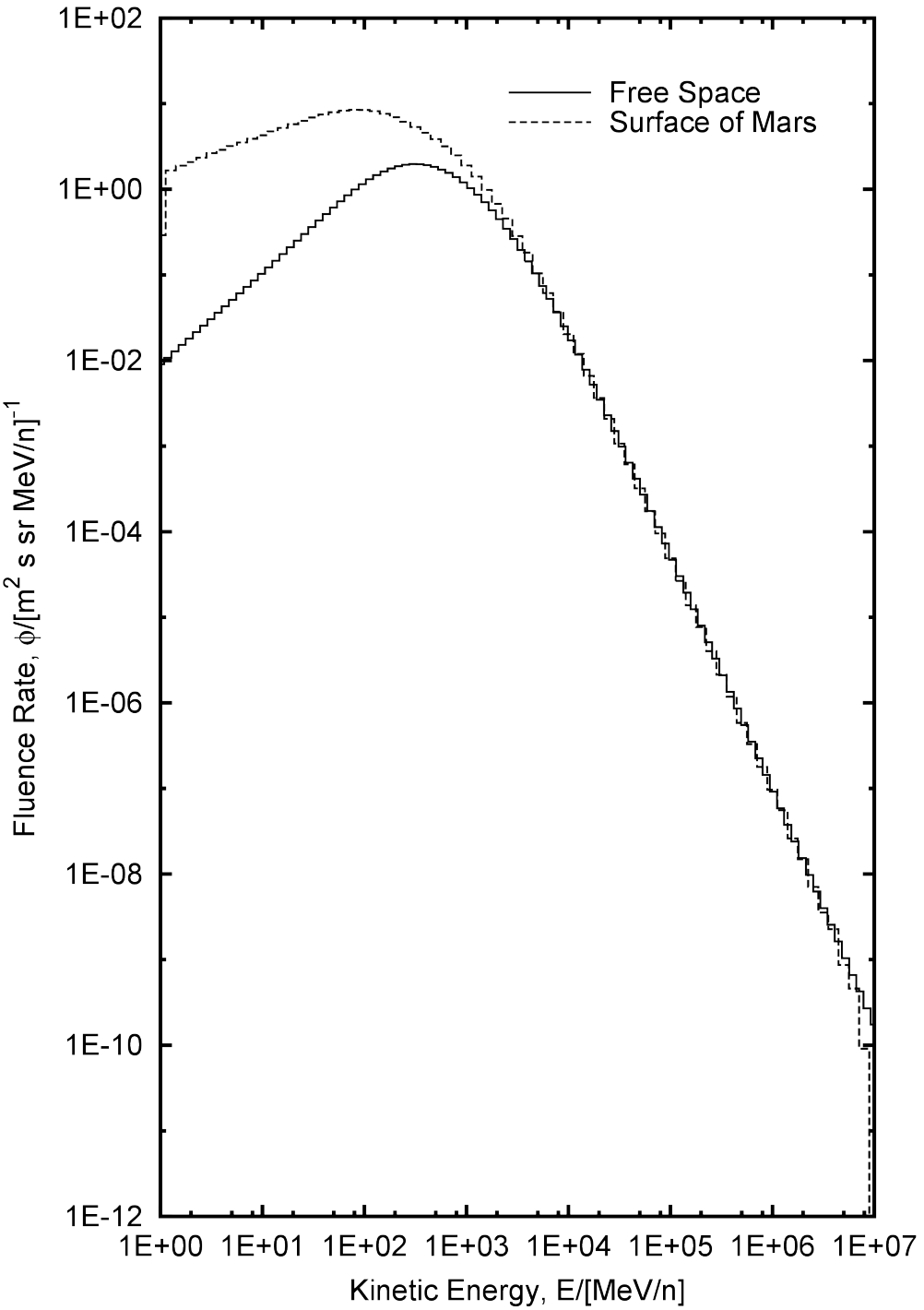

Figure 4.8. Comparison of free space and surface of Mars differential energy spectra for $z = 1$ (isotopes combined). The "Free Space" curve is from the Badhwar–O'Neill model and the "Surface of Mars" curve was generated from the particle fluence 1 m above the surface, including albedo ions, with the Badhwar–O'Neill model ($z = 1$ to $z = 28$) incident on the top of the Martian atmosphere.

Figure 4.8 represents a very small sampling of the differential energy spectra generated in the present study. The entire set of figures is presented in Appendix F. Additionally, the corresponding tabulated data files, from which the figures were plotted, are presented in Appendix G.

These data were generated by randomly sampling the Badhwar–O'Neill model 1.0×10^8 times. Each randomly sampled particle was assigned a random, inward-directed cosine vector and positioned at the top of the Martian atmosphere. Normalized to time, these 1.0×10^8 Monte Carlo histories correspond to a "counting time" of 0.545 y.

Even with a counting time of over half a year, many of the surface of Mars heavy ion spectra are far from appearing as smooth as their free space, Badhwar–O'Neill model, counterparts. These poor statistics are not an indication of an error in the present study. In fact, these spectra offer a realistic representation of the stochastic nature of dose from heavy ions–an aspect of space radiation protection that cannot be avoided. Even if an attempt was made to improve these spectra by increasing the number of primary particles by three orders of magnitude, for example, the corresponding simulated irradiation time would be 545 y. Such a length of time would make the spectra biologically irrelevant since it is no less than six times the average human life expectancy.

4.3.4 Frequency, Dose, Dose Equivalent Distributions

From these differential energy spectra it is possible to generate frequency, dose, and dose equivalent distributions for each elemental ion on the surface of Mars using the same integration methods as in free space.

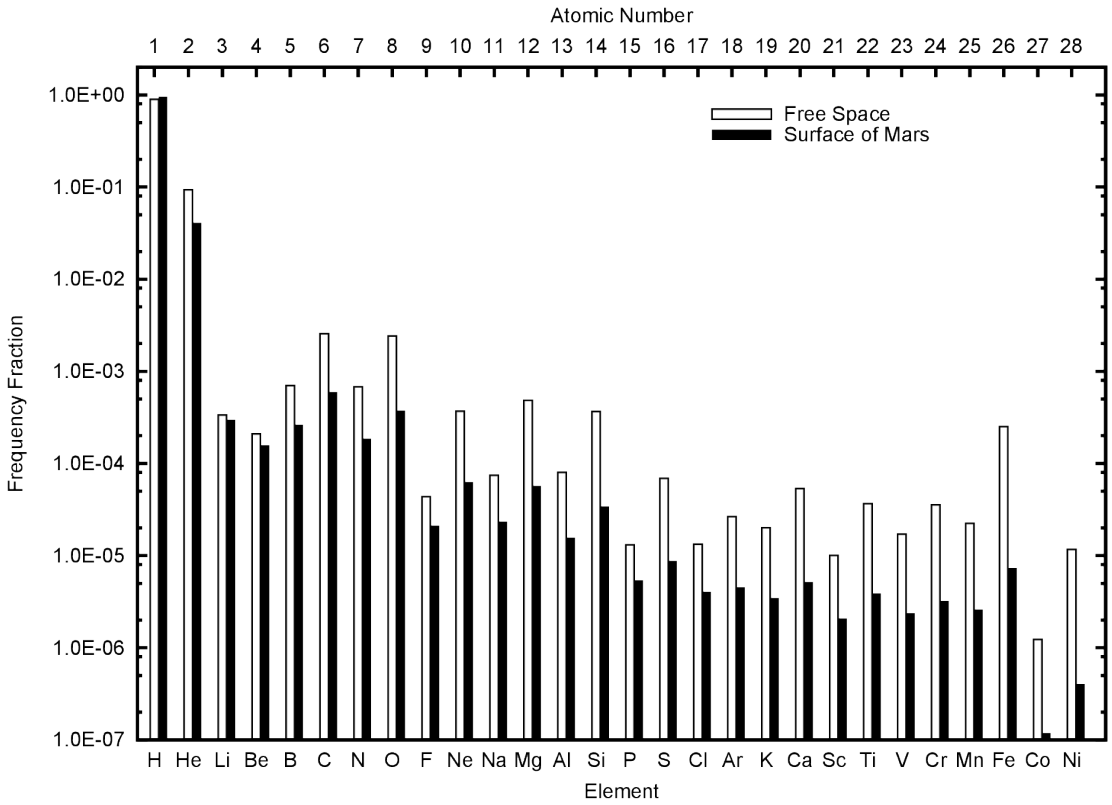

Figure 4.9. Comparison of the fractional contributions to frequency of each elemental ion in free space and on the surface of Mars. The "Free Space" distribution was generated from the Badhwar–O'Neill model. The "Surface of Mars" distribution was generated from the particle fluence 1 m above the surface, including albedo ions, with the Badhwar–O'Neill model ($z = 1$ to $z = 28$) incident on the top of the Martian atmosphere.

A comparison of the frequency distributions in free space and on the surface of Mars appears in Figure 4.9. The influence of the Martian atmosphere can be seen in the relative reduction of the number of ions with $z > 1$ reaching the surface.

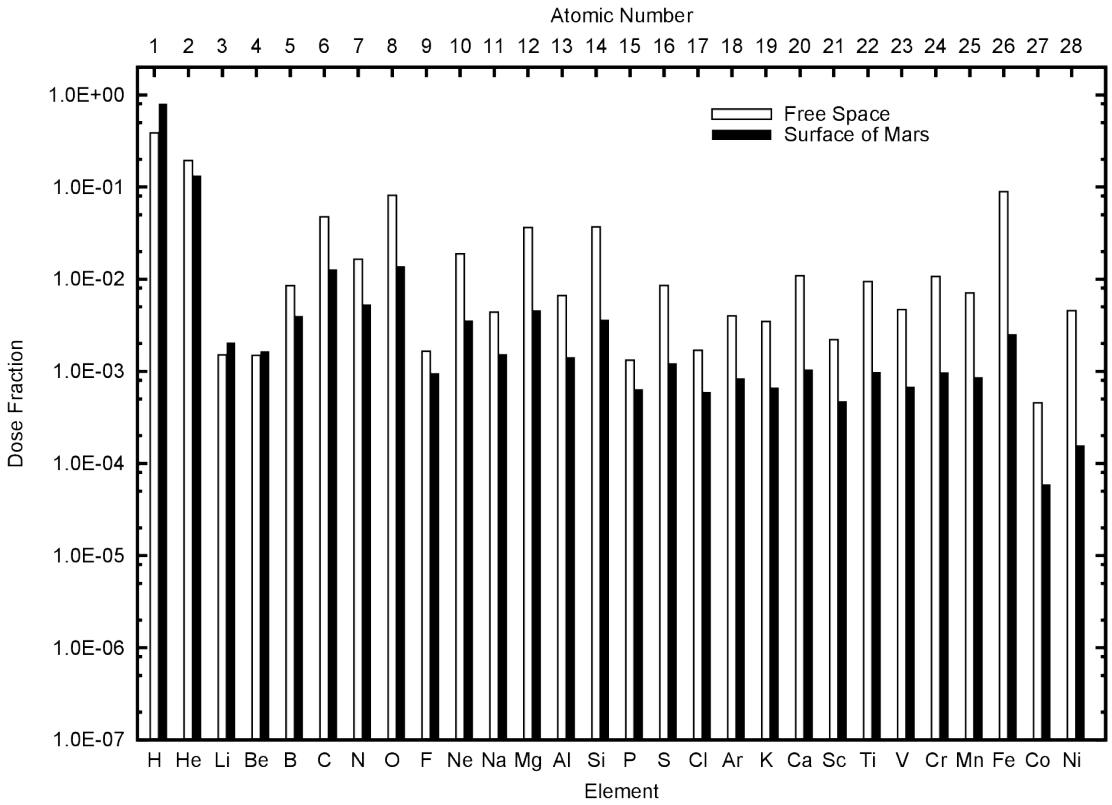

Figure 4.10. Comparison of the fractional contributions to dose of each elemental ion in free space and on the surface of Mars. The "Free Space" distribution was generated from the Badhwar–O'Neill model. The "Surface of Mars" distribution was generated from the particle fluence 1 m above the surface, including albedo ions, with the Badhwar–O'Neill model ($z = 1$ to $z = 28$) incident on the top of the Martian atmosphere. These values represent each ion's contribution to the elemental ion dose, not the total (all-particle) dose.

A comparison of the dose distributions in free space and on the surface of Mars appears in Figure 4.10. Following the trend of the frequency distribution, the relative contribution to the elemental ion dose decreased for every ion with the exception of H, Li, and Be. H accounted for the largest increase followed by Li then Be.

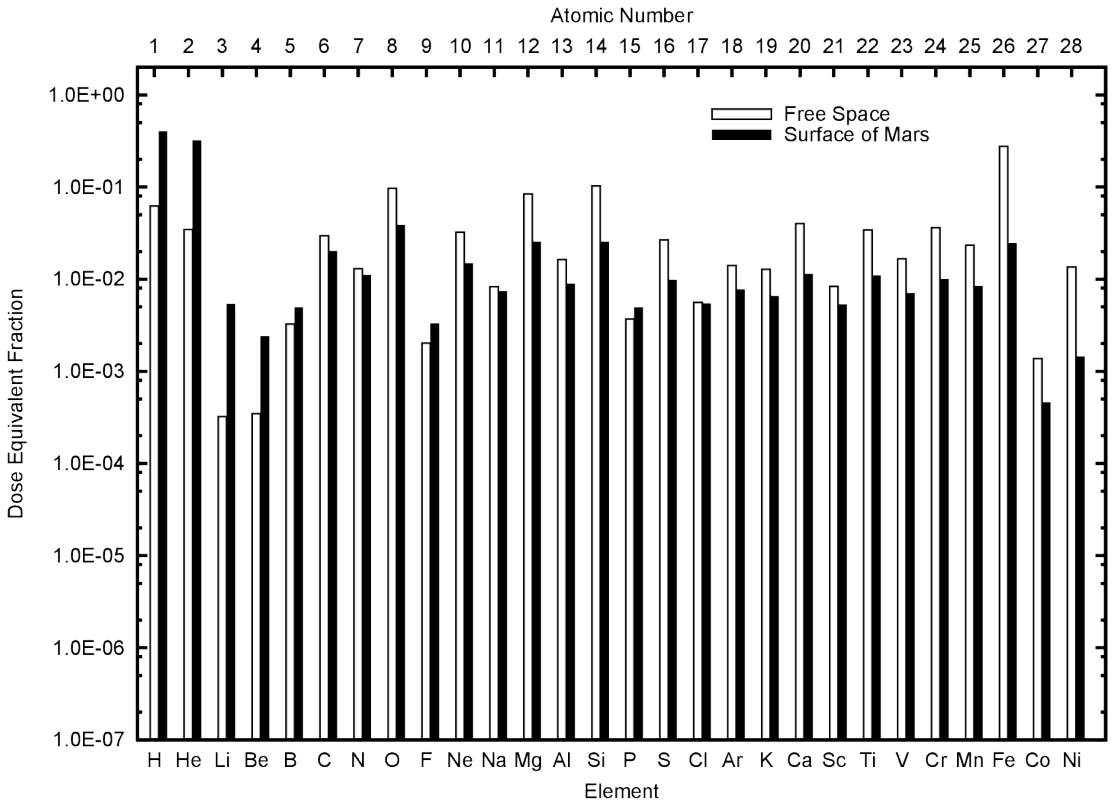

Figure 4.11. Comparison of the fractional contributions to dose equivalent of each elemental ion in free space and on the surface of Mars. The "Free Space" distribution was generated from the Badhwar–O'Neill model. The "Surface of Mars" distribution was generated from the particle fluence 1 m above the surface, including albedo ions, with the Badhwar–O'Neill model ($z = 1$ to $z = 28$) incident on the top of the Martian atmosphere. These values represent each ion's contribution to the elemental ion dose equivalent, not the total (all-particle) dose equivalent.

Finally, a comparison of the dose equivalent distributions in free space and on the surface of Mars appears in Figure 4.11. This comparison demonstrates the complexities involved in properly assessing the radiation risk to humans on the surface of Mars. The relative contribution to the elemental ion dose equivalent increased by an order of magnitude for H through Be. Slight increases resulted for B, F, and P and the decrease for Cl was almost negligible. The relative contribution to the elemental

ion dose equivalent decreased for all other elemental ions.

Fe ions suffered a full order-of-magnitude reduction in their fractional contribution to the elemental ion dose equivalent. While they account for 28% of the dose equivalent in free space, Fe ions represent only 2.5% of the elemental ion dose equivalent (1.3% of the dose equivalent from all particles) on the surface of Mars. Because of this, they are no longer the ion of interest from a radiation protection point of view.

Instead, H and He ions are the elemental ions of interest on the surface of Mars since they account for 40% and 32% of the elemental ion dose equivalent, respectively. Taking all particles into consideration, H and He ions account for 22% and 17% of the total dose equivalent, respectively.

5. CONCLUSION

5.1 Summary

The data generated in the present study offer insight into the radiation environment on the surface of Mars. The FLUKA model is meant to represent the worst-case scenario exposure to galactic cosmic rays: unshielded and at deep solar minimum conditions.

The unshielded free space scenario yielded a dose equivalent rate of 1.0 Sv/y with $\bar{Q} = 6.9$ and $\bar{y}_{\mathrm{D}} = 71.1$ keV/μm. The influence of the Martian atmosphere and regolith, along with the shielding offered by the planet, resulted in a net decrease in the dose equivalent rate to 0.18 Sv/y with $\bar{Q} = 2.9$ and $\bar{y}_{\mathrm{D}} = 18.4$ keV/μm. Of particular interest is the contribution to the dose equivalent on the surface of Mars from neutrons. Downward neutrons are responsible for 0.018 Sv/y, 9.5% of the total dose equivalent rate, and albedo neutrons are responsible for 0.047 Sv/y, 25.4% of the total dose equivalent rate.

The y spectra offer additional insight into the distribution of energy deposition in terms of radiation quality. A pronounced tendency towards higher values of y exists for both the downward and albedo neutron components as evidenced by the high values of $\bar{Q}$ and $\bar{y}_{\mathrm{D}}$. A comparison of the free space and surface of Mars y distributions shows how the presence of the Martian atmosphere greatly reduces the influence of HZE ions.

Finally, the generation of frequency, dose, and dose equivalent distributions from the differential energy spectra illustrated the effects of the atmosphere shielding. Fe ions, of particular interest in space radiation protection since they are responsible for 28% of the dose equivalent in free space, are responsible for 1.3% of the dose

equivalent on the surface of Mars. The elemental ions of interest on the surface of Mars are H which account for 40% of the elemental ion dose equivalent and 22% of the total, all-particle dose equivalent and He which is responsible for 32% of the elemental ion dose equivalent and 17% of the total, all-particle dose equivalent.

It is anticipated that these data will be useful in future mission planning studies and for comparison to the data collected by the RAD instrument.

5.2 Future Work

While every effort has been made to be complete in all aspects of the present study, several limitations do exist.

One major limitation was the use of a static atmosphere model for all simulations. The Martian atmosphere is by no means static in either space or time. Seasonal variations in atmospheric thickness lead to fluctuations in the amount of shielding from GCRs. Additionally, surface features can lead to altitudes many kilometers above or below mean planetary radius. The RAD instrument is located in Gale Crater, approximately 4 km below mean planet radius. In order to provide an accurate comparison to data collected by the RAD instrument, the atmospheric model used in the present study is thicker than average. Consequently, these data are less accurate for other locations on the planet.

Another limitation of the present study is the use of a fixed solar modulation parameter. All simulations used the Badhwar–O'Neill model with $\Phi = 450$ MV as the source spectrum. It could be argued that there is no problem with the use of such a conservative estimate. However, the use of a higher solar modulation parameter or the incorporation of a dynamic model might serve as a more realistic model.

Additionally, the Badhwar–O'Neill model presents differential energy spectra of GCR ions at 1 AU from the sun. However, the distance from the Sun to Mars varies

from 1.4 AU to 1.7 AU. Such a difference, even if only slight, should be considered in future studies.

In any realistic scenario, a human on the surface of Mars would either be inside a habitat or, if not in a habitat, wearing some type of suit for the entirety of their stay. No shielding was considered in the present study. Any addition of shielding has the potential to further complicate the radiation environment. The non-negligible change in the stopping power of incident ions, in addition to the generation of secondary particles, prohibits the use of any simple scaling factor to quantify the effect of varying the shielding thickness. Therefore, each unique scenario must be independently simulated, and the reliability of approximations of the effects of changes in shielding are called into question.

The radiation environment in space and on the surface of Mars is not just a product of galactic cosmic rays. The Sun, a source of ionizing radiation during intense solar events, has the potential to deliver significant doses to humans in transit to and on the surface of Mars. That said, determining a proper benchmark solar event is difficult because of the varying energy spectra and intensities of recorded events. In addition, uncertainty persists regarding what should be deemed the worst-case scenario solar event for conservative estimates.

Furthermore, the present study employed daily averages of atmospheric density and pressure in the Mars model. Fluctuations in these values that occur throughout each sol can largely be ignored with respect to GCRs. Ignoring these fluctuations is a reasonable assumption for GCR dosimetry since its fluence is isotropic and the rate is rather stable over the short time period of a sol. For solar events, however, the highly directional nature and large temporal variability of SPEs does not allow for such an assumption.

For these reasons, only galactic cosmic rays were considered in the present study

and the influence of solar events on the radiation environment on the surface of Mars has been left to future studies.

Modeling the radiation environment on the surface of Mars is a difficult task because of the large number of variables involved. Varying solar modulation, as well as daily and seasonal variations in atmospheric thickness, do not allow for the generation of an all-encompassing data set that can describe all possible scenarios. Likewise, introducing shielding and considering solar events adds further complications. Future mission planning studies will require detailed knowledge of the landing site, both location and specific time of stay, and shielding materials to develop an accurate estimate of the particle fluence spectrum a human would be exposed to along with the corresponding health risks. Perhaps the data generated in the present study can serve as a starting point for these future studies.

REFERENCES

1. Hand E. Mars rover sizes up the field. Nature. 2012; 488:137–138.

2. Grotzinger J, Crisp J, Vasavada A, Anderson R, Baker C, Barry R, et al. Mars Science Laboratory mission and science investigation. Space Science Reviews. 2012; 1:1–52.

3. Hassler D, Zeitlin C, Wimmer-Schweingruber R, Böttcher S, Martin C, Andrews J, et al. The Radiation Assessment Detector (RAD) investigation. Space Science Reviews. 2012; 1:503–558.

4. Ozasa K, Shimizu Y, Suyama A, Kasagi F, Soda M, Grant EJ, et al. Studies of the mortality of atomic bomb survivors, report 14, 1950–2003: an overview of cancer and noncancer diseases. Radiation Research. 2012; 177:229–243.

5. Mabuchi K, Soda M, Ron E, Tokunaga M, Ochikubo S, Sugimoto S, et al. Cancer incidence in atomic bomb survivors. Part I: use of the tumor registries in Hiroshima and Nagasaki for incidence studies. Radiation Research. 1994; 137:S1–S16.

6. Thompson DE, Mabuchi K, Ron E, Soda M, Tokunaga M, Ochikubo S, et al. Cancer incidence in atomic bomb survivors. Part II: solid tumors, 1958-1987. Radiation Research. 1994; 137:S17–S67.

7. Preston DL, Kusumi S, Tomonaga M, Izumi S, Ron E, Kuramoto A, et al. Cancer incidence in atomic bomb survivors. Part III: leukemia, lymphoma and multiple myeloma, 1950-1987. Radiation Research. 1994; 137:S68–S97.

8. Ron E, Preston DL, Mabuchi K, Thompson DE, Soda M. Cancer incidence in atomic bomb survivors. Part IV: comparison of cancer incidence and mortality. Radiation Research. 1994; 137:S98–S112.

9. Young RW, Kerr GD, editors. Reassessment of the atomic bomb radiation dosimetry for Hiroshima and Nagasaki: dosimetry system 2002. Hiroshima: Radiation Effects Research Foundation; 2005.

10. Cucinotta FA, Schimmerling W, Wilson JW, Peterson LE, Badhwar GD, Saganti PB, et al. Space radiation cancer risks and uncertainties for Mars missions. Radiation Research. 2001; 156:682–688.

11. Simpson JA. Elemental and isotopic composition of the galactic cosmic rays. Annual Reviews of Nuclear and Particle Science. 1983; 33:323–382.

12. Hess VF. Über Beobachtungen der durchdringenden Strahlung bei sieben Freiballonfahrten. Physikalische Zeitschrift. 1912; 13:1084–1091.

13. Binns WR. Cosmic-ray origins. Science. 2011; 334:1071–1072.

14. Information needed to make radiation protection recommendations for space missions beyond low-Earth orbit. Report 153. Bethesda, MD: National Council on Radiation Protection & Measurements; 2006.

15. Guidance on radiation received in space activities. Report 98. Bethesda, MD: National Council on Radiation Protection & Measurements; 1989.

16. Beringer J, Arguin JF, Barnett RM, Copic K, Dahl O, Groom DE, et al. Review of particle physics. Phys Rev D. 2012; 86:010001.

17. Meyer-Vernet N. Basics of the solar wind. Cambridge: Cambridge University Press; 2007.

18. Mewaldt RA, Davis AJ, Lave KA, Leske RA, Stone EC, Wiedenbeck ME, et al. Record-setting cosmic-ray intensities in 2009 and 2010. The Astrophysical Journal Letters. 2010; 723:L1–L6.

19. Badhwar GD, O'Neill PM. Galactic cosmic radiation model and its applications. Advances in Space Research. 1996; 17:7–17.

20. O'Neill PM. Badhwar–O'Neill galactic cosmic ray model update based on Advanced Composition Explorer (ACE) energy spectra from 1997 to present. Advances in Space Research. 2006; 37:1727–1733.

21. O'Neill PM. Badhwar–O'Neill 2010 galactic cosmic ray flux model–revised. IEEE Transactions on Nuclear Science. 2010; 57:3148–3153.

22. Guetersloh S, Zapp N. Energetic particles and manned spaceflight. In: Heliophysics: space storms and radiation: causes and effects. Cambridge: Cambridge University Press; 2010. p. 359–379.

23. George JS, Lave KA, Wiedenbeck ME, Binns WR, Cummings AC, Davis AJ, et al. Elemental composition and energy spectra of galactic cosmic rays during solar cycle 23. The Astrophysical Journal. 2009; 698:1666–1681.

24. Blakely EA, Kronenberg A. Heavy-ion radiobiology: new approaches to delineate mechanisms underlying enhanced biological effectiveness. Radiation Research. 1998; 150:S126–S145.

25. Townsend LW, Cucinotta FA, Wilson JW. Interplanetary crew exposure estimates for galactic cosmic rays. Radiation Research. 1992; 129:48–52.

26. Badhwar GD, Cucinotta FA, O'Neill PM. An analysis of interplanetary space radiation exposure for various solar cycles. Radiation Research. 1994; 138:201–208.

27. Badhwar GD, Cucinotta FA, O'Neill PM. Depth-dose equivalent relationship for cosmic rays at various solar minima. Radiation Research. 1993; 134:9–15.

28. Hoff JL, Townsend LW, Zapp EN. Interplanetary crew doses and dose equivalents: variations among different bone marrow and skin sites. Advances in Space Research. 2004; 34:1347–1352.

29. Borggräfe A, Quatmann M, Nölke D. Radiation protective structures on the base of a case study for a manned Mars mission. Acta Astronautica. 2009; 65:1292–1305.

30. Zeitlin C, Cleghorn T, Cucinotta F, Saganti P, Andersen V, Lee K, et al. Overview of the Martian radiation environment experiment. Advances in Space Research. 2004; 33:2204–2210.

31. Saganti PB, Cucinotta FA, Wilson JW, Cleghorn TF, Zeitlin CJ. Model calculations of the particle spectrum of the galactic cosmic ray (GCR) environment: Assessment with ACE/CRIS and MARIE measurements. Radiation Measurements. 2006; 41:1152–1157.

32. Hu S, Kim MHY, McClellan GE, Cucinotta FA. Modeling the acute health effects of astronauts from exposure to large solar particle events. Health Physics. 2009; 96:465–476.

33. Turner JE. Atoms, radiation, and radiation protection. 2nd ed. New York: Wiley; 1995.

34. Hapgood M. Astrophysics: prepare for the coming space weather storm. Nature. 2012; 484:311–313.

35. Carrington RC. Description of a singular appearance seen in the sun on September 1, 1859. Monthly Notices of the Royal Astronomical Society. 1859; 20:13–15.

36. McCracken KG, Dreschhoff GAM, Zeller EJ, Smart DF, Shea MA. Solar cosmic ray events for the period 1561–1994: 1. Identification in polar ice, 1561–1950. Journal of Geophysical Research. 2001; 106:21585–21598.

37. Townsend LW, Stephens DL, Hoff JL, Zapp EN, Moussa HM, Miller TM, et al. The Carrington event: possible doses to crews in space from a comparable event. Advances in Space Research. 2006; 38:226–231.

38. Wolff E, Bigler M, Curran M, Dibb J, Frey M, Legrand M, et al. The Carrington event not observed in most ice core nitrate records. Geophysical Research Letters. 2012; 39(8):L08503.

39. Luhmann JG, Zeitlin C, Turner R, Brain DA, Delory G, Lyon JG, et al. Solar energetic particles in near-Mars space. Journal of Geophysical Research. 2007; 112:E10001.

40. Zurek RW, Barnes JR, Haberle RM, Pollack JB, Tillman JE, Leovy CB. Dynamics of the atmosphere of Mars. In: Mars. Tucson, AZ: University of Arizona Press; 1992. p. 835–933.

41. Mitrofanov I, Litvak M, Varenikov A, Barmakov Y, Behar A, Bobrovnitsky Y, et al. Dynamic Albedo of Neutrons (DAN) experiment onboard NASA's Mars Science Laboratory. Space Science Reviews. 2012; p. 559–582.

42. Blakely EA. Biological effects of cosmic radiation: deterministic and stochastic. Health Physics. 2000; 79:495–506.

43. Berger MJ, Coursey JS, Zucker MA, Chang J. ESTAR, PSTAR, and ASTAR: Computer programs for calculating stopping-power and range tables for electrons, protons, and helium ions (version 1.2.3). (http://physics.nist.gov/Star)

44. Simonsen LC, Wilson JW, Kim MH, Cucinotta FA. Radiation exposure for human mars exploration. Health Physics. 2000; 79:515–525.

45. Morthekai P, Jain M, Dartnell L, Murray AS, Bøtter-Jensen L, Desorgher L. Modelling of the dose-rate variations with depth in the Martian regolith using GEANT4. Nuclear Instruments and Methods in Physics Research A. 2007; 580:667–670.

46. Gurtner M, Desorgher L, Flückiger EO, Moser MR. Simulation of the interaction of space radiation with the Martian atmosphere and surface. Advances in Space Research. 2005; 36:2176–2181.

47. Banerjee D, Dewangan A. Simulation of the cosmic-ray induced dose-rate within a Martian soil profile. Radiation Measurements. 2008; 43:797–801.

48. Cucinotta FA, Saganti PB, Wilson JW, Simonsen LC. Model predictions and visualization of the particle flux on the surface of Mars. Journal of Radiation Research. 2002; 43:S35–S39.

49. Keating A, Mohammadzadeh A, Nieminen P, Maia D, Coutinho S, Evans H, et al. A model for Mars radiation environment characterization. IEEE Transactions on Nuclear Science. 2005; 52:2287–2293.

50. Clowdsley MS, Wilson JW, Kim MHY, Singleterry RC, Tripathi RK, Heinbockel JH, et al. Neutron environments on the Martian surface. Physica Medica. 2001; 17:94–96.

51. De Angelis G, Wilson JW, Clowdsley MS, Qualls GD, Singleterry RC. Modeling of the Martian environment for radiation analysis. Radiation Measurements. 2006; 41:1097–1102.

52. Cucinotta FA, Kim MHY, Chappell LJ. Space radiation cancer risk projections and uncertainties – 2010. Houston, TX: NASA/TP-2011-216155; 2011.

53. Townsend LW, PourArsalan M, Cucinotta FA, Kim MY, Schwadron NA. Transmission of galactic cosmic rays through Mars atmosphere. Space Weather. 2011; 9:S00E11.

54. Zaider M. Microdosimetric-based risk factors for radiation received in space activities during a trip to Mars. Health Physics. 1996; 70:845–851.

55. Durante M, Cucinotta FA. Heavy ion carcinogenesis and human space exploration. Nature Reviews Cancer. 2008; 8:465–472.

56. Quantification and reporting of low-dose and other heterogeneous exposures. Report 86. Bethesda, MD: International Commission on Radiation Units and Measurements; 2011.

57. Fassò A, Ferrari A, Ranft J, Sala PR. FLUKA: a multi-particle transport code. Geneva: CERN-2005-010, INFN-TC-2005-11, SLAC-R-773; 2005.

58. Battistoni G, Muraro S, Sala PR, Cerutti F, Ferrari A, Roesler S, et al. The FLUKA code: description and benchmarking. In: Proceedings of the Hadronic Shower Simulation Workshop 2006 (AIP Conference Proceeding 896). Fermilab. Melville, New York: American Institute of Physics; 2007. p. 31–49.

59. Rollet S, Beck P, Ferrari A, Pelliccioni M, Autischer M. Dosimetric considerations on TEPC Fluka-simulation and measurements. Radiation Protection Dosimetry. 2004; 110:833–837.

60. Rollet S, Autischer M, Beck P, Latocha M. Measurement and simulation of lineal energy distribution at the CERN High Energy Facility with a tissue equivalent proportional counter. Radiation Protection Dosimetry. 2007; 125:425–428.

61. Rollet S, Colautti P, Grosswendt B, Moro D, Gargioni E, Conte V, et al. Monte carlo simulation of mini TEPC microdosimetric spectra: influence of low energy electrons. Radiation Measurements. 2010; 45:1330–1333.

62. Rollet S, Colautti P, Grosswendt B, Herault J, Wind M, Gargioni E, et al. Microdosimetric assessment of the radiation quality of a therapeutic proton beam: comparison between numerical simulation and experimental measurements. Radiation Protection Dosimetry. 2011; 143:445–449.

63. Böhlen TT, Dosanjh M, Ferrari A, Gudowska I, Mairani A. FLUKA simulations of the response of tissue-equivalent proportional counters to ion beams for applications in hadron therapy and space. Physics in Medicine and Biology. 2011; 56:6545–6561.

64. Böhlen TT, Dosanjh M, Ferrari A, Gudowska I. Simulations of microdosimetric quantities with the Monte Carlo code FLUKA for carbon ions at therapeutic energies. International Journal of Radiation Biology. 2012; 88:176–82.

65. Northum JD, Guetersloh SB, Braby LA. FLUKA capabilities for microdosimetric analysis. Radiation Research. 2012; 177:117–123.

66. Beck P, Ferrari A, Pelliccioni M, Rollet S, Villari R. FLUKA simulation of TEPC response to cosmic radiation. Radiation Protection Dosimetry. 2005; 116:327–330.

67. Wilson JW, Kim M, Schimmerling W, Badavi FF, Thibeault SA, Cucinotta FA, et al. Issues in space radiation protection. Health Physics. 1995; 68:50–58.

68. Attix FH. Introduction to radiological physics and radiation dosimetry. Weinheim, Germany: Wiley–VCH; 2004.

69. Stopping powers and ranges for protons and alpha particles. Report 49. Bethesda, MD: International Commission on Radiation Units and Measurements; 1993.

70. Griffiths DJ. Introduction to elementary particles. 2nd ed. Weinheim, Germany: Wiley–VCH; 2008.

71. Fernow R. Introduction to experimental particle physics. Cambridge: Cambridge University Press; 1989.

72. Turner JE. Calculation of stopping power of a heavy charged particle in matter. Health Physics. 1967; 13:1255–1263.

73. Knoll G. Radiation detection and measurement. New York: Wiley; 2000.

74. Bethe HA, Ashkin J. Passage of radiations through matter. In: Experimental Nuclear Physics. New York: Wiley; 1953. p. 166–357.

75. Stopping powers for electrons and positrons. Report 37. Bethesda, MD: International Commission on Radiation Units and Measurements; 1984.

76. Stopping of ions heavier than helium. Report 73. Bethesda, MD: International Commission on Radiation Units and Measurements; 2005.

77. Norbury JW, Miller J, Adamczyk AM, Heilbronn LH, Townsend LW, Blattnig SR, et al. Nuclear data for space radiation. Radiation Measurements. 2012; 47:315–363.

78. Zeitlin C, Heilbronn L, Miller J, Rademacher SE, Borak T, Carter TR, et al. Heavy fragment production cross sections from 1.05 GeV/nucleon ^{56}Fe in C, Al, Cu, Pb, and CH_2 targets. Phys Rev C. 1997; 56:388–397.

79. Zeitlin C, Fukumura A, Heilbronn L, Iwata Y, Miller J, Murakami T. Fragmentation cross sections of 600 MeV/nucleon ^{20}Ne on elemental targets. Phys Rev C. 2001; 64:024902.

80. Zeitlin C, Guetersloh S, Heilbronn L, Miller J, Fukumura A, Iwata Y, et al. Fragmentation cross sections of 290 and 400 MeV/nucleon ^{12}C beams on elemental targets. Phys Rev C. 2007; 76:014911.

81. Zeitlin C, Sihver L, Tessa CL, Mancusi D, Heilbronn L, Miller J, et al. Comparisons of fragmentation spectra using 1GeV/amu ^{56}Fe data and the PHITS model. Radiation Measurements. 2008; 43:1242–1253.

82. Zeitlin C, Guetersloh S, Heilbronn L, Miller J, Fukumura A, Iwata Y, et al. Nuclear fragmentation database for GCR transport code development. Advances in Space Research. 2010; 46:728–734.

83. Zeitlin C, Miller J, Guetersloh S, Heilbronn L, Fukumura A, Iwata Y, et al. Fragmentation of ^{14}N, ^{16}O, ^{20}Ne, and ^{24}Mg nuclei at 290 to 1000 MeV/nucleon. Phys Rev C. 2011; 83:034909.

84. Zeitlin C, Miller J, Heilbronn L, Frankel K, Gong W, Schimmerling W. The fragmentation of 510 MeV/nucleon iron-56 in polyethylene. I. Fragment fluence spectra. Radiation Research. 1996; 145:655–665.

85. Zeitlin C, Heilbronn L, Miller J, Schimmerling W, Townsend L, Tripathi R, et al. The fragmentation of 510 MeV/nucleon iron-56 in polyethylene. II. Comparisons between data and a model. Radiation Research. 1996; 145:666–672.

86. Guetersloh S, Zeitlin C, Heilbronn L, Miller J, Komiyama T, Fukumura A, et al. Polyethylene as a radiation shielding standard in simulated cosmic-ray environments. Nuclear Instruments and Methods in Physics Research B. 2006; 252:319–332.

87. Zeitlin C, Guetersloh SB, Heilbronn LH, Miller J. Measurements of materials shielding properties with 1 GeV/nuc ^{56}Fe. Nuclear Instruments and Methods in Physics Research B. 2006; 252:308–318.

88. Guetersloh S, Miller J, Taylor L, Zeitlin C, Heilbronn L, Komiyama T, et al. Lunar soil as in-situ shielding. In: Proceedings of Nuclear and Emerging Technologies for Space 2009 (NETS-2009). Atlanta, GA: American Nuclear Society; 2009. p. 1–10.

89. Zeitlin C, Guetersloh S, Heilbronn L, Miller J. Shielding and fragmentation studies. Radiation Protection Dosimetry. 2005; 116:123–124.

90. Zeitlin C, Guetersloh S, Heilbronn L, Miller J, Elkhayari N, Empl A, et al. Shielding experiments with high-energy heavy ions for spaceflight applications. New Journal of Physics. 2008; 10:075007.

91. Zhou D, Semones E, Guetersloh S, Zapp N, Weyland M, Benton ER. The experimental and simulated LET spectrum and charge spectrum from CR-39 detectors exposed to irons near CRaTER at BNL. Radiation Measurements. 2010; 45:916–922.

92. Miller J, Guetersloh SB, Heilbronn LH, Zeitlin CJ. Simulating elements of the space radiation environment on Earth. In: 2005 IEEE Aerospace Conference. Big Sky, MT: IEEE; 2005. p. 698 –703.

93. Zeitlin C, Heilbronn L, Miller J. Detailed characterization of the 1087 MeV/nucleon iron-56 beam used for radiobiology at the Alternating Gradient Synchrotron. Radiation Research. 1998; 149:560–569.

94. Chen CX, Albergo S, Caccia Z, Costa S, Crawford HJ, Cronqvist M, et al. Interactions in hydrogen of relativistic neon to nickel projectiles: total charge-changing cross sections. Phys Rev C. 1994; 49:3200–3210.

95. Miller J, Zeitlin C, Cucinotta FA, Heilbronn L, Stephensc D, Wilson JW. Benchmark studies of the effectiveness of structural and internal materials as radiation shielding for the International Space Station. Radiation Research. 2003; 159:381–390.

96. Fundamental quantities and units for ionizing radiation (*revised*). Report 85. Bethesda, MD: International Commission on Radiation Units and Measurements; 2011.

97. The 2007 recommendations of the International Commission on Radiological Protection. ICRP publication 103. Annals of the ICRP. 2007; 37:1–332.

98. The 1990 recommendations of the International Commission on Radiological Protection. ICRP publication 60. Annals of the ICRP. 1991; 21:1–201.

99. Relative biological effectiveness (RBE), quality factor (Q), and radiation weighting factor (w_{R}). ICRP publication 92. Annals of the ICRP. 2003; 33:1–118.

100. Technical evaluation of the NASA model for cancer risk to astronauts due to space radiation. Washington, DC: The National Academies Press; 2012.

101. Kellerer AM. Microdosimetry: reflections on Harald Rossi. Radiation Protection Dosimetry. 2002; 99:17–22.

102. Chatterjee A, Schaefer HJ. Microdosimetric structure of heavy ion tracks in tissue. Radiation and Environmental Biophysics. 1976; 13:215–227.

103. Kobetich E, Katz R. Energy deposition by electron beams and δ rays. Physical Review. 1968; 170:391–396.

104. Rossi HH, Zaider M. Microdosimetry and its applications. New York: Springer; 1996.

105. Microdosimetry. Report 36. Bethesda, MD: International Commission on Radiation Units and Measurements; 1983.

106. Ebert HG, editor. Proceedings second symposium on microdosimetry. Commission ot the European Communities. Stresa, Italy: Centre for Information and Documentation, Directorate General for Dissemination of Information, Commission of the European Communities; 1970.

107. Cauchy A. Mémoire sur la rectification des courbes et la quadrature des surfaces courbes. In: Oeuvres complètes. Paris: Gauthier–Villars; 1908. p. 167–177.

108. Bradley PD, Rosenfeld AB, Zaider M. Solid state microdosimetry. Nuclear Instruments and Methods in Physics Research B. 2001; 184:135–157.

109. Bracewell RN. The fourier transform and its applications. New York: McGraw-Hill; 1965.

110. Chu E. Discrete and continuous fourier transforms: analysis, applications and fast algorithms. Boca Raton, Florida: CRC Press; 2008.

111. Landau L. On the energy loss of fast particles by ionization. J Phys (USSR). 1944; 8:201–205.

112. Vavilov PV. Ionization losses of high-energy heavy particles. Soviet Physics - JETP. 1957; 5:749–751.

113. Brückner J, Dreibus G, Gellert R, Squyres SW, Wänke H, Yen A, et al. Mars Exploration Rovers: chemical composition by the APXS. In: The Martian surface: composition, mineralogy and physical properties. Cambridge: Cambridge University Press; 2008. p. 58–102.

114. Herkenhoff K, Golombek M, Guinness E, Johnson J, Kusack A, Richter L, et al. In situ observations of the physical properties of the Martian surface. In: The Martian surface: composition, mineralogy and physical properties. Cambridge: Cambridge University Press; 2008. p. 451–467.

115. Golombek M, Haldemann A, Simpson R, Fergason R, Putzig N, Arvidson R, et al. Martian surface properties from joint analysis of orbital, Earth-based, and surface observations. In: The Martian surface: composition, mineralogy and physical properties. Cambridge: Cambridge University Press; 2008. p. 468–497.

116. Williams DR. Mars fact sheet. (http://nssdc.gsfc.nasa.gov/planetary/factsheet/marsfact.html)

117. Justus CG, Johnson DL. Mars global reference atmospheric model 2001 version (Mars-GRAM 2001): Users guide. Marshall Space Flight Center, Alabama: NASA/TM-2001-210961; 2001.

118. Archinal B, A'Hearn M, Bowell E, Conrad A, Consolmagno G, Courtin R, et al. Report of the IAU working group on cartographic coordinates and rotational elements: 2009. Celestial Mechanics and Dynamical Astronomy. 2011; 109:101–135.

119. Zhou D, Semones E, Gaza R, Johnson S, Zapp N, Weyland M. Radiation measured for ISS-Expedition 12 with different dosimeters. Nuclear Instruments and Methods in Physics Research Section A. 2007; 580:1283–1289.

120. Zhou D, Semones E, Gaza R, Johnson S, Zapp N, Lee K, et al. Radiation measured during ISS-Expedition 13 with different dosimeters. Advances in Space Research. 2009; 43:1212–1219.

121. Zhou D, Semones E, Gaza R, Johnson S, Zapp N, Weyland M, et al. Radiation measured with different dosimeters during STS-121 space mission. Acta Astronautica. 2009; 64:437–447.

APPENDIX A

EXTRAPOLATION TECHNIQUE FOR LINEAL ENERGY DISTRIBUTIONS

The reliability of experimental microdosimetry is often called into question at low values of y due to electrical noise and gas multiplication statistics. For these reasons, the $N(y)$ distribution is often extrapolated below a specified value of y according to one of many extrapolation techniques. (*105*).

FLUKA was used to report energy deposition in the gas volume of a simulated TEPC, not charge collection via gas multiplication as in a real TEPC. Electrical noise and the statistics of gas multiplication are not an issue in Monte Carlo simulations. However, a separate issue is present which calls into question the reliability of y distributions at low values of y. In effect, the TEPC modeled by FLUKA has perfect resolution, a feature not present in experimental data.

This perfect resolution manifests itself in the form of distinctive peaks at low values of y, presumably corresponding to a discrete number of ionizations. An example of this phenomenon is found in Figure A.1.

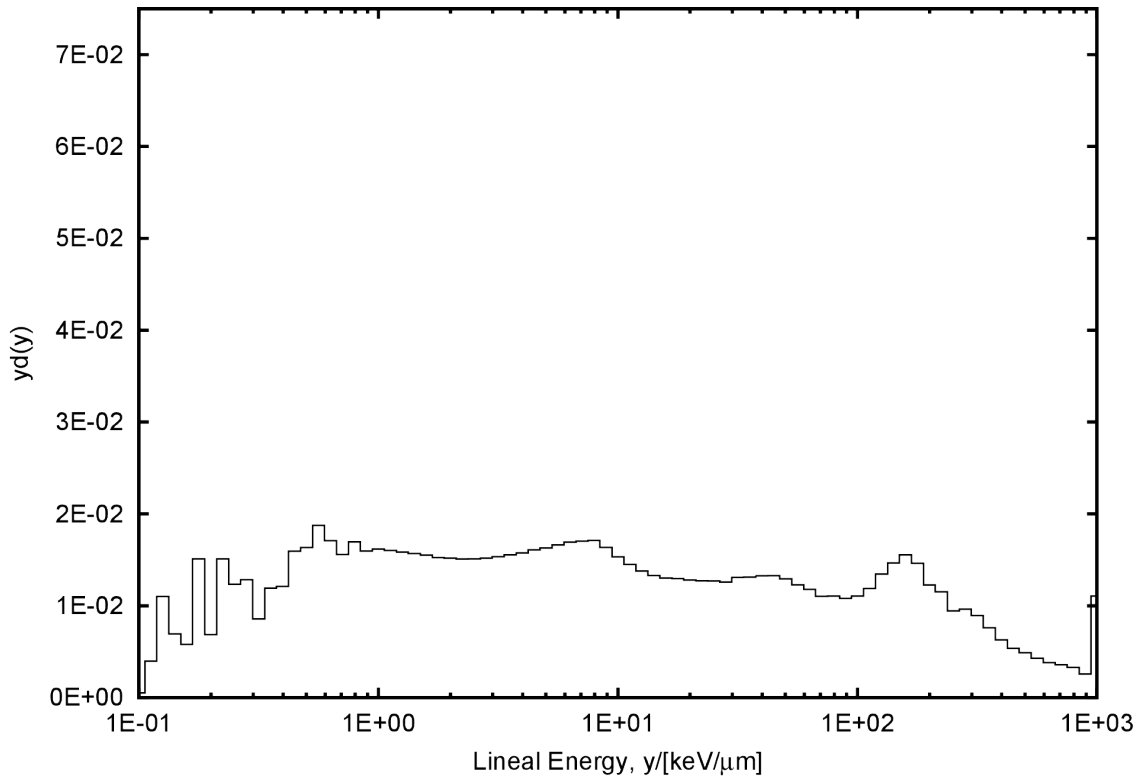

Figure A.1. Lineal energy distribution for a TEPC in free space without the use of an extrapolation technique for low values of y.

To smooth out these peaks, a linear extrapolation was implemented from 0.3 keV/μm down to 0.1 keV/μm. The bin value closest to 0.3 keV/μm in the log binning scheme used in the present study is the $y = 0.316$ keV/μm bin. Therefore, $N(y)$ was set equal to $N(0.316$ keV/μm$)$ for $y < 0.316$ keV/μm. Evidence of this extrapolation can be found in the tabulated data in Appendices B, C, D, and E. The result of the extrapolation technique applied to Figure A.1 is presented in Figure A.2.

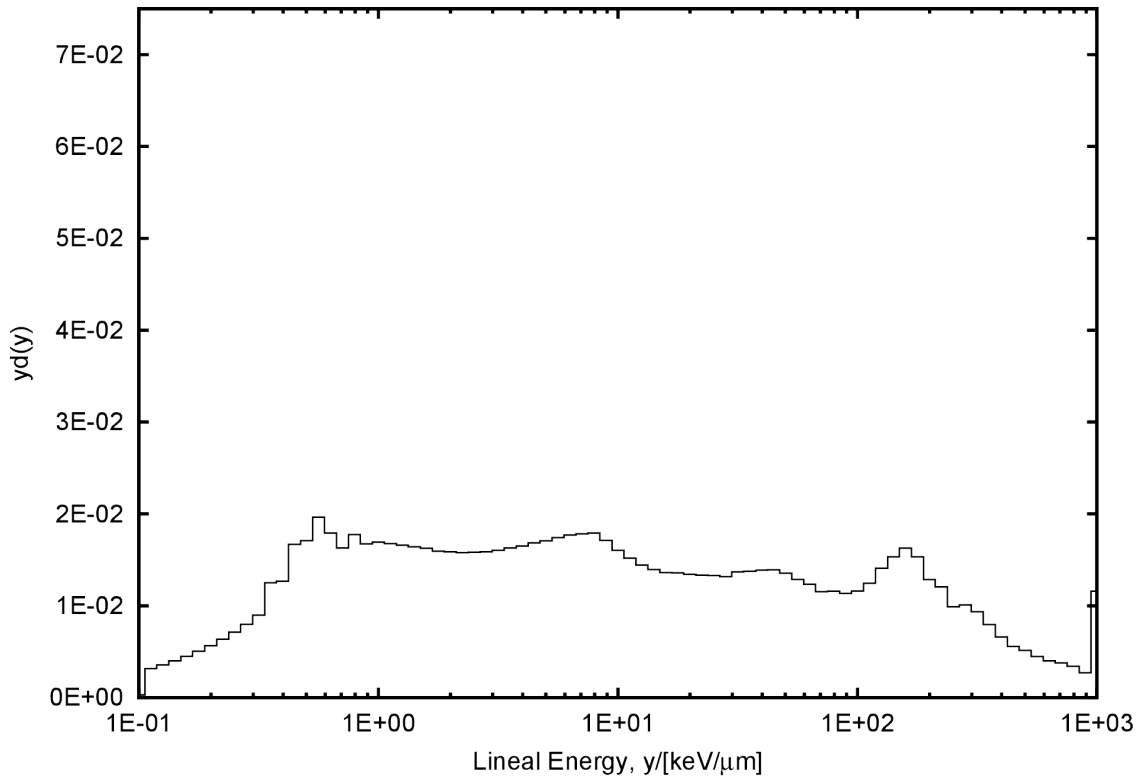

Figure A.2. Lineal energy distribution for a TEPC in free space with the use of an extrapolation technique for low values of y.

The graphical representation of the y distribution is improved with the implementation of this linear extrapolation technique. Its effect on $\bar{y}_{\mathrm{D}}$, $\dot{D}$, $\dot{H}$, and $\bar{Q}$ for this specific y distribution is presented in Table A.1.

Table A.1
Extrapolation Comparison

	$\bar{y}_{\mathrm{D}}$ [keV/μm]	$\dot{D}$ [Gy/y]	$\dot{H}$ [Sv/y]	$\bar{Q}$
Unextrapolated	67.9	0.15	1.0	6.6
Extrapolated	71.1	0.15	1.0	6.9

APPENDIX B

FREE SPACE LINEAL ENERGY DISTRIBUTION

This appendix contains the y distribution for the TEPC in free space. The figure shows a plot of $yd(y)$ as a function of y on a semi-log axis. $\bar{y}_{\mathrm{F}}$, $\bar{y}_{\mathrm{D}}$, D, H, and $\bar{Q}$ for the simulated irradiation are included in the tabulated data. D and H represent integral values for 1.0×10^8 incident particles. These 1.0×10^8 particles, 1.0×10^8 histories in FLUKA, correspond to a simulated irradiation time of 0.301 y. Dividing D and H by 0.301 will normalize these values to time in the form of $\dot{D}$ and $\dot{H}$ with units of Gy/y and Sv/y, respectively. The $f(y)$, $d(y)$, $yf(y)$, and $yd(y)$ distributions have all been normalized to unit area.

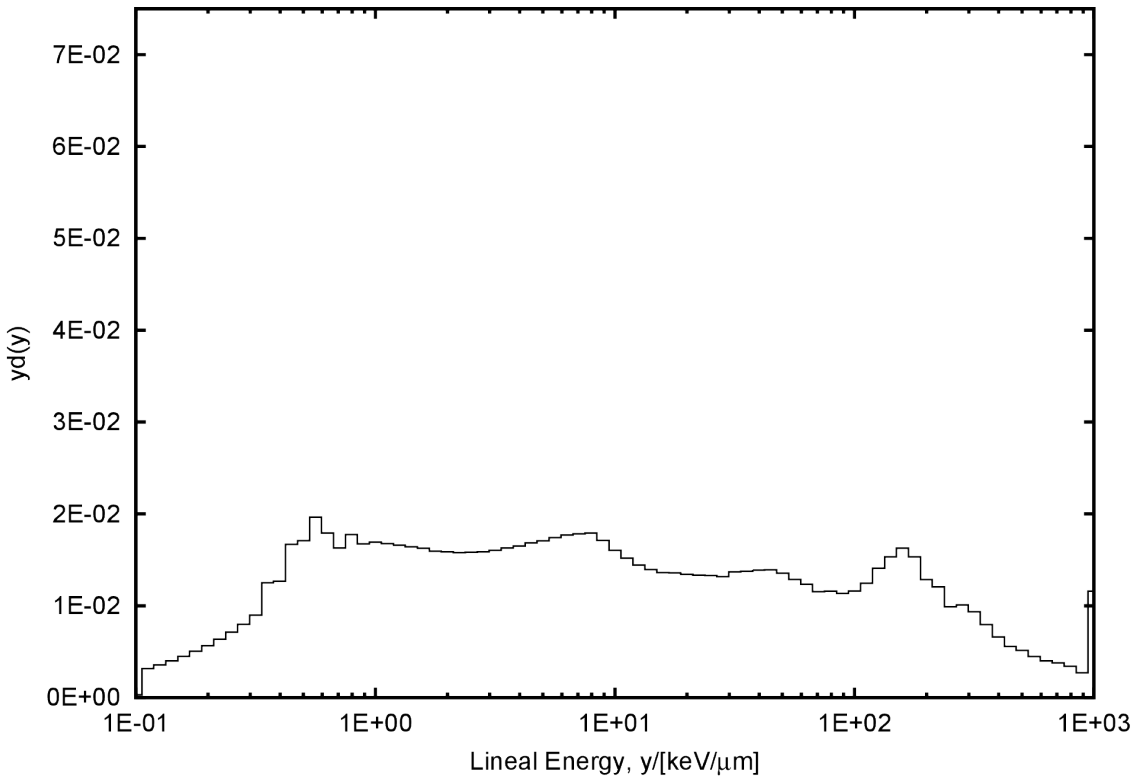

Figure B.1. Lineal energy distribution for a TEPC in free space.

Free Space:

```
# Using 80 Log Bins
# Min: 0.1 keV/μm              Max: 1000 keV/μm              20 bins/decade
#
# SiteSize: 1 μm               Mean Chord Length: 0.667 μm
#
# Using y Output with units of [keV/μm]
#
# y_F = 1.425 keV/μm
# y_D = 71.085 keV/μm
#
# D     = 4.385e-02 Gy
# H     = 3.020e-01 Sv
# Q_avg = 6.887e+00
#
# N = 25132584
#
# y [keV/μm] N(y)     f(y)         y*f(y)      d(y)         y*d(y)
1.0000e-01   980787   1.3895e-02  4.3968e-03  4.3968e-03  3.0852e-04
1.1220e-01   980787   1.1388e-01  4.0431e-02  4.0431e-02  3.1831e-03
1.2589e-01   980787   1.0149e-01  4.0431e-02  4.0431e-02  3.5715e-03
1.4125e-01   980787   9.0456e-02  4.0431e-02  4.0431e-02  4.0073e-03
1.5849e-01   980787   8.0619e-02  4.0431e-02  4.0431e-02  4.4963e-03
1.7783e-01   980787   7.1851e-02  4.0431e-02  4.0431e-02  5.0449e-03
1.9953e-01   980787   6.4038e-02  4.0431e-02  4.0431e-02  5.6605e-03
2.2387e-01   980787   5.7074e-02  4.0431e-02  4.0431e-02  6.3512e-03
2.5119e-01   980787   5.0867e-02  4.0431e-02  4.0431e-02  7.1261e-03
2.8184e-01   980787   4.5335e-02  4.0431e-02  4.0431e-02  7.9956e-03
3.1623e-01   980787   4.0405e-02  4.0431e-02  4.0431e-02  8.9713e-03
3.5481e-01   1216382  4.4661e-02  5.0143e-02  5.0143e-02  1.2484e-02
3.9811e-01   1099332  3.5974e-02  4.5317e-02  4.5317e-02  1.2659e-02
4.4668e-01   1291905  3.7678e-02  5.3256e-02  5.3256e-02  1.6692e-02
5.0119e-01   1179649  3.0663e-02  4.8628e-02  4.8628e-02  1.7101e-02
5.6234e-01   1207241  2.7968e-02  4.9766e-02  4.9766e-02  1.9637e-02
6.3096e-01   981119   2.0257e-02  4.0444e-02  4.0444e-02  1.7906e-02
7.0795e-01   795856   1.4645e-02  3.2807e-02  3.2807e-02  1.6297e-02
7.9433e-01   772782   1.2674e-02  3.1856e-02  3.1856e-02  1.7756e-02
8.9125e-01   648684   9.4819e-03  2.6741e-02  2.6741e-02  1.6723e-02
1.0000e+00   585208   7.6238e-03  2.4124e-02  2.4124e-02  1.6927e-02
1.1220e+00   516847   6.0010e-03  2.1306e-02  2.1306e-02  1.6774e-02
1.2589e+00   455634   4.7149e-03  1.8782e-02  1.8782e-02  1.6592e-02
1.4125e+00   402017   3.7077e-03  1.6572e-02  1.6572e-02  1.6426e-02
1.5849e+00   354199   2.9114e-03  1.4601e-02  1.4601e-02  1.6238e-02
1.7783e+00   310268   2.2730e-03  1.2790e-02  1.2790e-02  1.5959e-02
1.9953e+00   275119   1.7963e-03  1.1341e-02  1.1341e-02  1.5878e-02
2.2387e+00   243974   1.4197e-03  1.0057e-02  1.0057e-02  1.5799e-02
2.5119e+00   217547   1.1283e-03  8.9679e-03  8.9679e-03  1.5806e-02
2.8184e+00   194817   9.0051e-04  8.0309e-03  8.0309e-03  1.5882e-02
3.1623e+00   175619   7.2349e-04  7.2395e-03  7.2395e-03  1.6064e-02
```

3.5481e+00	158751	5.8288e-04	6.5442e-03	6.5442e-03	1.6293e-02
3.9811e+00	143329	4.6902e-04	5.9084e-03	5.9084e-03	1.6505e-02
4.4668e+00	130426	3.8039e-04	5.3765e-03	5.3765e-03	1.6852e-02
5.0119e+00	117683	3.0590e-04	4.8512e-03	4.8512e-03	1.7061e-02
5.6234e+00	107062	2.4803e-04	4.4134e-03	4.4134e-03	1.7415e-02
6.3096e+00	97084	2.0045e-04	4.0021e-03	4.0021e-03	1.7718e-02
7.0795e+00	87130	1.6034e-04	3.5917e-03	3.5917e-03	1.7842e-02
7.9433e+00	78021	1.2796e-04	3.2162e-03	3.2162e-03	1.7926e-02
8.9125e+00	66465	9.7152e-05	2.7399e-03	2.7399e-03	1.7135e-02
1.0000e+01	55474	7.2269e-05	2.2868e-03	2.2868e-03	1.6046e-02
1.1220e+01	46742	5.4271e-05	1.9268e-03	1.9268e-03	1.5170e-02
1.2589e+01	39629	4.1009e-05	1.6336e-03	1.6336e-03	1.4431e-02
1.4125e+01	34108	3.1457e-05	1.4060e-03	1.4060e-03	1.3936e-02
1.5849e+01	29711	2.4422e-05	1.2248e-03	1.2248e-03	1.3621e-02
1.7783e+01	26418	1.9354e-05	1.0890e-03	1.0890e-03	1.3589e-02
1.9953e+01	23223	1.5163e-05	9.5732e-04	9.5732e-04	1.3403e-02
2.2387e+01	20563	1.1966e-05	8.4766e-04	8.4766e-04	1.3316e-02
2.5119e+01	18304	9.4931e-06	7.5454e-04	7.5454e-04	1.3299e-02
2.8184e+01	16145	7.4628e-06	6.6554e-04	6.6554e-04	1.3162e-02
3.1623e+01	14977	6.1700e-06	6.1739e-04	6.1739e-04	1.3699e-02
3.5481e+01	13386	4.9149e-06	5.5181e-04	5.5181e-04	1.3738e-02
3.9811e+01	12071	3.9501e-06	4.9760e-04	4.9760e-04	1.3900e-02
4.4668e+01	10770	3.1411e-06	4.4397e-04	4.4397e-04	1.3915e-02
5.0119e+01	9343	2.4286e-06	3.8514e-04	3.8514e-04	1.3545e-02
5.6234e+01	7912	1.8329e-06	3.2615e-04	3.2615e-04	1.2870e-02
6.3096e+01	6759	1.3955e-06	2.7862e-04	2.7862e-04	1.2336e-02
7.0795e+01	5633	1.0366e-06	2.3221e-04	2.3221e-04	1.1535e-02
7.9433e+01	5044	8.2725e-07	2.0793e-04	2.0793e-04	1.1589e-02
8.9125e+01	4393	6.4213e-07	1.8109e-04	1.8109e-04	1.1325e-02
1.0000e+02	4011	5.2253e-07	1.6534e-04	1.6534e-04	1.1602e-02
1.1220e+02	3836	4.4539e-07	1.5813e-04	1.5813e-04	1.2450e-02
1.2589e+02	3866	4.0006e-07	1.5937e-04	1.5937e-04	1.4078e-02
1.4125e+02	3753	3.4613e-07	1.5471e-04	1.5471e-04	1.5334e-02
1.5849e+02	3551	2.9188e-07	1.4638e-04	1.4638e-04	1.6279e-02
1.7783e+02	2979	2.1824e-07	1.2280e-04	1.2280e-04	1.5323e-02
1.9953e+02	2226	1.4534e-07	9.1762e-05	9.1762e-05	1.2847e-02
2.2387e+02	1863	1.0841e-07	7.6798e-05	7.6798e-05	1.2064e-02
2.5119e+02	1362	7.0638e-08	5.6145e-05	5.6145e-05	9.8959e-03
2.8184e+02	1237	5.7178e-08	5.0993e-05	5.0993e-05	1.0084e-02
3.1623e+02	1021	4.2062e-08	4.2088e-05	4.2088e-05	9.3391e-03
3.5481e+02	775	2.8455e-08	3.1948e-05	3.1948e-05	7.9539e-03
3.9811e+02	573	1.8751e-08	2.3621e-05	2.3621e-05	6.5983e-03
4.4668e+02	433	1.2628e-08	1.7849e-05	1.7849e-05	5.5946e-03
5.0119e+02	354	9.2016e-09	1.4593e-05	1.4593e-05	5.1319e-03
5.6234e+02	275	6.3708e-09	1.1336e-05	1.1336e-05	4.4731e-03
6.3096e+02	219	4.5217e-09	9.0278e-06	9.0278e-06	3.9969e-03
7.0795e+02	184	3.3859e-09	7.5850e-06	7.5850e-06	3.7679e-03
7.9433e+02	149	2.4437e-09	6.1422e-06	6.1422e-06	3.4235e-03
8.9125e+02	105	1.5348e-09	4.3284e-06	4.3284e-06	2.7069e-03
1.0000e+03	400	5.2110e-09	1.6489e-05	1.6489e-05	1.1570e-02

APPENDIX C

SURFACE OF MARS LINEAL ENERGY DISTRIBUTIONS

This appendix contains the y distributions for the combined (downward plus albedo) components of the particle fluence for the TEPC positioned 1 m above the surface of Mars. The figures show a plot of $yd(y)$ as a function of y on a semi-log axis. $\bar{y}_{\mathrm{F}}$, $\bar{y}_{\mathrm{D}}$, D, H, and $\bar{Q}$ for the simulated irradiation are included in the tabulated data. D and H represent integral values for 1.0×10^8 incident particles. These 1.0×10^8 particles, 1.0×10^8 histories in FLUKA, correspond to a simulated irradiation time of 0.545 y. Dividing D and H by 0.545 will normalize these values to time in the form of $\dot{D}$ and $\dot{H}$ with units of Gy/y and Sv/y, respectively. The $f(y)$, $d(y)$, $yf(y)$, and $yd(y)$ distributions have all been normalized to unit area.

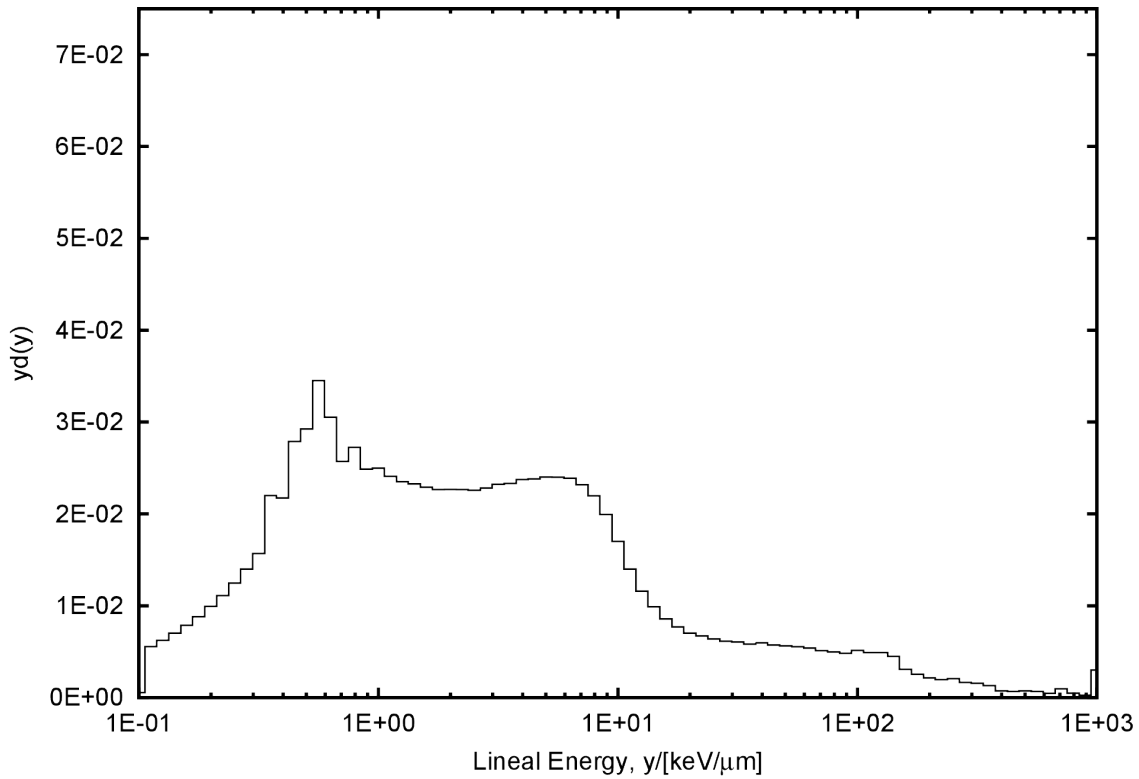

Figure C.1. Lineal energy distribution for the TEPC on the surface of Mars. This distribution contains all particle types.

Surface of Mars, all particle types:

```
# Using 80 Log Bins
# Min: 0.1 keV/μm              Max: 1000 keV/μm              20 bins/decade
#
# SiteSize: 1 μm               Mean Chord Length: 0.667 μm
#
# Using y Output with units of [keV/μm]
#
# y_F = 0.870 keV/μm
# y_D = 18.387 keV/μm
#
# D     = 3.500e-02 Gy
# H     = 1.007e-01 Sv
# Q_avg = 2.876e+00
#
# N = 32862971
#
# y [keV/μm] N(y)     f(y)         y*f(y)       d(y)         y*d(y)
1.0000e-01   1367046  1.4096e-02   4.6980e-03   4.6980e-03   5.3986e-04
1.1220e-01   1367046  1.1552e-01   4.3200e-02   4.3200e-02   5.5700e-03
1.2589e-01   1367046  1.0296e-01   4.3200e-02   4.3200e-02   6.2496e-03
1.4125e-01   1367046  9.1765e-02   4.3200e-02   4.3200e-02   7.0122e-03
1.5849e-01   1367046  8.1785e-02   4.3200e-02   4.3200e-02   7.8678e-03
1.7783e-01   1367046  7.2891e-02   4.3200e-02   4.3200e-02   8.8278e-03
1.9953e-01   1367046  6.4964e-02   4.3200e-02   4.3200e-02   9.9050e-03
2.2387e-01   1367046  5.7900e-02   4.3200e-02   4.3200e-02   1.1114e-02
2.5119e-01   1367046  5.1603e-02   4.3200e-02   4.3200e-02   1.2470e-02
2.8184e-01   1367046  4.5991e-02   4.3200e-02   4.3200e-02   1.3991e-02
3.1623e-01   1367046  4.0990e-02   4.3200e-02   4.3200e-02   1.5698e-02
3.5481e-01   1708587  4.5659e-02   5.3993e-02   5.3993e-02   2.2014e-02
3.9811e-01   1502577  3.5787e-02   4.7483e-02   4.7483e-02   2.1722e-02
4.4668e-01   1718319  3.6475e-02   5.4301e-02   5.4301e-02   2.7872e-02
5.0119e-01   1607305  3.0408e-02   5.0792e-02   5.0792e-02   2.9253e-02
5.6234e-01   1689752  2.8491e-02   5.3398e-02   5.3398e-02   3.4506e-02
6.3096e-01   1332110  2.0019e-02   4.2096e-02   4.2096e-02   3.0522e-02
7.0795e-01   999921   1.3392e-02   3.1598e-02   3.1598e-02   2.5706e-02
7.9433e-01   944552   1.1275e-02   2.9849e-02   2.9849e-02   2.7246e-02
8.9125e-01   767925   8.1698e-03   2.4267e-02   2.4267e-02   2.4854e-02
1.0000e+00   687305   6.5169e-03   2.1720e-02   2.1720e-02   2.4959e-02
1.1220e+00   591647   4.9998e-03   1.8697e-02   1.8697e-02   2.4106e-02
1.2589e+00   514184   3.8727e-03   1.6249e-02   1.6249e-02   2.3507e-02
1.4125e+00   453573   3.0447e-03   1.4333e-02   1.4333e-02   2.3266e-02
1.5849e+00   398005   2.3811e-03   1.2577e-02   1.2577e-02   2.2907e-02
1.7783e+00   350722   1.8701e-03   1.1083e-02   1.1083e-02   2.2648e-02
1.9953e+00   312894   1.4869e-03   9.8878e-03   9.8878e-03   2.2671e-02
2.2387e+00   278668   1.1803e-03   8.8062e-03   8.8062e-03   2.2655e-02
2.5119e+00   247326   9.3360e-04   7.8157e-03   7.8157e-03   2.2560e-02
2.8184e+00   222991   7.5020e-04   7.0467e-03   7.0467e-03   2.2822e-02
3.1623e+00   202215   6.0633e-04   6.3902e-03   6.3902e-03   2.3221e-02
```

3.5481e+00	180856	4.8331e-04	5.7152e-03	5.7152e-03	2.3303e-02
3.9811e+00	164309	3.9134e-04	5.1923e-03	5.1923e-03	2.3754e-02
4.4668e+00	146768	3.1155e-04	4.6380e-03	4.6380e-03	2.3807e-02
5.0119e+00	131949	2.4963e-04	4.1697e-03	4.1697e-03	2.4015e-02
5.6234e+00	117469	1.9807e-04	3.7121e-03	3.7121e-03	2.3988e-02
6.3096e+00	104196	1.5658e-04	3.2927e-03	3.2927e-03	2.3874e-02
7.0795e+00	90193	1.2080e-04	2.8502e-03	2.8502e-03	2.3187e-02
7.9433e+00	76098	9.0838e-05	2.4048e-03	2.4048e-03	2.1950e-02
8.9125e+00	61641	6.5579e-05	1.9479e-03	1.9479e-03	1.9950e-02
1.0000e+01	46841	4.4414e-05	1.4802e-03	1.4802e-03	1.7010e-02
1.1220e+01	34365	2.9041e-05	1.0860e-03	1.0860e-03	1.4002e-02
1.2589e+01	25335	1.9082e-05	8.0061e-04	8.0061e-04	1.1582e-02
1.4125e+01	19279	1.2941e-05	6.0924e-04	6.0924e-04	9.8891e-03
1.5849e+01	14876	8.8998e-06	4.7010e-04	4.7010e-04	8.5616e-03
1.7783e+01	11917	6.3542e-06	3.7659e-04	3.7659e-04	7.6955e-03
1.9953e+01	9685	4.6025e-06	3.0606e-04	3.0606e-04	7.0173e-03
2.2387e+01	8269	3.5022e-06	2.6131e-04	2.6131e-04	6.7224e-03
2.5119e+01	6998	2.6416e-06	2.2114e-04	2.2114e-04	6.3833e-03
2.8184e+01	5997	2.0176e-06	1.8951e-04	1.8951e-04	6.1377e-03
3.1623e+01	5266	1.5790e-06	1.6641e-04	1.6641e-04	6.0472e-03
3.5481e+01	4531	1.2108e-06	1.4318e-04	1.4318e-04	5.8380e-03
3.9811e+01	4138	9.8556e-07	1.3076e-04	1.3076e-04	5.9822e-03
4.4668e+01	3532	7.4974e-07	1.1161e-04	1.1161e-04	5.7292e-03
5.0119e+01	3102	5.8686e-07	9.8026e-05	9.8026e-05	5.6456e-03
5.6234e+01	2711	4.5711e-07	8.5670e-05	8.5670e-05	5.5361e-03
6.3096e+01	2356	3.5405e-07	7.4452e-05	7.4452e-05	5.3982e-03
7.0795e+01	1987	2.6613e-07	6.2791e-05	6.2791e-05	5.1082e-03
7.9433e+01	1727	2.0615e-07	5.4575e-05	5.4575e-05	4.9815e-03
8.9125e+01	1497	1.5926e-07	4.7307e-05	4.7307e-05	4.8450e-03
1.0000e+02	1416	1.3426e-07	4.4747e-05	4.4747e-05	5.1420e-03
1.1220e+02	1206	1.0192e-07	3.8111e-05	3.8111e-05	4.9138e-03
1.2589e+02	1074	8.0890e-08	3.3939e-05	3.3939e-05	4.9099e-03
1.4125e+02	877	5.8870e-08	2.7714e-05	2.7714e-05	4.4985e-03
1.5849e+02	538	3.2187e-08	1.7001e-05	1.7001e-05	3.0964e-03
1.7783e+02	391	2.0848e-08	1.2356e-05	1.2356e-05	2.5249e-03
1.9953e+02	298	1.4161e-08	9.4171e-06	9.4171e-06	2.1592e-03
2.2387e+02	240	1.0165e-08	7.5842e-06	7.5842e-06	1.9511e-03
2.5119e+02	228	8.6065e-09	7.2050e-06	7.2050e-06	2.0797e-03
2.8184e+02	162	5.4501e-09	5.1194e-06	5.1194e-06	1.6580e-03
3.1623e+02	136	4.0778e-09	4.2977e-06	4.2977e-06	1.5617e-03
3.5481e+02	101	2.6991e-09	3.1917e-06	3.1917e-06	1.3013e-03
3.9811e+02	51	1.2147e-09	1.6116e-06	1.6116e-06	7.3729e-04
4.4668e+02	42	8.9154e-10	1.3272e-06	1.3272e-06	6.8127e-04
5.0119e+02	41	7.7567e-10	1.2956e-06	1.2956e-06	7.4620e-04
5.6234e+02	34	5.7329e-10	1.0744e-06	1.0744e-06	6.9430e-04
6.3096e+02	20	3.0055e-10	6.3202e-07	6.3202e-07	4.5825e-04
7.0795e+02	37	4.9556e-10	1.1692e-06	1.1692e-06	9.5120e-04
7.9433e+02	16	1.9099e-10	5.0562e-07	5.0562e-07	4.6152e-04
8.9125e+02	8	8.5110e-11	2.5281e-07	2.5281e-07	2.5892e-04
1.0000e+03	83	7.8699e-10	2.6229e-06	2.6229e-06	3.0140e-03

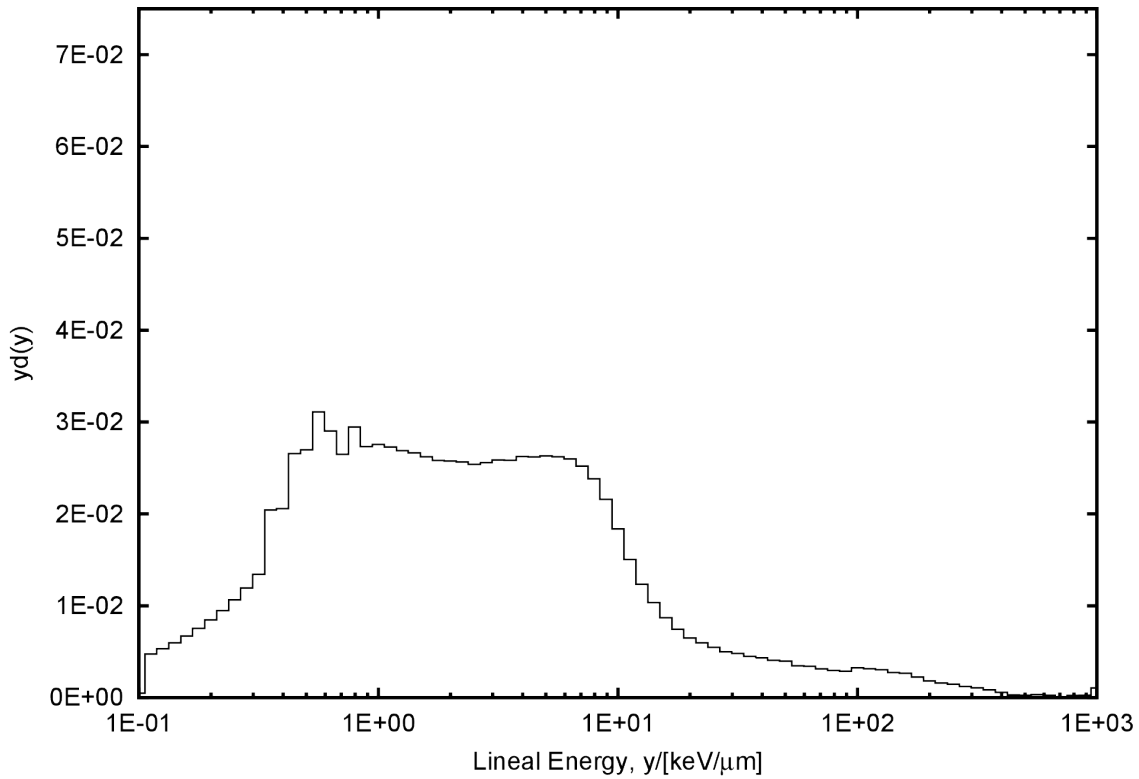

Figure C.2. Lineal energy distribution for the TEPC on the surface of Mars, elemental ion component.

Surface of Mars, elemental ion component:

```
# Using 80 Log Bins
# Min: 0.1 keV/μm              Max: 1000 keV/μm              20 bins/decade
#
# SiteSize: 1 μm               Mean Chord Length: 0.667 μm
#
# Using y Output with units of [keV/μm]
#
# y_F = 0.923 keV/μm
# y_D = 12.222 keV/μm
#
# D     = 2.531e-02 Gy
# H     = 5.790e-02 Sv
# Q_avg = 2.288e+00
#
# N = 22331110
#
# y [keV/μm] N(y)     f(y)         y*f(y)       d(y)         y*d(y)
1.0000e-01   844385   1.3604e-02   4.2554e-03   4.2554e-03   4.6080e-04
1.1220e-01   844385   1.1149e-01   3.9131e-02   3.9131e-02   4.7543e-03
1.2589e-01   844385   9.9366e-02   3.9131e-02   3.9131e-02   5.3345e-03
1.4125e-01   844385   8.8560e-02   3.9131e-02   3.9131e-02   5.9854e-03
1.5849e-01   844385   7.8929e-02   3.9131e-02   3.9131e-02   6.7157e-03
1.7783e-01   844385   7.0346e-02   3.9131e-02   3.9131e-02   7.5351e-03
1.9953e-01   844385   6.2696e-02   3.9131e-02   3.9131e-02   8.4546e-03
2.2387e-01   844385   5.5878e-02   3.9131e-02   3.9131e-02   9.4862e-03
2.5119e-01   844385   4.9801e-02   3.9131e-02   3.9131e-02   1.0644e-02
2.8184e-01   844385   4.4385e-02   3.9131e-02   3.9131e-02   1.1942e-02
3.1623e-01   844385   3.9558e-02   3.9131e-02   3.9131e-02   1.3400e-02
3.5481e-01   1147249  4.7902e-02   5.3166e-02   5.3166e-02   2.0427e-02
3.9811e-01   1029725  3.8319e-02   4.7720e-02   4.7720e-02   2.0572e-02
4.4668e-01   1185436  3.9317e-02   5.4936e-02   5.4936e-02   2.6572e-02
5.0119e-01   1072864  3.1713e-02   4.9719e-02   4.9719e-02   2.6983e-02
5.6234e-01   1102024  2.9033e-02   5.1070e-02   5.1070e-02   3.1099e-02
6.3096e-01   916490   2.1519e-02   4.2472e-02   4.2472e-02   2.9019e-02
7.0795e-01   745428   1.5599e-02   3.4545e-02   3.4545e-02   2.6482e-02
7.9433e-01   738998   1.3783e-02   3.4247e-02   3.4247e-02   2.9457e-02
8.9125e-01   611099   1.0158e-02   2.8320e-02   2.8320e-02   2.7331e-02
1.0000e+00   549708   8.1438e-03   2.5475e-02   2.5475e-02   2.7586e-02
1.1220e+00   484498   6.3972e-03   2.2453e-02   2.2453e-02   2.7280e-02
1.2589e+00   425546   5.0078e-03   1.9721e-02   1.9721e-02   2.6884e-02
1.4125e+00   376088   3.9445e-03   1.7429e-02   1.7429e-02   2.6659e-02
1.5849e+00   329473   3.0798e-03   1.5269e-02   1.5269e-02   2.6204e-02
1.7783e+00   289550   2.4122e-03   1.3418e-02   1.3418e-02   2.5839e-02
1.9953e+00   257368   1.9110e-03   1.1927e-02   1.1927e-02   2.5769e-02
2.2387e+00   228346   1.5111e-03   1.0582e-02   1.0582e-02   2.5653e-02
2.5119e+00   201364   1.1876e-03   9.3317e-03   9.3317e-03   2.5382e-02
2.8184e+00   180974   9.5129e-04   8.3868e-03   8.3868e-03   2.5596e-02
3.1623e+00   162937   7.6334e-04   7.5509e-03   7.5509e-03   2.5857e-02
```

3.5481e+00	145197	6.0625e-04	6.7288e-03	6.7288e-03	2.5853e-02
3.9811e+00	131489	4.8931e-04	6.0935e-03	6.0935e-03	2.6269e-02
4.4668e+00	116873	3.8762e-04	5.4162e-03	5.4162e-03	2.6198e-02
5.0119e+00	104621	3.0925e-04	4.8484e-03	4.8484e-03	2.6313e-02
5.6234e+00	92955	2.4489e-04	4.3077e-03	4.3077e-03	2.6231e-02
6.3096e+00	82057	1.9267e-04	3.8027e-03	3.8027e-03	2.5982e-02
7.0795e+00	70938	1.4845e-04	3.2874e-03	3.2874e-03	2.5202e-02
7.9433e+00	59755	1.1145e-04	2.7692e-03	2.7692e-03	2.3819e-02
8.9125e+00	48278	8.0250e-05	2.2373e-03	2.2373e-03	2.1592e-02
1.0000e+01	36629	5.4265e-05	1.6975e-03	1.6975e-03	1.8381e-02
1.1220e+01	26739	3.5306e-05	1.2391e-03	1.2391e-03	1.5056e-02
1.2589e+01	19524	2.2976e-05	9.0479e-04	9.0479e-04	1.2334e-02
1.4125e+01	14585	1.5297e-05	6.7590e-04	6.7590e-04	1.0338e-02
1.5849e+01	10940	1.0226e-05	5.0698e-04	5.0698e-04	8.7010e-03
1.7783e+01	8334	6.9431e-06	3.8622e-04	3.8622e-04	7.4371e-03
1.9953e+01	6501	4.8270e-06	3.0127e-04	3.0127e-04	6.5092e-03
2.2387e+01	5308	3.5126e-06	2.4599e-04	2.4599e-04	5.9632e-03
2.5119e+01	4355	2.5685e-06	2.0182e-04	2.0182e-04	5.4896e-03
2.8184e+01	3532	1.8566e-06	1.6368e-04	1.6368e-04	4.9954e-03
3.1623e+01	3033	1.4209e-06	1.4056e-04	1.4056e-04	4.8131e-03
3.5481e+01	2531	1.0568e-06	1.1729e-04	1.1729e-04	4.5065e-03
3.9811e+01	2178	8.1050e-07	1.0093e-04	1.0093e-04	4.3512e-03
4.4668e+01	1814	6.0164e-07	8.4065e-05	8.4065e-05	4.0662e-03
5.0119e+01	1575	4.6556e-07	7.2989e-05	7.2989e-05	3.9612e-03
5.6234e+01	1225	3.2273e-07	5.6769e-05	5.6769e-05	3.4569e-03
6.3096e+01	1081	2.5382e-07	5.0096e-05	5.0096e-05	3.4228e-03
7.0795e+01	882	1.8457e-07	4.0874e-05	4.0874e-05	3.1334e-03
7.9433e+01	738	1.3764e-07	3.4201e-05	3.4201e-05	2.9418e-03
8.9125e+01	639	1.0622e-07	2.9613e-05	2.9613e-05	2.8579e-03
1.0000e+02	647	9.5852e-08	2.9983e-05	2.9983e-05	3.2468e-03
1.1220e+02	560	7.3941e-08	2.5952e-05	2.5952e-05	3.1531e-03
1.2589e+02	478	5.6250e-08	2.2152e-05	2.2152e-05	3.0198e-03
1.4125e+02	386	4.0484e-08	1.7888e-05	1.7888e-05	2.7361e-03
1.5849e+02	334	3.1221e-08	1.5478e-05	1.5478e-05	2.6564e-03
1.7783e+02	251	2.0911e-08	1.1632e-05	1.1632e-05	2.2399e-03
1.9953e+02	181	1.3439e-08	8.3880e-06	8.3880e-06	1.8123e-03
2.2387e+02	141	9.3307e-09	6.5343e-06	6.5343e-06	1.5841e-03
2.5119e+02	115	6.7826e-09	5.3294e-06	5.3294e-06	1.4496e-03
2.8184e+02	86	4.5206e-09	3.9854e-06	3.9854e-06	1.2163e-03
3.1623e+02	68	3.1857e-09	3.1513e-06	3.1513e-06	1.0791e-03
3.5481e+02	48	2.0042e-09	2.2244e-06	2.2244e-06	8.5466e-04
3.9811e+02	29	1.0792e-09	1.3439e-06	1.3439e-06	5.7936e-04
4.4668e+02	13	4.3116e-10	6.0245e-07	6.0245e-07	2.9140e-04
5.0119e+02	10	2.9560e-10	4.6342e-07	4.6342e-07	2.5151e-04
5.6234e+02	12	3.1614e-10	5.5611e-07	5.5611e-07	3.3863e-04
6.3096e+02	9	2.1132e-10	4.1708e-07	4.1708e-07	2.8497e-04
7.0795e+02	3	6.2780e-11	1.3903e-07	1.3903e-07	1.0658e-04
7.9433e+02	6	1.1190e-10	2.7805e-07	2.7805e-07	2.3917e-04
8.9125e+02	6	9.9735e-11	2.7805e-07	2.7805e-07	2.6835e-04
1.0000e+03	21	3.1111e-10	9.7319e-07	9.7319e-07	1.0538e-03

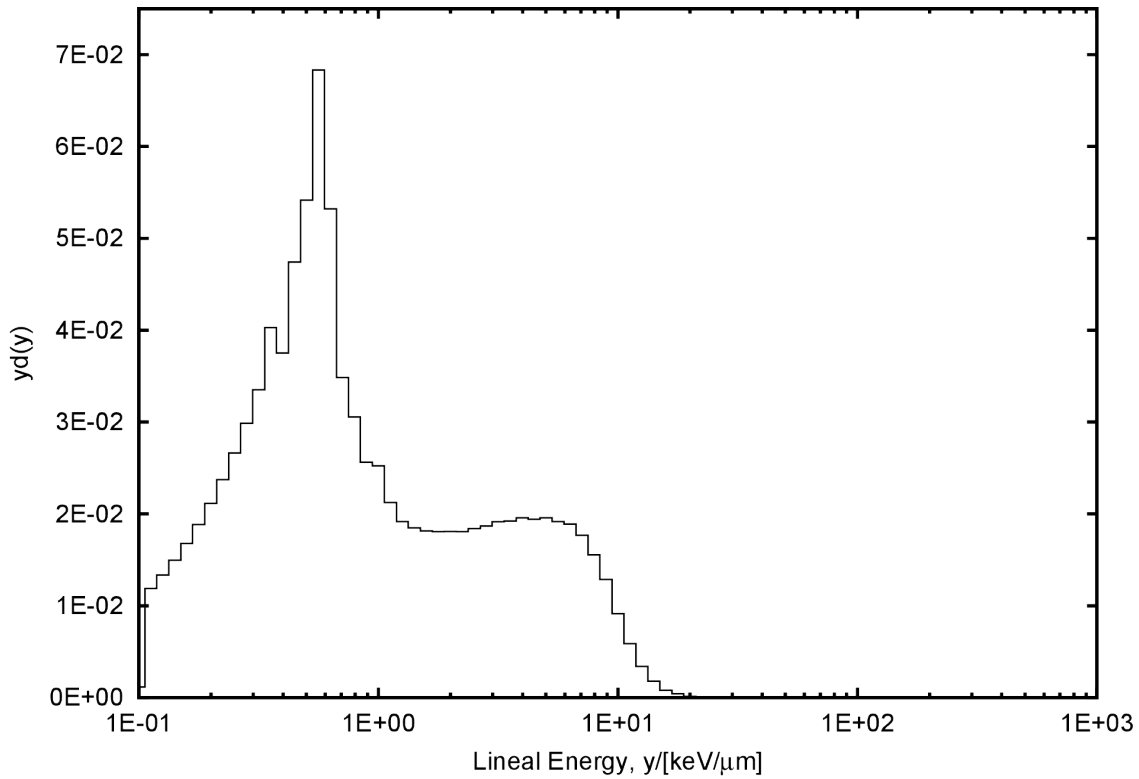

Figure C.3. Lineal energy distribution for the TEPC on the surface of Mars, electron component.

Surface of Mars, electron component:

```
# Using 80 Log Bins
# Min: 0.1 keV/μm              Max: 1000 keV/μm               20 bins/decade
#
# SiteSize: 1 μm               Mean Chord Length: 0.667 μm
#
# Using y Output with units of [keV/μm]
#
# y_F = 0.505 keV/μm
# y_D = 1.835 keV/μm
#
# D     = 5.173e-03 Gy
# H     = 5.228e-03 Sv
# Q_avg = 1.011e+00
#
# N = 8401054
#
# y [keV/μm] N(y)     f(y)         y*f(y)      d(y)         y*d(y)
1.0000e-01   429279   1.5041e-02  5.8220e-03  5.8220e-03  1.1525e-03
1.1220e-01   429279   1.2327e-01  5.3536e-02  5.3536e-02  1.1891e-02
1.2589e-01   429279   1.0986e-01  5.3536e-02  5.3536e-02  1.3342e-02
1.4125e-01   429279   9.7917e-02  5.3536e-02  5.3536e-02  1.4970e-02
1.5849e-01   429279   8.7269e-02  5.3536e-02  5.3536e-02  1.6797e-02
1.7783e-01   429279   7.7778e-02  5.3536e-02  5.3536e-02  1.8846e-02
1.9953e-01   429279   6.9320e-02  5.3536e-02  5.3536e-02  2.1146e-02
2.2387e-01   429279   6.1781e-02  5.3536e-02  5.3536e-02  2.3726e-02
2.5119e-01   429279   5.5063e-02  5.3536e-02  5.3536e-02  2.6621e-02
2.8184e-01   429279   4.9075e-02  5.3536e-02  5.3536e-02  2.9870e-02
3.1623e-01   429279   4.3738e-02  5.3536e-02  5.3536e-02  3.3514e-02
3.5481e-01   460056   4.1776e-02  5.7375e-02  5.7375e-02  4.0300e-02
3.9811e-01   381684   3.0890e-02  4.7601e-02  4.7601e-02  3.7514e-02
4.4668e-01   430001   3.1016e-02  5.3626e-02  5.3626e-02  4.7420e-02
5.0119e-01   437838   2.8147e-02  5.4604e-02  5.4604e-02  5.4176e-02
5.6234e-01   492062   2.8193e-02  6.1366e-02  6.1366e-02  6.8314e-02
6.3096e-01   341580   1.7443e-02  4.2599e-02  4.2599e-02  5.3209e-02
7.0795e-01   199292   9.0700e-03  2.4854e-02  2.4854e-02  3.4832e-02
7.9433e-01   155837   6.3210e-03  1.9435e-02  1.9435e-02  3.0560e-02
8.9125e-01   116414   4.2085e-03  1.4518e-02  1.4518e-02  2.5615e-02
1.0000e+00   102240   3.2941e-03  1.2751e-02  1.2751e-02  2.5241e-02
1.1220e+00   76607    2.1998e-03  9.5538e-03  9.5538e-03  2.1221e-02
1.2589e+00   61620    1.5770e-03  7.6848e-03  7.6848e-03  1.9152e-02
1.4125e+00   52971    1.2082e-03  6.6061e-03  6.6061e-03  1.8473e-02
1.5849e+00   46399    9.4325e-04  5.7865e-03  5.7865e-03  1.8155e-02
1.7783e+00   41135    7.4530e-04  5.1300e-03  5.1300e-03  1.8059e-02
1.9953e+00   36697    5.9258e-04  4.5766e-03  4.5766e-03  1.8077e-02
2.2387e+00   32672    4.7021e-04  4.0746e-03  4.0746e-03  1.8058e-02
2.5119e+00   29669    3.8056e-04  3.7001e-03  3.7001e-03  1.8399e-02
2.8184e+00   26846    3.0690e-04  3.3480e-03  3.3480e-03  1.8680e-02
3.1623e+00   24504    2.4966e-04  3.0559e-03  3.0559e-03  1.9131e-02
```

3.5481e+00	21940	1.9923e-04	2.7362e-03	2.7362e-03	1.9219e-02
3.9811e+00	19903	1.6108e-04	2.4821e-03	2.4821e-03	1.9562e-02
4.4668e+00	17608	1.2701e-04	2.1959e-03	2.1959e-03	1.9418e-02
5.0119e+00	15820	1.0170e-04	1.9729e-03	1.9729e-03	1.9575e-02
5.6234e+00	13809	7.9119e-05	1.7222e-03	1.7222e-03	1.9171e-02
6.3096e+00	12125	6.1916e-05	1.5121e-03	1.5121e-03	1.8887e-02
7.0795e+00	10109	4.6007e-05	1.2607e-03	1.2607e-03	1.7668e-02
7.9433e+00	7931	3.2170e-05	9.8909e-04	9.8909e-04	1.5553e-02
8.9125e+00	5847	2.1137e-05	7.2919e-04	7.2919e-04	1.2865e-02
1.0000e+01	3706	1.1941e-05	4.6218e-04	4.6218e-04	9.1495e-03
1.1220e+01	2120	6.0877e-06	2.6439e-04	2.6439e-04	5.8725e-03
1.2589e+01	1097	2.8075e-06	1.3681e-04	1.3681e-04	3.4095e-03
1.4125e+01	509	1.1610e-06	6.3479e-05	6.3479e-05	1.7750e-03
1.5849e+01	200	4.0658e-07	2.4942e-05	2.4942e-05	7.8256e-04
1.7783e+01	99	1.7937e-07	1.2347e-05	1.2347e-05	4.3464e-04
1.9953e+01	26	4.1985e-08	3.2425e-06	3.2425e-06	1.2807e-04
2.2387e+01	10	1.4392e-08	1.2471e-06	1.2471e-06	5.5270e-05
2.5119e+01	1	1.2827e-09	1.2471e-07	1.2471e-07	6.2014e-06
2.8184e+01	1	1.1432e-09	1.2471e-07	1.2471e-07	6.9581e-06
3.1623e+01	0	0.0000e+00	0.0000e+00	0.0000e+00	0.0000e+00
3.5481e+01	0	0.0000e+00	0.0000e+00	0.0000e+00	0.0000e+00
3.9811e+01	0	0.0000e+00	0.0000e+00	0.0000e+00	0.0000e+00
4.4668e+01	0	0.0000e+00	0.0000e+00	0.0000e+00	0.0000e+00
5.0119e+01	0	0.0000e+00	0.0000e+00	0.0000e+00	0.0000e+00
5.6234e+01	0	0.0000e+00	0.0000e+00	0.0000e+00	0.0000e+00
6.3096e+01	0	0.0000e+00	0.0000e+00	0.0000e+00	0.0000e+00
7.0795e+01	0	0.0000e+00	0.0000e+00	0.0000e+00	0.0000e+00
7.9433e+01	0	0.0000e+00	0.0000e+00	0.0000e+00	0.0000e+00
8.9125e+01	0	0.0000e+00	0.0000e+00	0.0000e+00	0.0000e+00
1.0000e+02	0	0.0000e+00	0.0000e+00	0.0000e+00	0.0000e+00
1.1220e+02	0	0.0000e+00	0.0000e+00	0.0000e+00	0.0000e+00
1.2589e+02	0	0.0000e+00	0.0000e+00	0.0000e+00	0.0000e+00
1.4125e+02	0	0.0000e+00	0.0000e+00	0.0000e+00	0.0000e+00
1.5849e+02	0	0.0000e+00	0.0000e+00	0.0000e+00	0.0000e+00
1.7783e+02	0	0.0000e+00	0.0000e+00	0.0000e+00	0.0000e+00
1.9953e+02	0	0.0000e+00	0.0000e+00	0.0000e+00	0.0000e+00
2.2387e+02	0	0.0000e+00	0.0000e+00	0.0000e+00	0.0000e+00
2.5119e+02	0	0.0000e+00	0.0000e+00	0.0000e+00	0.0000e+00
2.8184e+02	0	0.0000e+00	0.0000e+00	0.0000e+00	0.0000e+00
3.1623e+02	0	0.0000e+00	0.0000e+00	0.0000e+00	0.0000e+00
3.5481e+02	0	0.0000e+00	0.0000e+00	0.0000e+00	0.0000e+00
3.9811e+02	0	0.0000e+00	0.0000e+00	0.0000e+00	0.0000e+00
4.4668e+02	0	0.0000e+00	0.0000e+00	0.0000e+00	0.0000e+00
5.0119e+02	0	0.0000e+00	0.0000e+00	0.0000e+00	0.0000e+00
5.6234e+02	0	0.0000e+00	0.0000e+00	0.0000e+00	0.0000e+00
6.3096e+02	0	0.0000e+00	0.0000e+00	0.0000e+00	0.0000e+00
7.0795e+02	0	0.0000e+00	0.0000e+00	0.0000e+00	0.0000e+00
7.9433e+02	0	0.0000e+00	0.0000e+00	0.0000e+00	0.0000e+00
8.9125e+02	0	0.0000e+00	0.0000e+00	0.0000e+00	0.0000e+00
1.0000e+03	0	0.0000e+00	0.0000e+00	0.0000e+00	0.0000e+00

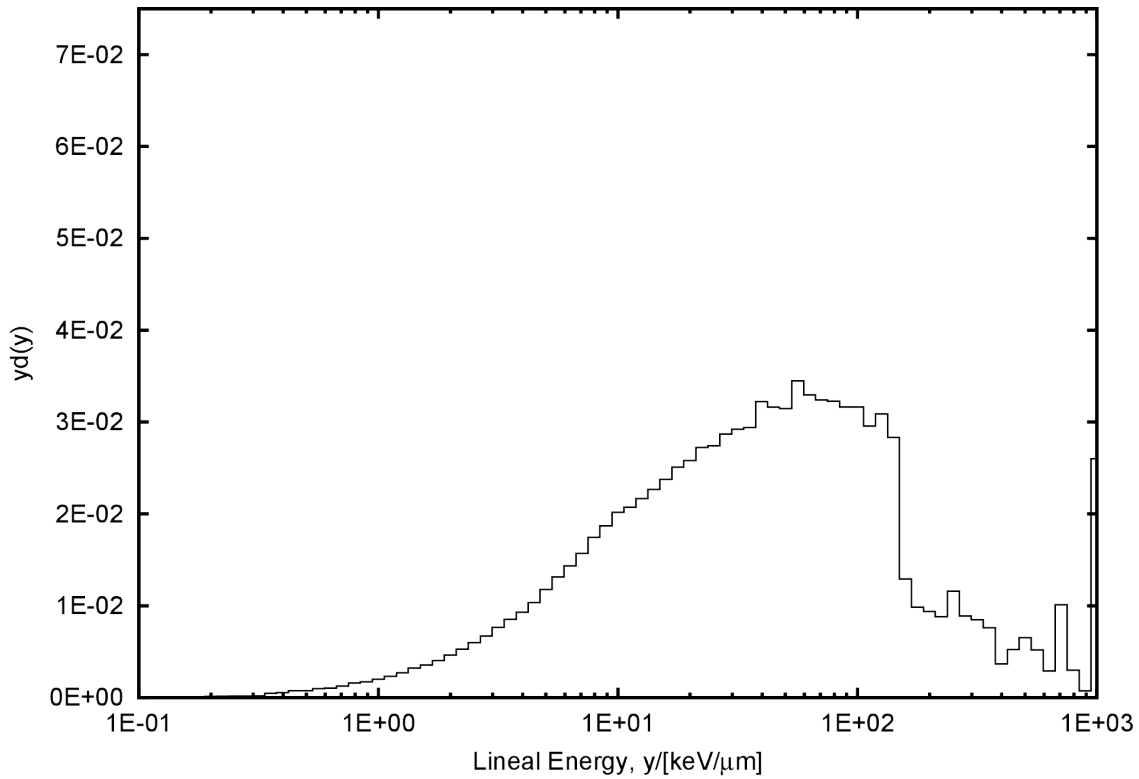

Figure C.4. Lineal energy distribution for the TEPC on the surface of Mars, neutron component.

Surface of Mars, neutron component:

```
# Using 80 Log Bins
# Min: 0.1 keV/μm              Max: 1000 keV/μm               20 bins/decade
#
# SiteSize: 1 μm               Mean Chord Length: 0.667 μm
#
# Using y Output with units of [keV/μm]
#
# y_F = 11.231 keV/μm
# y_D = 104.130 keV/μm
#
# D     = 3.015e-03 Gy
# H     = 3.528e-02 Sv
# Q_avg = 1.170e+01
#
# N = 213520
#
# y [keV/μm] N(y)     f(y)         y*f(y)       d(y)         y*d(y)
1.0000e-01   1482     8.2646e-03   7.5950e-04   7.5950e-04   6.7628e-06
1.1220e-01   1482     6.7732e-02   6.9840e-03   6.9840e-03   6.9776e-05
1.2589e-01   1482     6.0366e-02   6.9840e-03   6.9840e-03   7.8290e-05
1.4125e-01   1482     5.3802e-02   6.9840e-03   6.9840e-03   8.7842e-05
1.5849e-01   1482     4.7951e-02   6.9840e-03   6.9840e-03   9.8561e-05
1.7783e-01   1482     4.2736e-02   6.9840e-03   6.9840e-03   1.1059e-04
1.9953e-01   1482     3.8089e-02   6.9840e-03   6.9840e-03   1.2408e-04
2.2387e-01   1482     3.3946e-02   6.9840e-03   6.9840e-03   1.3922e-04
2.5119e-01   1482     3.0255e-02   6.9840e-03   6.9840e-03   1.5621e-04
2.8184e-01   1482     2.6965e-02   6.9840e-03   6.9840e-03   1.7527e-04
3.1623e-01   1482     2.4032e-02   6.9840e-03   6.9840e-03   1.9665e-04
3.5481e-01   3042     4.3965e-02   1.4336e-02   1.4336e-02   4.5291e-04
3.9811e-01   3162     4.0729e-02   1.4901e-02   1.4901e-02   5.2822e-04
4.4668e-01   4063     4.6644e-02   1.9147e-02   1.9147e-02   7.6156e-04
5.0119e-01   3660     3.7448e-02   1.7248e-02   1.7248e-02   7.6973e-04
5.6234e-01   4115     3.7525e-02   1.9392e-02   1.9392e-02   9.7101e-04
6.3096e-01   3952     3.2119e-02   1.8624e-02   1.8624e-02   1.0463e-03
7.0795e-01   4246     3.0756e-02   2.0010e-02   2.0010e-02   1.2614e-03
7.9433e-01   4763     3.0749e-02   2.2446e-02   2.2446e-02   1.5876e-03
8.9125e-01   4564     2.6260e-02   2.1508e-02   2.1508e-02   1.7069e-03
1.0000e+00   4774     2.4481e-02   2.2498e-02   2.2498e-02   2.0033e-03
1.1220e+00   4913     2.2454e-02   2.3153e-02   2.3153e-02   2.3131e-03
1.2589e+00   5108     2.0806e-02   2.4072e-02   2.4072e-02   2.6984e-03
1.4125e+00   5430     1.9713e-02   2.5589e-02   2.5589e-02   3.2185e-03
1.5849e+00   5340     1.7278e-02   2.5165e-02   2.5165e-02   3.5514e-03
1.7783e+00   5412     1.5606e-02   2.5504e-02   2.5504e-02   4.0384e-03
1.9953e+00   5535     1.4225e-02   2.6084e-02   2.6084e-02   4.6342e-03
2.2387e+00   5610     1.2850e-02   2.6437e-02   2.6437e-02   5.2701e-03
2.5119e+00   5691     1.1618e-02   2.6819e-02   2.6819e-02   5.9985e-03
2.8184e+00   5672     1.0320e-02   2.6730e-02   2.6730e-02   6.7080e-03
3.1623e+00   5771     9.3583e-03   2.7196e-02   2.7196e-02   7.6578e-03
```

3.5481e+00	5721	8.2683e-03	2.6961e-02	2.6961e-02	8.5178e-03
3.9811e+00	5572	7.1772e-03	2.6258e-02	2.6258e-02	9.3082e-03
4.4668e+00	5521	6.3382e-03	2.6018e-02	2.6018e-02	1.0348e-02
5.0119e+00	5595	5.7246e-03	2.6367e-02	2.6367e-02	1.1767e-02
5.6234e+00	5564	5.0738e-03	2.6221e-02	2.6221e-02	1.3129e-02
6.3096e+00	5416	4.4017e-03	2.5523e-02	2.5523e-02	1.4340e-02
7.0795e+00	5289	3.8311e-03	2.4925e-02	2.4925e-02	1.5712e-02
7.9433e+00	5239	3.3822e-03	2.4689e-02	2.4689e-02	1.7462e-02
8.9125e+00	5001	2.8774e-03	2.3567e-02	2.3567e-02	1.8703e-02
1.0000e+01	4806	2.4645e-03	2.2649e-02	2.2649e-02	2.0167e-02
1.1220e+01	4398	2.0100e-03	2.0726e-02	2.0726e-02	2.0707e-02
1.2589e+01	4104	1.6717e-03	1.9340e-02	1.9340e-02	2.1680e-02
1.4125e+01	3824	1.3882e-03	1.8021e-02	1.8021e-02	2.2666e-02
1.5849e+01	3575	1.1567e-03	1.6847e-02	1.6847e-02	2.3776e-02
1.7783e+01	3364	9.7007e-04	1.5853e-02	1.5853e-02	2.5102e-02
1.9953e+01	3083	7.9236e-04	1.4529e-02	1.4529e-02	2.5812e-02
2.2387e+01	2898	6.6381e-04	1.3657e-02	1.3657e-02	2.7224e-02
2.5119e+01	2601	5.3099e-04	1.2257e-02	1.2257e-02	2.7415e-02
2.8184e+01	2426	4.4141e-04	1.1433e-02	1.1433e-02	2.8691e-02
3.1623e+01	2201	3.5692e-04	1.0372e-02	1.0372e-02	2.9206e-02
3.5481e+01	1975	2.8544e-04	9.3073e-03	9.3073e-03	2.9405e-02
3.9811e+01	1930	2.4860e-04	9.0952e-03	9.0952e-03	3.2241e-02
4.4668e+01	1687	1.9367e-04	7.9501e-03	7.9501e-03	3.1621e-02
5.0119e+01	1496	1.5307e-04	7.0500e-03	7.0500e-03	3.1462e-02
5.6234e+01	1461	1.3323e-04	6.8850e-03	6.8850e-03	3.4475e-02
6.3096e+01	1245	1.0118e-04	5.8671e-03	5.8671e-03	3.2963e-02
7.0795e+01	1091	7.9026e-05	5.1414e-03	5.1414e-03	3.2410e-02
7.9433e+01	968	6.2492e-05	4.5618e-03	4.5618e-03	3.2265e-02
8.9125e+01	846	4.8676e-05	3.9868e-03	3.9868e-03	3.1639e-02
1.0000e+02	754	3.8665e-05	3.5533e-03	3.5533e-03	3.1639e-02
1.1220e+02	628	2.8702e-05	2.9595e-03	2.9595e-03	2.9568e-02
1.2589e+02	585	2.3829e-05	2.7568e-03	2.7568e-03	3.0904e-02
1.4125e+02	478	1.7353e-05	2.2526e-03	2.2526e-03	2.8332e-02
1.5849e+02	194	6.2769e-06	9.1424e-04	9.1424e-04	1.2902e-02
1.7783e+02	132	3.8065e-06	6.2206e-04	6.2206e-04	9.8498e-03
1.9953e+02	112	2.8785e-06	5.2781e-04	5.2781e-04	9.3772e-03
2.2387e+02	94	2.1532e-06	4.4298e-04	4.4298e-04	8.8305e-03
2.5119e+02	110	2.2456e-06	5.1838e-04	5.1838e-04	1.1594e-02
2.8184e+02	75	1.3646e-06	3.5344e-04	3.5344e-04	8.8699e-03
3.1623e+02	64	1.0378e-06	3.0160e-04	3.0160e-04	8.4925e-03
3.5481e+02	51	7.3708e-07	2.4034e-04	2.4034e-04	7.5932e-03
3.9811e+02	22	2.8338e-07	1.0368e-04	1.0368e-04	3.6752e-03
4.4668e+02	28	3.2144e-07	1.3195e-04	1.3195e-04	5.2482e-03
5.0119e+02	31	3.1718e-07	1.4609e-04	1.4609e-04	6.5195e-03
5.6234e+02	22	2.0062e-07	1.0368e-04	1.0368e-04	5.1913e-03
6.3096e+02	11	8.9400e-08	5.1838e-05	5.1838e-05	2.9124e-03
7.0795e+02	34	2.4628e-07	1.6023e-04	1.6023e-04	1.0100e-02
7.9433e+02	9	5.8102e-08	4.2413e-05	4.2413e-05	2.9998e-03
8.9125e+02	2	1.1507e-08	9.4251e-06	9.4251e-06	7.4797e-04
1.0000e+03	62	3.1793e-07	2.9218e-04	2.9218e-04	2.6016e-02

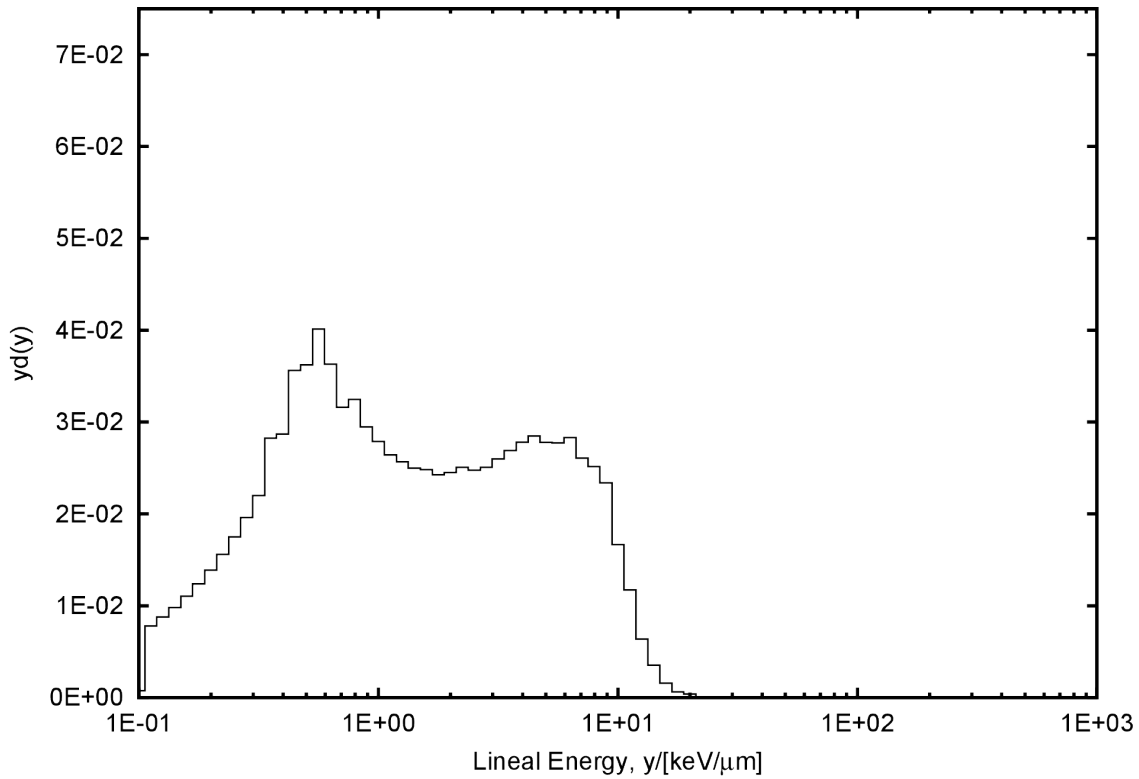

Figure C.5. Lineal energy distribution for the TEPC on the surface of Mars, photon component.

Surface of Mars, photon component:

```
# Using 80 Log Bins
# Min: 0.1 keV/μm              Max: 1000 keV/μm               20 bins/decade
#
# SiteSize: 1 μm               Mean Chord Length: 0.667 μm
#
# Using y Output with units of [keV/μm]
#
# y_F = 0.679 keV/μm
# y_D = 2.608 keV/μm
#
# D     = 6.264e-04 Gy
# H     = 6.392e-04 Sv
# Q_avg = 1.021e+00
#
# N = 755343
#
# y [keV/μm] N(y)     f(y)         y*f(y)      d(y)         y*d(y)
1.0000e-01   34251    1.4558e-02  5.1389e-03  5.1389e-03  7.5706e-04
1.1220e-01   34251    1.1931e-01  4.7255e-02  4.7255e-02  7.8110e-03
1.2589e-01   34251    1.0634e-01  4.7255e-02  4.7255e-02  8.7641e-03
1.4125e-01   34251    9.4773e-02  4.7255e-02  4.7255e-02  9.8335e-03
1.5849e-01   34251    8.4466e-02  4.7255e-02  4.7255e-02  1.1033e-02
1.7783e-01   34251    7.5281e-02  4.7255e-02  4.7255e-02  1.2380e-02
1.9953e-01   34251    6.7094e-02  4.7255e-02  4.7255e-02  1.3890e-02
2.2387e-01   34251    5.9798e-02  4.7255e-02  4.7255e-02  1.5585e-02
2.5119e-01   34251    5.3295e-02  4.7255e-02  4.7255e-02  1.7487e-02
2.8184e-01   34251    4.7499e-02  4.7255e-02  4.7255e-02  1.9620e-02
3.1623e-01   34251    4.2333e-02  4.7255e-02  4.7255e-02  2.2014e-02
3.5481e-01   39164    4.3142e-02  5.4033e-02  5.4033e-02  2.8244e-02
3.9811e-01   35453    3.4807e-02  4.8913e-02  4.8913e-02  2.8687e-02
4.4668e-01   39241    3.4336e-02  5.4139e-02  5.4139e-02  3.5627e-02
5.0119e-01   35566    2.7736e-02  4.9069e-02  4.9069e-02  3.6230e-02
5.6234e-01   35098    2.4395e-02  4.8423e-02  4.8423e-02  4.0116e-02
6.3096e-01   28320    1.7543e-02  3.9072e-02  3.9072e-02  3.6318e-02
7.0795e-01   21952    1.2119e-02  3.0286e-02  3.0286e-02  3.1587e-02
7.9433e-01   20119    9.8996e-03  2.7757e-02  2.7757e-02  3.2482e-02
8.9125e-01   16274    7.1368e-03  2.2453e-02  2.2453e-02  2.9480e-02
1.0000e+00   13709    5.3582e-03  1.8914e-02  1.8914e-02  2.7864e-02
1.1220e+00   11589    4.0370e-03  1.5989e-02  1.5989e-02  2.6429e-02
1.2589e+00   10036    3.1158e-03  1.3846e-02  1.3846e-02  2.5680e-02
1.4125e+00   8703     2.4081e-03  1.2007e-02  1.2007e-02  2.4986e-02
1.5849e+00   7705     1.9001e-03  1.0630e-02  1.0630e-02  2.4820e-02
1.7783e+00   6714     1.4757e-03  9.2630e-03  9.2630e-03  2.4267e-02
1.9953e+00   6045     1.1842e-03  8.3400e-03  8.3400e-03  2.4515e-02
2.2387e+00   5514     9.6267e-04  7.6074e-03  7.6074e-03  2.5090e-02
2.5119e+00   4853     7.5513e-04  6.6955e-03  6.6955e-03  2.4777e-02
2.8184e+00   4376     6.0686e-04  6.0374e-03  6.0374e-03  2.5067e-02
3.1623e+00   4044     4.9983e-04  5.5793e-03  5.5793e-03  2.5992e-02
```

3.5481e+00	3730	4.1088e-04	5.1461e-03	5.1461e-03	2.6899e-02
3.9811e+00	3435	3.3724e-04	4.7391e-03	4.7391e-03	2.7795e-02
4.4668e+00	3137	2.7449e-04	4.3280e-03	4.3280e-03	2.8481e-02
5.0119e+00	2726	2.1259e-04	3.7610e-03	3.7610e-03	2.7769e-02
5.6234e+00	2427	1.6869e-04	3.3484e-03	3.3484e-03	2.7740e-02
6.3096e+00	2209	1.3684e-04	3.0477e-03	3.0477e-03	2.8329e-02
7.0795e+00	1812	1.0004e-04	2.4999e-03	2.4999e-03	2.6073e-02
7.9433e+00	1558	7.6662e-05	2.1495e-03	2.1495e-03	2.5154e-02
8.9125e+00	1290	5.6572e-05	1.7798e-03	1.7798e-03	2.3368e-02
1.0000e+01	819	3.2011e-05	1.1299e-03	1.1299e-03	1.6646e-02
1.1220e+01	514	1.7905e-05	7.0914e-04	7.0914e-04	1.1722e-02
1.2589e+01	249	7.7305e-06	3.4354e-04	3.4354e-04	6.3714e-03
1.4125e+01	123	3.4034e-06	1.6970e-04	1.6970e-04	3.5313e-03
1.5849e+01	49	1.2084e-06	6.7603e-05	6.7603e-05	1.5784e-03
1.7783e+01	17	3.7365e-07	2.3454e-05	2.3454e-05	6.1444e-04
1.9953e+01	10	1.9589e-07	1.3797e-05	1.3797e-05	4.0554e-04
2.2387e+01	2	3.4917e-08	2.7593e-06	2.7593e-06	9.1005e-05
2.5119e+01	0	0.0000e+00	0.0000e+00	0.0000e+00	0.0000e+00
2.8184e+01	0	0.0000e+00	0.0000e+00	0.0000e+00	0.0000e+00
3.1623e+01	0	0.0000e+00	0.0000e+00	0.0000e+00	0.0000e+00
3.5481e+01	0	0.0000e+00	0.0000e+00	0.0000e+00	0.0000e+00
3.9811e+01	0	0.0000e+00	0.0000e+00	0.0000e+00	0.0000e+00
4.4668e+01	0	0.0000e+00	0.0000e+00	0.0000e+00	0.0000e+00
5.0119e+01	0	0.0000e+00	0.0000e+00	0.0000e+00	0.0000e+00
5.6234e+01	0	0.0000e+00	0.0000e+00	0.0000e+00	0.0000e+00
6.3096e+01	0	0.0000e+00	0.0000e+00	0.0000e+00	0.0000e+00
7.0795e+01	0	0.0000e+00	0.0000e+00	0.0000e+00	0.0000e+00
7.9433e+01	0	0.0000e+00	0.0000e+00	0.0000e+00	0.0000e+00
8.9125e+01	0	0.0000e+00	0.0000e+00	0.0000e+00	0.0000e+00
1.0000e+02	0	0.0000e+00	0.0000e+00	0.0000e+00	0.0000e+00
1.1220e+02	0	0.0000e+00	0.0000e+00	0.0000e+00	0.0000e+00
1.2589e+02	0	0.0000e+00	0.0000e+00	0.0000e+00	0.0000e+00
1.4125e+02	0	0.0000e+00	0.0000e+00	0.0000e+00	0.0000e+00
1.5849e+02	0	0.0000e+00	0.0000e+00	0.0000e+00	0.0000e+00
1.7783e+02	0	0.0000e+00	0.0000e+00	0.0000e+00	0.0000e+00
1.9953e+02	0	0.0000e+00	0.0000e+00	0.0000e+00	0.0000e+00
2.2387e+02	0	0.0000e+00	0.0000e+00	0.0000e+00	0.0000e+00
2.5119e+02	0	0.0000e+00	0.0000e+00	0.0000e+00	0.0000e+00
2.8184e+02	0	0.0000e+00	0.0000e+00	0.0000e+00	0.0000e+00
3.1623e+02	0	0.0000e+00	0.0000e+00	0.0000e+00	0.0000e+00
3.5481e+02	0	0.0000e+00	0.0000e+00	0.0000e+00	0.0000e+00
3.9811e+02	0	0.0000e+00	0.0000e+00	0.0000e+00	0.0000e+00
4.4668e+02	0	0.0000e+00	0.0000e+00	0.0000e+00	0.0000e+00
5.0119e+02	0	0.0000e+00	0.0000e+00	0.0000e+00	0.0000e+00
5.6234e+02	0	0.0000e+00	0.0000e+00	0.0000e+00	0.0000e+00
6.3096e+02	0	0.0000e+00	0.0000e+00	0.0000e+00	0.0000e+00
7.0795e+02	0	0.0000e+00	0.0000e+00	0.0000e+00	0.0000e+00
7.9433e+02	0	0.0000e+00	0.0000e+00	0.0000e+00	0.0000e+00
8.9125e+02	0	0.0000e+00	0.0000e+00	0.0000e+00	0.0000e+00
1.0000e+03	0	0.0000e+00	0.0000e+00	0.0000e+00	0.0000e+00

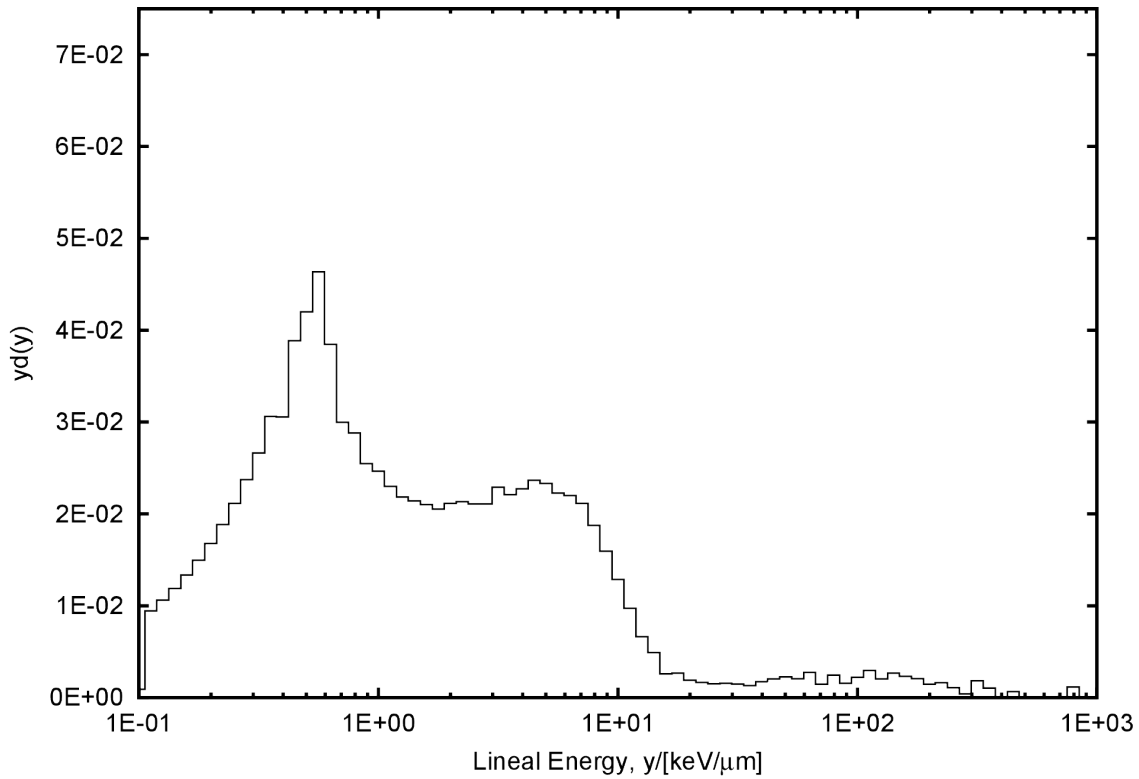

Figure C.6. Lineal energy distribution for the TEPC on the surface of Mars, other component.

Surface of Mars, other component:

```
# Using 80 Log Bins
# Min: 0.1 keV/μm              Max: 1000 keV/μm               20 bins/decade
#
# SiteSize: 1 μm               Mean Chord Length: 0.667 μm
#
# Using y Output with units of [keV/μm]
#
# y_F = 0.617 keV/μm
# y_D = 8.625 keV/μm
#
# D     = 8.730e-04 Gy
# H     = 1.613e-03 Sv
# Q_avg = 1.848e+00
#
# N = 1161944
#
# y [keV/μm] N(y)     f(y)         y*f(y)      d(y)         y*d(y)
1.0000e-01   57649    1.5019e-02  5.6451e-03  5.6451e-03  9.1548e-04
1.1220e-01   57649    1.2309e-01  5.1910e-02  5.1910e-02  9.4455e-03
1.2589e-01   57649    1.0970e-01  5.1910e-02  5.1910e-02  1.0598e-02
1.4125e-01   57649    9.7770e-02  5.1910e-02  5.1910e-02  1.1891e-02
1.5849e-01   57649    8.7138e-02  5.1910e-02  5.1910e-02  1.3342e-02
1.7783e-01   57649    7.7662e-02  5.1910e-02  5.1910e-02  1.4970e-02
1.9953e-01   57649    6.9216e-02  5.1910e-02  5.1910e-02  1.6797e-02
2.2387e-01   57649    6.1689e-02  5.1910e-02  5.1910e-02  1.8846e-02
2.5119e-01   57649    5.4980e-02  5.1910e-02  5.1910e-02  2.1146e-02
2.8184e-01   57649    4.9001e-02  5.1910e-02  5.1910e-02  2.3726e-02
3.1623e-01   57649    4.3672e-02  5.1910e-02  5.1910e-02  2.6621e-02
3.5481e-01   59076    3.9887e-02  5.3195e-02  5.3195e-02  3.0609e-02
3.9811e-01   52553    3.1624e-02  4.7321e-02  4.7321e-02  3.0551e-02
4.4668e-01   59578    3.1952e-02  5.3647e-02  5.3647e-02  3.8861e-02
5.0119e-01   57377    2.7425e-02  5.1665e-02  5.1665e-02  4.1992e-02
5.6234e-01   56453    2.4049e-02  5.0833e-02  5.0833e-02  4.6357e-02
6.3096e-01   41768    1.5858e-02  3.7610e-02  3.7610e-02  3.8484e-02
7.0795e-01   29003    9.8143e-03  2.6116e-02  2.6116e-02  2.9983e-02
7.9433e-01   24835    7.4900e-03  2.2363e-02  2.2363e-02  2.8807e-02
8.9125e-01   19574    5.2613e-03  1.7625e-02  1.7625e-02  2.5475e-02
1.0000e+00   16874    4.0423e-03  1.5194e-02  1.5194e-02  2.4640e-02
1.1220e+00   14040    2.9977e-03  1.2642e-02  1.2642e-02  2.3004e-02
1.2589e+00   11874    2.2595e-03  1.0692e-02  1.0692e-02  2.1829e-02
1.4125e+00   10381    1.7606e-03  9.3475e-03  9.3475e-03  2.1413e-02
1.5849e+00   9088     1.3737e-03  8.1832e-03  8.1832e-03  2.1033e-02
1.7783e+00   7911     1.0657e-03  7.1234e-03  7.1234e-03  2.0543e-02
1.9953e+00   7249     8.7035e-04  6.5273e-03  6.5273e-03  2.1121e-02
2.2387e+00   6526     6.9833e-04  5.8763e-03  5.8763e-03  2.1334e-02
2.5119e+00   5749     5.4829e-04  5.1766e-03  5.1766e-03  2.1087e-02
2.8184e+00   5123     4.3545e-04  4.6130e-03  4.6130e-03  2.1084e-02
3.1623e+00   4959     3.7567e-04  4.4653e-03  4.4653e-03  2.2899e-02
```

3.5481e+00	4268	2.8816e-04	3.8431e-03	3.8431e-03	2.2113e-02
3.9811e+00	3910	2.3528e-04	3.5207e-03	3.5207e-03	2.2730e-02
4.4668e+00	3629	1.9463e-04	3.2677e-03	3.2677e-03	2.3671e-02
5.0119e+00	3187	1.5233e-04	2.8697e-03	2.8697e-03	2.3325e-02
5.6234e+00	2714	1.1562e-04	2.4438e-03	2.4438e-03	2.2286e-02
6.3096e+00	2389	9.0705e-05	2.1512e-03	2.1512e-03	2.2011e-02
7.0795e+00	2045	6.9200e-05	1.8414e-03	1.8414e-03	2.1141e-02
7.9433e+00	1615	4.8707e-05	1.4542e-03	1.4542e-03	1.8733e-02
8.9125e+00	1225	3.2927e-05	1.1030e-03	1.1030e-03	1.5943e-02
1.0000e+01	881	2.1105e-05	7.9329e-04	7.9329e-04	1.2865e-02
1.1220e+01	594	1.2682e-05	5.3486e-04	5.3486e-04	9.7323e-03
1.2589e+01	361	6.8695e-06	3.2506e-04	3.2506e-04	6.6365e-03
1.4125e+01	238	4.0364e-06	2.1431e-04	2.1431e-04	4.9092e-03
1.5849e+01	112	1.6929e-06	1.0085e-04	1.0085e-04	2.5921e-03
1.7783e+01	103	1.3876e-06	9.2746e-05	9.2746e-05	2.6747e-03
1.9953e+01	65	7.8042e-07	5.8529e-05	5.8529e-05	1.8938e-03
2.2387e+01	51	5.4574e-07	4.5923e-05	4.5923e-05	1.6673e-03
2.5119e+01	41	3.9102e-07	3.6918e-05	3.6918e-05	1.5039e-03
2.8184e+01	38	3.2300e-07	3.4217e-05	3.4217e-05	1.5639e-03
3.1623e+01	32	2.4242e-07	2.8814e-05	2.8814e-05	1.4777e-03
3.5481e+01	25	1.6879e-07	2.2511e-05	2.2511e-05	1.2953e-03
3.9811e+01	30	1.8052e-07	2.7013e-05	2.7013e-05	1.7440e-03
4.4668e+01	31	1.6626e-07	2.7914e-05	2.7914e-05	2.0221e-03
5.0119e+01	31	1.4818e-07	2.7914e-05	2.7914e-05	2.2688e-03
5.6234e+01	25	1.0650e-07	2.2511e-05	2.2511e-05	2.0529e-03
6.3096e+01	30	1.1390e-07	2.7013e-05	2.7013e-05	2.7641e-03
7.0795e+01	14	4.7374e-08	1.2606e-05	1.2606e-05	1.4473e-03
7.9433e+01	21	6.3334e-08	1.8909e-05	1.8909e-05	2.4358e-03
8.9125e+01	12	3.2255e-08	1.0805e-05	1.0805e-05	1.5618e-03
1.0000e+02	15	3.5934e-08	1.3507e-05	1.3507e-05	2.1904e-03
1.1220e+02	18	3.8432e-08	1.6208e-05	1.6208e-05	2.9492e-03
1.2589e+02	11	2.0932e-08	9.9049e-06	9.9049e-06	2.0222e-03
1.4125e+02	13	2.2047e-08	1.1706e-05	1.1706e-05	2.6815e-03
1.5849e+02	10	1.5115e-08	9.0044e-06	9.0044e-06	2.3144e-03
1.7783e+02	8	1.0777e-08	7.2035e-06	7.2035e-06	2.0774e-03
1.9953e+02	5	6.0032e-09	4.5022e-06	4.5022e-06	1.4568e-03
2.2387e+02	5	5.3504e-09	4.5022e-06	4.5022e-06	1.6346e-03
2.5119e+02	3	2.8611e-09	2.7013e-06	2.7013e-06	1.1004e-03
2.8184e+02	1	8.4999e-10	9.0044e-07	9.0044e-07	4.1156e-04
3.1623e+02	4	3.0302e-09	3.6018e-06	3.6018e-06	1.8471e-03
3.5481e+02	2	1.3503e-09	1.8009e-06	1.8009e-06	1.0362e-03
3.9811e+02	0	0.0000e+00	0.0000e+00	0.0000e+00	0.0000e+00
4.4668e+02	1	5.3631e-10	9.0044e-07	9.0044e-07	6.5228e-04
5.0119e+02	0	0.0000e+00	0.0000e+00	0.0000e+00	0.0000e+00
5.6234e+02	0	0.0000e+00	0.0000e+00	0.0000e+00	0.0000e+00
6.3096e+02	0	0.0000e+00	0.0000e+00	0.0000e+00	0.0000e+00
7.0795e+02	0	0.0000e+00	0.0000e+00	0.0000e+00	0.0000e+00
7.9433e+02	1	3.0159e-10	9.0044e-07	9.0044e-07	1.1599e-03
8.9125e+02	0	0.0000e+00	0.0000e+00	0.0000e+00	0.0000e+00
1.0000e+03	0	0.0000e+00	0.0000e+00	0.0000e+00	0.0000e+00

APPENDIX D

SURFACE OF MARS DOWNWARD LINEAL ENERGY DISTRIBUTIONS

This appendix contains the y distributions for the downward components of the particle fluence for the TEPC positioned 1 m above the surface of Mars. The figures show a plot of $yd(y)$ as a function of y on a semi-log axis. $\bar{y}_{\mathrm{F}}$, $\bar{y}_{\mathrm{D}}$, D, H, and $\bar{Q}$ for the simulated irradiation are included in the tabulated data. D and H represent integral values for 1.0×10^8 incident particles. These 1.0×10^8 particles, 1.0×10^8 histories in FLUKA, correspond to a simulated irradiation time of 0.545 y. Dividing D and H by 0.545 will normalize these values to time in the form of $\dot{D}$ and $\dot{H}$ with units of Gy/y and Sv/y, respectively. The $f(y)$, $d(y)$, $yf(y)$, and $yd(y)$ distributions have all been normalized to unit area.

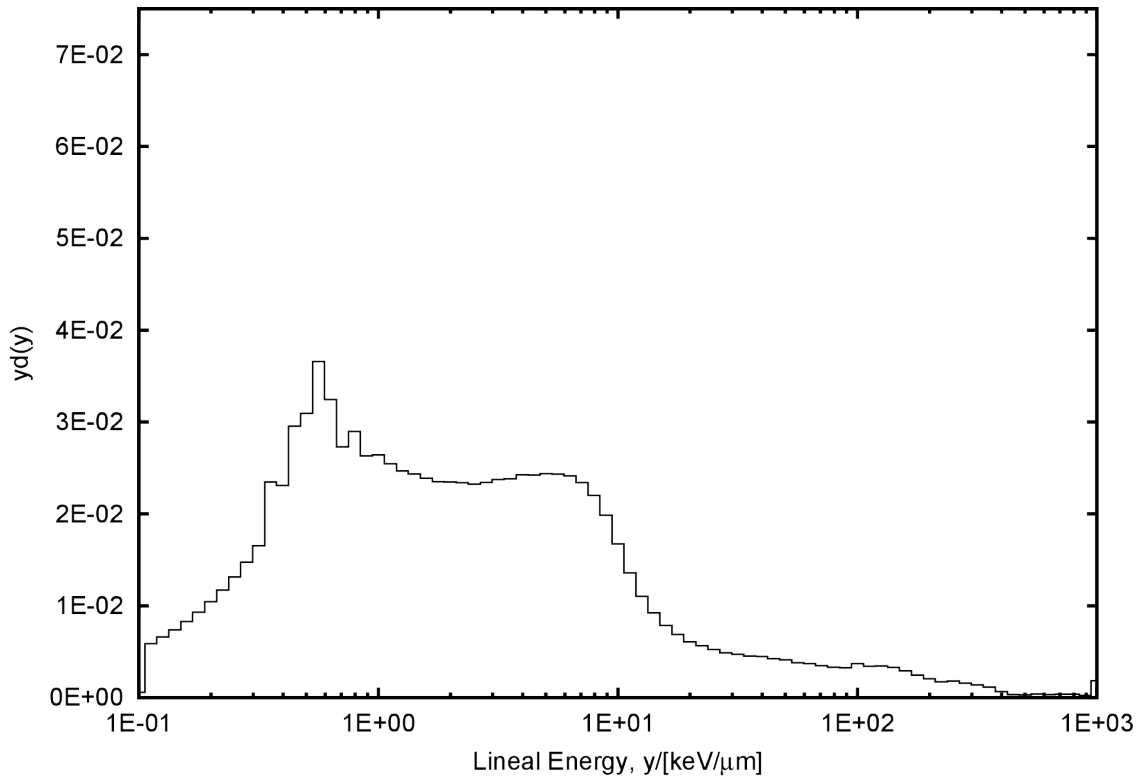

Figure D.1. Lineal energy distribution for the TEPC on the surface of Mars, downward (all-particle) component.

Surface of Mars, downward (all-particle) component:

```
# Using 80 Log Bins
# Min: 0.1 keV/μm              Max: 1000 keV/μm              20 bins/decade
#
# SiteSize: 1 μm               Mean Chord Length: 0.667 μm
#
# Using y Output with units of [keV/μm]
#
# y_F = 0.826 keV/μm
# y_D = 14.090 keV/μm
#
# D     = 2.824e-02 Gy
# H     = 6.814e-02 Sv
# Q_avg = 2.413e+00
#
# N = 27924753
#
# y [keV/μm] N(y)     f(y)         y*f(y)      d(y)         y*d(y)
1.0000e-01   1162378  1.4075e-02  4.7011e-03  4.7011e-03  5.6908e-04
1.1220e-01   1162378  1.1535e-01  4.3229e-02  4.3229e-02  5.8715e-03
1.2589e-01   1162378  1.0281e-01  4.3229e-02  4.3229e-02  6.5879e-03
1.4125e-01   1162378  9.1628e-02  4.3229e-02  4.3229e-02  7.3917e-03
1.5849e-01   1162378  8.1664e-02  4.3229e-02  4.3229e-02  8.2936e-03
1.7783e-01   1162378  7.2783e-02  4.3229e-02  4.3229e-02  9.3056e-03
1.9953e-01   1162378  6.4868e-02  4.3229e-02  4.3229e-02  1.0441e-02
2.2387e-01   1162378  5.7813e-02  4.3229e-02  4.3229e-02  1.1715e-02
2.5119e-01   1162378  5.1526e-02  4.3229e-02  4.3229e-02  1.3145e-02
2.8184e-01   1162378  4.5923e-02  4.3229e-02  4.3229e-02  1.4748e-02
3.1623e-01   1162378  4.0929e-02  4.3229e-02  4.3229e-02  1.6548e-02
3.5481e-01   1469617  4.6120e-02  5.4655e-02  5.4655e-02  2.3475e-02
3.9811e-01   1289113  3.6056e-02  4.7942e-02  4.7942e-02  2.3104e-02
4.4668e-01   1469816  3.6639e-02  5.4663e-02  5.4663e-02  2.9557e-02
5.0119e-01   1370658  3.0452e-02  5.0975e-02  5.0975e-02  3.0926e-02
5.6234e-01   1444935  2.8611e-02  5.3737e-02  5.3737e-02  3.6580e-02
6.3096e-01   1142429  2.0161e-02  4.2487e-02  4.2487e-02  3.2451e-02
7.0795e-01   856675   1.3474e-02  3.1860e-02  3.1860e-02  2.7303e-02
7.9433e-01   810539   1.1362e-02  3.0144e-02  3.0144e-02  2.8985e-02
8.9125e-01   656423   8.2010e-03  2.4413e-02  2.4413e-02  2.6338e-02
1.0000e+00   586858   6.5345e-03  2.1825e-02  2.1825e-02  2.6420e-02
1.1220e+00   503847   5.0001e-03  1.8738e-02  1.8738e-02  2.5451e-02
1.2589e+00   435579   3.8525e-03  1.6199e-02  1.6199e-02  2.4687e-02
1.4125e+00   383151   3.0203e-03  1.4249e-02  1.4249e-02  2.4365e-02
1.5849e+00   334577   2.3506e-03  1.2443e-02  1.2443e-02  2.3872e-02
1.7783e+00   293989   1.8408e-03  1.0934e-02  1.0934e-02  2.3536e-02
1.9953e+00   261380   1.4587e-03  9.7208e-03  9.7208e-03  2.3479e-02
2.2387e+00   232137   1.1546e-03  8.6332e-03  8.6332e-03  2.3396e-02
2.5119e+00   205515   9.1101e-04  7.6432e-03  7.6432e-03  2.3240e-02
2.8184e+00   184707   7.2973e-04  6.8693e-03  6.8693e-03  2.3436e-02
3.1623e+00   166894   5.8765e-04  6.2068e-03  6.2068e-03  2.3760e-02
```

3.5481e+00	149178	4.6815e-04	5.5480e-03	5.5480e-03	2.3829e-02
3.9811e+00	135459	3.7887e-04	5.0378e-03	5.0378e-03	2.4278e-02
4.4668e+00	120424	3.0019e-04	4.4786e-03	4.4786e-03	2.4216e-02
5.0119e+00	108043	2.4004e-04	4.0181e-03	4.0181e-03	2.4378e-02
5.6234e+00	96068	1.9022e-04	3.5728e-03	3.5728e-03	2.4321e-02
6.3096e+00	84991	1.4999e-04	3.1608e-03	3.1608e-03	2.4142e-02
7.0795e+00	73469	1.1555e-04	2.7323e-03	2.7323e-03	2.3415e-02
7.9433e+00	61575	8.6315e-05	2.2900e-03	2.2900e-03	2.2019e-02
8.9125e+00	49496	6.1837e-05	1.8408e-03	1.8408e-03	1.9859e-02
1.0000e+01	37179	4.1398e-05	1.3827e-03	1.3827e-03	1.6738e-02
1.1220e+01	26882	2.6677e-05	9.9975e-04	9.9975e-04	1.3579e-02
1.2589e+01	19448	1.7201e-05	7.2328e-04	7.2328e-04	1.1022e-02
1.4125e+01	14528	1.1452e-05	5.4030e-04	5.4030e-04	9.2386e-03
1.5849e+01	11004	7.7309e-06	4.0924e-04	4.0924e-04	7.8514e-03
1.7783e+01	8571	5.3668e-06	3.1876e-04	3.1876e-04	6.8617e-03
1.9953e+01	6771	3.7786e-06	2.5182e-04	2.5182e-04	6.0821e-03
2.2387e+01	5609	2.7898e-06	2.0860e-04	2.0860e-04	5.6531e-03
2.5119e+01	4651	2.0617e-06	1.7297e-04	1.7297e-04	5.2595e-03
2.8184e+01	3852	1.5218e-06	1.4326e-04	1.4326e-04	4.8875e-03
3.1623e+01	3309	1.1651e-06	1.2306e-04	1.2306e-04	4.7108e-03
3.5481e+01	2823	8.8591e-07	1.0499e-04	1.0499e-04	4.5093e-03
3.9811e+01	2497	6.9839e-07	9.2864e-05	9.2864e-05	4.4752e-03
4.4668e+01	2119	5.2822e-07	7.8806e-05	7.8806e-05	4.2612e-03
5.0119e+01	1818	4.0390e-07	6.7612e-05	6.7612e-05	4.1020e-03
5.6234e+01	1505	2.9800e-07	5.5971e-05	5.5971e-05	3.8101e-03
6.3096e+01	1303	2.2995e-07	4.8459e-05	4.8459e-05	3.7012e-03
7.0795e+01	1099	1.7285e-07	4.0872e-05	4.0872e-05	3.5026e-03
7.9433e+01	924	1.2952e-07	3.4364e-05	3.4364e-05	3.3042e-03
8.9125e+01	810	1.0120e-07	3.0124e-05	3.0124e-05	3.2500e-03
1.0000e+02	818	9.1082e-08	3.0422e-05	3.0422e-05	3.6826e-03
1.1220e+02	677	6.7185e-08	2.5178e-05	2.5178e-05	3.4197e-03
1.2589e+02	608	5.3775e-08	2.2612e-05	2.2612e-05	3.4459e-03
1.4125e+02	515	4.0596e-08	1.9153e-05	1.9153e-05	3.2750e-03
1.5849e+02	410	2.8805e-08	1.5248e-05	1.5248e-05	2.9254e-03
1.7783e+02	307	1.9223e-08	1.1417e-05	1.1417e-05	2.4577e-03
1.9953e+02	229	1.2780e-08	8.5166e-06	8.5166e-06	2.0570e-03
2.2387e+02	171	8.5050e-09	6.3595e-06	6.3595e-06	1.7234e-03
2.5119e+02	159	7.0482e-09	5.9132e-06	5.9132e-06	1.7980e-03
2.8184e+02	124	4.8989e-09	4.6116e-06	4.6116e-06	1.5733e-03
3.1623e+02	97	3.4155e-09	3.6075e-06	3.6075e-06	1.3809e-03
3.5481e+02	71	2.2281e-09	2.6405e-06	2.6405e-06	1.1341e-03
3.9811e+02	37	1.0349e-09	1.3760e-06	1.3760e-06	6.6313e-04
4.4668e+02	17	4.2377e-10	6.3223e-07	6.3223e-07	3.4186e-04
5.0119e+02	14	3.1103e-10	5.2066e-07	5.2066e-07	3.1588e-04
5.6234e+02	16	3.1681e-10	5.9504e-07	5.9504e-07	4.0506e-04
6.3096e+02	12	2.1177e-10	4.4628e-07	4.4628e-07	3.4086e-04
7.0795e+02	12	1.8874e-10	4.4628e-07	4.4628e-07	3.8245e-04
7.9433e+02	10	1.4018e-10	3.7190e-07	3.7190e-07	3.5760e-04
8.9125e+02	6	7.4960e-11	2.2314e-07	2.2314e-07	2.4074e-04
1.0000e+03	41	4.5653e-10	1.5248e-06	1.5248e-06	1.8458e-03

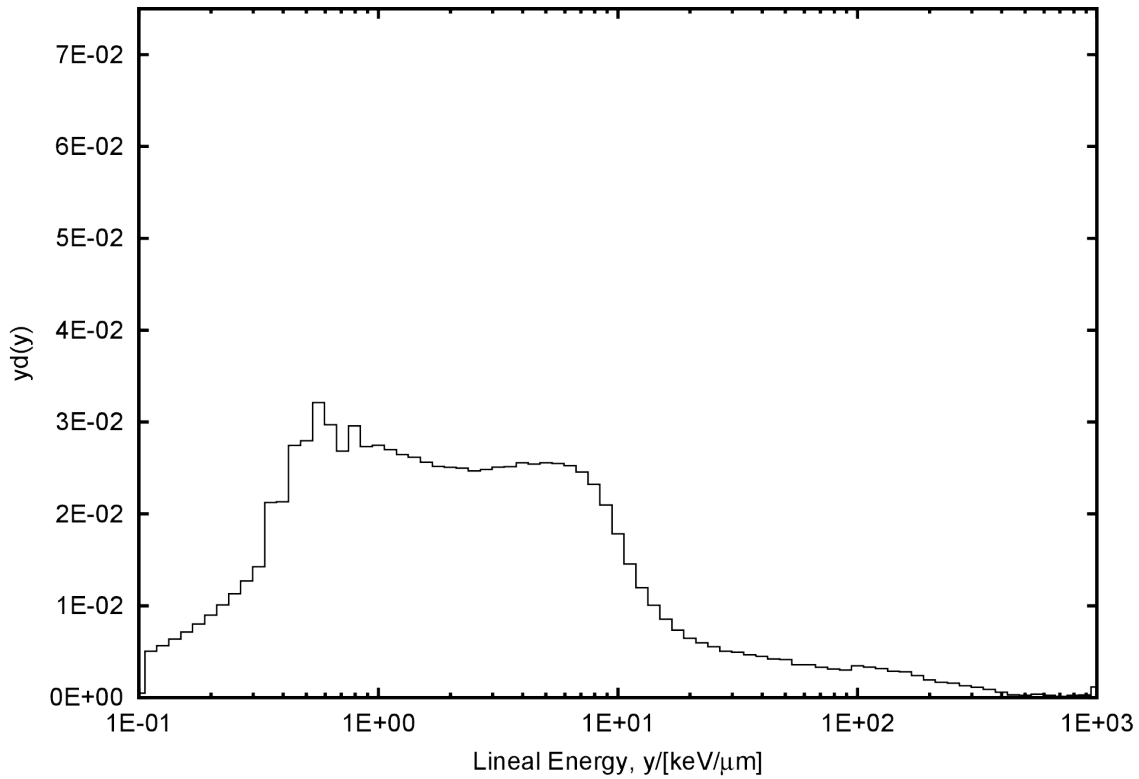

Figure D.2. Lineal energy distribution for the TEPC on the surface of Mars, downward elemental ion component.

Surface of Mars, downward elemental ion component:

```
# Using 80 Log Bins
# Min: 0.1 keV/μm              Max: 1000 keV/μm              20 bins/decade
#
# SiteSize: 1 μm               Mean Chord Length: 0.667 μm
#
# Using y Output with units of [keV/μm]
#
# y_F = 0.895 keV/μm
# y_D = 12.700 keV/μm
#
# D     = 2.309e-02 Gy
# H     = 5.418e-02 Sv
# Q_avg = 2.346e+00
#
# N = 21030866
#
# y [keV/μm] N(y)     f(y)         y*f(y)       d(y)         y*d(y)
1.0000e-01   818598   1.3748e-02   4.3850e-03   4.3850e-03   4.8975e-04
1.1220e-01   818598   1.1267e-01   4.0322e-02   4.0322e-02   5.0530e-03
1.2589e-01   818598   1.0042e-01   4.0322e-02   4.0322e-02   5.6696e-03
1.4125e-01   818598   8.9496e-02   4.0322e-02   4.0322e-02   6.3614e-03
1.5849e-01   818598   7.9763e-02   4.0322e-02   4.0322e-02   7.1376e-03
1.7783e-01   818598   7.1089e-02   4.0322e-02   4.0322e-02   8.0085e-03
1.9953e-01   818598   6.3358e-02   4.0322e-02   4.0322e-02   8.9857e-03
2.2387e-01   818598   5.6468e-02   4.0322e-02   4.0322e-02   1.0082e-02
2.5119e-01   818598   5.0327e-02   4.0322e-02   4.0322e-02   1.1312e-02
2.8184e-01   818598   4.4854e-02   4.0322e-02   4.0322e-02   1.2693e-02
3.1623e-01   818598   3.9976e-02   4.0322e-02   4.0322e-02   1.4241e-02
3.5481e-01   1087696  4.7341e-02   5.3578e-02   5.3578e-02   2.1232e-02
3.9811e-01   973394   3.7759e-02   4.7947e-02   4.7947e-02   2.1319e-02
4.4668e-01   1116451  3.8599e-02   5.4994e-02   5.4994e-02   2.7436e-02
5.0119e-01   1014062  3.1246e-02   4.9951e-02   4.9951e-02   2.7961e-02
5.6234e-01   1038004  2.8506e-02   5.1130e-02   5.1130e-02   3.2113e-02
6.3096e-01   856019   2.0952e-02   4.2166e-02   4.2166e-02   2.9714e-02
7.0795e-01   689374   1.5038e-02   3.3957e-02   3.3957e-02   2.6850e-02
7.9433e-01   676902   1.3160e-02   3.3343e-02   3.3343e-02   2.9581e-02
8.9125e-01   557379   9.6579e-03   2.7455e-02   2.7455e-02   2.7330e-02
1.0000e+00   499236   7.7097e-03   2.4591e-02   2.4591e-02   2.7466e-02
1.1220e+00   437538   6.0221e-03   2.1552e-02   2.1552e-02   2.7008e-02
1.2589e+00   382031   4.6863e-03   1.8818e-02   1.8818e-02   2.6459e-02
1.4125e+00   336801   3.6822e-03   1.6590e-02   1.6590e-02   2.6173e-02
1.5849e+00   293812   2.8629e-03   1.4473e-02   1.4473e-02   2.5618e-02
1.7783e+00   257566   2.2368e-03   1.2687e-02   1.2687e-02   2.5198e-02
1.9953e+00   228557   1.7690e-03   1.1258e-02   1.1258e-02   2.5089e-02
2.2387e+00   202657   1.3980e-03   9.9825e-03   9.9825e-03   2.4960e-02
2.5119e+00   178708   1.0987e-03   8.8028e-03   8.8028e-03   2.4696e-02
2.8184e+00   160283   8.7825e-04   7.8952e-03   7.8952e-03   2.4852e-02
3.1623e+00   144286   7.0462e-04   7.1072e-03   7.1072e-03   2.5102e-02
```

3.5481e+00	128752	5.6039e-04	6.3421e-03	6.3421e-03	2.5133e-02
3.9811e+00	116717	4.5276e-04	5.7492e-03	5.7492e-03	2.5563e-02
4.4668e+00	103518	3.5789e-04	5.0991e-03	5.0991e-03	2.5439e-02
5.0119e+00	92758	2.8581e-04	4.5691e-03	4.5691e-03	2.5576e-02
5.6234e+00	82443	2.2641e-04	4.0610e-03	4.0610e-03	2.5506e-02
6.3096e+00	72778	1.7813e-04	3.5849e-03	3.5849e-03	2.5263e-02
7.0795e+00	63014	1.3746e-04	3.1039e-03	3.1039e-03	2.4543e-02
7.9433e+00	53084	1.0320e-04	2.6148e-03	2.6148e-03	2.3198e-02
8.9125e+00	42779	7.4125e-05	2.1072e-03	2.1072e-03	2.0976e-02
1.0000e+01	32418	5.0063e-05	1.5968e-03	1.5968e-03	1.7835e-02
1.1220e+01	23584	3.2460e-05	1.1617e-03	1.1617e-03	1.4558e-02
1.2589e+01	17277	2.1193e-05	8.5103e-04	8.5103e-04	1.1966e-02
1.4125e+01	12952	1.4160e-05	6.3799e-04	6.3799e-04	1.0065e-02
1.5849e+01	9777	9.5266e-06	4.8160e-04	4.8160e-04	8.5249e-03
1.7783e+01	7521	6.5314e-06	3.7047e-04	3.7047e-04	7.3580e-03
1.9953e+01	5883	4.5534e-06	2.8978e-04	2.8978e-04	6.4577e-03
2.2387e+01	4848	3.3442e-06	2.3880e-04	2.3880e-04	5.9710e-03
2.5119e+01	4001	2.4598e-06	1.9708e-04	1.9708e-04	5.5290e-03
2.8184e+01	3260	1.7863e-06	1.6058e-04	1.6058e-04	5.0547e-03
3.1623e+01	2839	1.3864e-06	1.3984e-04	1.3984e-04	4.9391e-03
3.5481e+01	2391	1.0407e-06	1.1778e-04	1.1778e-04	4.6673e-03
3.9811e+01	2056	7.9755e-07	1.0127e-04	1.0127e-04	4.5030e-03
4.4668e+01	1721	5.9500e-07	8.4773e-05	8.4773e-05	4.2292e-03
5.0119e+01	1504	4.6343e-07	7.4084e-05	7.4084e-05	4.1470e-03
5.6234e+01	1165	3.1993e-07	5.7386e-05	5.7386e-05	3.6042e-03
6.3096e+01	1032	2.5259e-07	5.0834e-05	5.0834e-05	3.5823e-03
7.0795e+01	847	1.8476e-07	4.1721e-05	4.1721e-05	3.2989e-03
7.9433e+01	711	1.3823e-07	3.5022e-05	3.5022e-05	3.1071e-03
8.9125e+01	613	1.0622e-07	3.0195e-05	3.0195e-05	3.0057e-03
1.0000e+02	628	9.6982e-08	3.0934e-05	3.0934e-05	3.4549e-03
1.1220e+02	537	7.3911e-08	2.6452e-05	2.6452e-05	3.3148e-03
1.2589e+02	460	5.6427e-08	2.2659e-05	2.2659e-05	3.1860e-03
1.4125e+02	368	4.0233e-08	1.8127e-05	1.8127e-05	2.8598e-03
1.5849e+02	324	3.1570e-08	1.5960e-05	1.5960e-05	2.8251e-03
1.7783e+02	246	2.1363e-08	1.2117e-05	1.2117e-05	2.4067e-03
1.9953e+02	176	1.3622e-08	8.6694e-06	8.6694e-06	1.9319e-03
2.2387e+02	136	9.3815e-09	6.6991e-06	6.6991e-06	1.6750e-03
2.5119e+02	114	7.0087e-09	5.6154e-06	5.6154e-06	1.5754e-03
2.8184e+02	83	4.5479e-09	4.0884e-06	4.0884e-06	1.2869e-03
3.1623e+02	65	3.1743e-09	3.2018e-06	3.2018e-06	1.1308e-03
3.5481e+02	45	1.9586e-09	2.2166e-06	2.2166e-06	8.7840e-04
3.9811e+02	28	1.0862e-09	1.3792e-06	1.3792e-06	6.1325e-04
4.4668e+02	13	4.4944e-10	6.4035e-07	6.4035e-07	3.1947e-04
5.0119e+02	10	3.0813e-10	4.9258e-07	4.9258e-07	2.7573e-04
5.6234e+02	12	3.2954e-10	5.9110e-07	5.9110e-07	3.7125e-04
6.3096e+02	8	1.9580e-10	3.9406e-07	3.9406e-07	2.7770e-04
7.0795e+02	3	6.5442e-11	1.4777e-07	1.4777e-07	1.1684e-04
7.9433e+02	6	1.1665e-10	2.9555e-07	2.9555e-07	2.6220e-04
8.9125e+02	6	1.0396e-10	2.9555e-07	2.9555e-07	2.9419e-04
1.0000e+03	21	3.2430e-10	1.0344e-06	1.0344e-06	1.1553e-03

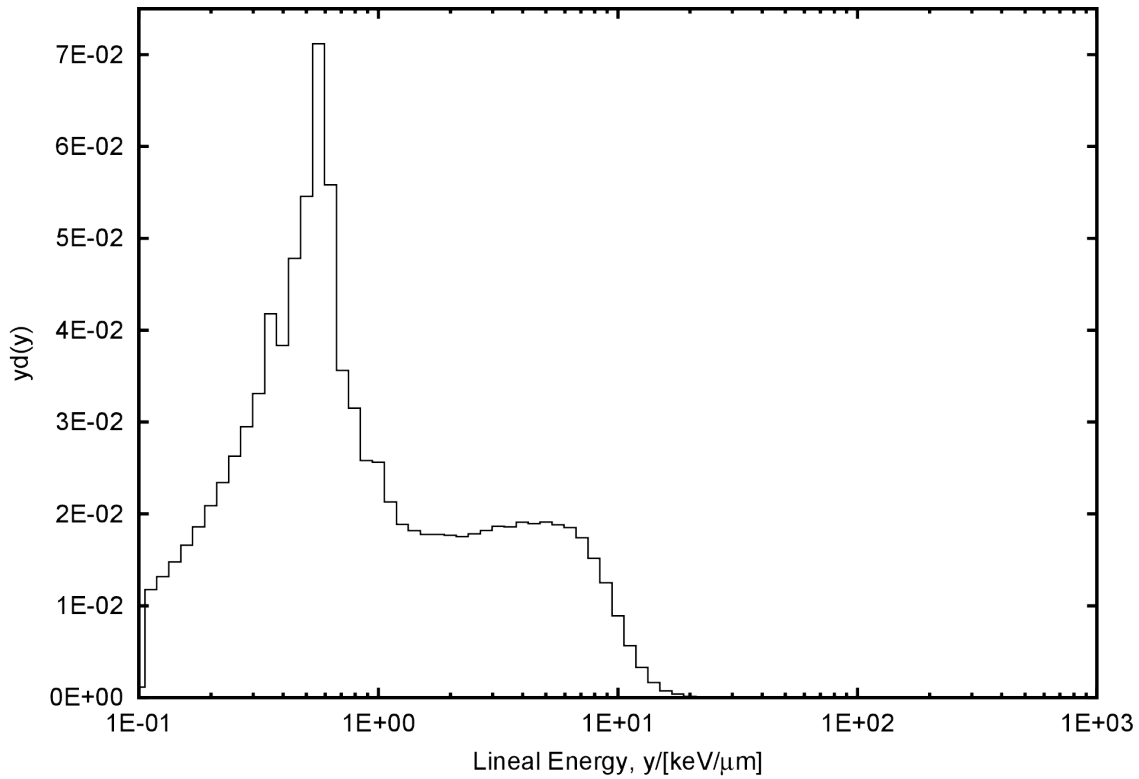

Figure D.3. Lineal energy distribution for the TEPC on the surface of Mars, downward electron component.

Surface of Mars, downward electron component:

```
# Using 80 Log Bins
# Min: 0.1 keV/μm              Max: 1000 keV/μm              20 bins/decade
#
# SiteSize: 1 μm               Mean Chord Length: 0.667 μm
#
# Using y Output with units of [keV/μm]
#
# y_F = 0.504 keV/μm
# y_D = 1.801 keV/μm
#
# D     = 3.710e-03 Gy
# H     = 3.747e-03 Sv
# Q_avg = 1.010e+00
#
# N = 6032843
#
# y [keV/μm] N(y)     f(y)         y*f(y)      d(y)         y*d(y)
1.0000e-01   303944   1.4924e-02  5.7365e-03  5.7365e-03  1.1379e-03
1.1220e-01   303944   1.2231e-01  5.2750e-02  5.2750e-02  1.1740e-02
1.2589e-01   303944   1.0901e-01  5.2750e-02  5.2750e-02  1.3173e-02
1.4125e-01   303944   9.7154e-02  5.2750e-02  5.2750e-02  1.4780e-02
1.5849e-01   303944   8.6588e-02  5.2750e-02  5.2750e-02  1.6584e-02
1.7783e-01   303944   7.7172e-02  5.2750e-02  5.2750e-02  1.8607e-02
1.9953e-01   303944   6.8779e-02  5.2750e-02  5.2750e-02  2.0878e-02
2.2387e-01   303944   6.1300e-02  5.2750e-02  5.2750e-02  2.3425e-02
2.5119e-01   303944   5.4633e-02  5.2750e-02  5.2750e-02  2.6284e-02
2.8184e-01   303944   4.8692e-02  5.2750e-02  5.2750e-02  2.9491e-02
3.1623e-01   303944   4.3397e-02  5.2750e-02  5.2750e-02  3.3089e-02
3.5481e-01   342221   4.3548e-02  5.9393e-02  5.9393e-02  4.1802e-02
3.9811e-01   279605   3.1711e-02  4.8526e-02  4.8526e-02  3.8321e-02
4.4668e-01   311024   3.1438e-02  5.3979e-02  5.3979e-02  4.7828e-02
5.0119e-01   316385   2.8502e-02  5.4909e-02  5.4909e-02  5.4589e-02
5.6234e-01   367792   2.9530e-02  6.3831e-02  6.3831e-02  7.1202e-02
6.3096e-01   257016   1.8392e-02  4.4606e-02  4.4606e-02  5.5828e-02
7.0795e-01   146169   9.3222e-03  2.5368e-02  2.5368e-02  3.5624e-02
7.9433e-01   115180   6.5470e-03  1.9990e-02  1.9990e-02  3.1497e-02
8.9125e-01   84104    4.2607e-03  1.4596e-02  1.4596e-02  2.5805e-02
1.0000e+00   74412    3.3598e-03  1.2914e-02  1.2914e-02  2.5617e-02
1.1220e+00   55134    2.2186e-03  9.5686e-03  9.5686e-03  2.1297e-02
1.2589e+00   43535    1.5614e-03  7.5556e-03  7.5556e-03  1.8868e-02
1.4125e+00   37397    1.1954e-03  6.4903e-03  6.4903e-03  1.8186e-02
1.5849e+00   32559    9.2755e-04  5.6507e-03  5.6507e-03  1.7765e-02
1.7783e+00   29012    7.3662e-04  5.0351e-03  5.0351e-03  1.7761e-02
1.9953e+00   25708    5.8175e-04  4.4617e-03  4.4617e-03  1.7659e-02
2.2387e+00   22771    4.5925e-04  3.9520e-03  3.9520e-03  1.7550e-02
2.5119e+00   20625    3.7073e-04  3.5795e-03  3.5795e-03  1.7835e-02
2.8184e+00   18764    3.0060e-04  3.2565e-03  3.2565e-03  1.8206e-02
3.1623e+00   17124    2.4450e-04  2.9719e-03  2.9719e-03  1.8642e-02
```

3.5481e+00	15226	1.9375e-04	2.6425e-03	2.6425e-03	1.8598e-02
3.9811e+00	13932	1.5801e-04	2.4179e-03	2.4179e-03	1.9094e-02
4.4668e+00	12322	1.2455e-04	2.1385e-03	2.1385e-03	1.8948e-02
5.0119e+00	11076	9.9781e-05	1.9223e-03	1.9223e-03	1.9111e-02
5.6234e+00	9718	7.8027e-05	1.6866e-03	1.6866e-03	1.8813e-02
6.3096e+00	8523	6.0990e-05	1.4792e-03	1.4792e-03	1.8513e-02
7.0795e+00	7140	4.5537e-05	1.2392e-03	1.2392e-03	1.7402e-02
7.9433e+00	5543	3.1507e-05	9.6200e-04	9.6200e-04	1.5158e-02
8.9125e+00	4069	2.0614e-05	7.0618e-04	7.0618e-04	1.2485e-02
1.0000e+01	2588	1.1685e-05	4.4915e-04	4.4915e-04	8.9095e-03
1.1220e+01	1466	5.8993e-06	2.5443e-04	2.5443e-04	5.6627e-03
1.2589e+01	754	2.7042e-06	1.3086e-04	1.3086e-04	3.2678e-03
1.4125e+01	338	1.0804e-06	5.8661e-05	5.8661e-05	1.6436e-03
1.5849e+01	136	3.8744e-07	2.3603e-05	2.3603e-05	7.4204e-04
1.7783e+01	66	1.6758e-07	1.1454e-05	1.1454e-05	4.0405e-04
1.9953e+01	18	4.0732e-08	3.1239e-06	3.1239e-06	1.2364e-04
2.2387e+01	6	1.2101e-08	1.0413e-06	1.0413e-06	4.6242e-05
2.5119e+01	1	1.7975e-09	1.7355e-07	1.7355e-07	8.6475e-06
2.8184e+01	0	0.0000e+00	0.0000e+00	0.0000e+00	0.0000e+00
3.1623e+01	0	0.0000e+00	0.0000e+00	0.0000e+00	0.0000e+00
3.5481e+01	0	0.0000e+00	0.0000e+00	0.0000e+00	0.0000e+00
3.9811e+01	0	0.0000e+00	0.0000e+00	0.0000e+00	0.0000e+00
4.4668e+01	0	0.0000e+00	0.0000e+00	0.0000e+00	0.0000e+00
5.0119e+01	0	0.0000e+00	0.0000e+00	0.0000e+00	0.0000e+00
5.6234e+01	0	0.0000e+00	0.0000e+00	0.0000e+00	0.0000e+00
6.3096e+01	0	0.0000e+00	0.0000e+00	0.0000e+00	0.0000e+00
7.0795e+01	0	0.0000e+00	0.0000e+00	0.0000e+00	0.0000e+00
7.9433e+01	0	0.0000e+00	0.0000e+00	0.0000e+00	0.0000e+00
8.9125e+01	0	0.0000e+00	0.0000e+00	0.0000e+00	0.0000e+00
1.0000e+02	0	0.0000e+00	0.0000e+00	0.0000e+00	0.0000e+00
1.1220e+02	0	0.0000e+00	0.0000e+00	0.0000e+00	0.0000e+00
1.2589e+02	0	0.0000e+00	0.0000e+00	0.0000e+00	0.0000e+00
1.4125e+02	0	0.0000e+00	0.0000e+00	0.0000e+00	0.0000e+00
1.5849e+02	0	0.0000e+00	0.0000e+00	0.0000e+00	0.0000e+00
1.7783e+02	0	0.0000e+00	0.0000e+00	0.0000e+00	0.0000e+00
1.9953e+02	0	0.0000e+00	0.0000e+00	0.0000e+00	0.0000e+00
2.2387e+02	0	0.0000e+00	0.0000e+00	0.0000e+00	0.0000e+00
2.5119e+02	0	0.0000e+00	0.0000e+00	0.0000e+00	0.0000e+00
2.8184e+02	0	0.0000e+00	0.0000e+00	0.0000e+00	0.0000e+00
3.1623e+02	0	0.0000e+00	0.0000e+00	0.0000e+00	0.0000e+00
3.5481e+02	0	0.0000e+00	0.0000e+00	0.0000e+00	0.0000e+00
3.9811e+02	0	0.0000e+00	0.0000e+00	0.0000e+00	0.0000e+00
4.4668e+02	0	0.0000e+00	0.0000e+00	0.0000e+00	0.0000e+00
5.0119e+02	0	0.0000e+00	0.0000e+00	0.0000e+00	0.0000e+00
5.6234e+02	0	0.0000e+00	0.0000e+00	0.0000e+00	0.0000e+00
6.3096e+02	0	0.0000e+00	0.0000e+00	0.0000e+00	0.0000e+00
7.0795e+02	0	0.0000e+00	0.0000e+00	0.0000e+00	0.0000e+00
7.9433e+02	0	0.0000e+00	0.0000e+00	0.0000e+00	0.0000e+00
8.9125e+02	0	0.0000e+00	0.0000e+00	0.0000e+00	0.0000e+00
1.0000e+03	0	0.0000e+00	0.0000e+00	0.0000e+00	0.0000e+00

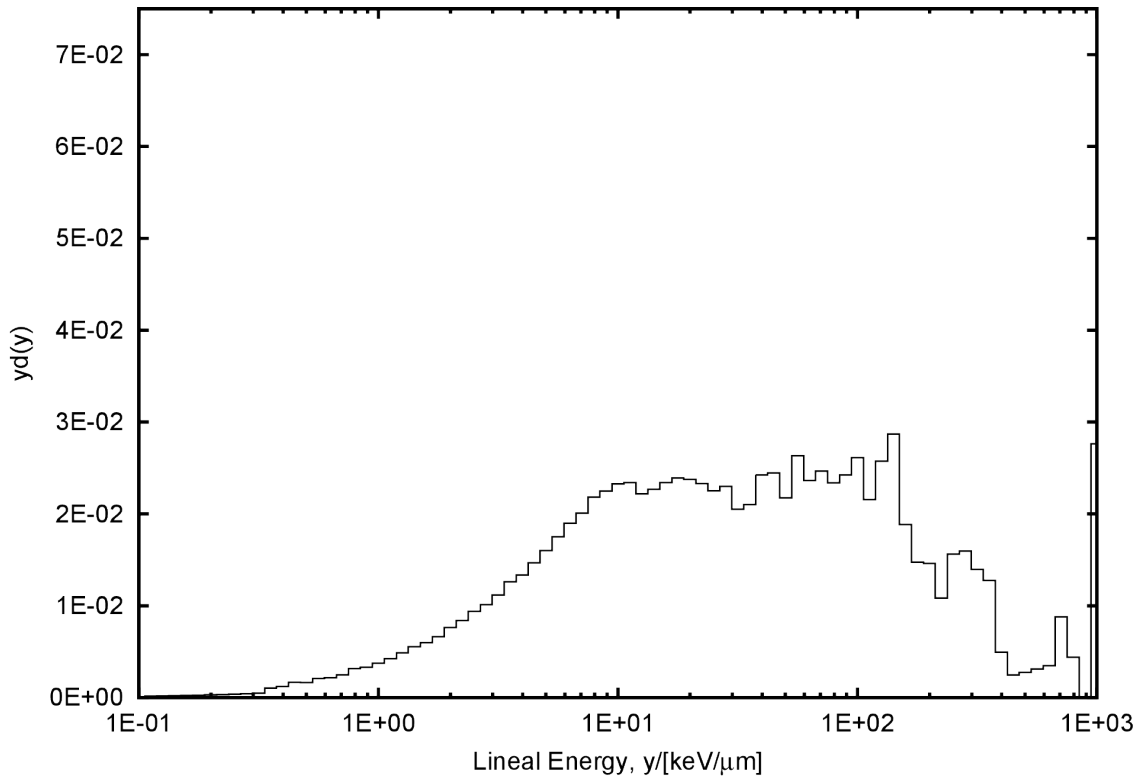

Figure D.4. Lineal energy distribution for the TEPC on the surface of Mars, downward neutron component.

Surface of Mars, downward neutron component:

```
# Using 80 Log Bins
# Min: 0.1 keV/μm              Max: 1000 keV/μm              20 bins/decade
#
# SiteSize: 1 μm               Mean Chord Length: 0.667 μm
#
# Using y Output with units of [keV/μm]
#
# y_F = 7.335 keV/μm
# y_D = 104.944 keV/μm
#
# D     = 9.158e-04 Gy
# H     = 9.669e-03 Sv
# Q_avg = 1.056e+01
#
# N = 99640
#
# y [keV/μm] N(y)     f(y)         y*f(y)      d(y)         y*d(y)
1.0000e-01   1105     9.4589e-03   1.2181e-03  1.2181e-03   1.6605e-05
1.1220e-01   1105     7.7521e-02   1.1201e-02  1.1201e-02   1.7132e-04
1.2589e-01   1105     6.9090e-02   1.1201e-02  1.1201e-02   1.9223e-04
1.4125e-01   1105     6.1577e-02   1.1201e-02  1.1201e-02   2.1568e-04
1.5849e-01   1105     5.4880e-02   1.1201e-02  1.1201e-02   2.4200e-04
1.7783e-01   1105     4.8912e-02   1.1201e-02  1.1201e-02   2.7153e-04
1.9953e-01   1105     4.3593e-02   1.1201e-02  1.1201e-02   3.0466e-04
2.2387e-01   1105     3.8852e-02   1.1201e-02  1.1201e-02   3.4184e-04
2.5119e-01   1105     3.4627e-02   1.1201e-02  1.1201e-02   3.8355e-04
2.8184e-01   1105     3.0861e-02   1.1201e-02  1.1201e-02   4.3035e-04
3.1623e-01   1105     2.7505e-02   1.1201e-02  1.1201e-02   4.8286e-04
3.5481e-01   2121     4.7054e-02   2.1499e-02  2.1499e-02   1.0399e-03
3.9811e-01   2165     4.2807e-02   2.1945e-02  2.1945e-02   1.1910e-03
4.4668e-01   2709     4.7738e-02   2.7459e-02  2.7459e-02   1.6721e-03
5.0119e-01   2383     3.7426e-02   2.4155e-02  2.4155e-02   1.6504e-03
5.6234e-01   2698     3.7766e-02   2.7348e-02  2.7348e-02   2.0965e-03
6.3096e-01   2494     3.1114e-02   2.5280e-02  2.5280e-02   2.1745e-03
7.0795e-01   2539     2.8230e-02   2.5736e-02  2.5736e-02   2.4838e-03
7.9433e-01   2891     2.8649e-02   2.9304e-02  2.9304e-02   3.1733e-03
8.9125e-01   2682     2.3687e-02   2.7186e-02  2.7186e-02   3.3031e-03
1.0000e+00   2723     2.1434e-02   2.7601e-02  2.7601e-02   3.7627e-03
1.1220e+00   2742     1.9236e-02   2.7794e-02  2.7794e-02   4.2513e-03
1.2589e+00   2807     1.7551e-02   2.8453e-02  2.8453e-02   4.8831e-03
1.4125e+00   2834     1.5793e-02   2.8726e-02  2.8726e-02   5.5317e-03
1.5849e+00   2738     1.3598e-02   2.7753e-02  2.7753e-02   5.9964e-03
1.7783e+00   2706     1.1978e-02   2.7429e-02  2.7429e-02   6.6494e-03
1.9953e+00   2769     1.0924e-02   2.8067e-02  2.8067e-02   7.6345e-03
2.2387e+00   2719     9.5601e-03   2.7561e-02  2.7561e-02   8.4114e-03
2.5119e+00   2711     8.4954e-03   2.7480e-02  2.7480e-02   9.4099e-03
2.8184e+00   2600     7.2615e-03   2.6354e-02  2.6354e-02   1.0126e-02
3.1623e+00   2559     6.3698e-03   2.5939e-02  2.5939e-02   1.1182e-02
```

3.5481e+00	2575	5.7126e-03	2.6101e-02	2.6101e-02	1.2625e-02
3.9811e+00	2427	4.7987e-03	2.4601e-02	2.4601e-02	1.3351e-02
4.4668e+00	2376	4.1870e-03	2.4084e-02	2.4084e-02	1.4666e-02
5.0119e+00	2311	3.6296e-03	2.3425e-02	2.3425e-02	1.6005e-02
5.6234e+00	2255	3.1565e-03	2.2857e-02	2.2857e-02	1.7523e-02
6.3096e+00	2177	2.7159e-03	2.2067e-02	2.2067e-02	1.8981e-02
7.0795e+00	2051	2.2804e-03	2.0790e-02	2.0790e-02	2.0064e-02
7.9433e+00	1988	1.9700e-03	2.0151e-02	2.0151e-02	2.1821e-02
8.9125e+00	1825	1.6118e-03	1.8499e-02	1.8499e-02	2.2476e-02
1.0000e+01	1684	1.3256e-03	1.7070e-02	1.7070e-02	2.3270e-02
1.1220e+01	1510	1.0593e-03	1.5306e-02	1.5306e-02	2.3412e-02
1.2589e+01	1276	7.9782e-04	1.2934e-02	1.2934e-02	2.2198e-02
1.4125e+01	1162	6.4753e-04	1.1778e-02	1.1778e-02	2.2681e-02
1.5849e+01	1070	5.3142e-04	1.0846e-02	1.0846e-02	2.3434e-02
1.7783e+01	973	4.3069e-04	9.8626e-03	9.8626e-03	2.3909e-02
1.9953e+01	862	3.4006e-04	8.7375e-03	8.7375e-03	2.3766e-02
2.2387e+01	753	2.6476e-04	7.6326e-03	7.6326e-03	2.3294e-02
2.5119e+01	649	2.0338e-04	6.5785e-03	6.5785e-03	2.2527e-02
2.8184e+01	591	1.6506e-04	5.9906e-03	5.9906e-03	2.3017e-02
3.1623e+01	469	1.1674e-04	4.7539e-03	4.7539e-03	2.0494e-02
3.5481e+01	429	9.5173e-05	4.3485e-03	4.3485e-03	2.1034e-02
3.9811e+01	441	8.7195e-05	4.4701e-03	4.4701e-03	2.4260e-02
4.4668e+01	396	6.9783e-05	4.0140e-03	4.0140e-03	2.4443e-02
5.0119e+01	314	4.9316e-05	3.1828e-03	3.1828e-03	2.1746e-02
5.6234e+01	339	4.7452e-05	3.4362e-03	3.4362e-03	2.6343e-02
6.3096e+01	271	3.3808e-05	2.7469e-03	2.7469e-03	2.3628e-02
7.0795e+01	252	2.8019e-05	2.5544e-03	2.5544e-03	2.4652e-02
7.9433e+01	213	2.1107e-05	2.1590e-03	2.1590e-03	2.3380e-02
8.9125e+01	197	1.7399e-05	1.9969e-03	1.9969e-03	2.4262e-02
1.0000e+02	189	1.4877e-05	1.9158e-03	1.9158e-03	2.6117e-02
1.1220e+02	139	9.7514e-06	1.4089e-03	1.4089e-03	2.1551e-02
1.2589e+02	148	9.2537e-06	1.5002e-03	1.5002e-03	2.5747e-02
1.4125e+02	147	8.1917e-06	1.4900e-03	1.4900e-03	2.8693e-02
1.5849e+02	86	4.2712e-06	8.7172e-04	8.7172e-04	1.8835e-02
1.7783e+02	60	2.6559e-06	6.0818e-04	6.0818e-04	1.4744e-02
1.9953e+02	53	2.0909e-06	5.3722e-04	5.3722e-04	1.4613e-02
2.2387e+02	35	1.2306e-06	3.5477e-04	3.5477e-04	1.0827e-02
2.5119e+02	45	1.4102e-06	4.5613e-04	4.5613e-04	1.5620e-02
2.8184e+02	41	1.1451e-06	4.1559e-04	4.1559e-04	1.5968e-02
3.1623e+02	32	7.9653e-07	3.2436e-04	3.2436e-04	1.3983e-02
3.5481e+02	26	5.7680e-07	2.6354e-04	2.6354e-04	1.2748e-02
3.9811e+02	9	1.7795e-07	9.1227e-05	9.1227e-05	4.9511e-03
4.4668e+02	4	7.0488e-08	4.0545e-05	4.0545e-05	2.4690e-03
5.0119e+02	4	6.2822e-08	4.0545e-05	4.0545e-05	2.7702e-03
5.6234e+02	4	5.5990e-08	4.0545e-05	4.0545e-05	3.1083e-03
6.3096e+02	4	4.9902e-08	4.0545e-05	4.0545e-05	3.4875e-03
7.0795e+02	9	1.0007e-07	9.1227e-05	9.1227e-05	8.8044e-03
7.9433e+02	4	3.9638e-08	4.0545e-05	4.0545e-05	4.3905e-03
8.9125e+02	0	0.0000e+00	0.0000e+00	0.0000e+00	0.0000e+00
1.0000e+03	20	1.5743e-07	2.0273e-04	2.0273e-04	2.7637e-02

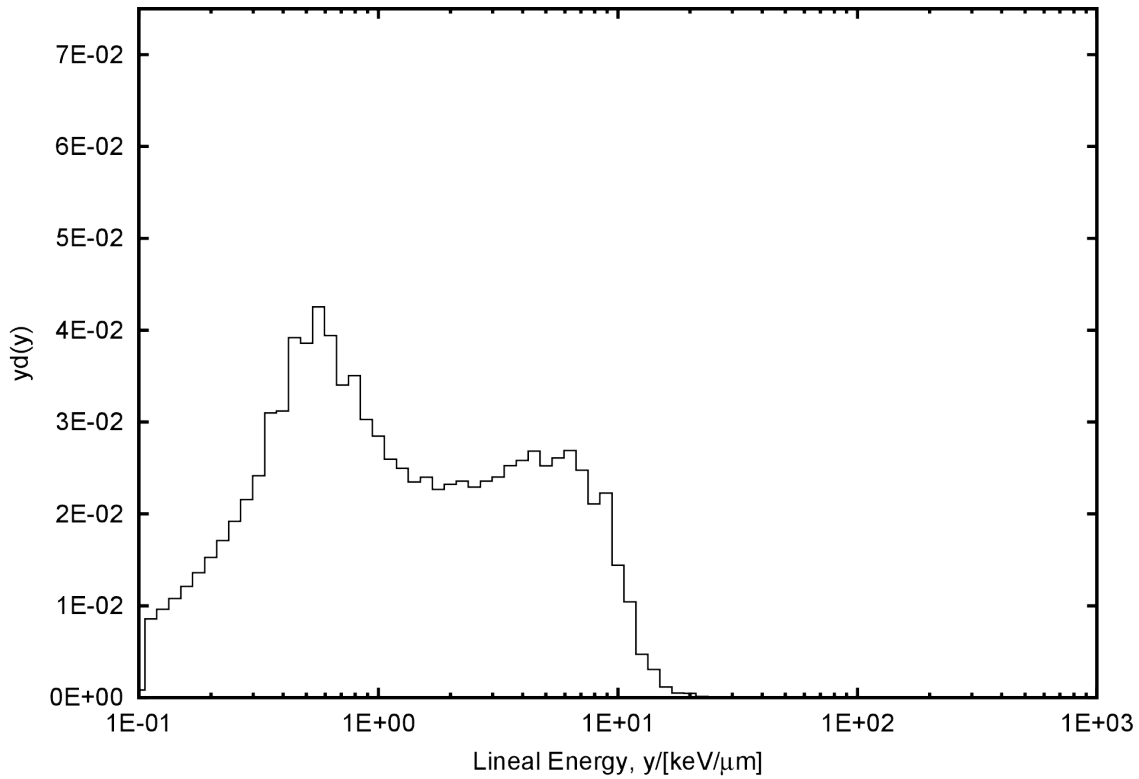

Figure D.5. Lineal energy distribution for the TEPC on the surface of Mars, downward photon component.

Surface of Mars, downward photon component:

```
# Using 80 Log Bins
# Min: 0.1 keV/μm              Max: 1000 keV/μm              20 bins/decade
#
# SiteSize: 1 μm               Mean Chord Length: 0.667 μm
#
# Using y Output with units of [keV/μm]
#
# y_F = 0.635 keV/μm
# y_D = 2.420 keV/μm
#
# D     = 2.280e-04 Gy
# H     = 2.319e-04 Sv
# Q_avg = 1.017e+00
#
# N = 294195
#
# y [keV/μm] N(y)     f(y)         y*f(y)      d(y)         y*d(y)
1.0000e-01   13680    1.4645e-02  5.2754e-03  5.2754e-03  8.3139e-04
1.1220e-01   13680    1.2002e-01  4.8510e-02  4.8510e-02  8.5779e-03
1.2589e-01   13680    1.0697e-01  4.8510e-02  4.8510e-02  9.6245e-03
1.4125e-01   13680    9.5335e-02  4.8510e-02  4.8510e-02  1.0799e-02
1.5849e-01   13680    8.4968e-02  4.8510e-02  4.8510e-02  1.2117e-02
1.7783e-01   13680    7.5728e-02  4.8510e-02  4.8510e-02  1.3595e-02
1.9953e-01   13680    6.7492e-02  4.8510e-02  4.8510e-02  1.5254e-02
2.2387e-01   13680    6.0153e-02  4.8510e-02  4.8510e-02  1.7115e-02
2.5119e-01   13680    5.3611e-02  4.8510e-02  4.8510e-02  1.9203e-02
2.8184e-01   13680    4.7781e-02  4.8510e-02  4.8510e-02  2.1547e-02
3.1623e-01   13680    4.2585e-02  4.8510e-02  4.8510e-02  2.4176e-02
3.5481e-01   15626    4.3353e-02  5.5411e-02  5.5411e-02  3.0984e-02
3.9811e-01   14020    3.4667e-02  4.9716e-02  4.9716e-02  3.1192e-02
4.4668e-01   15701    3.4602e-02  5.5677e-02  5.5677e-02  3.9194e-02
5.0119e-01   13773    2.7052e-02  4.8840e-02  4.8840e-02  3.8576e-02
5.6234e-01   13539    2.3700e-02  4.8010e-02  4.8010e-02  4.2548e-02
6.3096e-01   11176    1.7436e-02  3.9631e-02  3.9631e-02  3.9408e-02
7.0795e-01   8603     1.1962e-02  3.0507e-02  3.0507e-02  3.4036e-02
7.9433e-01   7901     9.7915e-03  2.8017e-02  2.8017e-02  3.5073e-02
8.9125e-01   6077     6.7121e-03  2.1549e-02  2.1549e-02  3.0268e-02
1.0000e+00   5092     5.0125e-03  1.8057e-02  1.8057e-02  2.8456e-02
1.1220e+00   4138     3.6304e-03  1.4674e-02  1.4674e-02  2.5947e-02
1.2589e+00   3546     2.7727e-03  1.2574e-02  1.2574e-02  2.4948e-02
1.4125e+00   2975     2.0733e-03  1.0550e-02  1.0550e-02  2.3484e-02
1.5849e+00   2709     1.6826e-03  9.6063e-03  9.6063e-03  2.3994e-02
1.7783e+00   2280     1.2621e-03  8.0850e-03  8.0850e-03  2.2658e-02
1.9953e+00   2082     1.0272e-03  7.3829e-03  7.3829e-03  2.3215e-02
2.2387e+00   1884     8.2842e-04  6.6808e-03  6.6808e-03  2.3571e-02
2.5119e+00   1633     6.3996e-04  5.7907e-03  5.7907e-03  2.2923e-02
2.8184e+00   1496     5.2252e-04  5.3049e-03  5.3049e-03  2.3563e-02
3.1623e+00   1359     4.2305e-04  4.8191e-03  4.8191e-03  2.4017e-02
```

3.5481e+00	1274	3.5346e-04	4.5177e-03	4.5177e-03	2.5262e-02
3.9811e+00	1161	2.8708e-04	4.1170e-03	4.1170e-03	2.5830e-02
4.4668e+00	1075	2.3691e-04	3.8120e-03	3.8120e-03	2.6835e-02
5.0119e+00	901	1.7697e-04	3.1950e-03	3.1950e-03	2.5236e-02
5.6234e+00	830	1.4529e-04	2.9432e-03	2.9432e-03	2.6084e-02
6.3096e+00	763	1.1904e-04	2.7056e-03	2.7056e-03	2.6904e-02
7.0795e+00	626	8.7045e-05	2.2198e-03	2.2198e-03	2.4767e-02
7.9433e+00	475	5.8866e-05	1.6844e-03	1.6844e-03	2.1086e-02
8.9125e+00	447	4.9371e-05	1.5851e-03	1.5851e-03	2.2264e-02
1.0000e+01	258	2.5397e-05	9.1488e-04	9.1488e-04	1.4418e-02
1.1220e+01	166	1.4564e-05	5.8865e-04	5.8865e-04	1.0409e-02
1.2589e+01	67	5.2389e-06	2.3759e-04	2.3759e-04	4.7138e-03
1.4125e+01	39	2.7179e-06	1.3830e-04	1.3830e-04	3.0786e-03
1.5849e+01	13	8.0744e-07	4.6099e-05	4.6099e-05	1.1514e-03
1.7783e+01	5	2.7678e-07	1.7730e-05	1.7730e-05	4.9689e-04
1.9953e+01	4	1.9735e-07	1.4184e-05	1.4184e-05	4.4602e-04
2.2387e+01	1	4.3971e-08	3.5461e-06	3.5461e-06	1.2511e-04
2.5119e+01	0	0.0000e+00	0.0000e+00	0.0000e+00	0.0000e+00
2.8184e+01	0	0.0000e+00	0.0000e+00	0.0000e+00	0.0000e+00
3.1623e+01	0	0.0000e+00	0.0000e+00	0.0000e+00	0.0000e+00
3.5481e+01	0	0.0000e+00	0.0000e+00	0.0000e+00	0.0000e+00
3.9811e+01	0	0.0000e+00	0.0000e+00	0.0000e+00	0.0000e+00
4.4668e+01	0	0.0000e+00	0.0000e+00	0.0000e+00	0.0000e+00
5.0119e+01	0	0.0000e+00	0.0000e+00	0.0000e+00	0.0000e+00
5.6234e+01	0	0.0000e+00	0.0000e+00	0.0000e+00	0.0000e+00
6.3096e+01	0	0.0000e+00	0.0000e+00	0.0000e+00	0.0000e+00
7.0795e+01	0	0.0000e+00	0.0000e+00	0.0000e+00	0.0000e+00
7.9433e+01	0	0.0000e+00	0.0000e+00	0.0000e+00	0.0000e+00
8.9125e+01	0	0.0000e+00	0.0000e+00	0.0000e+00	0.0000e+00
1.0000e+02	0	0.0000e+00	0.0000e+00	0.0000e+00	0.0000e+00
1.1220e+02	0	0.0000e+00	0.0000e+00	0.0000e+00	0.0000e+00
1.2589e+02	0	0.0000e+00	0.0000e+00	0.0000e+00	0.0000e+00
1.4125e+02	0	0.0000e+00	0.0000e+00	0.0000e+00	0.0000e+00
1.5849e+02	0	0.0000e+00	0.0000e+00	0.0000e+00	0.0000e+00
1.7783e+02	0	0.0000e+00	0.0000e+00	0.0000e+00	0.0000e+00
1.9953e+02	0	0.0000e+00	0.0000e+00	0.0000e+00	0.0000e+00
2.2387e+02	0	0.0000e+00	0.0000e+00	0.0000e+00	0.0000e+00
2.5119e+02	0	0.0000e+00	0.0000e+00	0.0000e+00	0.0000e+00
2.8184e+02	0	0.0000e+00	0.0000e+00	0.0000e+00	0.0000e+00
3.1623e+02	0	0.0000e+00	0.0000e+00	0.0000e+00	0.0000e+00
3.5481e+02	0	0.0000e+00	0.0000e+00	0.0000e+00	0.0000e+00
3.9811e+02	0	0.0000e+00	0.0000e+00	0.0000e+00	0.0000e+00
4.4668e+02	0	0.0000e+00	0.0000e+00	0.0000e+00	0.0000e+00
5.0119e+02	0	0.0000e+00	0.0000e+00	0.0000e+00	0.0000e+00
5.6234e+02	0	0.0000e+00	0.0000e+00	0.0000e+00	0.0000e+00
6.3096e+02	0	0.0000e+00	0.0000e+00	0.0000e+00	0.0000e+00
7.0795e+02	0	0.0000e+00	0.0000e+00	0.0000e+00	0.0000e+00
7.9433e+02	0	0.0000e+00	0.0000e+00	0.0000e+00	0.0000e+00
8.9125e+02	0	0.0000e+00	0.0000e+00	0.0000e+00	0.0000e+00
1.0000e+03	0	0.0000e+00	0.0000e+00	0.0000e+00	0.0000e+00

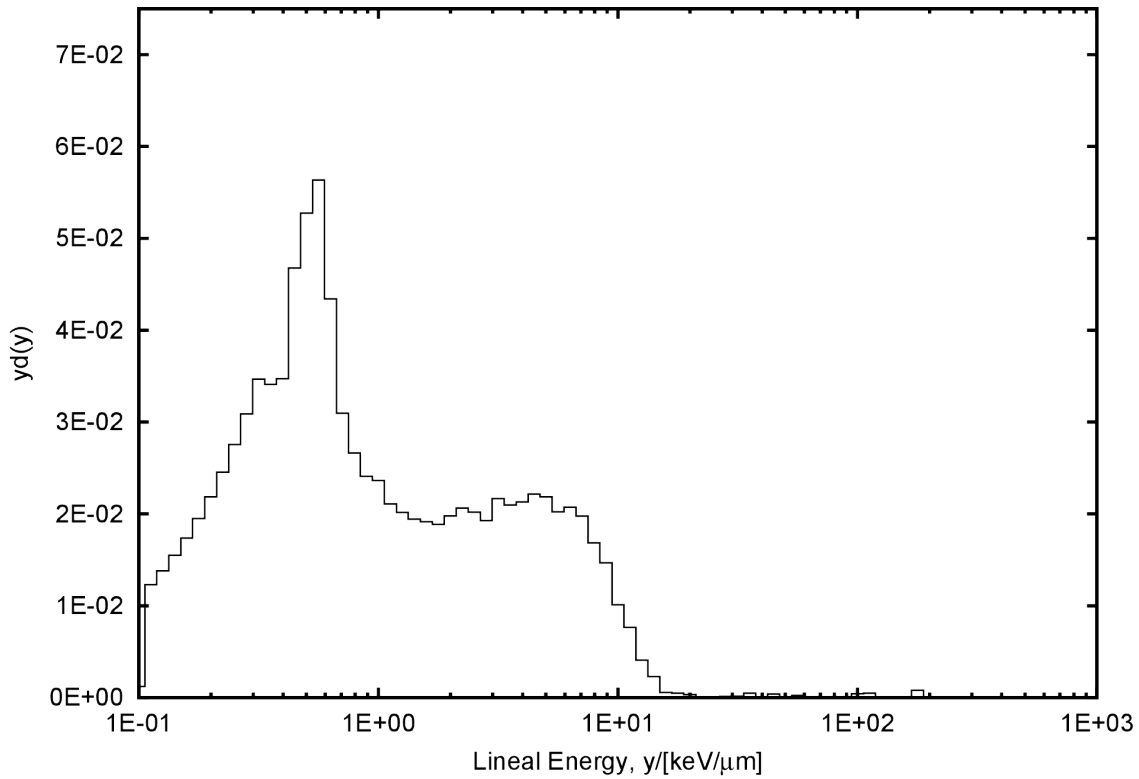

Figure D.6. Lineal energy distribution for the TEPC on the surface of Mars, downward other component.

Surface of Mars, downward other component:

```
# Using 80 Log Bins
# Min: 0.1 keV/μm              Max: 1000 keV/μm              20 bins/decade
#
# SiteSize: 1 μm               Mean Chord Length: 0.667 μm
#
# Using y Output with units of [keV/μm]
#
# y_F = 0.514 keV/μm
# y_D = 2.275 keV/μm
#
# D     = 2.920e-04 Gy
# H     = 3.120e-04 Sv
# Q_avg = 1.069e+00
#
# N = 467209
#
# y [keV/μm] N(y)     f(y)         y*f(y)      d(y)         y*d(y)
1.0000e-01   25051    1.5445e-02  6.1236e-03  6.1236e-03  1.1921e-03
1.1220e-01   25051    1.2658e-01  5.6309e-02  5.6309e-02  1.2300e-02
1.2589e-01   25051    1.1281e-01  5.6309e-02  5.6309e-02  1.3801e-02
1.4125e-01   25051    1.0054e-01  5.6309e-02  5.6309e-02  1.5485e-02
1.5849e-01   25051    8.9610e-02  5.6309e-02  5.6309e-02  1.7374e-02
1.7783e-01   25051    7.9865e-02  5.6309e-02  5.6309e-02  1.9494e-02
1.9953e-01   25051    7.1180e-02  5.6309e-02  5.6309e-02  2.1873e-02
2.2387e-01   25051    6.3439e-02  5.6309e-02  5.6309e-02  2.4541e-02
2.5119e-01   25051    5.6540e-02  5.6309e-02  5.6309e-02  2.7536e-02
2.8184e-01   25051    5.0392e-02  5.6309e-02  5.6309e-02  3.0896e-02
3.1623e-01   25051    4.4912e-02  5.6309e-02  5.6309e-02  3.4666e-02
3.5481e-01   21953    3.5077e-02  4.9346e-02  4.9346e-02  3.4085e-02
3.9811e-01   19929    2.8380e-02  4.4796e-02  4.4796e-02  3.4719e-02
4.4668e-01   23931    3.0373e-02  5.3792e-02  5.3792e-02  4.6777e-02
5.0119e-01   24055    2.7211e-02  5.4070e-02  5.4070e-02  5.2757e-02
5.6234e-01   22902    2.3089e-02  5.1479e-02  5.1479e-02  5.6357e-02
6.3096e-01   15724    1.4129e-02  3.5344e-02  3.5344e-02  4.3415e-02
7.0795e-01   9990     8.0002e-03  2.2455e-02  2.2455e-02  3.0949e-02
7.9433e-01   7665     5.4707e-03  1.7229e-02  1.7229e-02  2.6643e-02
8.9125e-01   6181     3.9318e-03  1.3894e-02  1.3894e-02  2.4107e-02
1.0000e+00   5395     3.0586e-03  1.2127e-02  1.2127e-02  2.3608e-02
1.1220e+00   4295     2.1702e-03  9.6542e-03  9.6542e-03  2.1088e-02
1.2589e+00   3660     1.6482e-03  8.2269e-03  8.2269e-03  2.0163e-02
1.4125e+00   3144     1.2619e-03  7.0670e-03  7.0670e-03  1.9434e-02
1.5849e+00   2759     9.8693e-04  6.2016e-03  6.2016e-03  1.9135e-02
1.7783e+00   2425     7.7312e-04  5.4509e-03  5.4509e-03  1.8871e-02
1.9953e+00   2264     6.4329e-04  5.0890e-03  5.0890e-03  1.9768e-02
2.2387e+00   2106     5.3332e-04  4.7338e-03  4.7338e-03  2.0632e-02
2.5119e+00   1838     4.1484e-04  4.1314e-03  4.1314e-03  2.0203e-02
2.8184e+00   1564     3.1461e-04  3.5155e-03  3.5155e-03  1.9289e-02
3.1623e+00   1566     2.8075e-04  3.5200e-03  3.5200e-03  2.1670e-02
```

3.5481e+00	1351	2.1587e-04	3.0368e-03	3.0368e-03	2.0976e-02
3.9811e+00	1222	1.7402e-04	2.7468e-03	2.7468e-03	2.1289e-02
4.4668e+00	1133	1.4380e-04	2.5467e-03	2.5467e-03	2.2147e-02
5.0119e+00	997	1.1278e-04	2.2410e-03	2.2410e-03	2.1866e-02
5.6234e+00	822	8.2872e-05	1.8477e-03	1.8477e-03	2.0228e-02
6.3096e+00	750	6.7390e-05	1.6858e-03	1.6858e-03	2.0708e-02
7.0795e+00	638	5.1092e-05	1.4341e-03	1.4341e-03	1.9765e-02
7.9433e+00	485	3.4616e-05	1.0902e-03	1.0902e-03	1.6858e-02
8.9125e+00	376	2.3918e-05	8.4517e-04	8.4517e-04	1.4664e-02
1.0000e+01	231	1.3096e-05	5.1924e-04	5.1924e-04	1.0109e-02
1.1220e+01	156	7.8824e-06	3.5065e-04	3.5065e-04	7.6595e-03
1.2589e+01	74	3.3325e-06	1.6634e-04	1.6634e-04	4.0767e-03
1.4125e+01	37	1.4850e-06	8.3168e-05	8.3168e-05	2.2871e-03
1.5849e+01	8	2.8617e-07	1.7982e-05	1.7982e-05	5.5484e-04
1.7783e+01	6	1.9129e-07	1.3487e-05	1.3487e-05	4.6690e-04
1.9953e+01	4	1.1366e-07	8.9911e-06	8.9911e-06	3.4925e-04
2.2387e+01	1	2.5324e-08	2.2478e-06	2.2478e-06	9.7966e-05
2.5119e+01	0	0.0000e+00	0.0000e+00	0.0000e+00	0.0000e+00
2.8184e+01	1	2.0116e-08	2.2478e-06	2.2478e-06	1.2333e-04
3.1623e+01	1	1.7928e-08	2.2478e-06	2.2478e-06	1.3838e-04
3.5481e+01	3	4.7935e-08	6.7434e-06	6.7434e-06	4.6580e-04
3.9811e+01	0	0.0000e+00	0.0000e+00	0.0000e+00	0.0000e+00
4.4668e+01	2	2.5384e-08	4.4956e-06	4.4956e-06	3.9094e-04
5.0119e+01	0	0.0000e+00	0.0000e+00	0.0000e+00	0.0000e+00
5.6234e+01	1	1.0082e-08	2.2478e-06	2.2478e-06	2.4608e-04
6.3096e+01	0	0.0000e+00	0.0000e+00	0.0000e+00	0.0000e+00
7.0795e+01	0	0.0000e+00	0.0000e+00	0.0000e+00	0.0000e+00
7.9433e+01	0	0.0000e+00	0.0000e+00	0.0000e+00	0.0000e+00
8.9125e+01	0	0.0000e+00	0.0000e+00	0.0000e+00	0.0000e+00
1.0000e+02	1	5.6694e-09	2.2478e-06	2.2478e-06	4.3760e-04
1.1220e+02	1	5.0528e-09	2.2478e-06	2.2478e-06	4.9099e-04
1.2589e+02	0	0.0000e+00	0.0000e+00	0.0000e+00	0.0000e+00
1.4125e+02	0	0.0000e+00	0.0000e+00	0.0000e+00	0.0000e+00
1.5849e+02	0	0.0000e+00	0.0000e+00	0.0000e+00	0.0000e+00
1.7783e+02	1	3.1881e-09	2.2478e-06	2.2478e-06	7.7817e-04
1.9953e+02	0	0.0000e+00	0.0000e+00	0.0000e+00	0.0000e+00
2.2387e+02	0	0.0000e+00	0.0000e+00	0.0000e+00	0.0000e+00
2.5119e+02	0	0.0000e+00	0.0000e+00	0.0000e+00	0.0000e+00
2.8184e+02	0	0.0000e+00	0.0000e+00	0.0000e+00	0.0000e+00
3.1623e+02	0	0.0000e+00	0.0000e+00	0.0000e+00	0.0000e+00
3.5481e+02	0	0.0000e+00	0.0000e+00	0.0000e+00	0.0000e+00
3.9811e+02	0	0.0000e+00	0.0000e+00	0.0000e+00	0.0000e+00
4.4668e+02	0	0.0000e+00	0.0000e+00	0.0000e+00	0.0000e+00
5.0119e+02	0	0.0000e+00	0.0000e+00	0.0000e+00	0.0000e+00
5.6234e+02	0	0.0000e+00	0.0000e+00	0.0000e+00	0.0000e+00
6.3096e+02	0	0.0000e+00	0.0000e+00	0.0000e+00	0.0000e+00
7.0795e+02	0	0.0000e+00	0.0000e+00	0.0000e+00	0.0000e+00
7.9433e+02	0	0.0000e+00	0.0000e+00	0.0000e+00	0.0000e+00
8.9125e+02	0	0.0000e+00	0.0000e+00	0.0000e+00	0.0000e+00
1.0000e+03	0	0.0000e+00	0.0000e+00	0.0000e+00	0.0000e+00

APPENDIX E

SURFACE OF MARS ALBEDO LINEAL ENERGY DISTRIBUTIONS

This appendix contains the y distributions for the albedo components of the particle fluence for the TEPC positioned 1 m above the surface of Mars. The figures show a plot of $yd(y)$ as a function of y on a semi-log axis. $\bar{y}_{\mathrm{F}}$, $\bar{y}_{\mathrm{D}}$, D, H, and $\bar{Q}$ for the simulated irradiation are included in the tabulated data. D and H represent integral values for 1.0×10^8 incident particles. These 1.0×10^8 particles, 1.0×10^8 histories in FLUKA, correspond to a simulated irradiation time of 0.545 y. Dividing D and H by 0.545 will normalize these values to time in the form of $\dot{D}$ and $\dot{H}$ with units of Gy/y and Sv/y, respectively. The $f(y)$, $d(y)$, $yf(y)$, and $yd(y)$ distributions have all been normalized to unit area.

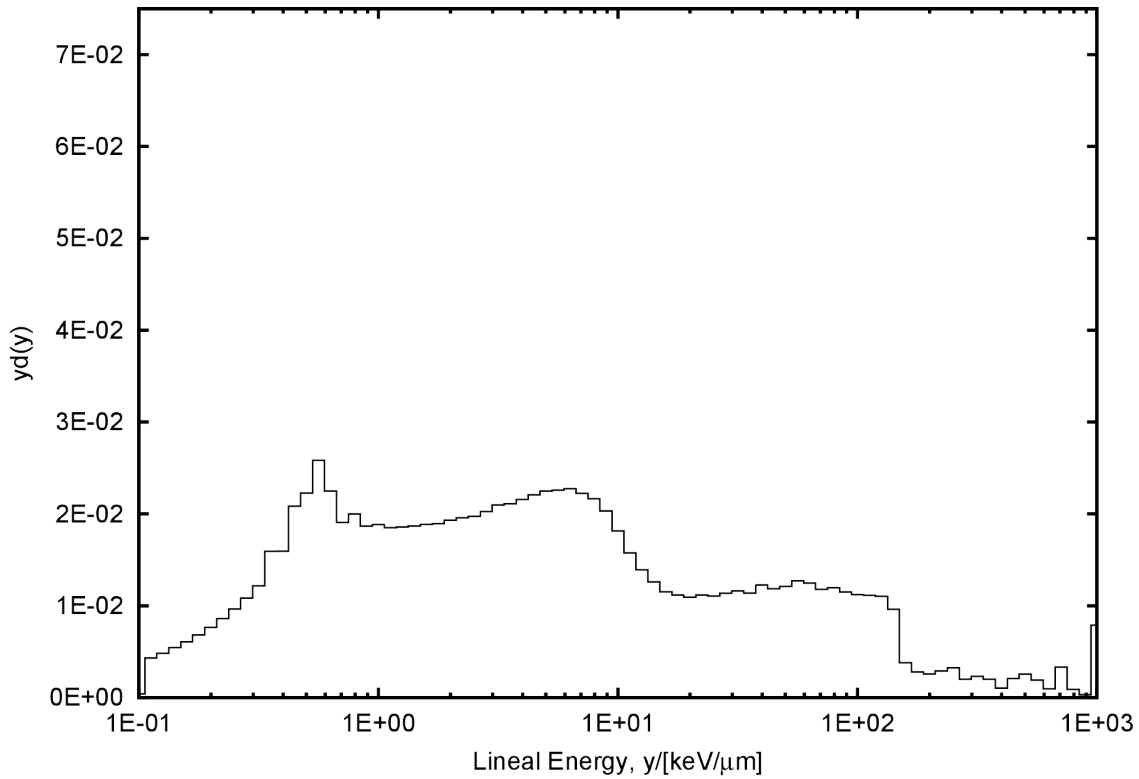

Figure E.1. Lineal energy distribution for the TEPC on the surface of Mars, albedo (all-particle) component.

Surface of Mars, albedo (all-particle) component:

```
# Using 80 Log Bins
# Min: 0.1 keV/μm              Max: 1000 keV/μm              20 bins/decade
#
# SiteSize: 1 μm               Mean Chord Length: 0.667 μm
#
# Using y Output with units of [keV/μm]
#
# y_F = 1.120 keV/μm
# y_D = 36.310 keV/μm
#
# D     = 6.761e-03 Gy
# H     = 3.252e-02 Sv
# Q_avg = 4.811e+00
#
# N = 4938218
#
# y [keV/μm] N(y)     f(y)         y*f(y)      d(y)         y*d(y)
1.0000e-01   204668   1.4217e-02  4.6801e-03  4.6801e-03  4.1797e-04
1.1220e-01   204668   1.1651e-01  4.3035e-02  4.3035e-02  4.3125e-03
1.2589e-01   204668   1.0384e-01  4.3035e-02  4.3035e-02  4.8387e-03
1.4125e-01   204668   9.2549e-02  4.3035e-02  4.3035e-02  5.4291e-03
1.5849e-01   204668   8.2484e-02  4.3035e-02  4.3035e-02  6.0915e-03
1.7783e-01   204668   7.3514e-02  4.3035e-02  4.3035e-02  6.8348e-03
1.9953e-01   204668   6.5519e-02  4.3035e-02  4.3035e-02  7.6687e-03
2.2387e-01   204668   5.8394e-02  4.3035e-02  4.3035e-02  8.6045e-03
2.5119e-01   204668   5.2044e-02  4.3035e-02  4.3035e-02  9.6544e-03
2.8184e-01   204668   4.6384e-02  4.3035e-02  4.3035e-02  1.0832e-02
3.1623e-01   204668   4.1340e-02  4.3035e-02  4.3035e-02  1.2154e-02
3.5481e-01   238970   4.3019e-02  5.0248e-02  5.0248e-02  1.5923e-02
3.9811e-01   213464   3.4249e-02  4.4885e-02  4.4885e-02  1.5959e-02
4.4668e-01   248503   3.5535e-02  5.2253e-02  5.2253e-02  2.0845e-02
5.0119e-01   236647   3.0159e-02  4.9760e-02  4.9760e-02  2.2273e-02
5.6234e-01   244817   2.7808e-02  5.1477e-02  5.1477e-02  2.5853e-02
6.3096e-01   189681   1.9202e-02  3.9884e-02  3.9884e-02  2.2475e-02
7.0795e-01   143246   1.2924e-02  3.0120e-02  3.0120e-02  1.9044e-02
7.9433e-01   134013   1.0776e-02  2.8179e-02  2.8179e-02  1.9990e-02
8.9125e-01   111502   7.9910e-03  2.3445e-02  2.3445e-02  1.8662e-02
1.0000e+00   100447   6.4159e-03  2.1121e-02  2.1121e-02  1.8863e-02
1.1220e+00   87800    4.9982e-03  1.8462e-02  1.8462e-02  1.8500e-02
1.2589e+00   78605    3.9881e-03  1.6528e-02  1.6528e-02  1.8583e-02
1.4125e+00   70422    3.1844e-03  1.4808e-02  1.4808e-02  1.8680e-02
1.5849e+00   63428    2.5562e-03  1.3337e-02  1.3337e-02  1.8878e-02
1.7783e+00   56733    2.0378e-03  1.1929e-02  1.1929e-02  1.8946e-02
1.9953e+00   51514    1.6491e-03  1.0832e-02  1.0832e-02  1.9302e-02
2.2387e+00   46531    1.3276e-03  9.7840e-03  9.7840e-03  1.9562e-02
2.5119e+00   41811    1.0632e-03  8.7916e-03  8.7916e-03  1.9723e-02
2.8184e+00   38284    8.6764e-04  8.0499e-03  8.0499e-03  2.0262e-02
3.1623e+00   35321    7.1343e-04  7.4269e-03  7.4269e-03  2.0975e-02
```

3.5481e+00	31678	5.7027e-04	6.6609e-03	6.6609e-03	2.1107e-02
3.9811e+00	28850	4.6288e-04	6.0663e-03	6.0663e-03	2.1569e-02
4.4668e+00	26344	3.7671e-04	5.5393e-03	5.5393e-03	2.2098e-02
5.0119e+00	23906	3.0467e-04	5.0267e-03	5.0267e-03	2.2500e-02
5.6234e+00	21401	2.4308e-04	4.5000e-03	4.5000e-03	2.2600e-02
6.3096e+00	19205	1.9442e-04	4.0382e-03	4.0382e-03	2.2756e-02
7.0795e+00	16724	1.5089e-04	3.5165e-03	3.5165e-03	2.2234e-02
7.9433e+00	14523	1.1678e-04	3.0537e-03	3.0537e-03	2.1664e-02
8.9125e+00	12145	8.7040e-05	2.5537e-03	2.5537e-03	2.0327e-02
1.0000e+01	9662	6.1715e-05	2.0316e-03	2.0316e-03	1.8144e-02
1.1220e+01	7483	4.2599e-05	1.5734e-03	1.5734e-03	1.5767e-02
1.2589e+01	5887	2.9869e-05	1.2379e-03	1.2379e-03	1.3918e-02
1.4125e+01	4751	2.1484e-05	9.9899e-04	9.9899e-04	1.2603e-02
1.5849e+01	3872	1.5605e-05	8.1416e-04	8.1416e-04	1.1524e-02
1.7783e+01	3346	1.2018e-05	7.0356e-04	7.0356e-04	1.1174e-02
1.9953e+01	2914	9.3285e-06	6.1272e-04	6.1272e-04	1.0919e-02
2.2387e+01	2660	7.5893e-06	5.5932e-04	5.5932e-04	1.1183e-02
2.5119e+01	2347	5.9681e-06	4.9350e-04	4.9350e-04	1.1071e-02
2.8184e+01	2145	4.8612e-06	4.5103e-04	4.5103e-04	1.1353e-02
3.1623e+01	1957	3.9529e-06	4.1150e-04	4.1150e-04	1.1622e-02
3.5481e+01	1708	3.0747e-06	3.5914e-04	3.5914e-04	1.1381e-02
3.9811e+01	1641	2.6329e-06	3.4505e-04	3.4505e-04	1.2268e-02
4.4668e+01	1413	2.0205e-06	2.9711e-04	2.9711e-04	1.1853e-02
5.0119e+01	1284	1.6364e-06	2.6999e-04	2.6999e-04	1.2085e-02
5.6234e+01	1206	1.3698e-06	2.5358e-04	2.5358e-04	1.2736e-02
6.3096e+01	1053	1.0660e-06	2.2141e-04	2.2141e-04	1.2477e-02
7.0795e+01	888	8.0119e-07	1.8672e-04	1.8672e-04	1.1806e-02
7.9433e+01	803	6.4571e-07	1.6885e-04	1.6885e-04	1.1978e-02
8.9125e+01	687	4.9235e-07	1.4445e-04	1.4445e-04	1.1498e-02
1.0000e+02	598	3.8196e-07	1.2574e-04	1.2574e-04	1.1230e-02
1.1220e+02	529	3.0115e-07	1.1123e-04	1.1123e-04	1.1146e-02
1.2589e+02	466	2.3643e-07	9.7985e-05	9.7985e-05	1.1017e-02
1.4125e+02	362	1.6369e-07	7.6117e-05	7.6117e-05	9.6025e-03
1.5849e+02	128	5.1586e-08	2.6914e-05	2.6914e-05	3.8096e-03
1.7783e+02	84	3.0172e-08	1.7663e-05	1.7663e-05	2.8051e-03
1.9953e+02	69	2.2089e-08	1.4509e-05	1.4509e-05	2.5854e-03
2.2387e+02	69	1.9687e-08	1.4509e-05	1.4509e-05	2.9008e-03
2.5119e+02	69	1.7546e-08	1.4509e-05	1.4509e-05	3.2548e-03
2.8184e+02	38	8.6120e-09	7.9902e-06	7.9902e-06	2.0112e-03
3.1623e+02	39	7.8774e-09	8.2005e-06	8.2005e-06	2.3160e-03
3.5481e+02	30	5.4006e-09	6.3081e-06	6.3081e-06	1.9989e-03
3.9811e+02	14	2.2462e-09	2.9438e-06	2.9438e-06	1.0467e-03
4.4668e+02	25	3.5749e-09	5.2567e-06	5.2567e-06	2.0971e-03
5.0119e+02	27	3.4410e-09	5.6773e-06	5.6773e-06	2.5412e-03
5.6234e+02	18	2.0445e-09	3.7848e-06	3.7848e-06	1.9008e-03
6.3096e+02	8	8.0986e-10	1.6822e-06	1.6822e-06	9.4790e-04
7.0795e+02	25	2.2556e-09	5.2567e-06	5.2567e-06	3.3236e-03
7.9433e+02	6	4.8247e-10	1.2616e-06	1.2616e-06	8.9501e-04
8.9125e+02	2	1.4333e-10	4.2054e-07	4.2054e-07	3.3474e-04
1.0000e+03	42	2.6827e-09	8.8313e-06	8.8313e-06	7.8872e-03

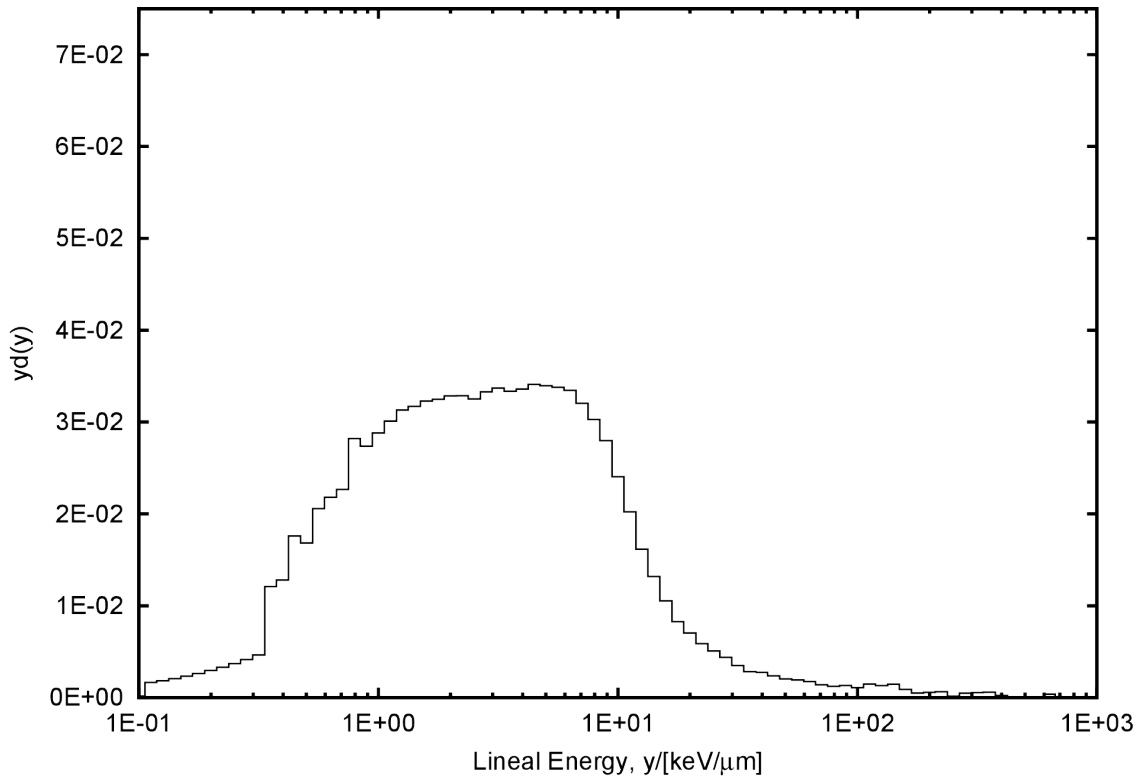

Figure E.2. Lineal energy distribution for the TEPC on the surface of Mars, albedo elemental ion component.

Surface of Mars, albedo elemental ion component:

```
# Using 80 Log Bins
# Min: 0.1 keV/μm              Max: 1000 keV/μm              20 bins/decade
#
# SiteSize: 1 μm               Mean Chord Length: 0.667 μm
#
# Using y Output with units of [keV/μm]
#
# y_F = 1.371 keV/μm
# y_D = 7.259 keV/μm
#
# D     = 2.218e-03 Gy
# H     = 3.721e-03 Sv
# Q_avg = 1.678e+00
#
# N = 1300244
#
# y [keV/μm] N(y)     f(y)         y*f(y)      d(y)         y*d(y)
1.0000e-01   25787    1.0213e-02  2.1956e-03  2.1956e-03  1.6020e-04
1.1220e-01   25787    8.3704e-02  2.0189e-02  2.0189e-02  1.6528e-03
1.2589e-01   25787    7.4601e-02  2.0189e-02  2.0189e-02  1.8545e-03
1.4125e-01   25787    6.6488e-02  2.0189e-02  2.0189e-02  2.0808e-03
1.5849e-01   25787    5.9258e-02  2.0189e-02  2.0189e-02  2.3347e-03
1.7783e-01   25787    5.2814e-02  2.0189e-02  2.0189e-02  2.6196e-03
1.9953e-01   25787    4.7070e-02  2.0189e-02  2.0189e-02  2.9392e-03
2.2387e-01   25787    4.1951e-02  2.0189e-02  2.0189e-02  3.2978e-03
2.5119e-01   25787    3.7389e-02  2.0189e-02  2.0189e-02  3.7002e-03
2.8184e-01   25787    3.3323e-02  2.0189e-02  2.0189e-02  4.1517e-03
3.1623e-01   25787    2.9699e-02  2.0189e-02  2.0189e-02  4.6583e-03
3.5481e-01   59553    6.1129e-02  4.6626e-02  4.6626e-02  1.2071e-02
3.9811e-01   56331    5.1534e-02  4.4103e-02  4.4103e-02  1.2811e-02
4.4668e-01   68985    5.6247e-02  5.4010e-02  5.4010e-02  1.7603e-02
5.0119e-01   58802    4.2730e-02  4.6038e-02  4.6038e-02  1.6835e-02
5.6234e-01   64020    4.1463e-02  5.0123e-02  5.0123e-02  2.0566e-02
6.3096e-01   60471    3.4905e-02  4.7344e-02  4.7344e-02  2.1796e-02
7.0795e-01   56054    2.8837e-02  4.3886e-02  4.3886e-02  2.2669e-02
7.9433e-01   62096    2.8471e-02  4.8617e-02  4.8617e-02  2.8177e-02
8.9125e-01   53720    2.1952e-02  4.2059e-02  4.2059e-02  2.7351e-02
1.0000e+00   50472    1.8382e-02  3.9516e-02  3.9516e-02  2.8832e-02
1.1220e+00   46960    1.5243e-02  3.6766e-02  3.6766e-02  3.0099e-02
1.2589e+00   43515    1.2589e-02  3.4069e-02  3.4069e-02  3.1295e-02
1.4125e+00   39287    1.0130e-02  3.0759e-02  3.0759e-02  3.1701e-02
1.5849e+00   35661    8.1948e-03  2.7920e-02  2.7920e-02  3.2287e-02
1.7783e+00   31984    6.5505e-03  2.5041e-02  2.5041e-02  3.2491e-02
1.9953e+00   28811    5.2590e-03  2.2557e-02  2.2557e-02  3.2839e-02
2.2387e+00   25689    4.1792e-03  2.0113e-02  2.0113e-02  3.2853e-02
2.5119e+00   22656    3.2849e-03  1.7738e-02  1.7738e-02  3.2510e-02
2.8184e+00   20691    2.6738e-03  1.6200e-02  1.6200e-02  3.3313e-02
3.1623e+00   18651    2.1481e-03  1.4602e-02  1.4602e-02  3.3692e-02
```

3.5481e+00	16445	1.6880e-03	1.2875e-02	1.2875e-02	3.3332e-02
3.9811e+00	14772	1.3514e-03	1.1565e-02	1.1565e-02	3.3595e-02
4.4668e+00	13355	1.0889e-03	1.0456e-02	1.0456e-02	3.4078e-02
5.0119e+00	11863	8.6206e-04	9.2878e-03	9.2878e-03	3.3964e-02
5.6234e+00	10512	6.8082e-04	8.2301e-03	8.2301e-03	3.3769e-02
6.3096e+00	9279	5.3561e-04	7.2648e-03	7.2648e-03	3.3445e-02
7.0795e+00	7924	4.0765e-04	6.2039e-03	6.2039e-03	3.2046e-02
7.9433e+00	6671	3.0587e-04	5.2229e-03	5.2229e-03	3.0271e-02
8.9125e+00	5499	2.2471e-04	4.3053e-03	4.3053e-03	2.7997e-02
1.0000e+01	4211	1.5337e-04	3.2969e-03	3.2969e-03	2.4056e-02
1.1220e+01	3155	1.0241e-04	2.4701e-03	2.4701e-03	2.0222e-02
1.2589e+01	2247	6.5005e-05	1.7592e-03	1.7592e-03	1.6160e-02
1.4125e+01	1633	4.2105e-05	1.2785e-03	1.2785e-03	1.3177e-02
1.5849e+01	1163	2.6725e-05	9.1054e-04	9.1054e-04	1.0530e-02
1.7783e+01	813	1.6651e-05	6.3652e-04	6.3652e-04	8.2589e-03
1.9953e+01	618	1.1281e-05	4.8385e-04	4.8385e-04	7.0440e-03
2.2387e+01	460	7.4835e-06	3.6015e-04	3.6015e-04	5.8828e-03
2.5119e+01	354	5.1327e-06	2.7716e-04	2.7716e-04	5.0796e-03
2.8184e+01	272	3.5149e-06	2.1296e-04	2.1296e-04	4.3792e-03
3.1623e+01	194	2.2343e-06	1.5189e-04	1.5189e-04	3.5045e-03
3.5481e+01	140	1.4371e-06	1.0961e-04	1.0961e-04	2.8376e-03
3.9811e+01	122	1.1161e-06	9.5517e-05	9.5517e-05	2.7745e-03
4.4668e+01	93	7.5828e-07	7.2812e-05	7.2812e-05	2.3731e-03
5.0119e+01	71	5.1594e-07	5.5588e-05	5.5588e-05	2.0328e-03
5.6234e+01	60	3.8859e-07	4.6976e-05	4.6976e-05	1.9274e-03
6.3096e+01	49	2.8284e-07	3.8363e-05	3.8363e-05	1.7661e-03
7.0795e+01	35	1.8006e-07	2.7402e-05	2.7402e-05	1.4155e-03
7.9433e+01	27	1.2380e-07	2.1139e-05	2.1139e-05	1.2252e-03
8.9125e+01	26	1.0625e-07	2.0356e-05	2.0356e-05	1.3237e-03
1.0000e+02	19	6.9199e-08	1.4876e-05	1.4876e-05	1.0854e-03
1.1220e+02	23	7.4657e-08	1.8007e-05	1.8007e-05	1.4742e-03
1.2589e+02	18	5.2074e-08	1.4093e-05	1.4093e-05	1.2945e-03
1.4125e+02	18	4.6411e-08	1.4093e-05	1.4093e-05	1.4525e-03
1.5849e+02	10	2.2980e-08	7.8293e-06	7.8293e-06	9.0538e-04
1.7783e+02	5	1.0240e-08	3.9146e-06	3.9146e-06	5.0793e-04
1.9953e+02	5	9.1267e-09	3.9146e-06	3.9146e-06	5.6990e-04
2.2387e+02	5	8.1342e-09	3.9146e-06	3.9146e-06	6.3944e-04
2.5119e+02	1	1.4499e-09	7.8293e-07	7.8293e-07	1.4349e-04
2.8184e+02	3	3.8767e-09	2.3488e-06	2.3488e-06	4.8300e-04
3.1623e+02	3	3.4551e-09	2.3488e-06	2.3488e-06	5.4194e-04
3.5481e+02	3	3.0794e-09	2.3488e-06	2.3488e-06	6.0807e-04
3.9811e+02	1	9.1484e-10	7.8293e-07	7.8293e-07	2.2742e-04
4.4668e+02	0	0.0000e+00	0.0000e+00	0.0000e+00	0.0000e+00
5.0119e+02	0	0.0000e+00	0.0000e+00	0.0000e+00	0.0000e+00
5.6234e+02	0	0.0000e+00	0.0000e+00	0.0000e+00	0.0000e+00
6.3096e+02	1	5.7722e-10	7.8293e-07	7.8293e-07	3.6044e-04
7.0795e+02	0	0.0000e+00	0.0000e+00	0.0000e+00	0.0000e+00
7.9433e+02	0	0.0000e+00	0.0000e+00	0.0000e+00	0.0000e+00
8.9125e+02	0	0.0000e+00	0.0000e+00	0.0000e+00	0.0000e+00
1.0000e+03	0	0.0000e+00	0.0000e+00	0.0000e+00	0.0000e+00

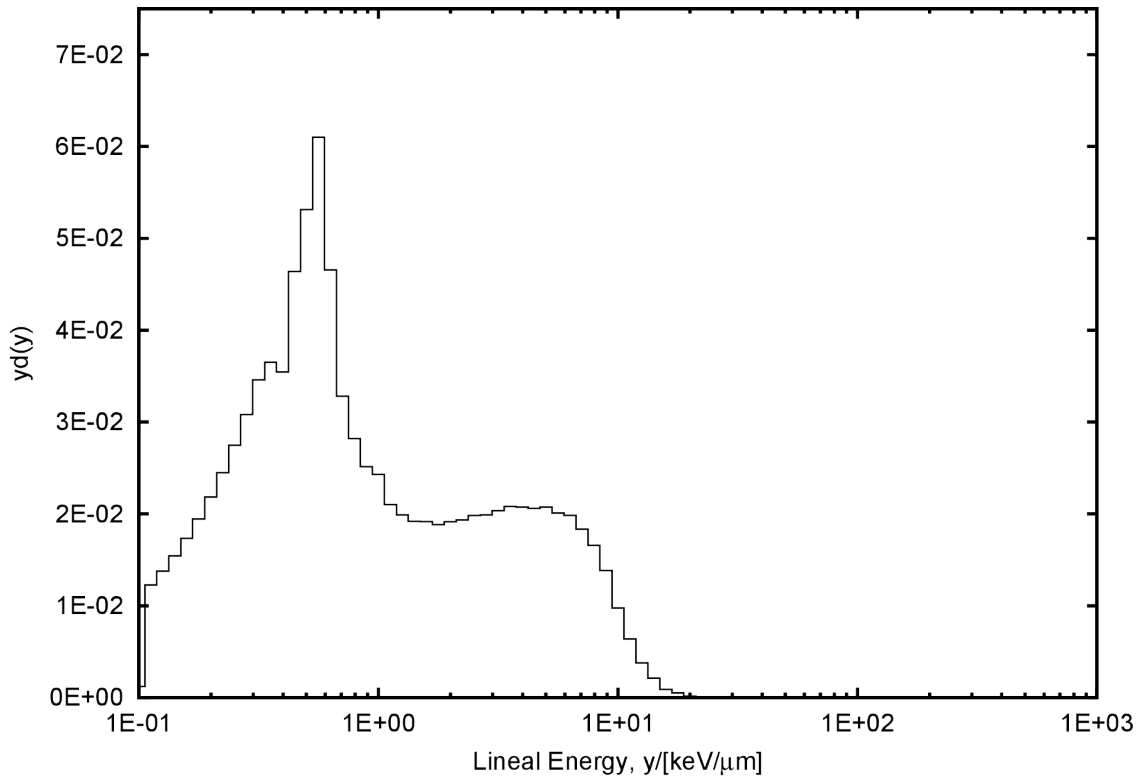

Figure E.3. Lineal energy distribution for the TEPC on the surface of Mars, albedo electron component.

Surface of Mars, albedo electron component:

```
# Using 80 Log Bins
# Min: 0.1 keV/μm              Max: 1000 keV/μm               20 bins/decade
#
# SiteSize: 1 μm               Mean Chord Length: 0.667 μm
#
# Using y Output with units of [keV/μm]
#
# y_F = 0.508 keV/μm
# y_D = 1.920 keV/μm
#
# D     = 1.464e-03 Gy
# H     = 1.482e-03 Sv
# Q_avg = 1.012e+00
#
# N = 2368211
#
# y [keV/μm] N(y)     f(y)         y*f(y)      d(y)         y*d(y)
1.0000e-01   125335   1.5333e-02  6.0403e-03  6.0403e-03  1.1896e-03
1.1220e-01   125335   1.2566e-01  5.5544e-02  5.5544e-02  1.2274e-02
1.2589e-01   125335   1.1200e-01  5.5544e-02  5.5544e-02  1.3771e-02
1.4125e-01   125335   9.9819e-02  5.5544e-02  5.5544e-02  1.5452e-02
1.5849e-01   125335   8.8963e-02  5.5544e-02  5.5544e-02  1.7337e-02
1.7783e-01   125335   7.9289e-02  5.5544e-02  5.5544e-02  1.9453e-02
1.9953e-01   125335   7.0666e-02  5.5544e-02  5.5544e-02  2.1826e-02
2.2387e-01   125335   6.2981e-02  5.5544e-02  5.5544e-02  2.4490e-02
2.5119e-01   125335   5.6132e-02  5.5544e-02  5.5544e-02  2.7478e-02
2.8184e-01   125335   5.0028e-02  5.5544e-02  5.5544e-02  3.0831e-02
3.1623e-01   125335   4.4587e-02  5.5544e-02  5.5544e-02  3.4592e-02
3.5481e-01   117835   3.7361e-02  5.2220e-02  5.2220e-02  3.6491e-02
3.9811e-01   102079   2.8845e-02  4.5238e-02  4.5238e-02  3.5469e-02
4.4668e-01   118977   2.9964e-02  5.2726e-02  5.2726e-02  4.6384e-02
5.0119e-01   121453   2.7261e-02  5.3823e-02  5.3823e-02  5.3127e-02
5.6234e-01   124270   2.4860e-02  5.5072e-02  5.5072e-02  6.0992e-02
6.3096e-01   84564    1.5077e-02  3.7476e-02  3.7476e-02  4.6569e-02
7.0795e-01   53123    8.4415e-03  2.3542e-02  2.3542e-02  3.2824e-02
7.9433e-01   40657    5.7580e-03  1.8018e-02  1.8018e-02  2.8187e-02
8.9125e-01   32310    4.0783e-03  1.4319e-02  1.4319e-02  2.5133e-02
1.0000e+00   27828    3.1306e-03  1.2332e-02  1.2332e-02  2.4288e-02
1.1220e+00   21473    2.1529e-03  9.5160e-03  9.5160e-03  2.1028e-02
1.2589e+00   18085    1.6161e-03  8.0146e-03  8.0146e-03  1.9871e-02
1.4125e+00   15574    1.2403e-03  6.9018e-03  6.9018e-03  1.9200e-02
1.5849e+00   13840    9.8237e-04  6.1334e-03  6.1334e-03  1.9145e-02
1.7783e+00   12123    7.6692e-04  5.3725e-03  5.3725e-03  1.8816e-02
1.9953e+00   10989    6.1958e-04  4.8699e-03  4.8699e-03  1.9137e-02
2.2387e+00   9901     4.9753e-04  4.3878e-03  4.3878e-03  1.9346e-02
2.5119e+00   9044     4.0504e-04  4.0080e-03  4.0080e-03  1.9828e-02
2.8184e+00   8082     3.2260e-04  3.5816e-03  3.5816e-03  1.9881e-02
3.1623e+00   7380     2.6254e-04  3.2705e-03  3.2705e-03  2.0369e-02
```

3.5481e+00	6714	2.1287e-04	2.9754e-03	2.9754e-03	2.0792e-02
3.9811e+00	5971	1.6873e-04	2.6461e-03	2.6461e-03	2.0747e-02
4.4668e+00	5286	1.3313e-04	2.3426e-03	2.3426e-03	2.0608e-02
5.0119e+00	4744	1.0648e-04	2.1024e-03	2.1024e-03	2.0752e-02
5.6234e+00	4091	8.1841e-05	1.8130e-03	1.8130e-03	2.0079e-02
6.3096e+00	3602	6.4222e-05	1.5963e-03	1.5963e-03	1.9836e-02
7.0795e+00	2969	4.7179e-05	1.3158e-03	1.3158e-03	1.8345e-02
7.9433e+00	2388	3.3820e-05	1.0583e-03	1.0583e-03	1.6556e-02
8.9125e+00	1778	2.2442e-05	7.8794e-04	7.8794e-04	1.3831e-02
1.0000e+01	1118	1.2577e-05	4.9546e-04	4.9546e-04	9.7578e-03
1.1220e+01	654	6.5572e-06	2.8983e-04	2.8983e-04	6.4045e-03
1.2589e+01	343	3.0650e-06	1.5200e-04	1.5200e-04	3.7688e-03
1.4125e+01	171	1.3619e-06	7.5781e-05	7.5781e-05	2.1082e-03
1.5849e+01	64	4.5428e-07	2.8362e-05	2.8362e-05	8.8530e-04
1.7783e+01	33	2.0876e-07	1.4624e-05	1.4624e-05	5.1218e-04
1.9953e+01	8	4.5105e-08	3.5453e-06	3.5453e-06	1.3932e-04
2.2387e+01	4	2.0100e-08	1.7727e-06	1.7727e-06	7.8157e-05
2.5119e+01	0	0.0000e+00	0.0000e+00	0.0000e+00	0.0000e+00
2.8184e+01	1	3.9915e-09	4.4316e-07	4.4316e-07	2.4599e-05
3.1623e+01	0	0.0000e+00	0.0000e+00	0.0000e+00	0.0000e+00
3.5481e+01	0	0.0000e+00	0.0000e+00	0.0000e+00	0.0000e+00
3.9811e+01	0	0.0000e+00	0.0000e+00	0.0000e+00	0.0000e+00
4.4668e+01	0	0.0000e+00	0.0000e+00	0.0000e+00	0.0000e+00
5.0119e+01	0	0.0000e+00	0.0000e+00	0.0000e+00	0.0000e+00
5.6234e+01	0	0.0000e+00	0.0000e+00	0.0000e+00	0.0000e+00
6.3096e+01	0	0.0000e+00	0.0000e+00	0.0000e+00	0.0000e+00
7.0795e+01	0	0.0000e+00	0.0000e+00	0.0000e+00	0.0000e+00
7.9433e+01	0	0.0000e+00	0.0000e+00	0.0000e+00	0.0000e+00
8.9125e+01	0	0.0000e+00	0.0000e+00	0.0000e+00	0.0000e+00
1.0000e+02	0	0.0000e+00	0.0000e+00	0.0000e+00	0.0000e+00
1.1220e+02	0	0.0000e+00	0.0000e+00	0.0000e+00	0.0000e+00
1.2589e+02	0	0.0000e+00	0.0000e+00	0.0000e+00	0.0000e+00
1.4125e+02	0	0.0000e+00	0.0000e+00	0.0000e+00	0.0000e+00
1.5849e+02	0	0.0000e+00	0.0000e+00	0.0000e+00	0.0000e+00
1.7783e+02	0	0.0000e+00	0.0000e+00	0.0000e+00	0.0000e+00
1.9953e+02	0	0.0000e+00	0.0000e+00	0.0000e+00	0.0000e+00
2.2387e+02	0	0.0000e+00	0.0000e+00	0.0000e+00	0.0000e+00
2.5119e+02	0	0.0000e+00	0.0000e+00	0.0000e+00	0.0000e+00
2.8184e+02	0	0.0000e+00	0.0000e+00	0.0000e+00	0.0000e+00
3.1623e+02	0	0.0000e+00	0.0000e+00	0.0000e+00	0.0000e+00
3.5481e+02	0	0.0000e+00	0.0000e+00	0.0000e+00	0.0000e+00
3.9811e+02	0	0.0000e+00	0.0000e+00	0.0000e+00	0.0000e+00
4.4668e+02	0	0.0000e+00	0.0000e+00	0.0000e+00	0.0000e+00
5.0119e+02	0	0.0000e+00	0.0000e+00	0.0000e+00	0.0000e+00
5.6234e+02	0	0.0000e+00	0.0000e+00	0.0000e+00	0.0000e+00
6.3096e+02	0	0.0000e+00	0.0000e+00	0.0000e+00	0.0000e+00
7.0795e+02	0	0.0000e+00	0.0000e+00	0.0000e+00	0.0000e+00
7.9433e+02	0	0.0000e+00	0.0000e+00	0.0000e+00	0.0000e+00
8.9125e+02	0	0.0000e+00	0.0000e+00	0.0000e+00	0.0000e+00
1.0000e+03	0	0.0000e+00	0.0000e+00	0.0000e+00	0.0000e+00

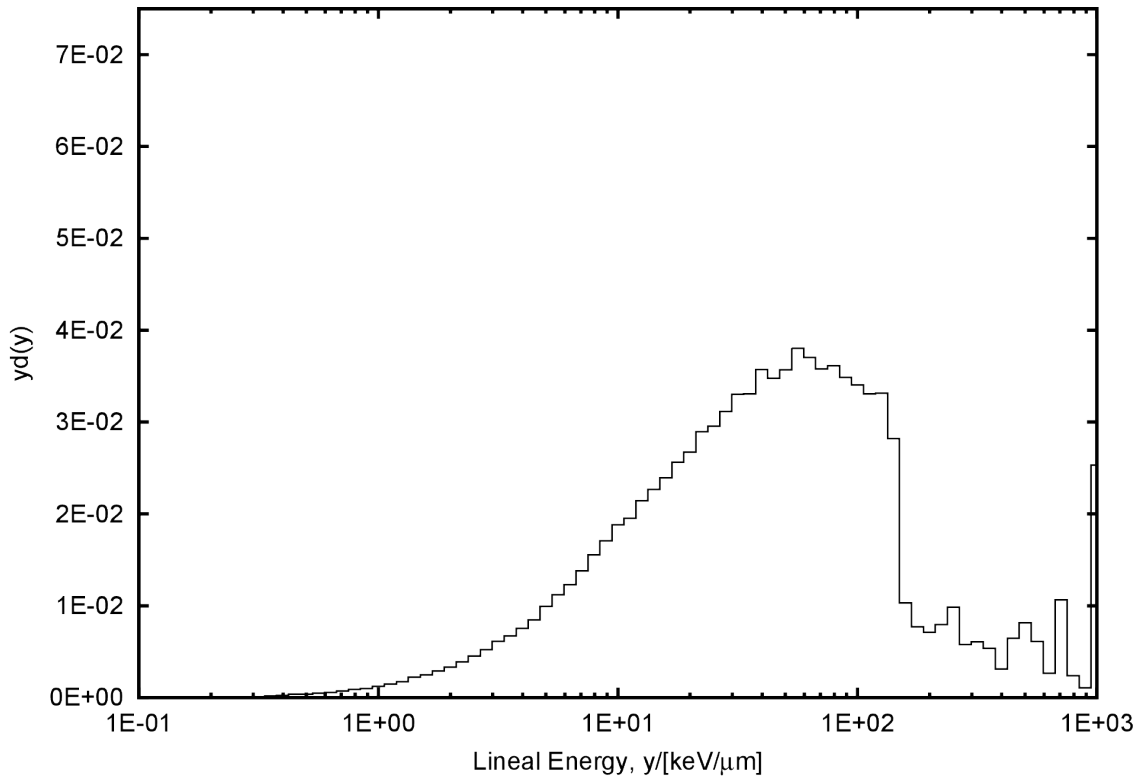

Figure E.4. Lineal energy distribution for the TEPC on the surface of Mars, albedo neutron component.

Surface of Mars, albedo neutron component:

```
# Using 80 Log Bins
# Min: 0.1 keV/μm              Max: 1000 keV/μm              20 bins/decade
#
# SiteSize: 1 μm               Mean Chord Length: 0.667 μm
#
# Using y Output with units of [keV/μm]
#
# y_F = 14.615 keV/μm
# y_D = 103.775 keV/μm
#
# D     = 2.100e-03 Gy
# H     = 2.561e-02 Sv
# Q_avg = 1.220e+01
#
# N = 113880
#
# y [keV/μm] N(y)     f(y)         y*f(y)      d(y)         y*d(y)
1.0000e-01   377      6.0321e-03   3.6108e-04  3.6108e-04   2.4706e-06
1.1220e-01   377      4.9436e-02   3.3203e-03  3.3203e-03   2.5491e-05
1.2589e-01   377      4.4060e-02   3.3203e-03  3.3203e-03   2.8601e-05
1.4125e-01   377      3.9268e-02   3.3203e-03  3.3203e-03   3.2091e-05
1.5849e-01   377      3.4998e-02   3.3203e-03  3.3203e-03   3.6006e-05
1.7783e-01   377      3.1192e-02   3.3203e-03  3.3203e-03   4.0400e-05
1.9953e-01   377      2.7800e-02   3.3203e-03  3.3203e-03   4.5329e-05
2.2387e-01   377      2.4777e-02   3.3203e-03  3.3203e-03   5.0860e-05
2.5119e-01   377      2.2082e-02   3.3203e-03  3.3203e-03   5.7066e-05
2.8184e-01   377      1.9681e-02   3.3203e-03  3.3203e-03   6.4030e-05
3.1623e-01   377      1.7541e-02   3.3203e-03  3.3203e-03   7.1842e-05
3.5481e-01   921      3.8191e-02   8.1114e-03  8.1114e-03   1.9692e-04
3.9811e-01   997      3.6847e-02   8.7807e-03  8.7807e-03   2.3919e-04
4.4668e-01   1354     4.4599e-02   1.1925e-02  1.1925e-02   3.6447e-04
5.0119e-01   1277     3.7488e-02   1.1247e-02  1.1247e-02   3.8568e-04
5.6234e-01   1417     3.7074e-02   1.2480e-02  1.2480e-02   4.8019e-04
6.3096e-01   1458     3.3998e-02   1.2841e-02  1.2841e-02   5.5437e-04
7.0795e-01   1707     3.5476e-02   1.5034e-02  1.5034e-02   7.2824e-04
7.9433e-01   1872     3.4674e-02   1.6487e-02  1.6487e-02   8.9608e-04
8.9125e-01   1882     3.1069e-02   1.6575e-02  1.6575e-02   1.0108e-03
1.0000e+00   2051     3.0176e-02   1.8063e-02  1.8063e-02   1.2360e-03
1.1220e+00   2171     2.8468e-02   1.9120e-02  1.9120e-02   1.4679e-03
1.2589e+00   2301     2.6892e-02   2.0265e-02  2.0265e-02   1.7456e-03
1.4125e+00   2596     2.7040e-02   2.2863e-02  2.2863e-02   2.2098e-03
1.5849e+00   2602     2.4155e-02   2.2916e-02  2.2916e-02   2.4851e-03
1.7783e+00   2706     2.2389e-02   2.3832e-02  2.3832e-02   2.8998e-03
1.9953e+00   2766     2.0396e-02   2.4361e-02  2.4361e-02   3.3258e-03
2.2387e+00   2891     1.9000e-02   2.5461e-02  2.5461e-02   3.9002e-03
2.5119e+00   2980     1.7455e-02   2.6245e-02  2.6245e-02   4.5108e-03
2.8184e+00   3072     1.6037e-02   2.7056e-02  2.7056e-02   5.2175e-03
3.1623e+00   3212     1.4944e-02   2.8289e-02  2.8289e-02   6.1209e-03
```

3.5481e+00	3146	1.3046e-02	2.7707e-02	2.7707e-02	6.7266e-03
3.9811e+00	3145	1.1623e-02	2.7699e-02	2.7699e-02	7.5450e-03
4.4668e+00	3145	1.0359e-02	2.7699e-02	2.7699e-02	8.4656e-03
5.0119e+00	3284	9.6406e-03	2.8923e-02	2.8923e-02	9.9184e-03
5.6234e+00	3309	8.6576e-03	2.9143e-02	2.9143e-02	1.1213e-02
6.3096e+00	3239	7.5529e-03	2.8526e-02	2.8526e-02	1.2315e-02
7.0795e+00	3238	6.7294e-03	2.8518e-02	2.8518e-02	1.3814e-02
7.9433e+00	3251	6.0217e-03	2.8632e-02	2.8632e-02	1.5562e-02
8.9125e+00	3176	5.2430e-03	2.7972e-02	2.7972e-02	1.7058e-02
1.0000e+01	3122	4.5934e-03	2.7496e-02	2.7496e-02	1.8814e-02
1.1220e+01	2888	3.7870e-03	2.5435e-02	2.5435e-02	1.9527e-02
1.2589e+01	2828	3.3051e-03	2.4907e-02	2.4907e-02	2.1454e-02
1.4125e+01	2662	2.7727e-03	2.3445e-02	2.3445e-02	2.2659e-02
1.5849e+01	2505	2.3255e-03	2.2062e-02	2.2062e-02	2.3925e-02
1.7783e+01	2391	1.9783e-03	2.1058e-02	2.1058e-02	2.5622e-02
1.9953e+01	2221	1.6378e-03	1.9561e-02	1.9561e-02	2.6705e-02
2.2387e+01	2145	1.4097e-03	1.8891e-02	1.8891e-02	2.8938e-02
2.5119e+01	1952	1.1434e-03	1.7192e-02	1.7192e-02	2.9547e-02
2.8184e+01	1835	9.5794e-04	1.6161e-02	1.6161e-02	3.1166e-02
3.1623e+01	1732	8.0584e-04	1.5254e-02	1.5254e-02	3.3006e-02
3.5481e+01	1546	6.4108e-04	1.3616e-02	1.3616e-02	3.3056e-02
3.9811e+01	1489	5.5030e-04	1.3114e-02	1.3114e-02	3.5722e-02
4.4668e+01	1291	4.2523e-04	1.1370e-02	1.1370e-02	3.4751e-02
5.0119e+01	1182	3.4699e-04	1.0410e-02	1.0410e-02	3.5699e-02
5.6234e+01	1122	2.9356e-04	9.8816e-03	9.8816e-03	3.8022e-02
6.3096e+01	974	2.2712e-04	8.5782e-03	8.5782e-03	3.7034e-02
7.0795e+01	839	1.7437e-04	7.3892e-03	7.3892e-03	3.5793e-02
7.9433e+01	755	1.3985e-04	6.6494e-03	6.6494e-03	3.6140e-02
8.9125e+01	649	1.0714e-04	5.7158e-03	5.7158e-03	3.4856e-02
1.0000e+02	565	8.3129e-05	4.9760e-03	4.9760e-03	3.4048e-02
1.1220e+02	489	6.4123e-05	4.3067e-03	4.3067e-03	3.3063e-02
1.2589e+02	437	5.1072e-05	3.8487e-03	3.8487e-03	3.3153e-02
1.4125e+02	331	3.4477e-05	2.9152e-03	2.9152e-03	2.8175e-02
1.5849e+02	108	1.0026e-05	9.5117e-04	9.5117e-04	1.0315e-02
1.7783e+02	72	5.9571e-06	6.3412e-04	6.3412e-04	7.7156e-03
1.9953e+02	59	4.3506e-06	5.1962e-04	5.1962e-04	7.0940e-03
2.2387e+02	59	3.8775e-06	5.1962e-04	5.1962e-04	7.9596e-03
2.5119e+02	65	3.8073e-06	5.7247e-04	5.7247e-04	9.8390e-03
2.8184e+02	34	1.7749e-06	2.9944e-04	2.9944e-04	5.7745e-03
3.1623e+02	32	1.4889e-06	2.8183e-04	2.8183e-04	6.0980e-03
3.5481e+02	25	1.0367e-06	2.2018e-04	2.2018e-04	5.3454e-03
3.9811e+02	13	4.8045e-07	1.1449e-04	1.1449e-04	3.1188e-03
4.4668e+02	24	7.9052e-07	2.1137e-04	2.1137e-04	6.4603e-03
5.0119e+02	27	7.9262e-07	2.3779e-04	2.3779e-04	8.1546e-03
5.6234e+02	18	4.7095e-07	1.5853e-04	1.5853e-04	6.0997e-03
6.3096e+02	7	1.6323e-07	6.1650e-05	6.1650e-05	2.6616e-03
7.0795e+02	25	5.1957e-07	2.2018e-04	2.2018e-04	1.0665e-02
7.9433e+02	5	9.2613e-08	4.4036e-05	4.4036e-05	2.3934e-03
8.9125e+02	2	3.3017e-08	1.7614e-05	1.7614e-05	1.0742e-03
1.0000e+03	42	6.1795e-07	3.6990e-04	3.6990e-04	2.5310e-02

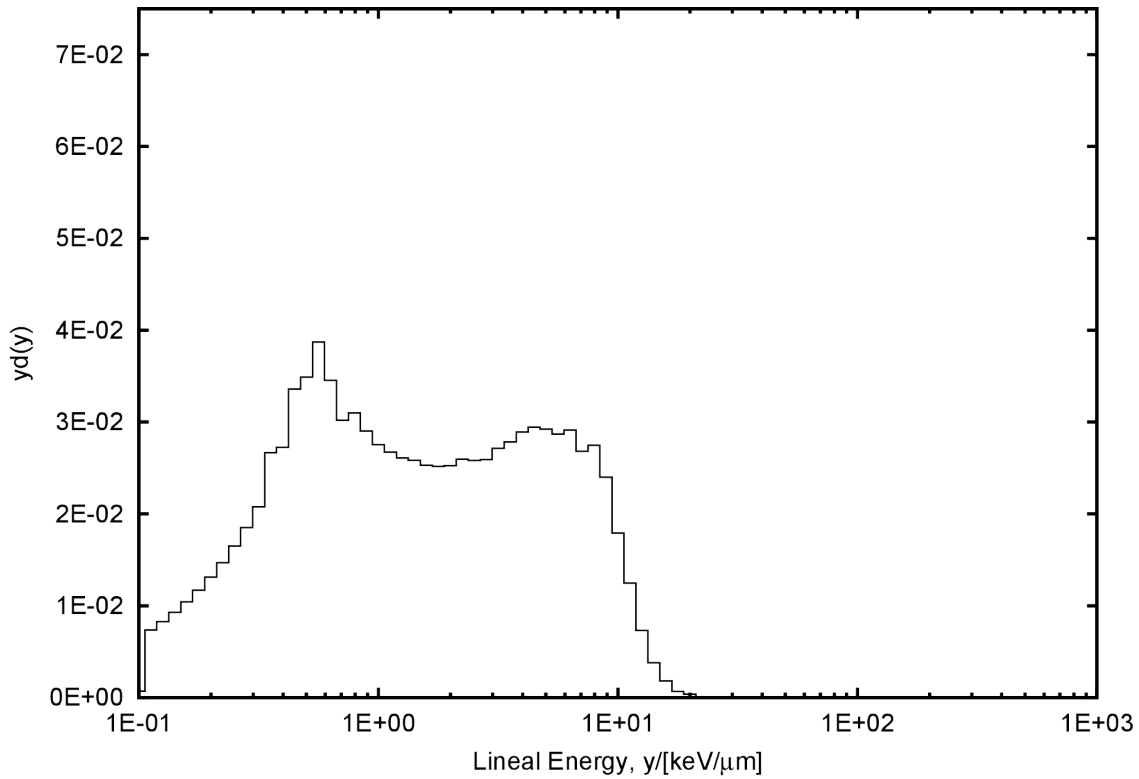

Figure E.5. Lineal energy distribution for the TEPC on the surface of Mars, albedo photon component.

Surface of Mars, albedo photon component:

```
# Using 80 Log Bins
# Min: 0.1 keV/μm              Max: 1000 keV/μm              20 bins/decade
#
# SiteSize: 1 μm               Mean Chord Length: 0.667 μm
#
# Using y Output with units of [keV/μm]
#
# y_F = 0.707 keV/μm
# y_D = 2.715 keV/μm
#
# D     = 3.984e-04 Gy
# H     = 4.074e-04 Sv
# Q_avg = 1.022e+00
#
# N = 461148
#
# y [keV/μm] N(y)     f(y)         y*f(y)      d(y)         y*d(y)
1.0000e-01   20571    1.4501e-02  5.0520e-03  5.0520e-03  7.1458e-04
1.1220e-01   20571    1.1885e-01  4.6455e-02  4.6455e-02  7.3727e-03
1.2589e-01   20571    1.0592e-01  4.6455e-02  4.6455e-02  8.2723e-03
1.4125e-01   20571    9.4402e-02  4.6455e-02  4.6455e-02  9.2817e-03
1.5849e-01   20571    8.4136e-02  4.6455e-02  4.6455e-02  1.0414e-02
1.7783e-01   20571    7.4986e-02  4.6455e-02  4.6455e-02  1.1685e-02
1.9953e-01   20571    6.6832e-02  4.6455e-02  4.6455e-02  1.3111e-02
2.2387e-01   20571    5.9564e-02  4.6455e-02  4.6455e-02  1.4710e-02
2.5119e-01   20571    5.3086e-02  4.6455e-02  4.6455e-02  1.6505e-02
2.8184e-01   20571    4.7313e-02  4.6455e-02  4.6455e-02  1.8519e-02
3.1623e-01   20571    4.2168e-02  4.6455e-02  4.6455e-02  2.0779e-02
3.5481e-01   23538    4.3003e-02  5.3155e-02  5.3155e-02  2.6677e-02
3.9811e-01   21433    3.4899e-02  4.8402e-02  4.8402e-02  2.7255e-02
4.4668e-01   23540    3.4161e-02  5.3160e-02  5.3160e-02  3.3587e-02
5.0119e-01   21793    2.8187e-02  4.9215e-02  4.9215e-02  3.4889e-02
5.6234e-01   21559    2.4852e-02  4.8686e-02  4.8686e-02  3.8726e-02
6.3096e-01   17144    1.7613e-02  3.8716e-02  3.8716e-02  3.4553e-02
7.0795e-01   13349    1.2223e-02  3.0146e-02  3.0146e-02  3.0187e-02
7.9433e-01   12218    9.9707e-03  2.7592e-02  2.7592e-02  3.1001e-02
8.9125e-01   10197    7.4165e-03  2.3028e-02  2.3028e-02  2.9030e-02
1.0000e+00   8617     5.5858e-03  1.9460e-02  1.9460e-02  2.7525e-02
1.1220e+00   7451     4.3047e-03  1.6826e-02  1.6826e-02  2.6705e-02
1.2589e+00   6490     3.3417e-03  1.4656e-02  1.4656e-02  2.6098e-02
1.4125e+00   5728     2.6286e-03  1.2935e-02  1.2935e-02  2.5845e-02
1.5849e+00   4996     2.0434e-03  1.1282e-02  1.1282e-02  2.5293e-02
1.7783e+00   4434     1.6163e-03  1.0013e-02  1.0013e-02  2.5186e-02
1.9953e+00   3963     1.2875e-03  8.9496e-03  8.9496e-03  2.5258e-02
2.2387e+00   3630     1.0511e-03  8.1976e-03  8.1976e-03  2.5958e-02
2.5119e+00   3220     8.3097e-04  7.2717e-03  7.2717e-03  2.5836e-02
2.8184e+00   2880     6.6240e-04  6.5039e-03  6.5039e-03  2.5928e-02
3.1623e+00   2685     5.5039e-04  6.0635e-03  6.0635e-03  2.7122e-02
```

3.5481e+00	2456	4.4870e-04	5.5463e-03	5.5463e-03	2.7835e-02
3.9811e+00	2274	3.7027e-04	5.1353e-03	5.1353e-03	2.8917e-02
4.4668e+00	2062	2.9924e-04	4.6566e-03	4.6566e-03	2.9421e-02
5.0119e+00	1825	2.3604e-04	4.1214e-03	4.1214e-03	2.9217e-02
5.6234e+00	1597	1.8409e-04	3.6065e-03	3.6065e-03	2.8686e-02
6.3096e+00	1446	1.4856e-04	3.2655e-03	3.2655e-03	2.9143e-02
7.0795e+00	1186	1.0860e-04	2.6783e-03	2.6783e-03	2.6820e-02
7.9433e+00	1083	8.8380e-05	2.4457e-03	2.4457e-03	2.7479e-02
8.9125e+00	843	6.1313e-05	1.9037e-03	1.9037e-03	2.3999e-02
1.0000e+01	561	3.6366e-05	1.2669e-03	1.2669e-03	1.7920e-02
1.1220e+01	348	2.0105e-05	7.8588e-04	7.8588e-04	1.2472e-02
1.2589e+01	182	9.3713e-06	4.1101e-04	4.1101e-04	7.3188e-03
1.4125e+01	84	3.8548e-06	1.8970e-04	1.8970e-04	3.7901e-03
1.5849e+01	36	1.4724e-06	8.1298e-05	8.1298e-05	1.8225e-03
1.7783e+01	12	4.3743e-07	2.7099e-05	2.7099e-05	6.8163e-04
1.9953e+01	6	1.9493e-07	1.3550e-05	1.3550e-05	3.8240e-04
2.2387e+01	1	2.8955e-08	2.2583e-06	2.2583e-06	7.1511e-05
2.5119e+01	0	0.0000e+00	0.0000e+00	0.0000e+00	0.0000e+00
2.8184e+01	0	0.0000e+00	0.0000e+00	0.0000e+00	0.0000e+00
3.1623e+01	0	0.0000e+00	0.0000e+00	0.0000e+00	0.0000e+00
3.5481e+01	0	0.0000e+00	0.0000e+00	0.0000e+00	0.0000e+00
3.9811e+01	0	0.0000e+00	0.0000e+00	0.0000e+00	0.0000e+00
4.4668e+01	0	0.0000e+00	0.0000e+00	0.0000e+00	0.0000e+00
5.0119e+01	0	0.0000e+00	0.0000e+00	0.0000e+00	0.0000e+00
5.6234e+01	0	0.0000e+00	0.0000e+00	0.0000e+00	0.0000e+00
6.3096e+01	0	0.0000e+00	0.0000e+00	0.0000e+00	0.0000e+00
7.0795e+01	0	0.0000e+00	0.0000e+00	0.0000e+00	0.0000e+00
7.9433e+01	0	0.0000e+00	0.0000e+00	0.0000e+00	0.0000e+00
8.9125e+01	0	0.0000e+00	0.0000e+00	0.0000e+00	0.0000e+00
1.0000e+02	0	0.0000e+00	0.0000e+00	0.0000e+00	0.0000e+00
1.1220e+02	0	0.0000e+00	0.0000e+00	0.0000e+00	0.0000e+00
1.2589e+02	0	0.0000e+00	0.0000e+00	0.0000e+00	0.0000e+00
1.4125e+02	0	0.0000e+00	0.0000e+00	0.0000e+00	0.0000e+00
1.5849e+02	0	0.0000e+00	0.0000e+00	0.0000e+00	0.0000e+00
1.7783e+02	0	0.0000e+00	0.0000e+00	0.0000e+00	0.0000e+00
1.9953e+02	0	0.0000e+00	0.0000e+00	0.0000e+00	0.0000e+00
2.2387e+02	0	0.0000e+00	0.0000e+00	0.0000e+00	0.0000e+00
2.5119e+02	0	0.0000e+00	0.0000e+00	0.0000e+00	0.0000e+00
2.8184e+02	0	0.0000e+00	0.0000e+00	0.0000e+00	0.0000e+00
3.1623e+02	0	0.0000e+00	0.0000e+00	0.0000e+00	0.0000e+00
3.5481e+02	0	0.0000e+00	0.0000e+00	0.0000e+00	0.0000e+00
3.9811e+02	0	0.0000e+00	0.0000e+00	0.0000e+00	0.0000e+00
4.4668e+02	0	0.0000e+00	0.0000e+00	0.0000e+00	0.0000e+00
5.0119e+02	0	0.0000e+00	0.0000e+00	0.0000e+00	0.0000e+00
5.6234e+02	0	0.0000e+00	0.0000e+00	0.0000e+00	0.0000e+00
6.3096e+02	0	0.0000e+00	0.0000e+00	0.0000e+00	0.0000e+00
7.0795e+02	0	0.0000e+00	0.0000e+00	0.0000e+00	0.0000e+00
7.9433e+02	0	0.0000e+00	0.0000e+00	0.0000e+00	0.0000e+00
8.9125e+02	0	0.0000e+00	0.0000e+00	0.0000e+00	0.0000e+00
1.0000e+03	0	0.0000e+00	0.0000e+00	0.0000e+00	0.0000e+00

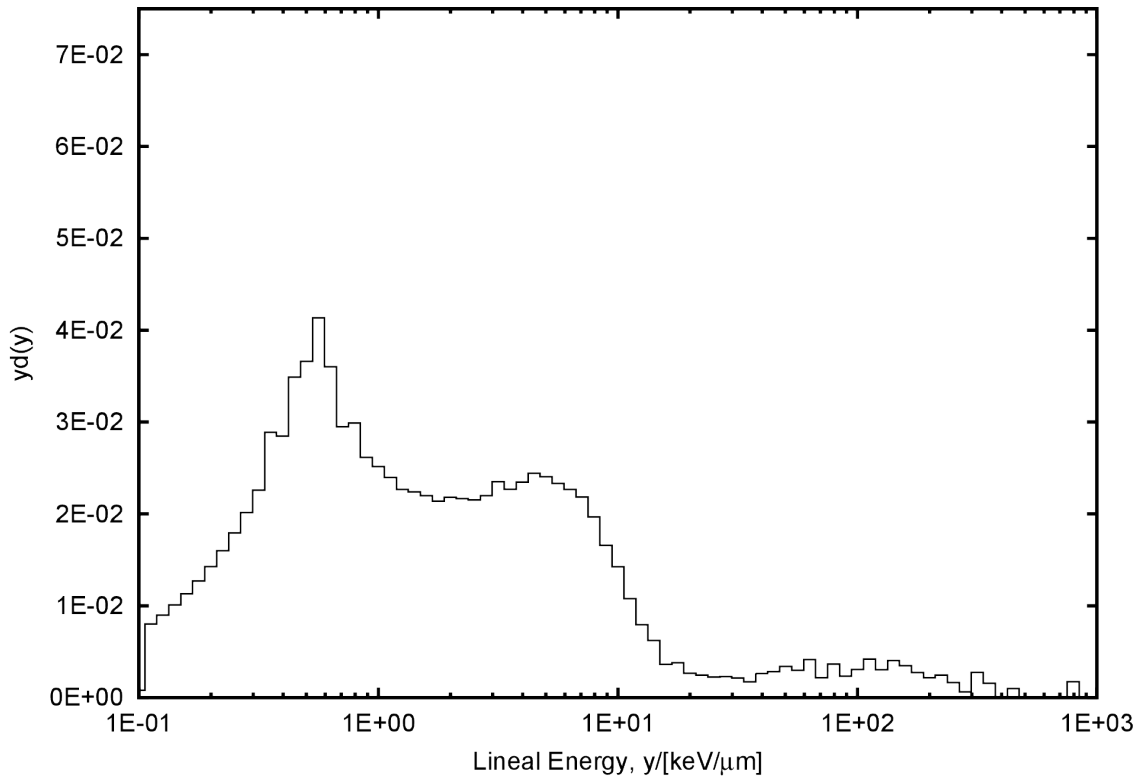

Figure E.6. Lineal energy distribution for the TEPC on the surface of Mars, albedo other component.

Surface of Mars, albedo other component:

```
# Using 80 Log Bins
# Min: 0.1 keV/μm              Max: 1000 keV/μm              20 bins/decade
#
# SiteSize: 1 μm               Mean Chord Length: 0.667 μm
#
# Using y Output with units of [keV/μm]
#
# y_F = 0.685 keV/μm
# y_D = 11.806 keV/μm
#
# D     = 5.810e-04 Gy
# H     = 1.301e-03 Sv
# Q_avg = 2.240e+00
#
# N = 694735
#
# y [keV/μm] N(y)     f(y)         y*f(y)      d(y)         y*d(y)
1.0000e-01   32598    1.4707e-02   5.3254e-03  5.3254e-03   7.7692e-04
1.1220e-01   32598    1.2053e-01   4.8969e-02  4.8969e-02   8.0159e-03
1.2589e-01   32598    1.0742e-01   4.8969e-02  4.8969e-02   8.9940e-03
1.4125e-01   32598    9.5740e-02   4.8969e-02  4.8969e-02   1.0091e-02
1.5849e-01   32598    8.5328e-02   4.8969e-02  4.8969e-02   1.1323e-02
1.7783e-01   32598    7.6049e-02   4.8969e-02  4.8969e-02   1.2704e-02
1.9953e-01   32598    6.7779e-02   4.8969e-02  4.8969e-02   1.4255e-02
2.2387e-01   32598    6.0408e-02   4.8969e-02  4.8969e-02   1.5994e-02
2.5119e-01   32598    5.3839e-02   4.8969e-02  4.8969e-02   1.7945e-02
2.8184e-01   32598    4.7984e-02   4.8969e-02  4.8969e-02   2.0135e-02
3.1623e-01   32598    4.2766e-02   4.8969e-02  4.8969e-02   2.2592e-02
3.5481e-01   37123    4.3406e-02   5.5767e-02  5.5767e-02   2.8867e-02
3.9811e-01   32624    3.3997e-02   4.9008e-02  4.9008e-02   2.8464e-02
4.4668e-01   35647    3.3107e-02   5.3550e-02  5.3550e-02   3.4897e-02
5.0119e-01   33322    2.7583e-02   5.0057e-02  5.0057e-02   3.6601e-02
5.6234e-01   33551    2.4752e-02   5.0401e-02  5.0401e-02   4.1349e-02
6.3096e-01   26044    1.7124e-02   3.9124e-02  3.9124e-02   3.6014e-02
7.0795e-01   19013    1.1142e-02   2.8562e-02  2.8562e-02   2.9499e-02
7.9433e-01   17170    8.9675e-03   2.5793e-02  2.5793e-02   2.9890e-02
8.9125e-01   13393    6.2342e-03   2.0119e-02  2.0119e-02   2.6160e-02
1.0000e+00   11479    4.7622e-03   1.7244e-02  1.7244e-02   2.5157e-02
1.1220e+00   9745     3.6032e-03   1.4639e-02  1.4639e-02   2.3963e-02
1.2589e+00   8214     2.7068e-03   1.2339e-02  1.2339e-02   2.2663e-02
1.4125e+00   7237     2.1255e-03   1.0872e-02  1.0872e-02   2.2404e-02
1.5849e+00   6329     1.6567e-03   9.5075e-03  9.5075e-03   2.1983e-02
1.7783e+00   5486     1.2798e-03   8.2412e-03  8.2412e-03   2.1380e-02
1.9953e+00   4985     1.0365e-03   7.4886e-03  7.4886e-03   2.1798e-02
2.2387e+00   4420     8.1908e-04   6.6398e-03  6.6398e-03   2.1686e-02
2.5119e+00   3911     6.4594e-04   5.8752e-03  5.8752e-03   2.1530e-02
2.8184e+00   3559     5.2388e-04   5.3464e-03  5.3464e-03   2.1983e-02
3.1623e+00   3393     4.4513e-04   5.0970e-03  5.0970e-03   2.3515e-02
```

3.5481e+00	2917	3.4107e-04	4.3820e-03	4.3820e-03	2.2683e-02
3.9811e+00	2688	2.8011e-04	4.0380e-03	4.0380e-03	2.3453e-02
4.4668e+00	2496	2.3182e-04	3.7495e-03	3.7495e-03	2.4435e-02
5.0119e+00	2190	1.8128e-04	3.2899e-03	3.2899e-03	2.4055e-02
5.6234e+00	1892	1.3958e-04	2.8422e-03	2.8422e-03	2.3318e-02
6.3096e+00	1639	1.0777e-04	2.4621e-03	2.4621e-03	2.2664e-02
7.0795e+00	1407	8.2451e-05	2.1136e-03	2.1136e-03	2.1830e-02
7.9433e+00	1130	5.9018e-05	1.6975e-03	1.6975e-03	1.9672e-02
8.9125e+00	849	3.9519e-05	1.2754e-03	1.2754e-03	1.6583e-02
1.0000e+01	650	2.6966e-05	9.7644e-04	9.7644e-04	1.4245e-02
1.1220e+01	438	1.6195e-05	6.5797e-04	6.5797e-04	1.0770e-02
1.2589e+01	287	9.4577e-06	4.3114e-04	4.3114e-04	7.9185e-03
1.4125e+01	201	5.9034e-06	3.0195e-04	3.0195e-04	6.2224e-03
1.5849e+01	104	2.7223e-06	1.5623e-04	1.5623e-04	3.6124e-03
1.7783e+01	97	2.2629e-06	1.4572e-04	1.4572e-04	3.7804e-03
1.9953e+01	61	1.2683e-06	9.1635e-05	9.1635e-05	2.6674e-03
2.2387e+01	50	9.2656e-07	7.5111e-05	7.5111e-05	2.4532e-03
2.5119e+01	41	6.7715e-07	6.1591e-05	6.1591e-05	2.2571e-03
2.8184e+01	37	5.4463e-07	5.5582e-05	5.5582e-05	2.2854e-03
3.1623e+01	31	4.0669e-07	4.6569e-05	4.6569e-05	2.1484e-03
3.5481e+01	22	2.5723e-07	3.3049e-05	3.3049e-05	1.7107e-03
3.9811e+01	30	3.1263e-07	4.5067e-05	4.5067e-05	2.6175e-03
4.4668e+01	29	2.6934e-07	4.3564e-05	4.3564e-05	2.8390e-03
5.0119e+01	31	2.5660e-07	4.6569e-05	4.6569e-05	3.4050e-03
5.6234e+01	24	1.7706e-07	3.6053e-05	3.6053e-05	2.9578e-03
6.3096e+01	30	1.9725e-07	4.5067e-05	4.5067e-05	4.1484e-03
7.0795e+01	14	8.2041e-08	2.1031e-05	2.1031e-05	2.1721e-03
7.9433e+01	21	1.0968e-07	3.1547e-05	3.1547e-05	3.6558e-03
8.9125e+01	12	5.5858e-08	1.8027e-05	1.8027e-05	2.3439e-03
1.0000e+02	14	5.8081e-08	2.1031e-05	2.1031e-05	3.0682e-03
1.1220e+02	17	6.2857e-08	2.5538e-05	2.5538e-05	4.1803e-03
1.2589e+02	11	3.6249e-08	1.6524e-05	1.6524e-05	3.0350e-03
1.4125e+02	13	3.8181e-08	1.9529e-05	1.9529e-05	4.0244e-03
1.5849e+02	10	2.6176e-08	1.5022e-05	1.5022e-05	3.4735e-03
1.7783e+02	7	1.6331e-08	1.0516e-05	1.0516e-05	2.7281e-03
1.9953e+02	5	1.0396e-08	7.5111e-06	7.5111e-06	2.1864e-03
2.2387e+02	5	9.2656e-09	7.5111e-06	7.5111e-06	2.4532e-03
2.5119e+02	3	4.9548e-09	4.5067e-06	4.5067e-06	1.6515e-03
2.8184e+02	1	1.4720e-09	1.5022e-06	1.5022e-06	6.1768e-04
3.1623e+02	4	5.2476e-09	6.0089e-06	6.0089e-06	2.7722e-03
3.5481e+02	2	2.3385e-09	3.0044e-06	3.0044e-06	1.5552e-03
3.9811e+02	0	0.0000e+00	0.0000e+00	0.0000e+00	0.0000e+00
4.4668e+02	1	9.2876e-10	1.5022e-06	1.5022e-06	9.7895e-04
5.0119e+02	0	0.0000e+00	0.0000e+00	0.0000e+00	0.0000e+00
5.6234e+02	0	0.0000e+00	0.0000e+00	0.0000e+00	0.0000e+00
6.3096e+02	0	0.0000e+00	0.0000e+00	0.0000e+00	0.0000e+00
7.0795e+02	0	0.0000e+00	0.0000e+00	0.0000e+00	0.0000e+00
7.9433e+02	1	5.2228e-10	1.5022e-06	1.5022e-06	1.7408e-03
8.9125e+02	0	0.0000e+00	0.0000e+00	0.0000e+00	0.0000e+00
1.0000e+03	0	0.0000e+00	0.0000e+00	0.0000e+00	0.0000e+00

APPENDIX F

DIFFERENTIAL ENERGY SPECTRA

This appendix contains the elemental ion differential energy spectra from $z = 1$ to $z = 28$. These data were generated from 1.0×10^8 FLUKA histories which corresponds to a simulated counting time of 0.545 y.

A distinction is made between isotopes for $z = 1$ and $z = 2$ such that the order of these figures is: H-1, H-2, H-3, $z = 1$ (isotopes combined), He-3, He-4, $z = 2$ (isotopes combined), $z = 3$ (isotopes combined), and so on. In every figure the "Surface of Mars" curves were produced from FLUKA-generated results of the present study and the "Free Space" curves were produced from the Badhwar–O'Neill model. The figures for the individual isotopes of H and He do not have a "Free Space" comparison because the Badhwar–O'Neill model does not specify mass and the masses of $z = 1$ and $z = 2$ were set to 1 and 4, respectively, in free space. Therefore, any H-2, H-3, or He-3 ions can be regarded as secondary particles produced in either the atmosphere or the regolith. All other ions with $z > 2$ were assigned the mass of their most abundant natural isotope.

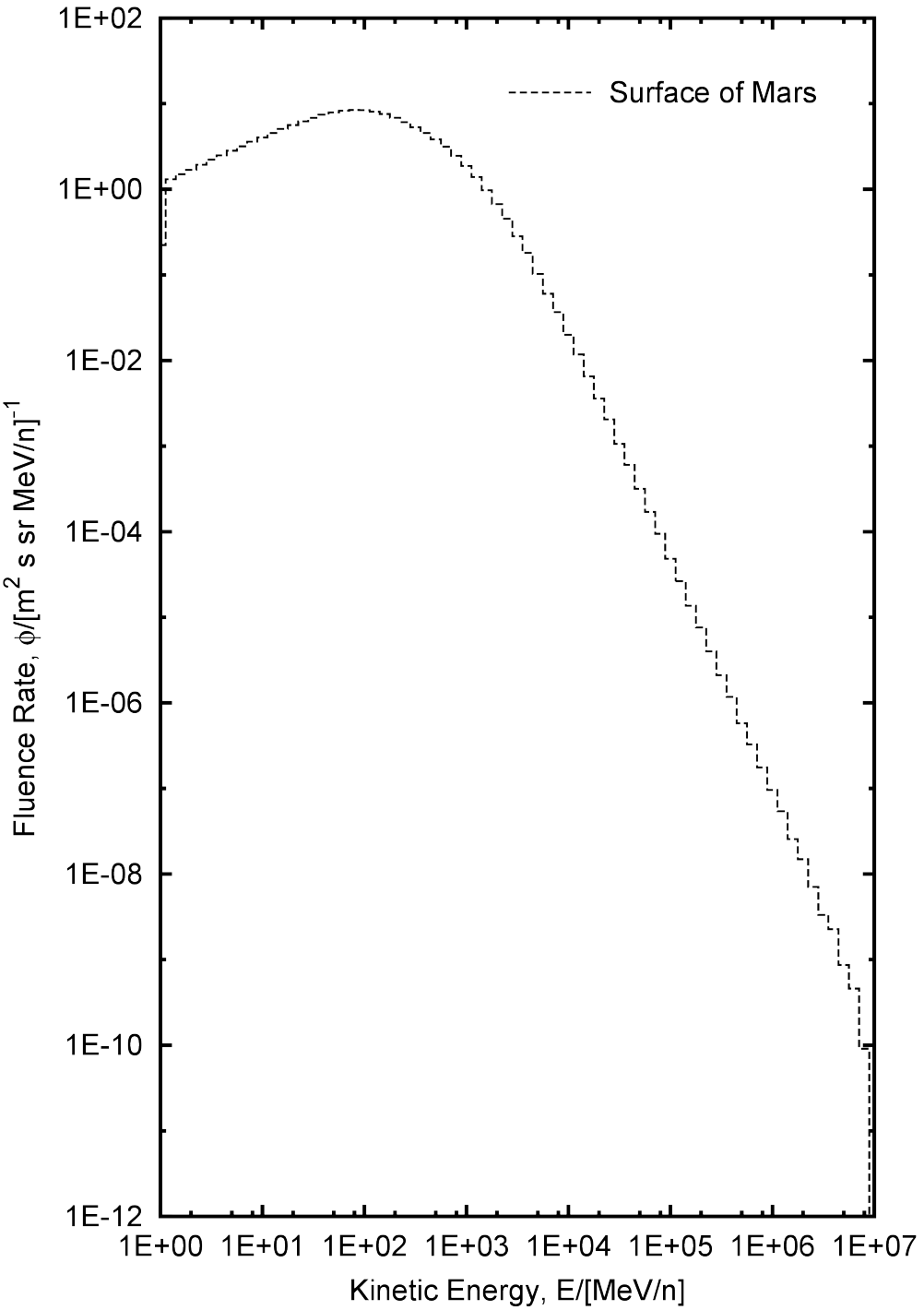

Figure F.1. Surface of Mars differential energy spectrum for H-1. These data were generated from the particle fluence 1 m above the surface, including albedo ions, with the Badhwar–O'Neill model ($z = 1$ to $z = 28$) incident on the top of the Martian atmosphere.

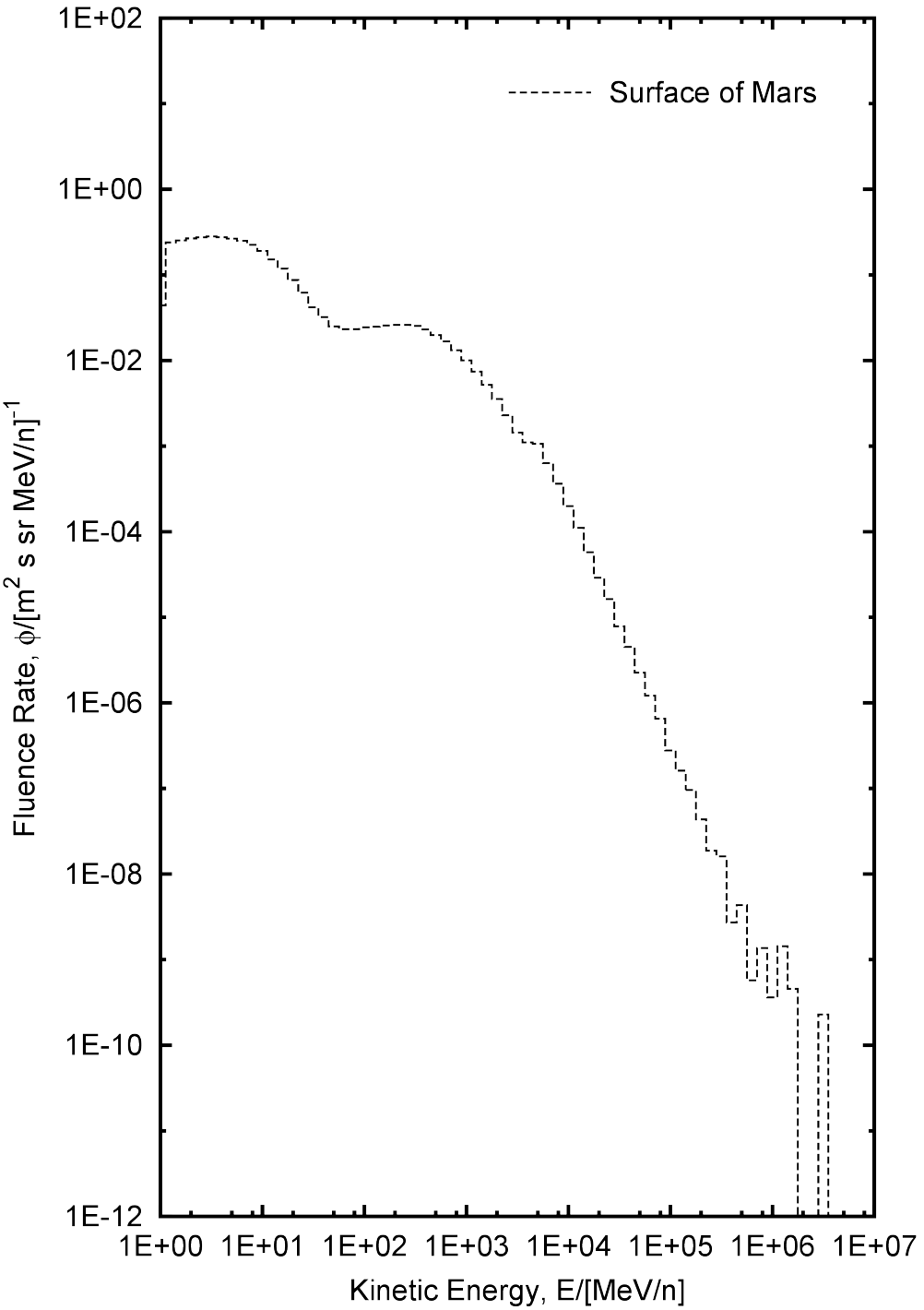

Figure F.2. Surface of Mars differential energy spectrum for H-2. These data were generated from the particle fluence 1 m above the surface, including albedo ions, with the Badhwar–O'Neill model ($z = 1$ to $z = 28$) incident on the top of the Martian atmosphere.

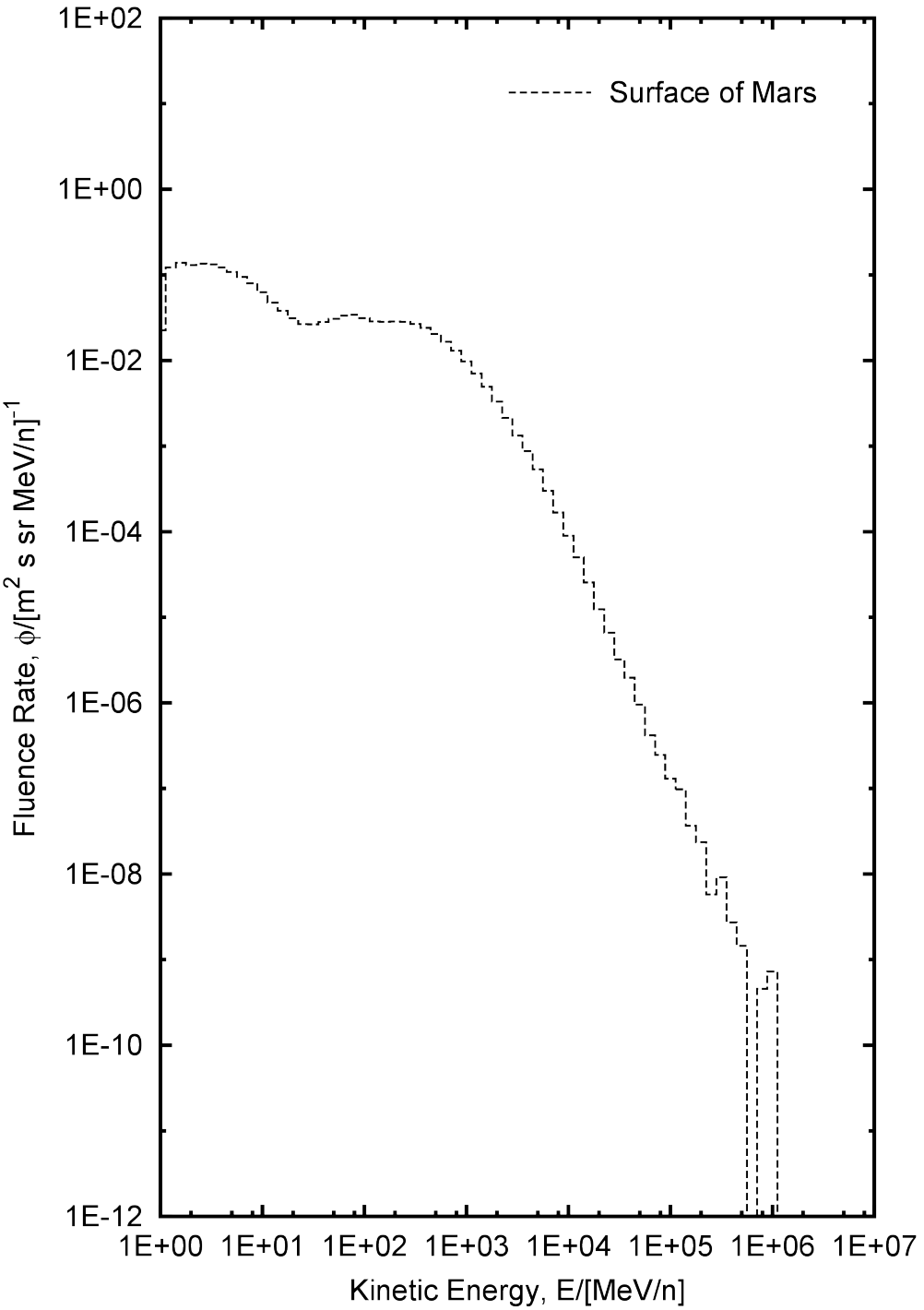

Figure F.3. Surface of Mars differential energy spectrum for H-3. These data were generated from the particle fluence 1 m above the surface, including albedo ions, with the Badhwar–O'Neill model ($z = 1$ to $z = 28$) incident on the top of the Martian atmosphere.

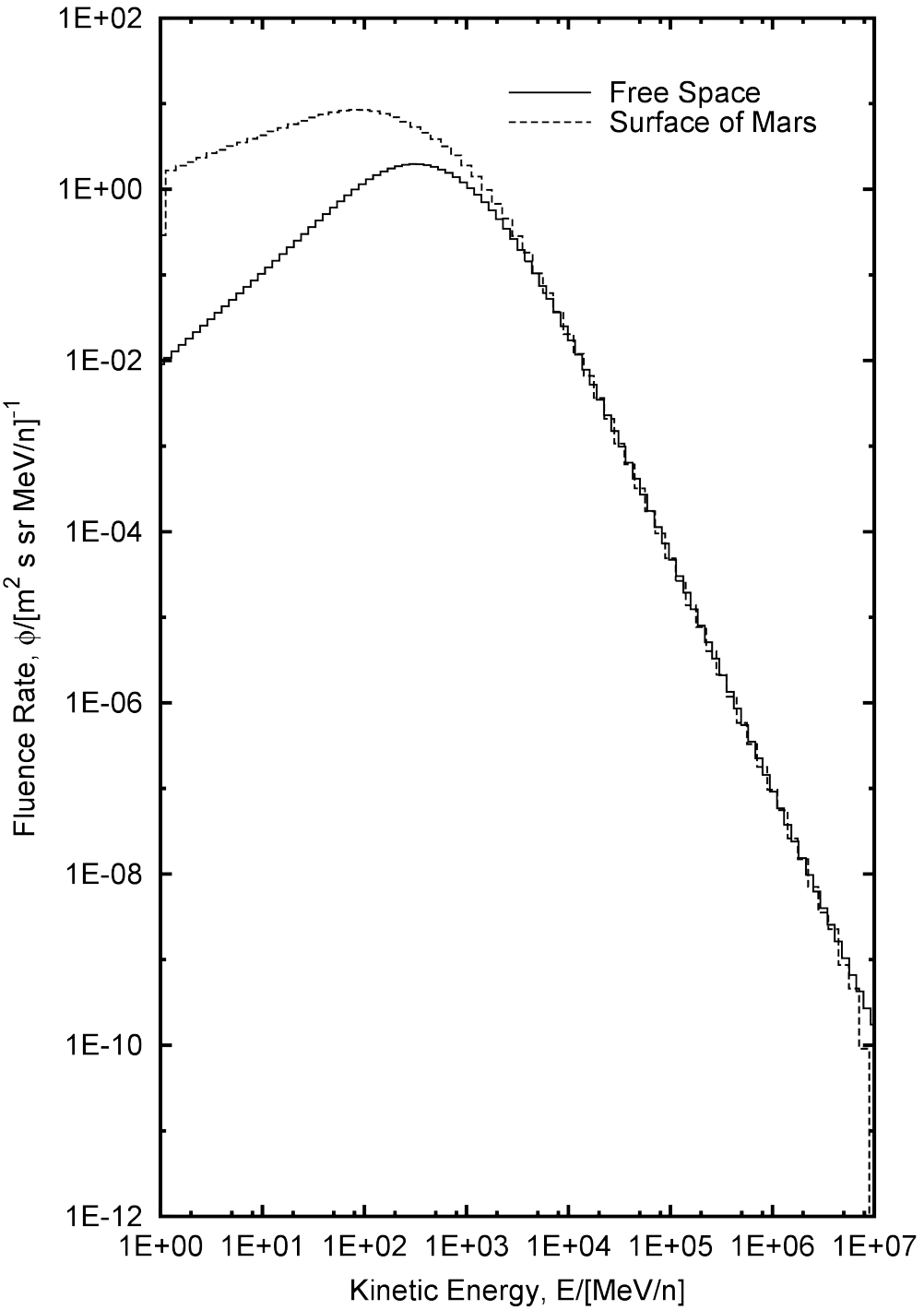

Figure F.4. Comparison of free space and surface of Mars differential energy spectra for $z = 1$ (isotopes combined). The "Free Space" curve is from the Badhwar–O'Neill model and the "Surface of Mars" curve was generated from the particle fluence 1 m above the surface, including albedo ions, with the Badhwar–O'Neill model ($z = 1$ to $z = 28$) incident on the top of the Martian atmosphere.

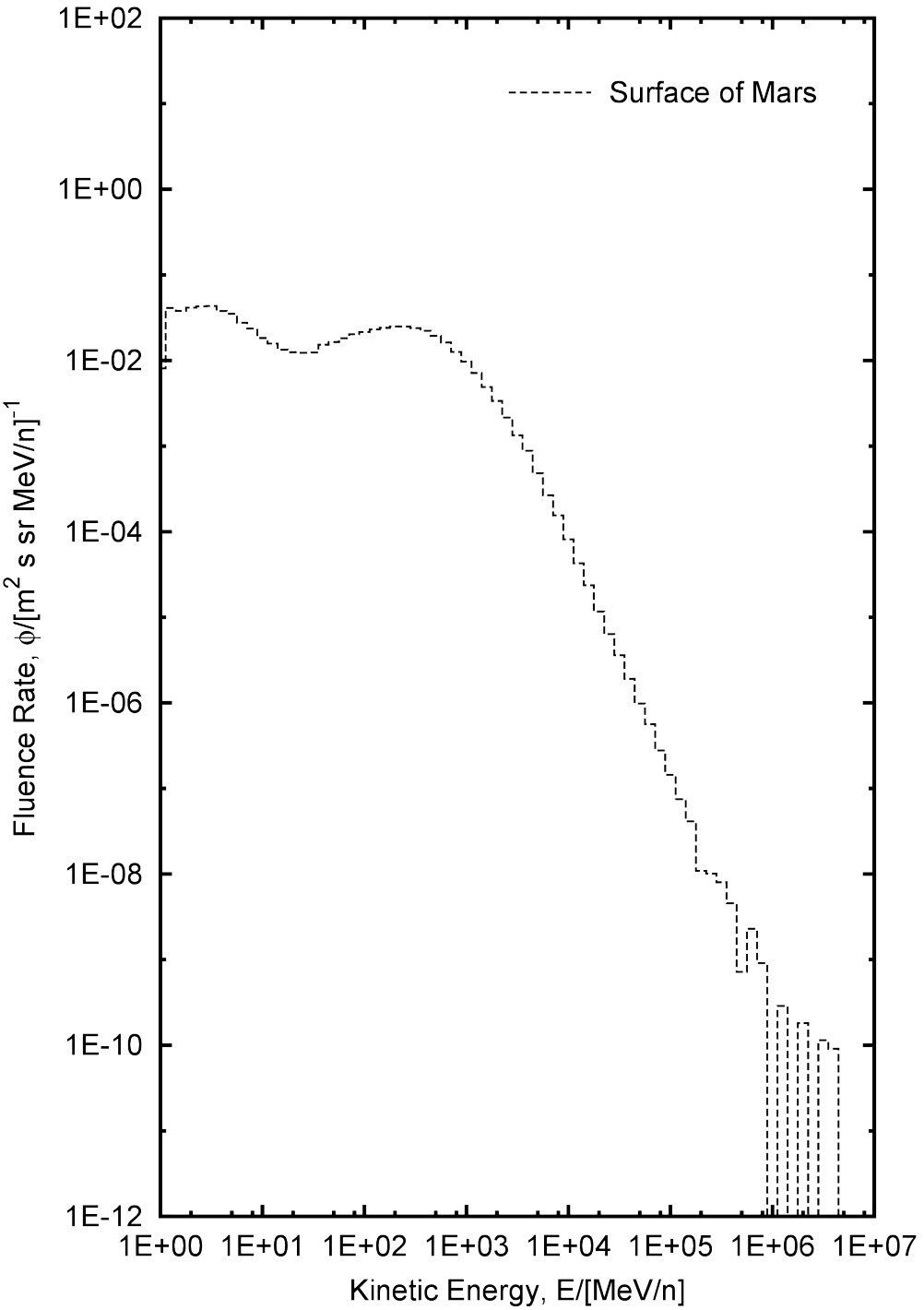

Figure F.5. Surface of Mars differential energy spectrum for He-3. These data were generated from the particle fluence 1 m above the surface, including albedo ions, with the Badhwar–O'Neill model ($z = 1$ to $z = 28$) incident on the top of the Martian atmosphere.

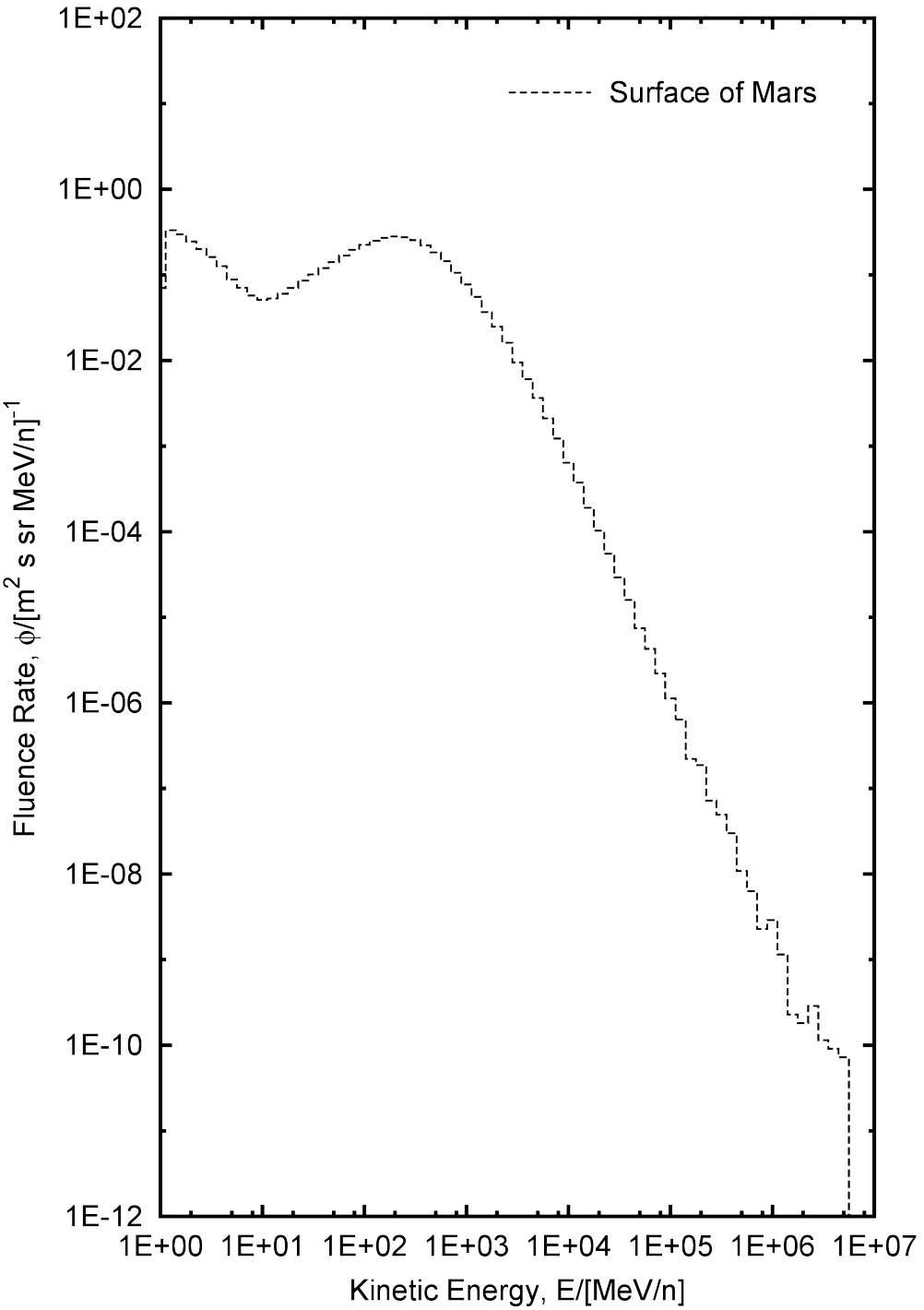

Figure F.6. Surface of Mars differential energy spectrum for He-4. These data were generated from the particle fluence 1 m above the surface, including albedo ions, with the Badhwar–O'Neill model ($z = 1$ to $z = 28$) incident on the top of the Martian atmosphere.

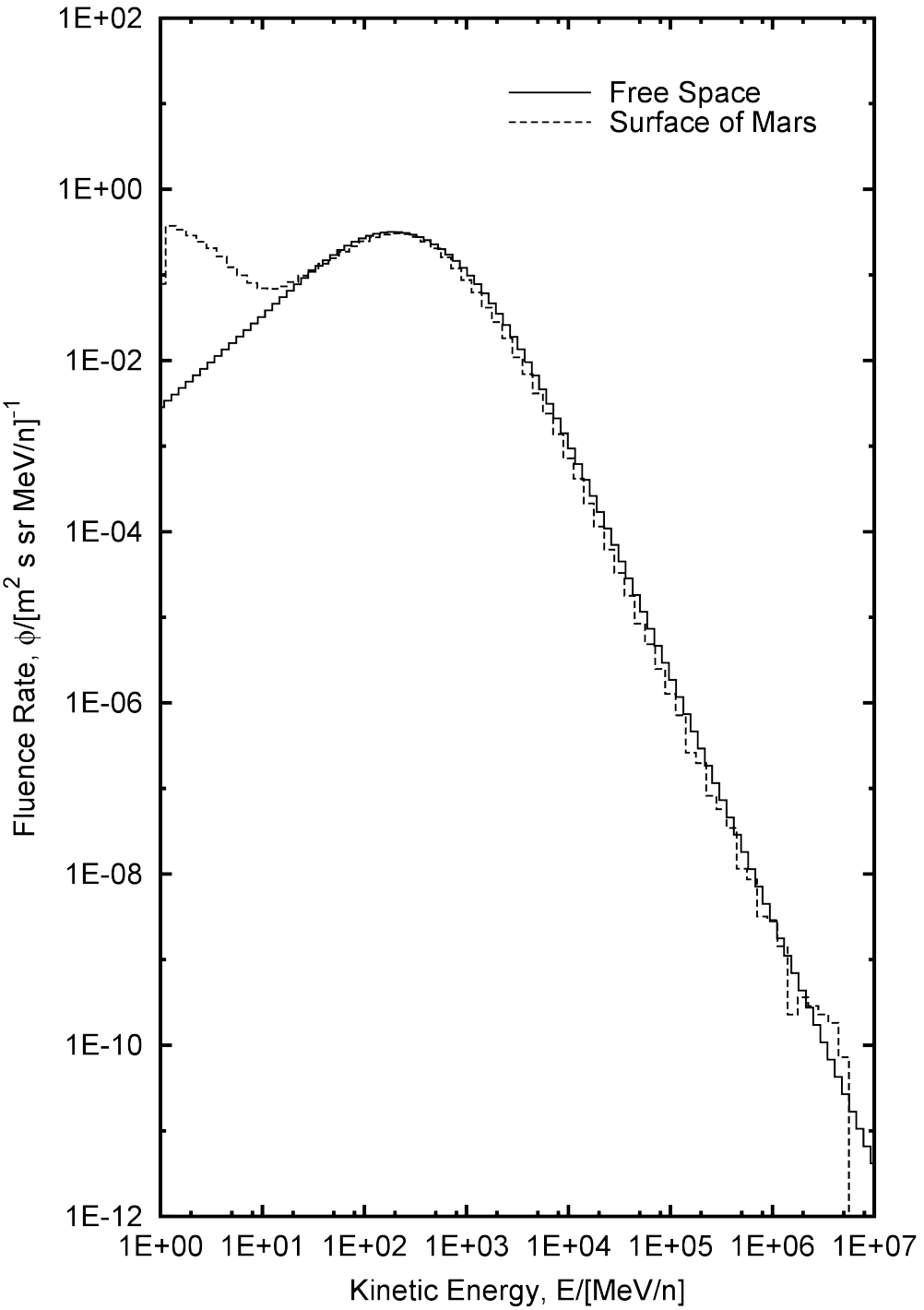

Figure F.7. Comparison of free space and surface of Mars differential energy spectra for $z = 2$ (isotopes combined). The "Free Space" curve is from the Badhwar–O'Neill model and the "Surface of Mars" curve was generated from the particle fluence 1 m above the surface, including albedo ions, with the Badhwar–O'Neill model ($z = 1$ to $z = 28$) incident on the top of the Martian atmosphere.

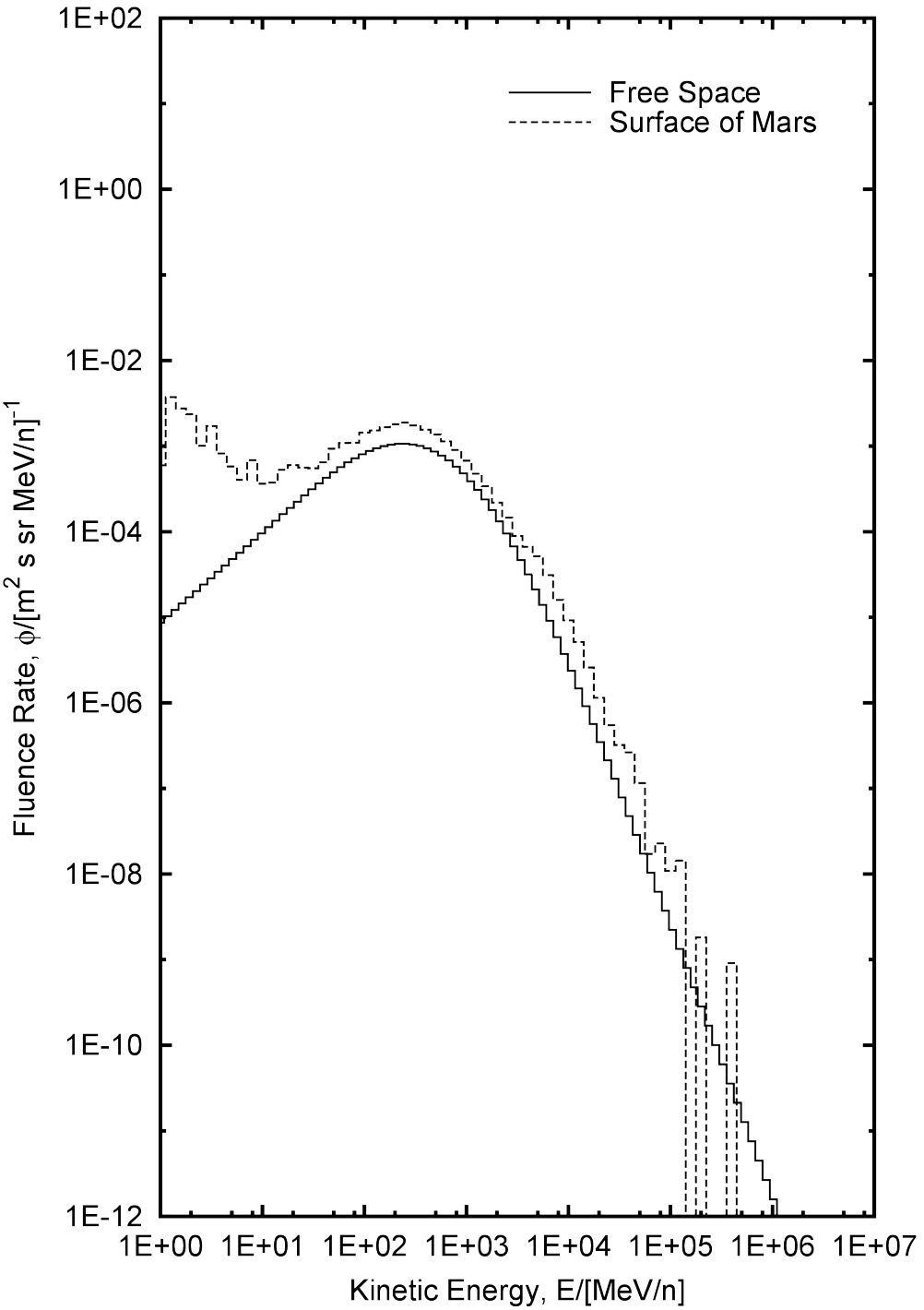

Figure F.8. Comparison of free space and surface of Mars differential energy spectra for $z = 3$ (isotopes combined). The "Free Space" curve is from the Badhwar–O'Neill model and the "Surface of Mars" curve was generated from the particle fluence 1 m above the surface, including albedo ions, with the Badhwar–O'Neill model ($z = 1$ to $z = 28$) incident on the top of the Martian atmosphere.

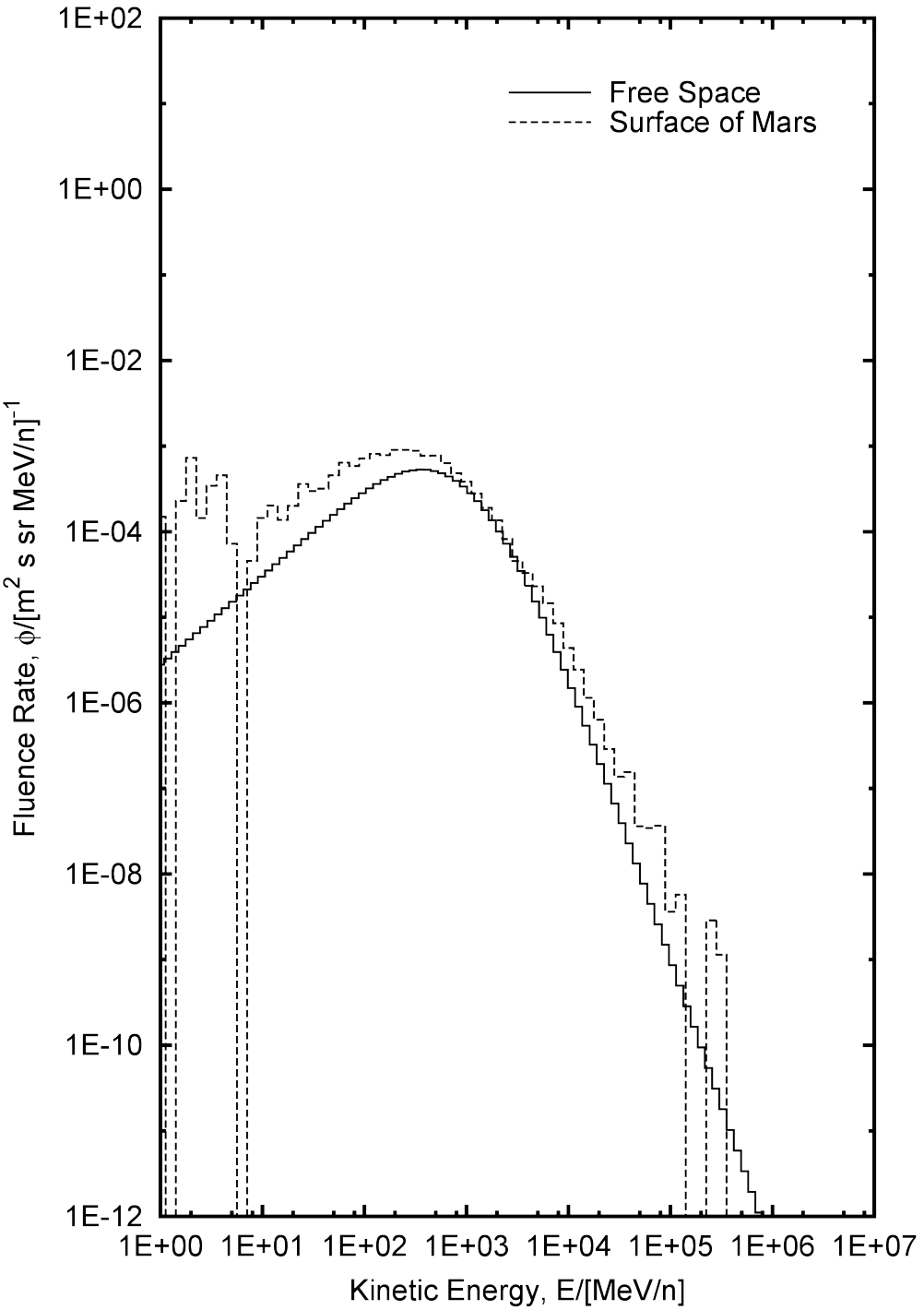

Figure F.9. Comparison of free space and surface of Mars differential energy spectra for $z = 4$ (isotopes combined). The "Free Space" curve is from the Badhwar–O'Neill model and the "Surface of Mars" curve was generated from the particle fluence 1 m above the surface, including albedo ions, with the Badhwar–O'Neill model ($z = 1$ to $z = 28$) incident on the top of the Martian atmosphere.

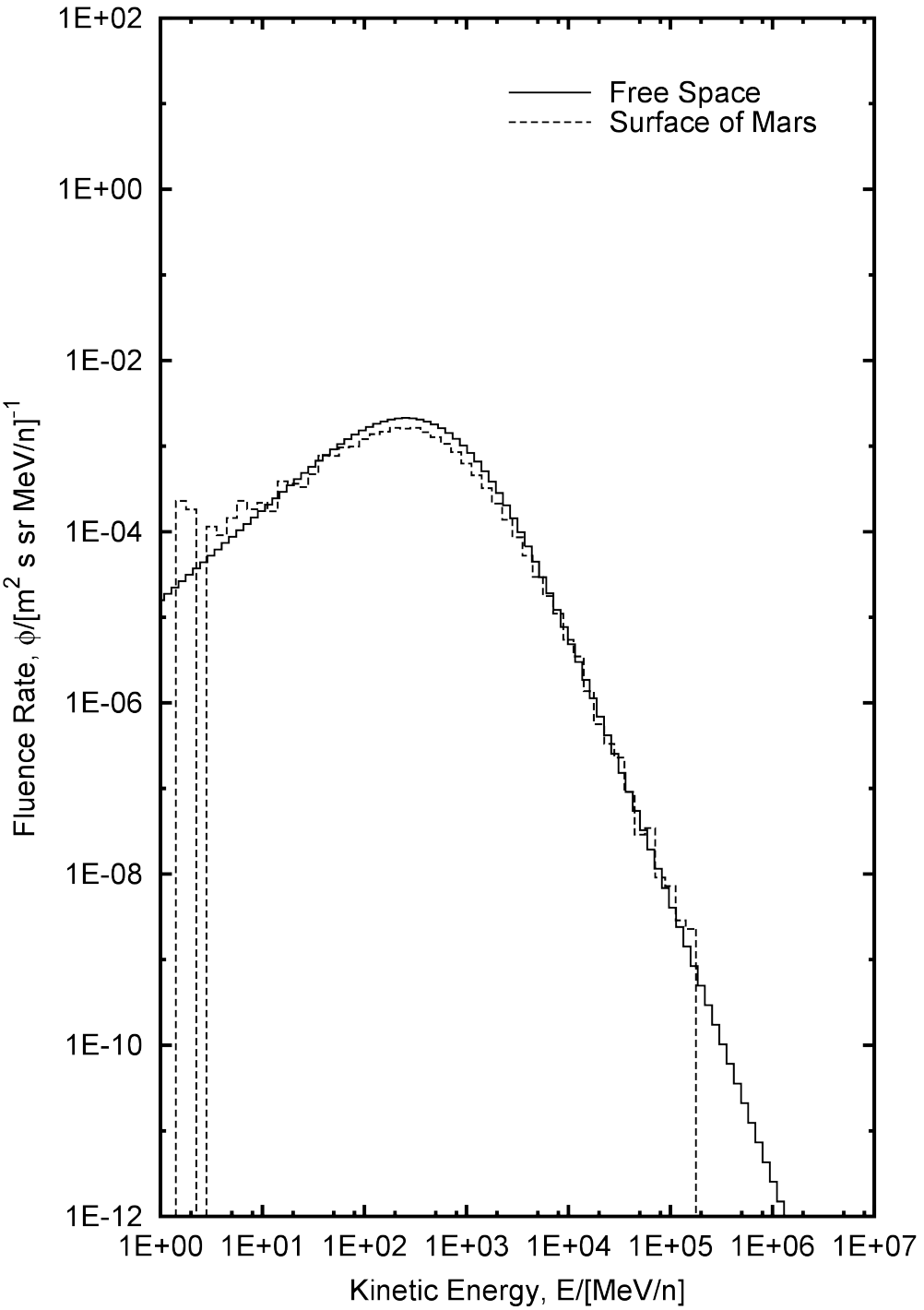

Figure F.10. Comparison of free space and surface of Mars differential energy spectra for $z = 5$ (isotopes combined). The "Free Space" curve is from the Badhwar–O'Neill model and the "Surface of Mars" curve was generated from the particle fluence 1 m above the surface, including albedo ions, with the Badhwar–O'Neill model ($z = 1$ to $z = 28$) incident on the top of the Martian atmosphere.

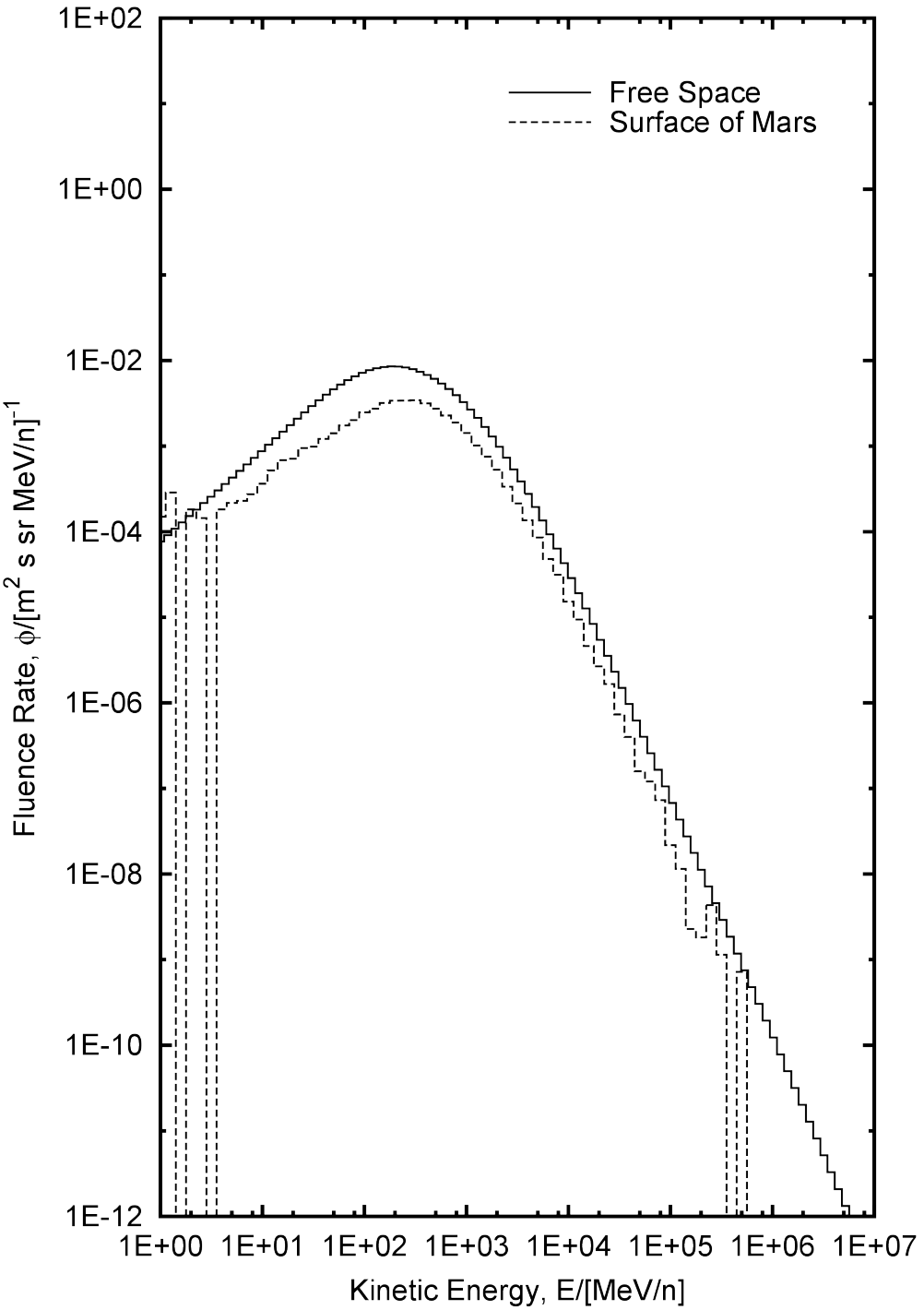

Figure F.11. Comparison of free space and surface of Mars differential energy spectra for $z = 6$ (isotopes combined). The "Free Space" curve is from the Badhwar–O'Neill model and the "Surface of Mars" curve was generated from the particle fluence 1 m above the surface, including albedo ions, with the Badhwar–O'Neill model ($z = 1$ to $z = 28$) incident on the top of the Martian atmosphere.

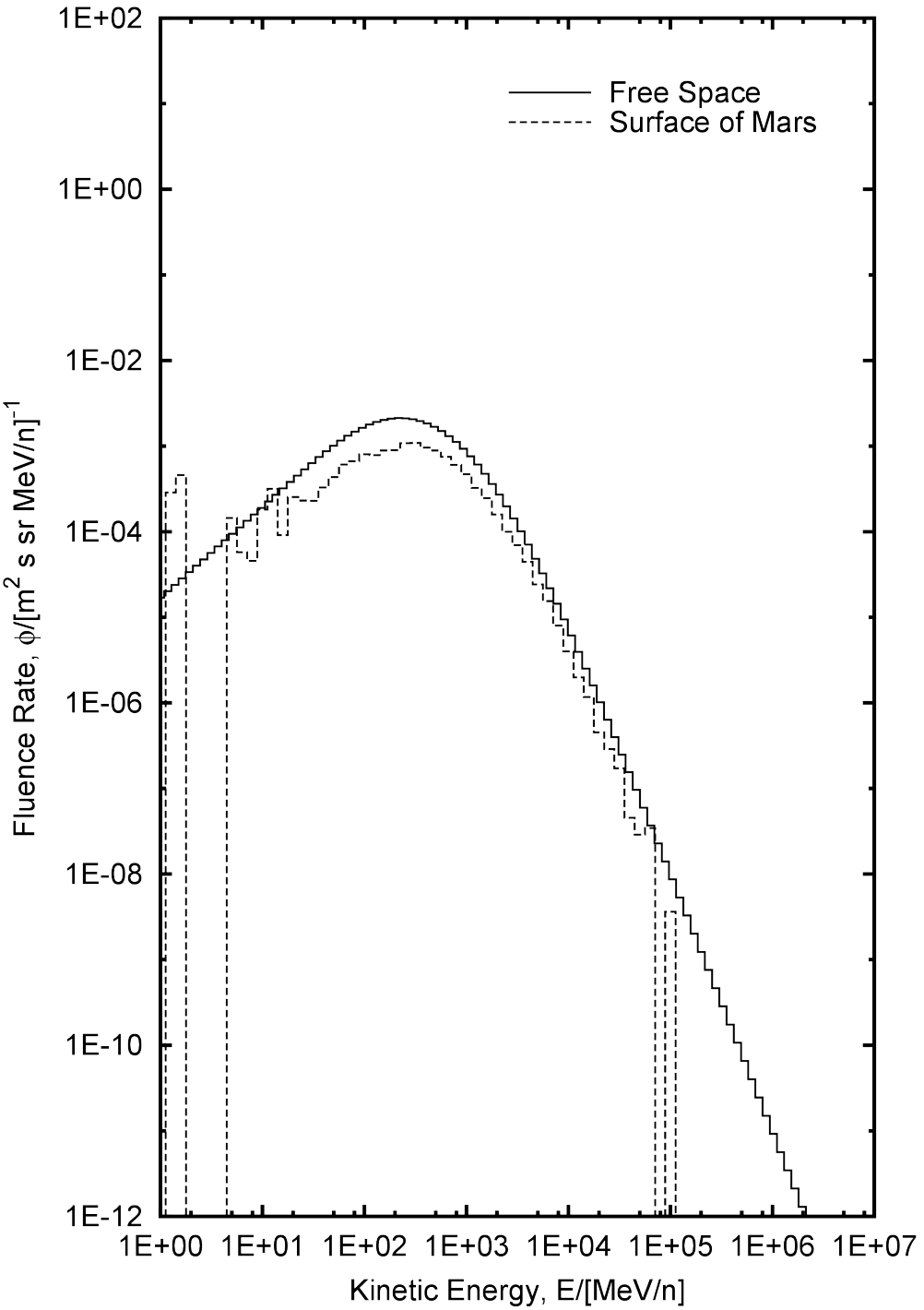

Figure F.12. Comparison of free space and surface of Mars differential energy spectra for $z = 7$ (isotopes combined). The "Free Space" curve is from the Badhwar–O'Neill model and the "Surface of Mars" curve was generated from the particle fluence 1 m above the surface, including albedo ions, with the Badhwar–O'Neill model ($z = 1$ to $z = 28$) incident on the top of the Martian atmosphere.

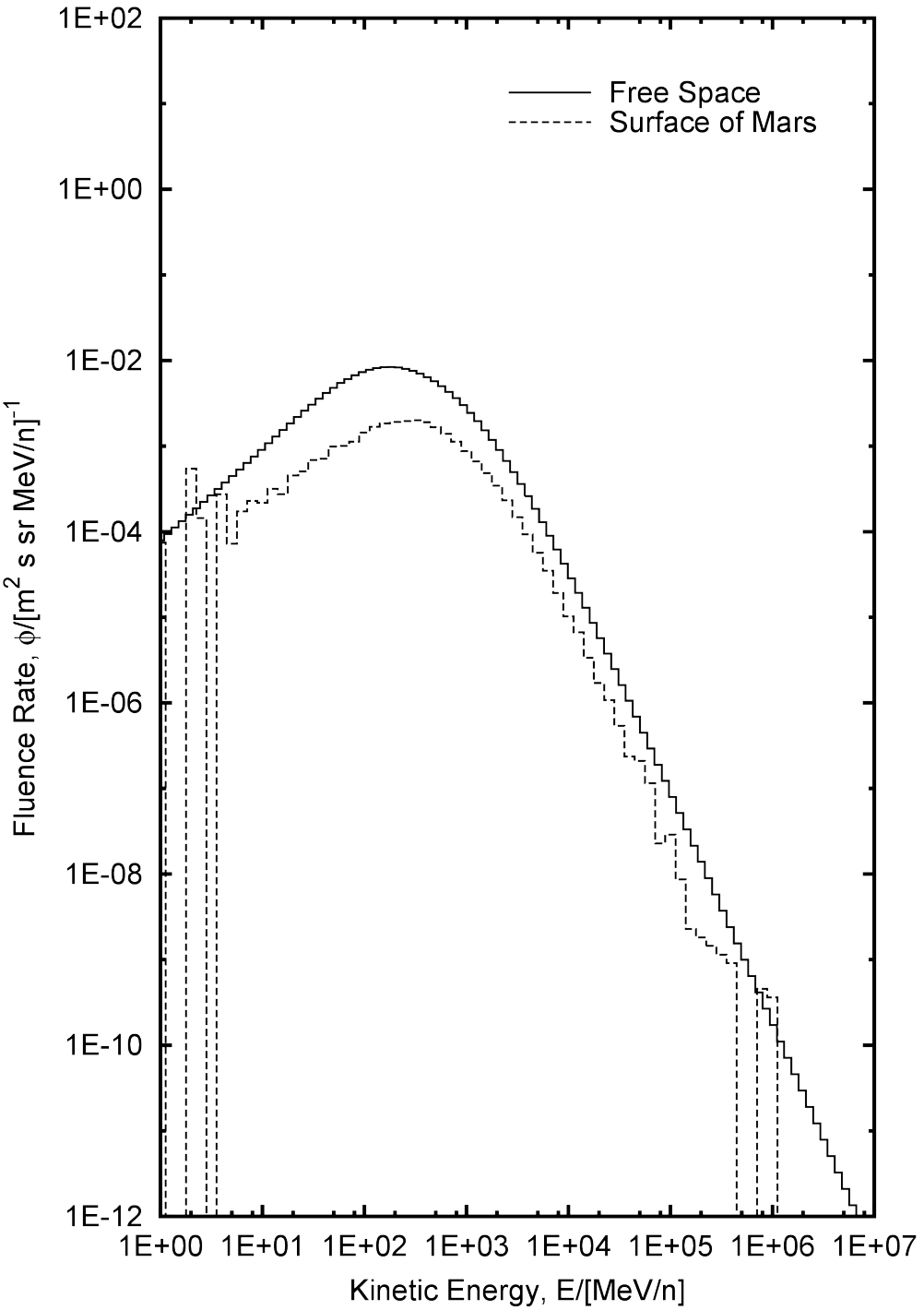

Figure F.13. Comparison of free space and surface of Mars differential energy spectra for $z = 8$ (isotopes combined). The "Free Space" curve is from the Badhwar–O'Neill model and the "Surface of Mars" curve was generated from the particle fluence 1 m above the surface, including albedo ions, with the Badhwar–O'Neill model ($z = 1$ to $z = 28$) incident on the top of the Martian atmosphere.

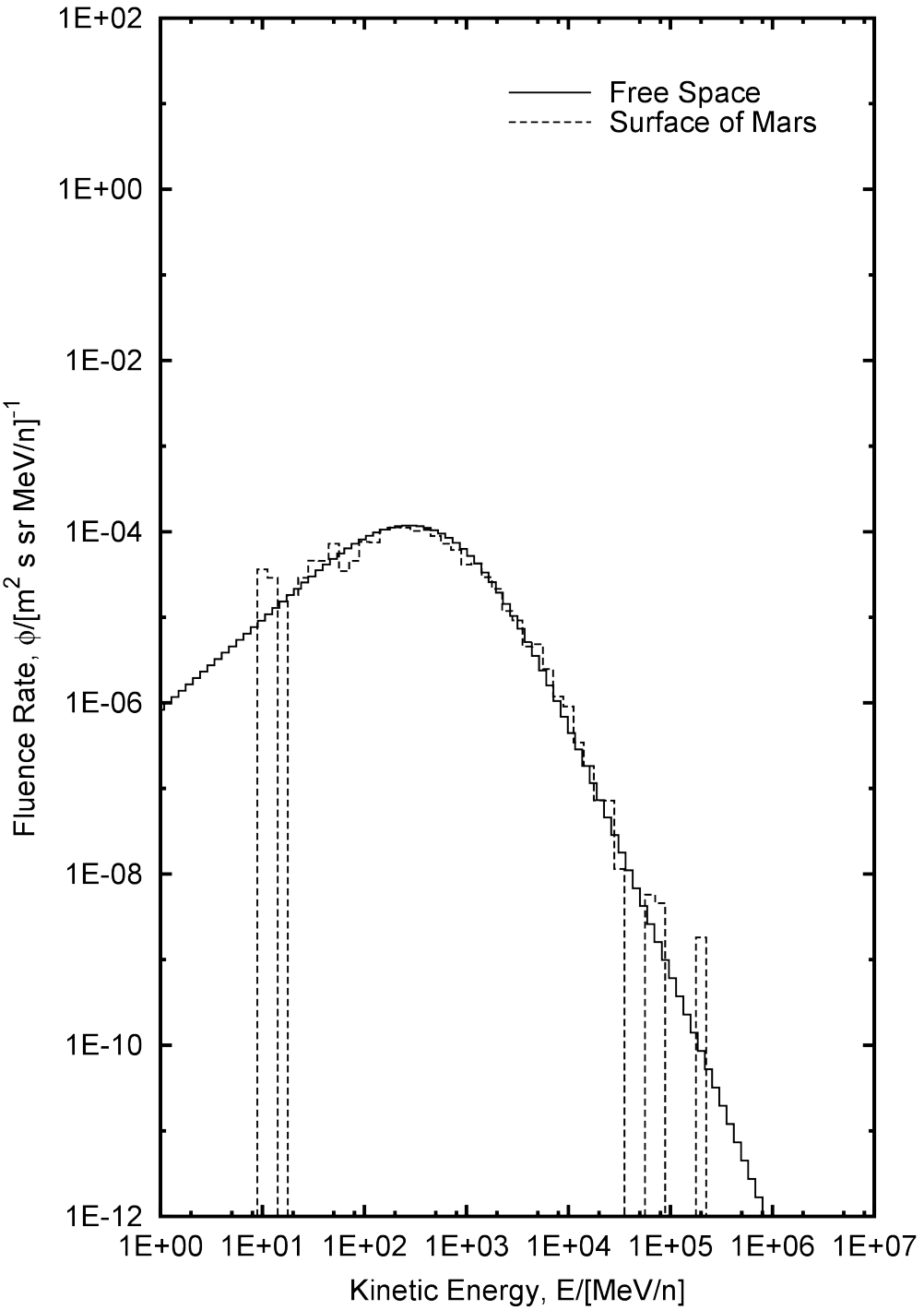

Figure F.14. Comparison of free space and surface of Mars differential energy spectra for $z = 9$ (isotopes combined). The "Free Space" curve is from the Badhwar–O'Neill model and the "Surface of Mars" curve was generated from the particle fluence 1 m above the surface, including albedo ions, with the Badhwar–O'Neill model ($z = 1$ to $z = 28$) incident on the top of the Martian atmosphere.

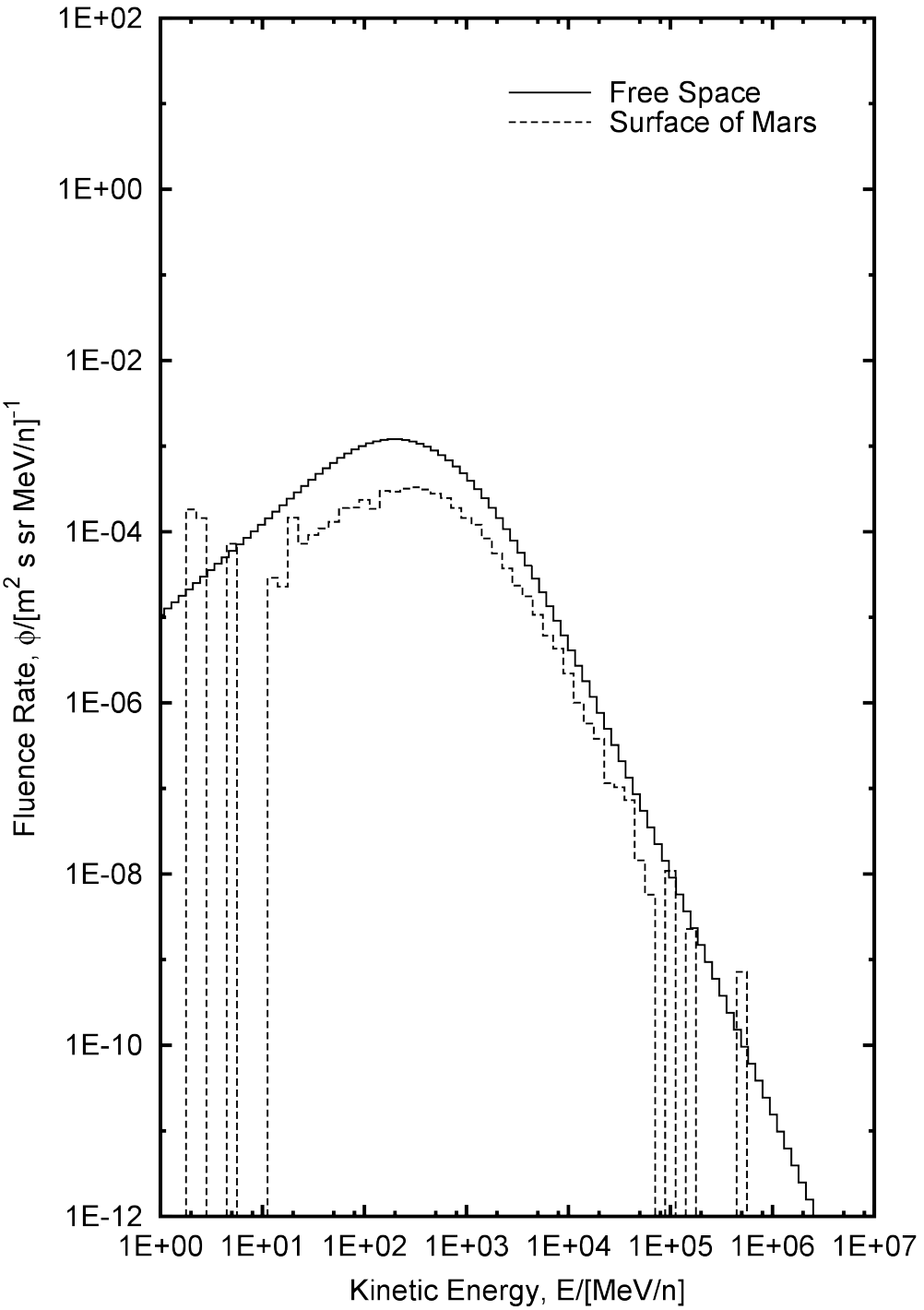

Figure F.15. Comparison of free space and surface of Mars differential energy spectra for $z = 10$ (isotopes combined). The "Free Space" curve is from the Badhwar–O'Neill model and the "Surface of Mars" curve was generated from the particle fluence 1 m above the surface, including albedo ions, with the Badhwar–O'Neill model ($z = 1$ to $z = 28$) incident on the top of the Martian atmosphere.

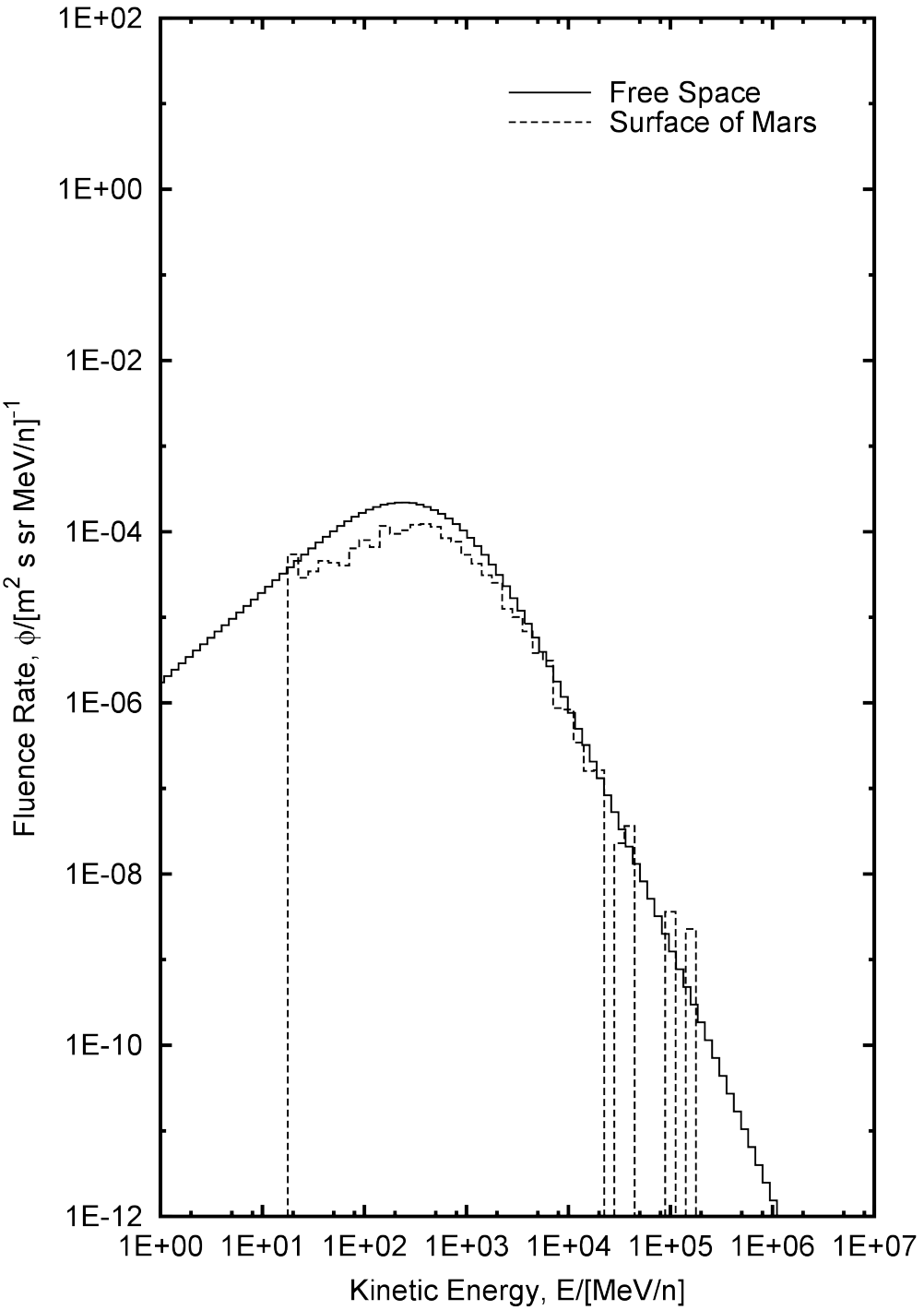

Figure F.16. Comparison of free space and surface of Mars differential energy spectra for $z = 11$ (isotopes combined). The "Free Space" curve is from the Badhwar–O'Neill model and the "Surface of Mars" curve was generated from the particle fluence 1 m above the surface, including albedo ions, with the Badhwar–O'Neill model ($z = 1$ to $z = 28$) incident on the top of the Martian atmosphere.

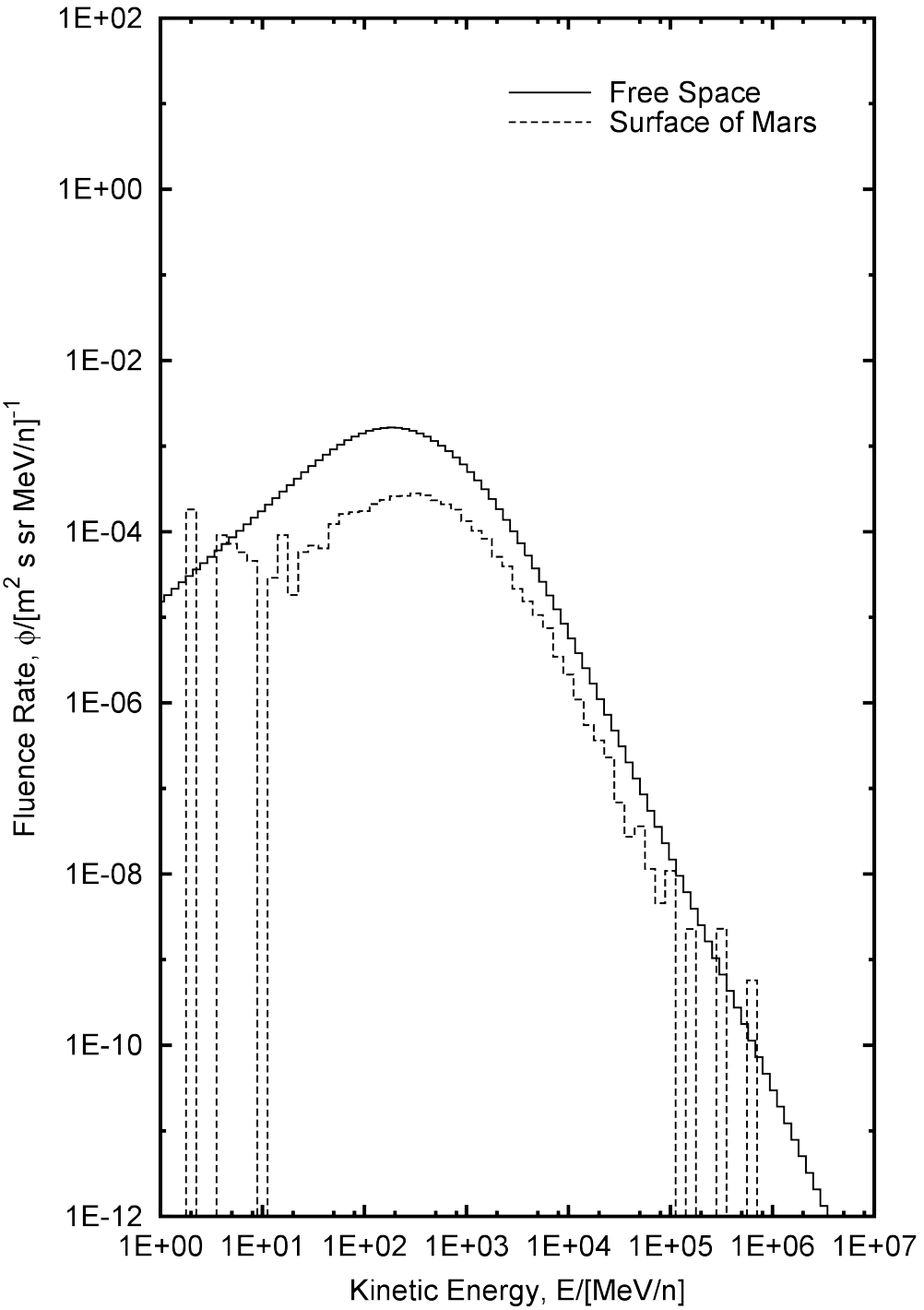

Figure F.17. Comparison of free space and surface of Mars differential energy spectra for $z = 12$ (isotopes combined). The "Free Space" curve is from the Badhwar–O'Neill model and the "Surface of Mars" curve was generated from the particle fluence 1 m above the surface, including albedo ions, with the Badhwar–O'Neill model ($z = 1$ to $z = 28$) incident on the top of the Martian atmosphere.

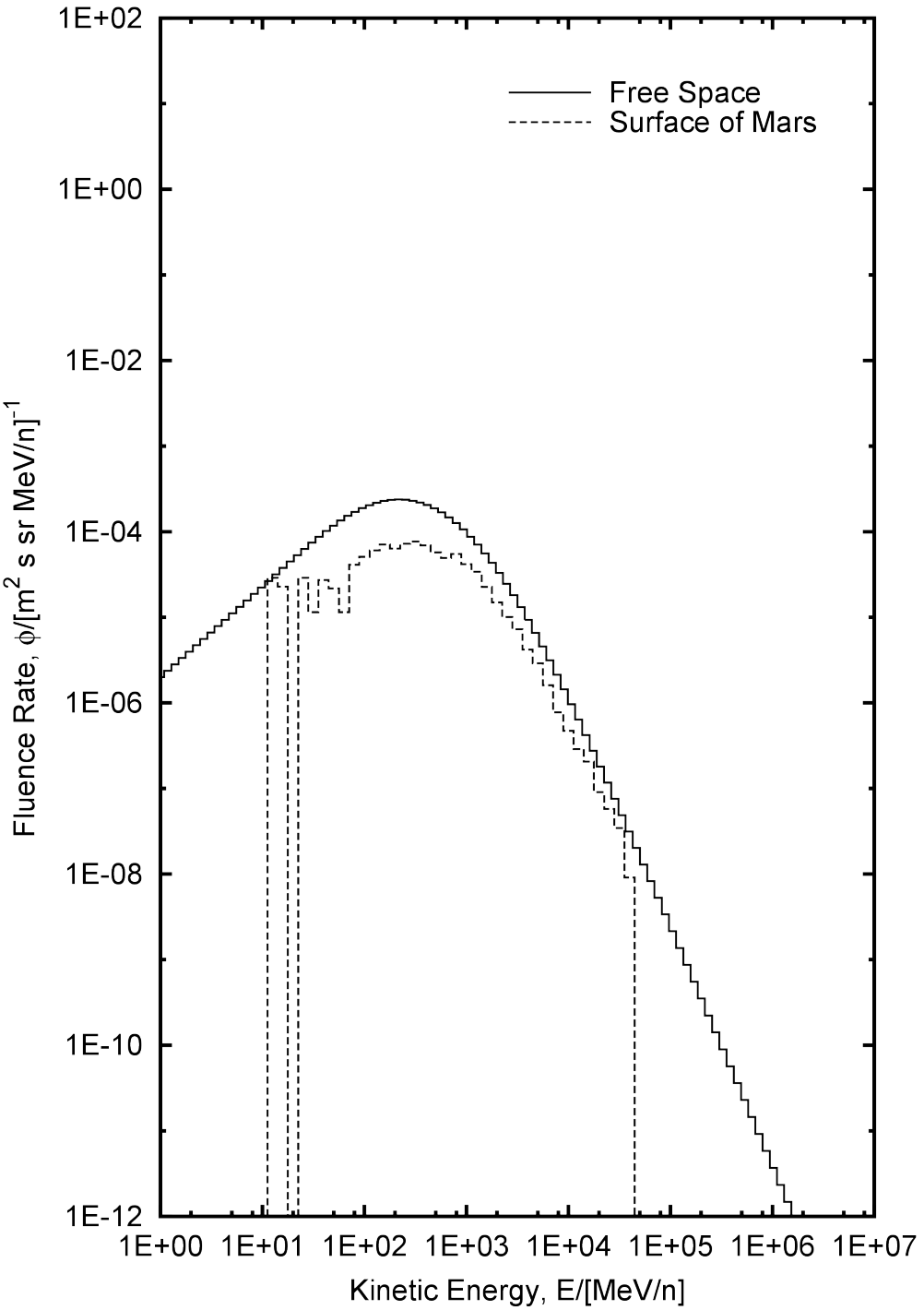

Figure F.18. Comparison of free space and surface of Mars differential energy spectra for $z = 13$ (isotopes combined). The "Free Space" curve is from the Badhwar–O'Neill model and the "Surface of Mars" curve was generated from the particle fluence 1 m above the surface, including albedo ions, with the Badhwar–O'Neill model ($z = 1$ to $z = 28$) incident on the top of the Martian atmosphere.

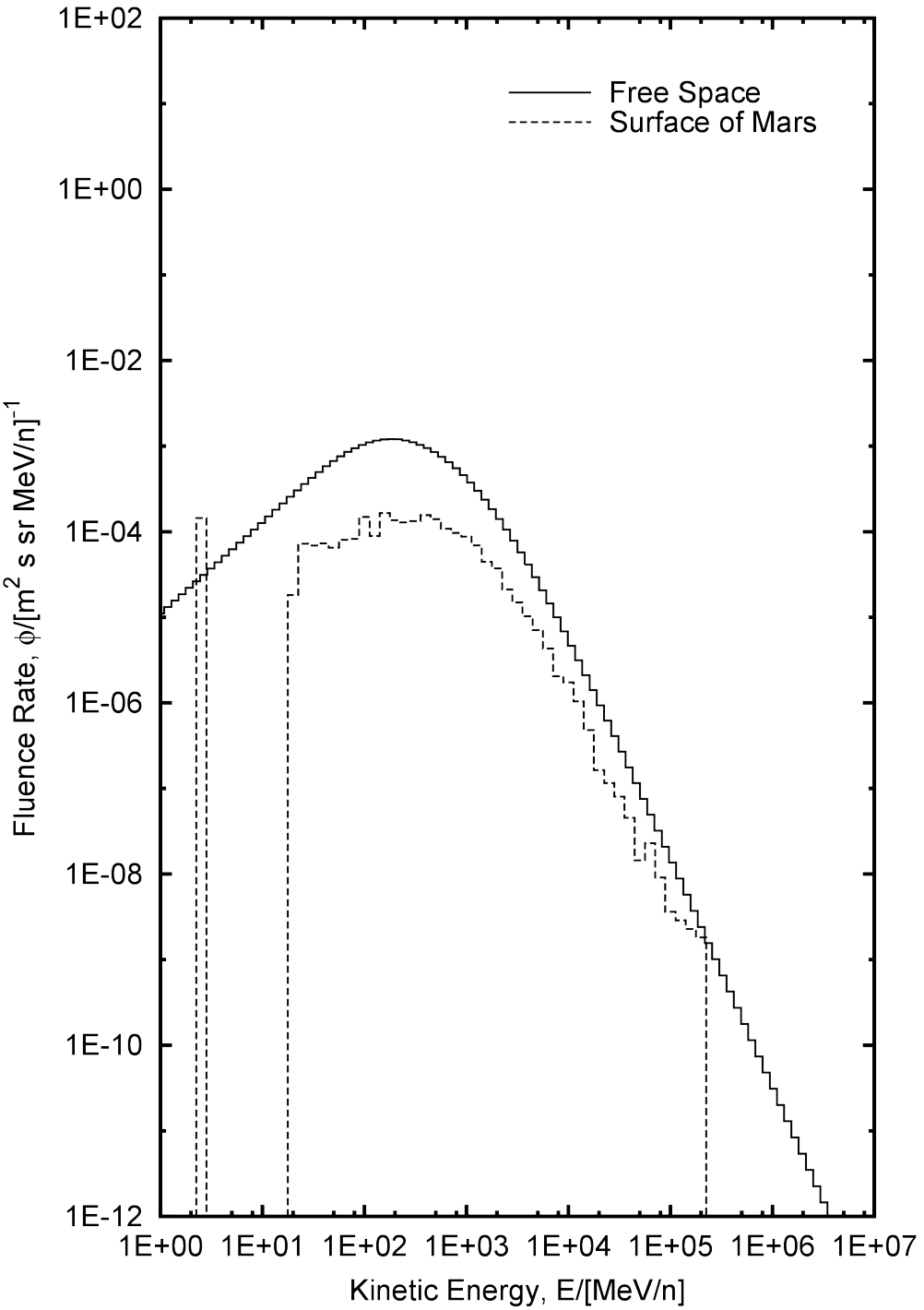

Figure F.19. Comparison of free space and surface of Mars differential energy spectra for $z = 14$ (isotopes combined). The "Free Space" curve is from the Badhwar–O'Neill model and the "Surface of Mars" curve was generated from the particle fluence 1 m above the surface, including albedo ions, with the Badhwar–O'Neill model ($z = 1$ to $z = 28$) incident on the top of the Martian atmosphere.

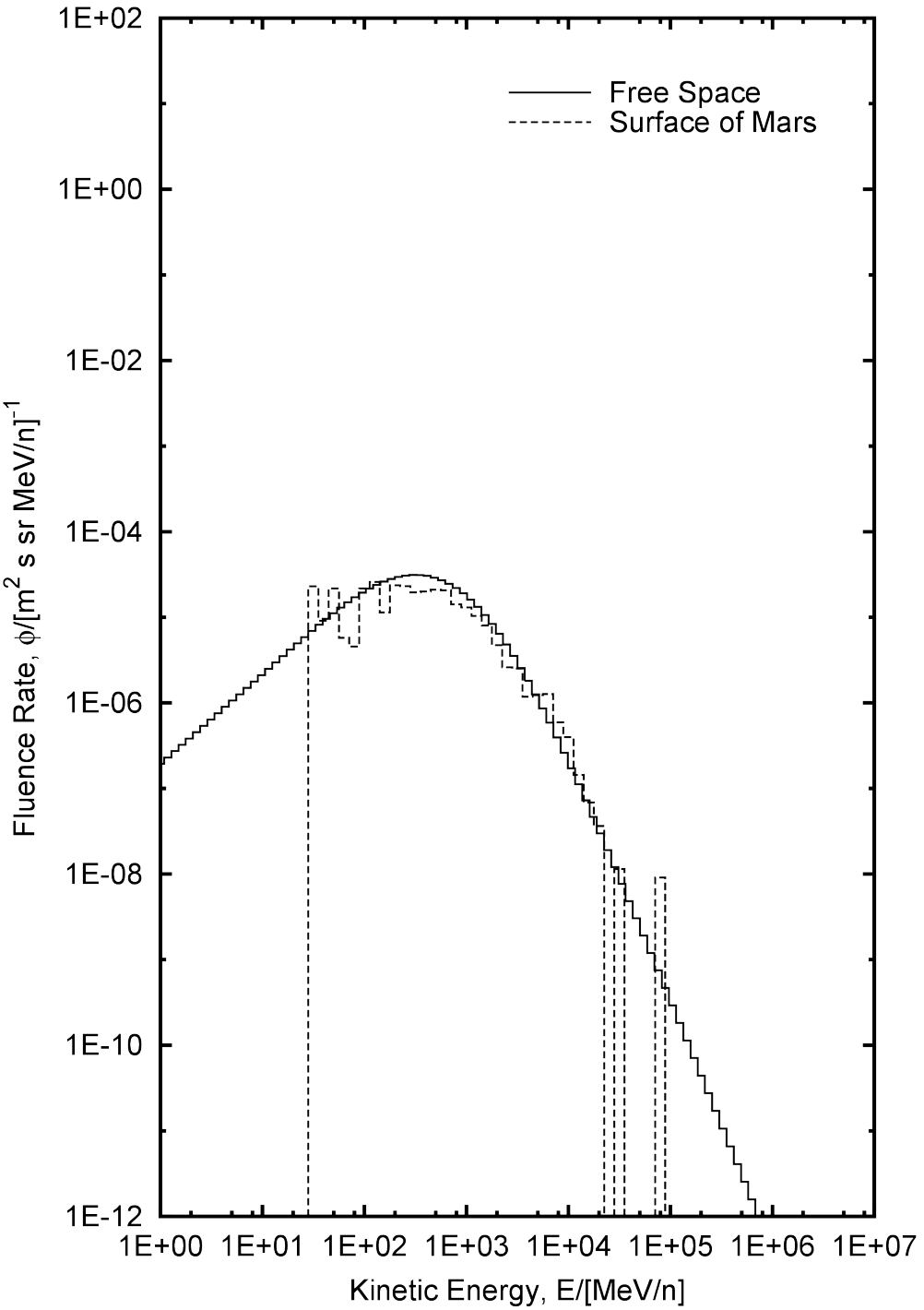

Figure F.20. Comparison of free space and surface of Mars differential energy spectra for $z = 15$ (isotopes combined). The "Free Space" curve is from the Badhwar–O'Neill model and the "Surface of Mars" curve was generated from the particle fluence 1 m above the surface, including albedo ions, with the Badhwar–O'Neill model ($z = 1$ to $z = 28$) incident on the top of the Martian atmosphere.

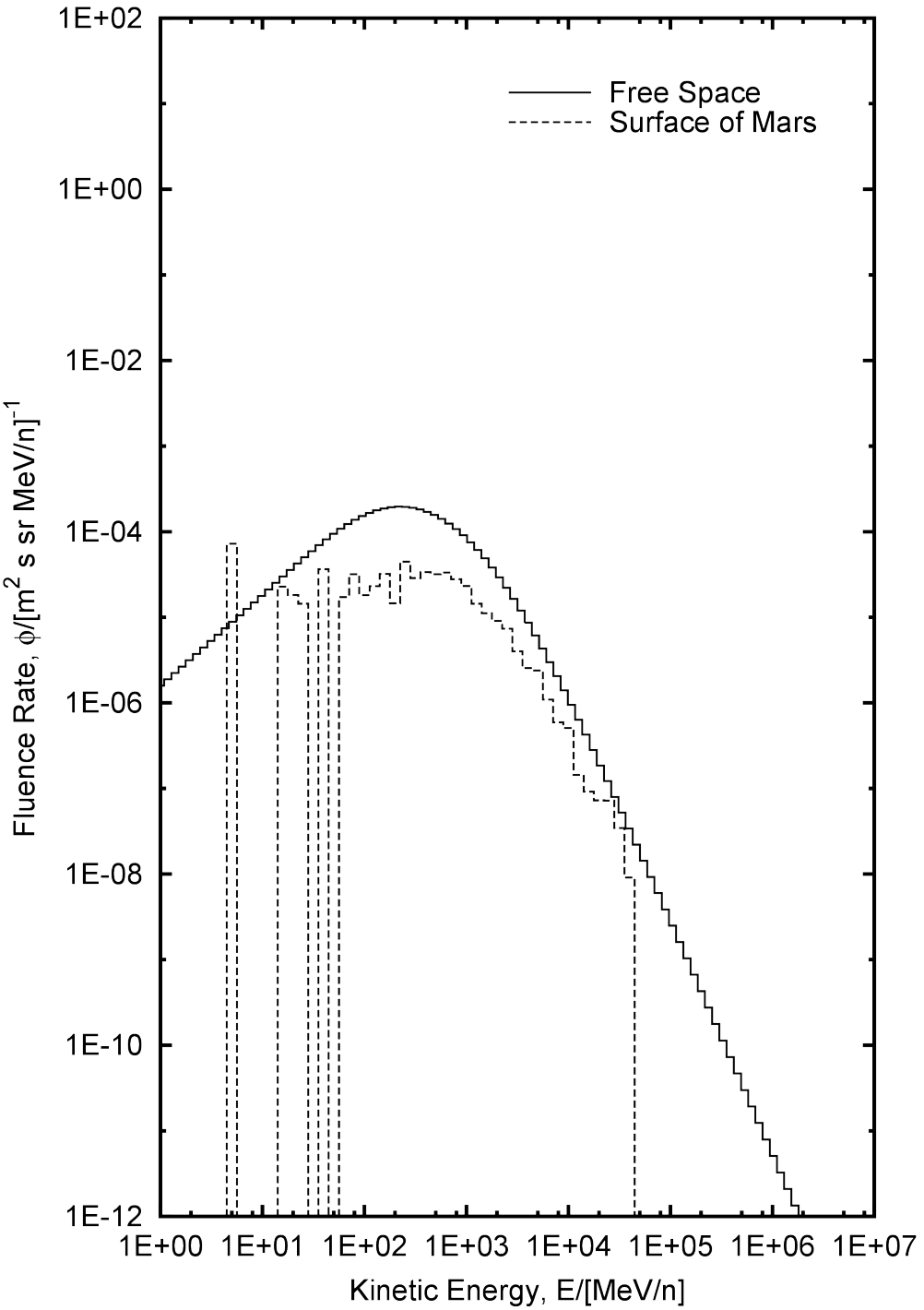

Figure F.21. Comparison of free space and surface of Mars differential energy spectra for $z = 16$ (isotopes combined). The "Free Space" curve is from the Badhwar–O'Neill model and the "Surface of Mars" curve was generated from the particle fluence 1 m above the surface, including albedo ions, with the Badhwar–O'Neill model ($z = 1$ to $z = 28$) incident on the top of the Martian atmosphere.

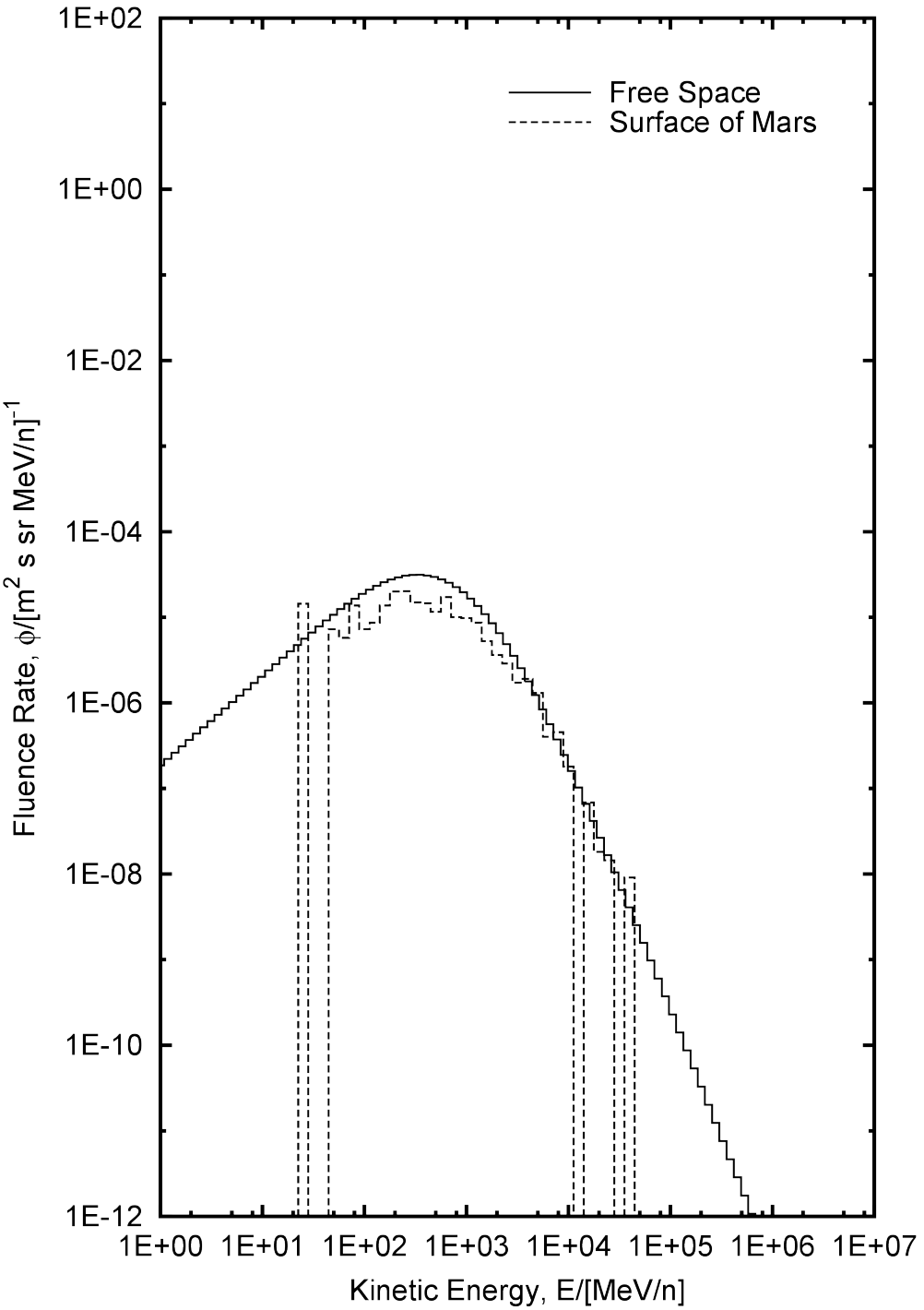

Figure F.22. Comparison of free space and surface of Mars differential energy spectra for $z = 17$ (isotopes combined). The "Free Space" curve is from the Badhwar–O'Neill model and the "Surface of Mars" curve was generated from the particle fluence 1 m above the surface, including albedo ions, with the Badhwar–O'Neill model ($z = 1$ to $z = 28$) incident on the top of the Martian atmosphere.

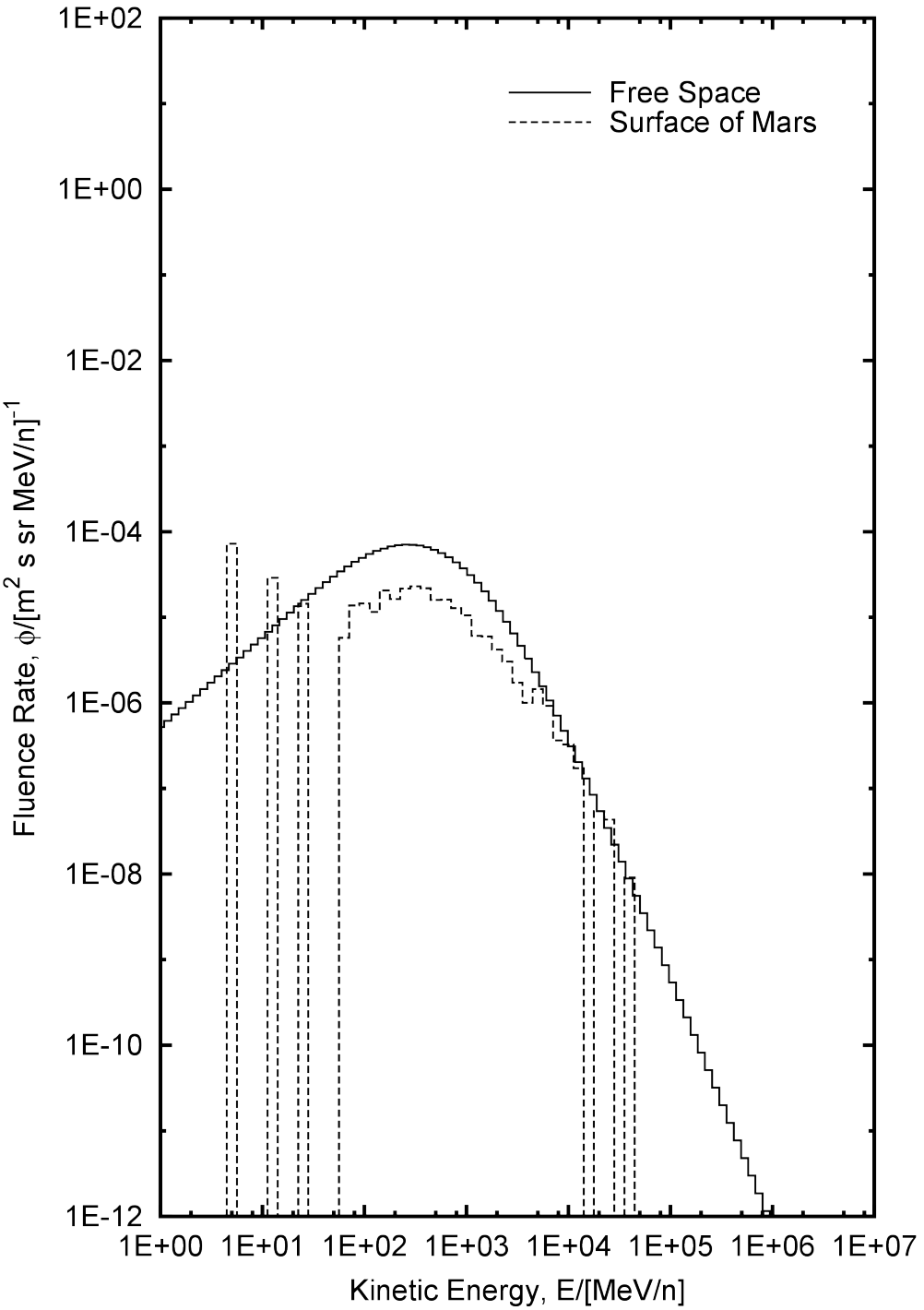

Figure F.23. Comparison of free space and surface of Mars differential energy spectra for $z = 18$ (isotopes combined). The "Free Space" curve is from the Badhwar–O'Neill model and the "Surface of Mars" curve was generated from the particle fluence 1 m above the surface, including albedo ions, with the Badhwar–O'Neill model ($z = 1$ to $z = 28$) incident on the top of the Martian atmosphere.

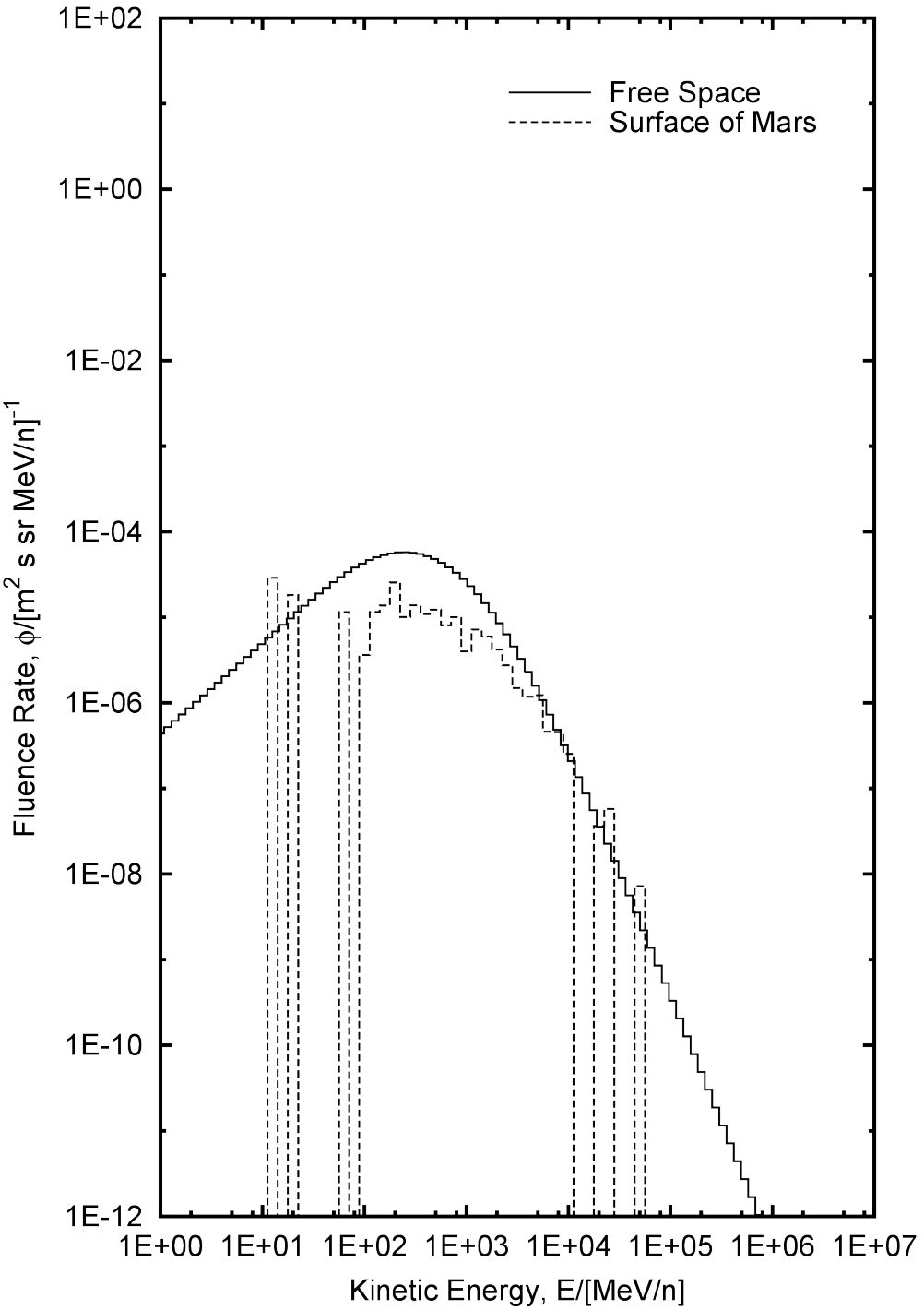

Figure F.24. Comparison of free space and surface of Mars differential energy spectra for $z = 19$ (isotopes combined). The "Free Space" curve is from the Badhwar–O'Neill model and the "Surface of Mars" curve was generated from the particle fluence 1 m above the surface, including albedo ions, with the Badhwar–O'Neill model ($z = 1$ to $z = 28$) incident on the top of the Martian atmosphere.

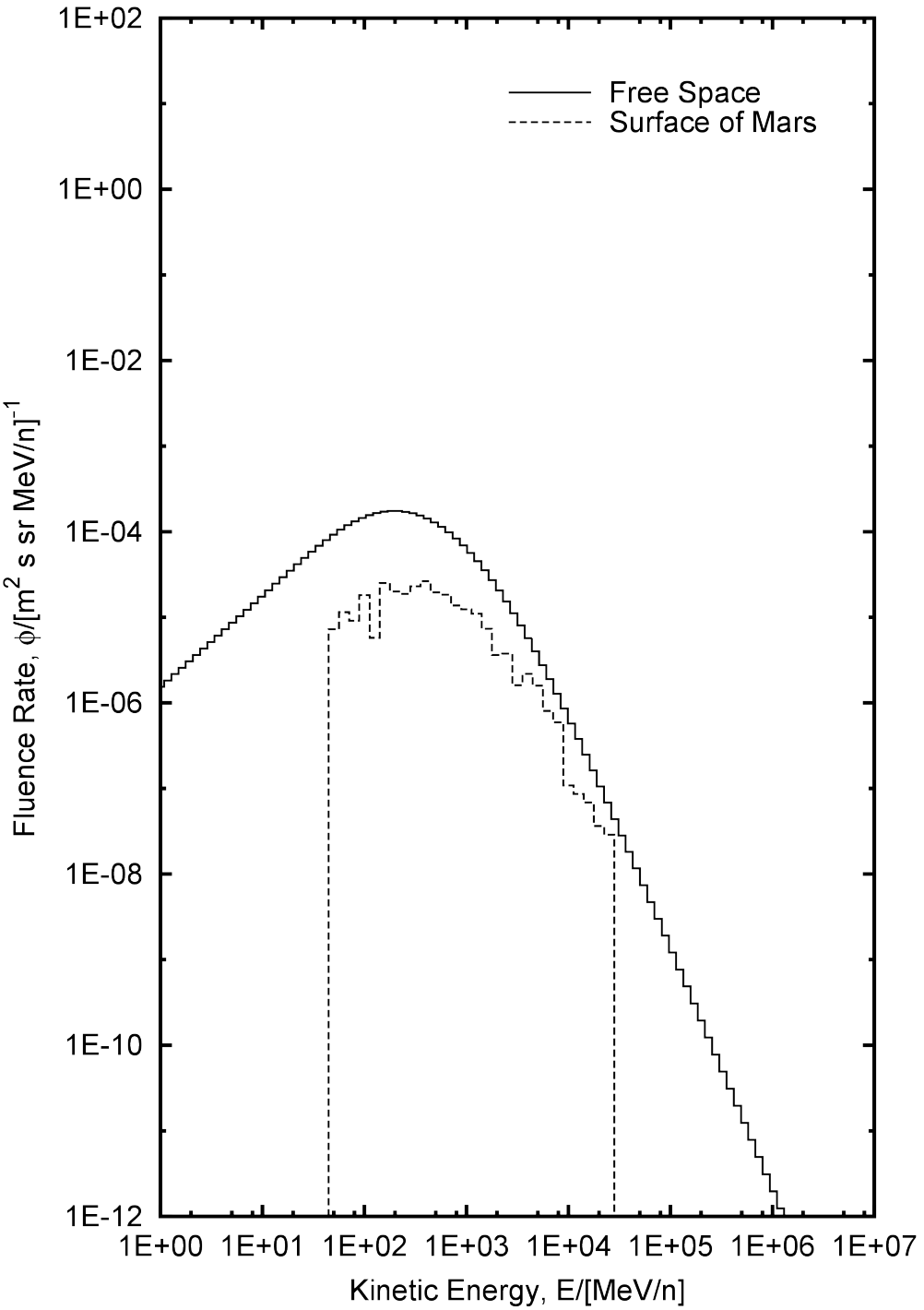

Figure F.25. Comparison of free space and surface of Mars differential energy spectra for $z = 20$ (isotopes combined). The "Free Space" curve is from the Badhwar–O'Neill model and the "Surface of Mars" curve was generated from the particle fluence 1 m above the surface, including albedo ions, with the Badhwar–O'Neill model ($z = 1$ to $z = 28$) incident on the top of the Martian atmosphere.

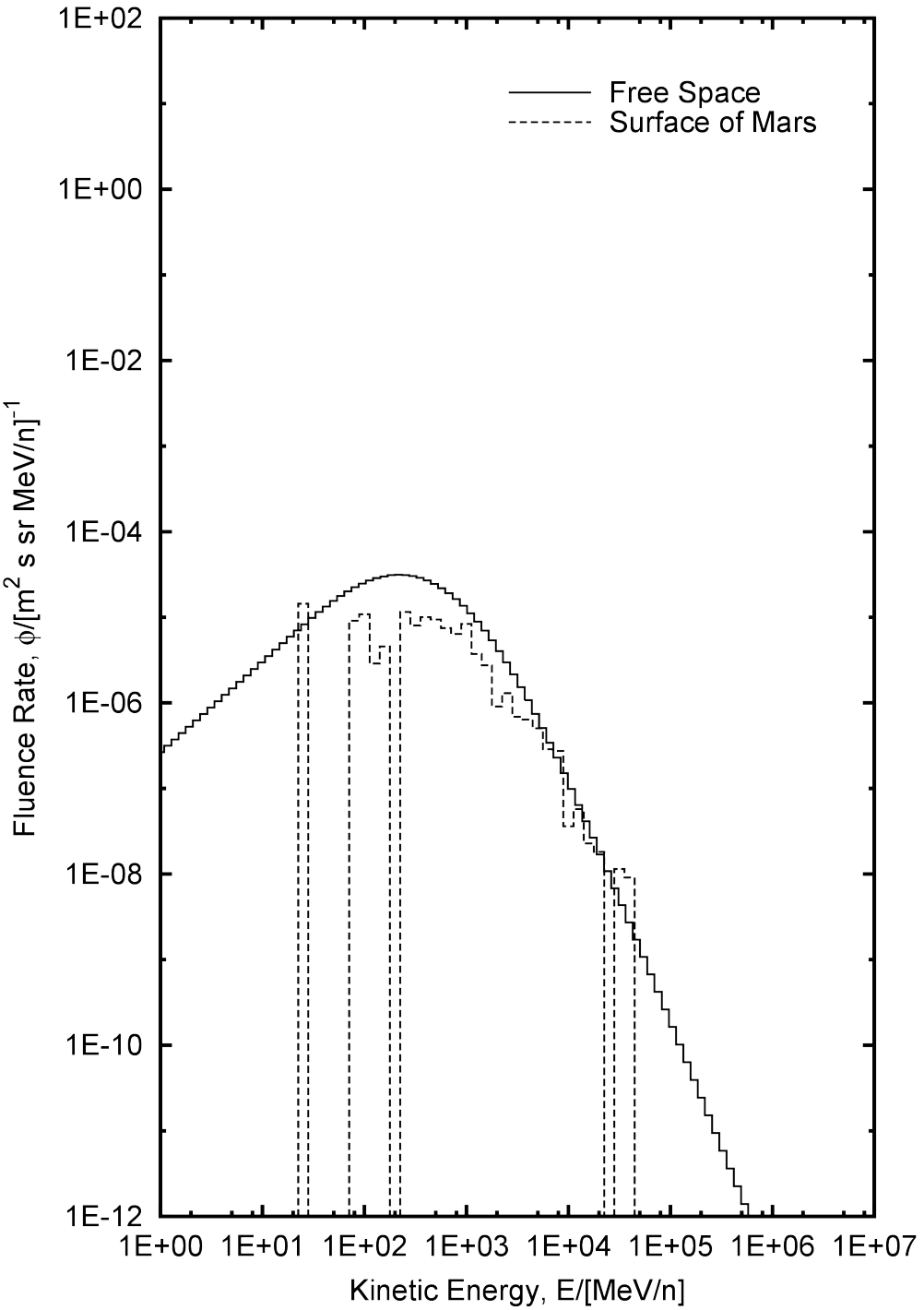

Figure F.26. Comparison of free space and surface of Mars differential energy spectra for $z = 21$ (isotopes combined). The "Free Space" curve is from the Badhwar–O'Neill model and the "Surface of Mars" curve was generated from the particle fluence 1 m above the surface, including albedo ions, with the Badhwar–O'Neill model ($z = 1$ to $z = 28$) incident on the top of the Martian atmosphere.

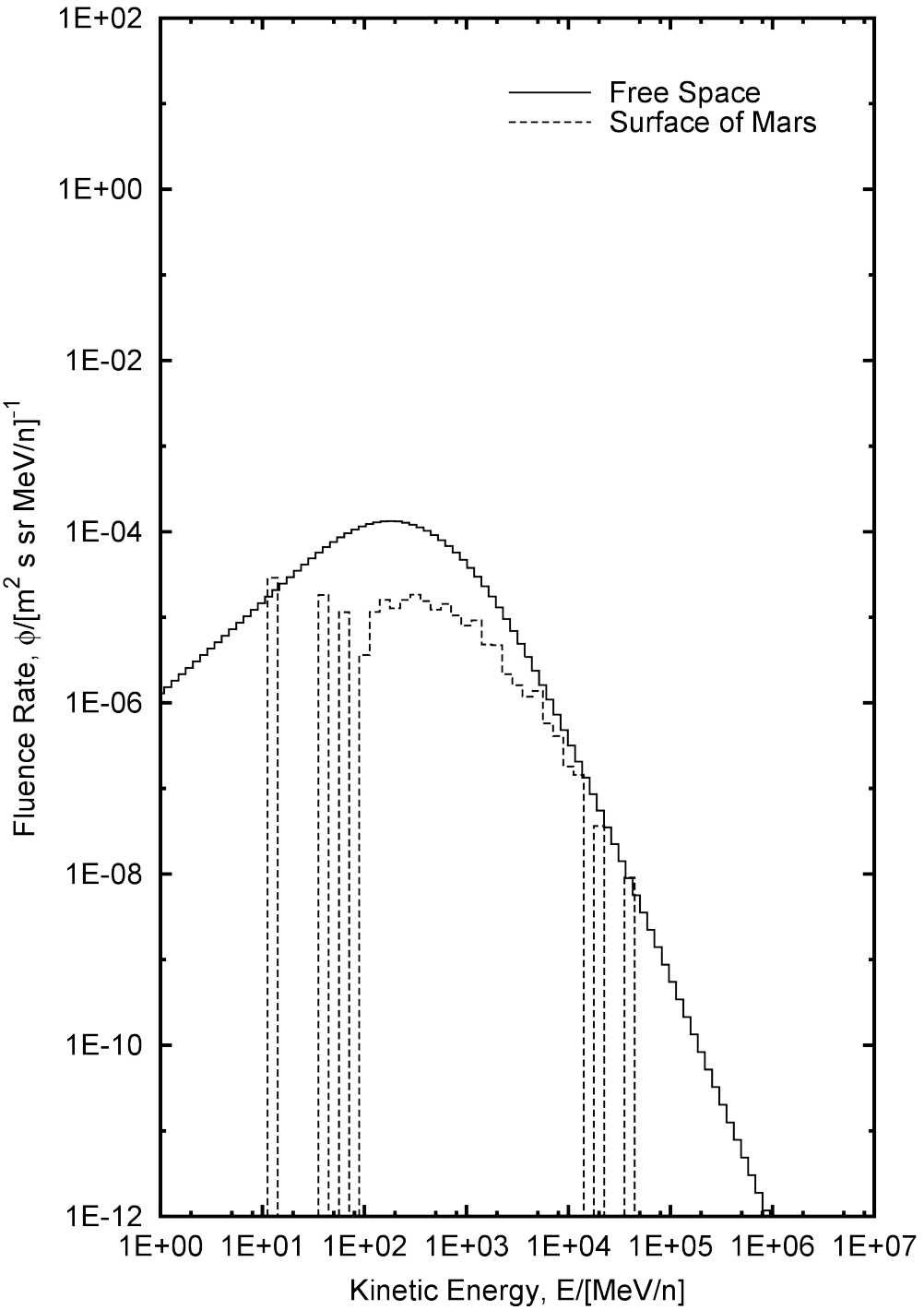

Figure F.27. Comparison of free space and surface of Mars differential energy spectra for $z = 22$ (isotopes combined). The "Free Space" curve is from the Badhwar–O'Neill model and the "Surface of Mars" curve was generated from the particle fluence 1 m above the surface, including albedo ions, with the Badhwar–O'Neill model ($z = 1$ to $z = 28$) incident on the top of the Martian atmosphere.

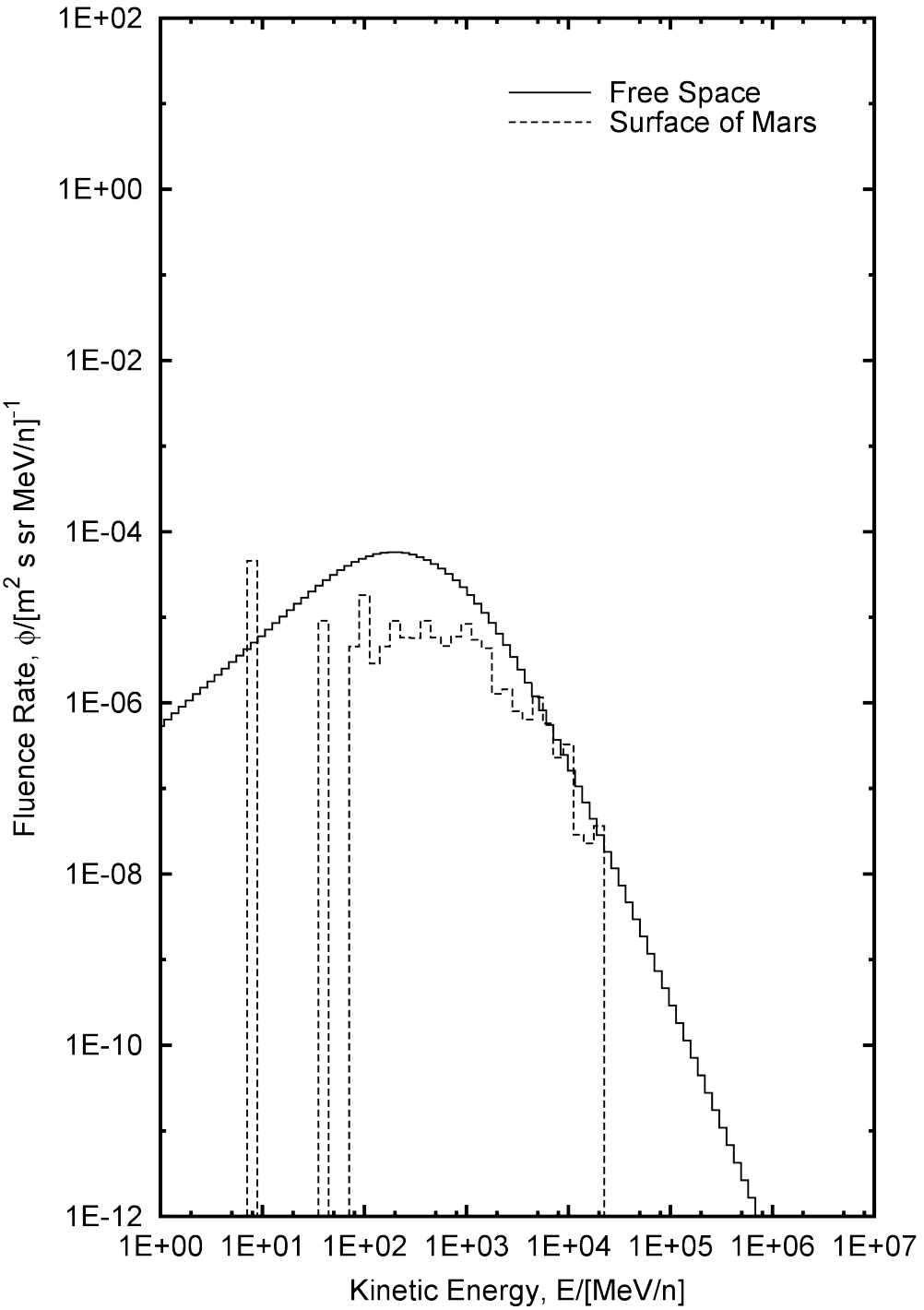

Figure F.28. Comparison of free space and surface of Mars differential energy spectra for $z = 23$ (isotopes combined). The "Free Space" curve is from the Badhwar–O'Neill model and the "Surface of Mars" curve was generated from the particle fluence 1 m above the surface, including albedo ions, with the Badhwar–O'Neill model ($z = 1$ to $z = 28$) incident on the top of the Martian atmosphere.

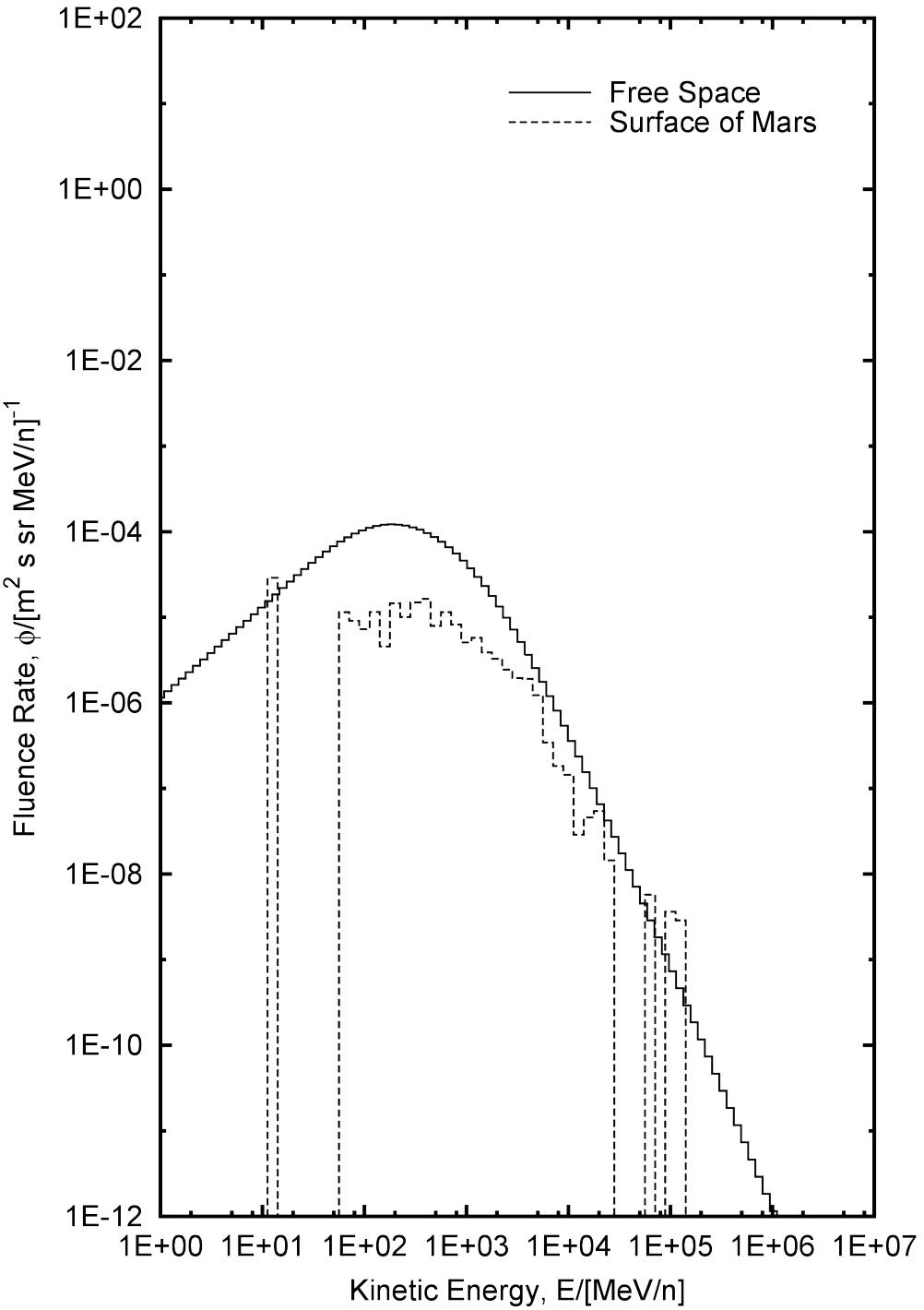

Figure F.29. Comparison of free space and surface of Mars differential energy spectra for $z = 24$ (isotopes combined). The "Free Space" curve is from the Badhwar–O'Neill model and the "Surface of Mars" curve was generated from the particle fluence 1 m above the surface, including albedo ions, with the Badhwar–O'Neill model ($z = 1$ to $z = 28$) incident on the top of the Martian atmosphere.

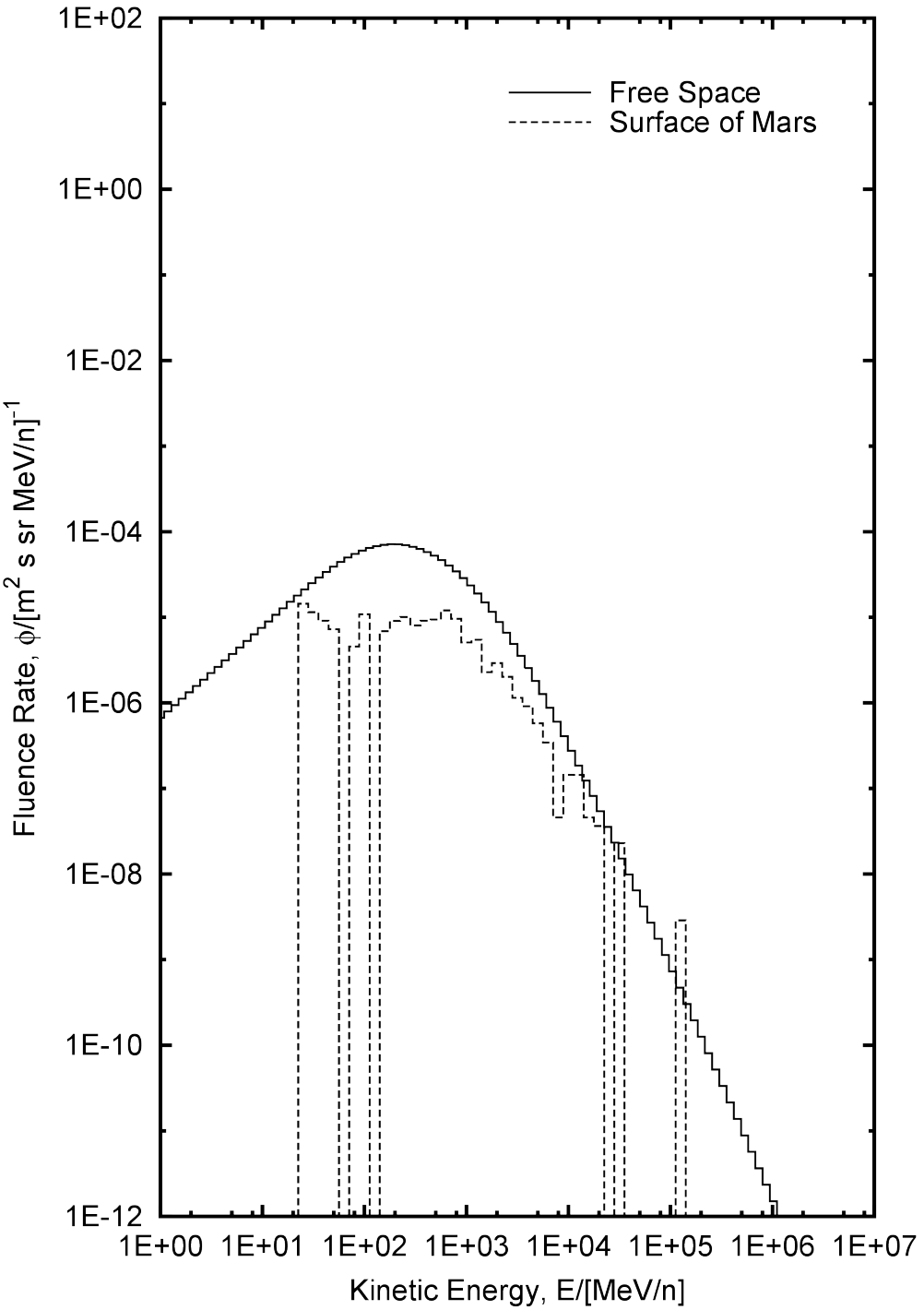

Figure F.30. Comparison of free space and surface of Mars differential energy spectra for $z = 25$ (isotopes combined). The "Free Space" curve is from the Badhwar–O'Neill model and the "Surface of Mars" curve was generated from the particle fluence 1 m above the surface, including albedo ions, with the Badhwar–O'Neill model ($z = 1$ to $z = 28$) incident on the top of the Martian atmosphere.

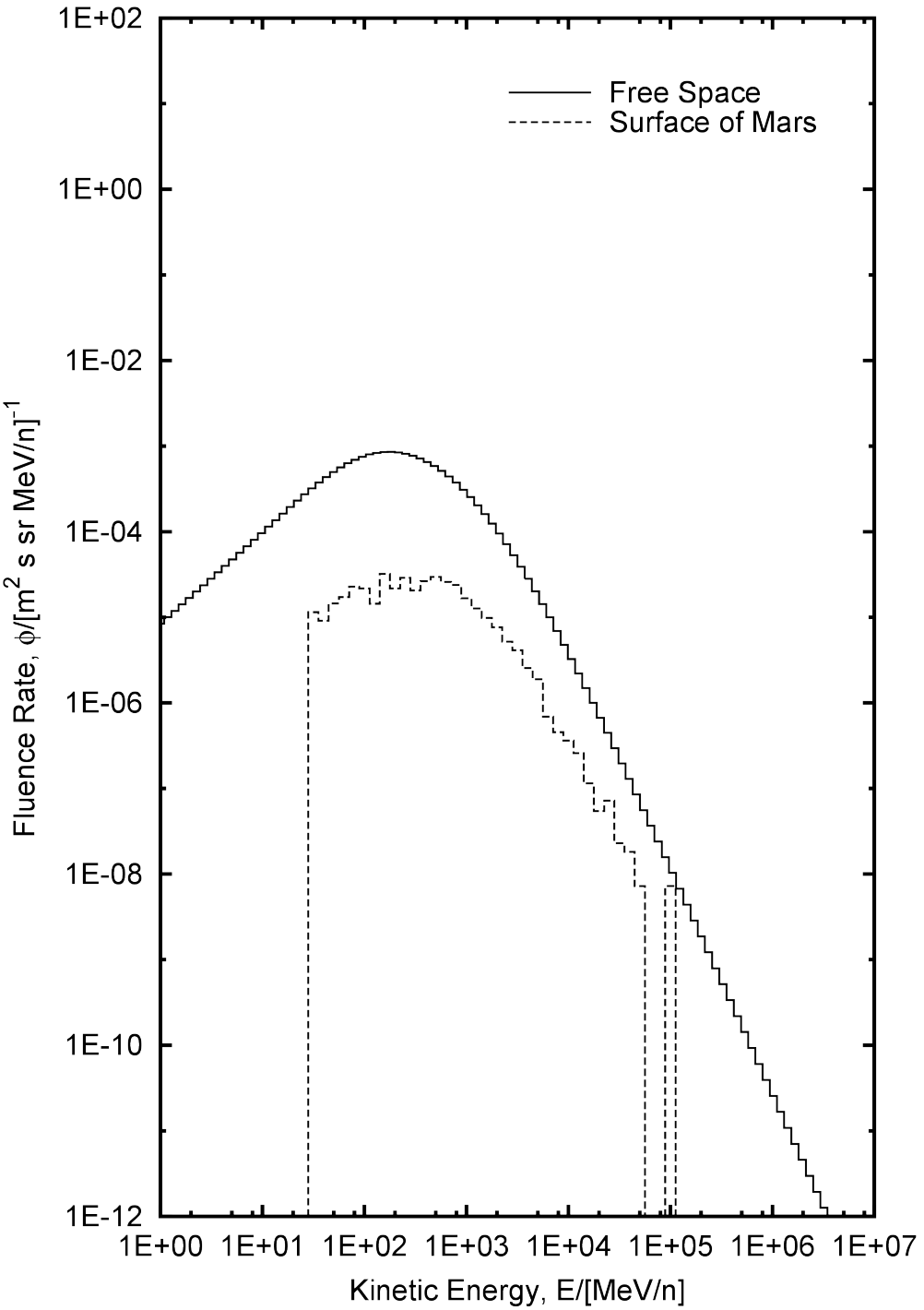

Figure F.31. Comparison of free space and surface of Mars differential energy spectra for $z = 26$ (isotopes combined). The "Free Space" curve is from the Badhwar–O'Neill model and the "Surface of Mars" curve was generated from the particle fluence 1 m above the surface, including albedo ions, with the Badhwar–O'Neill model ($z = 1$ to $z = 28$) incident on the top of the Martian atmosphere.

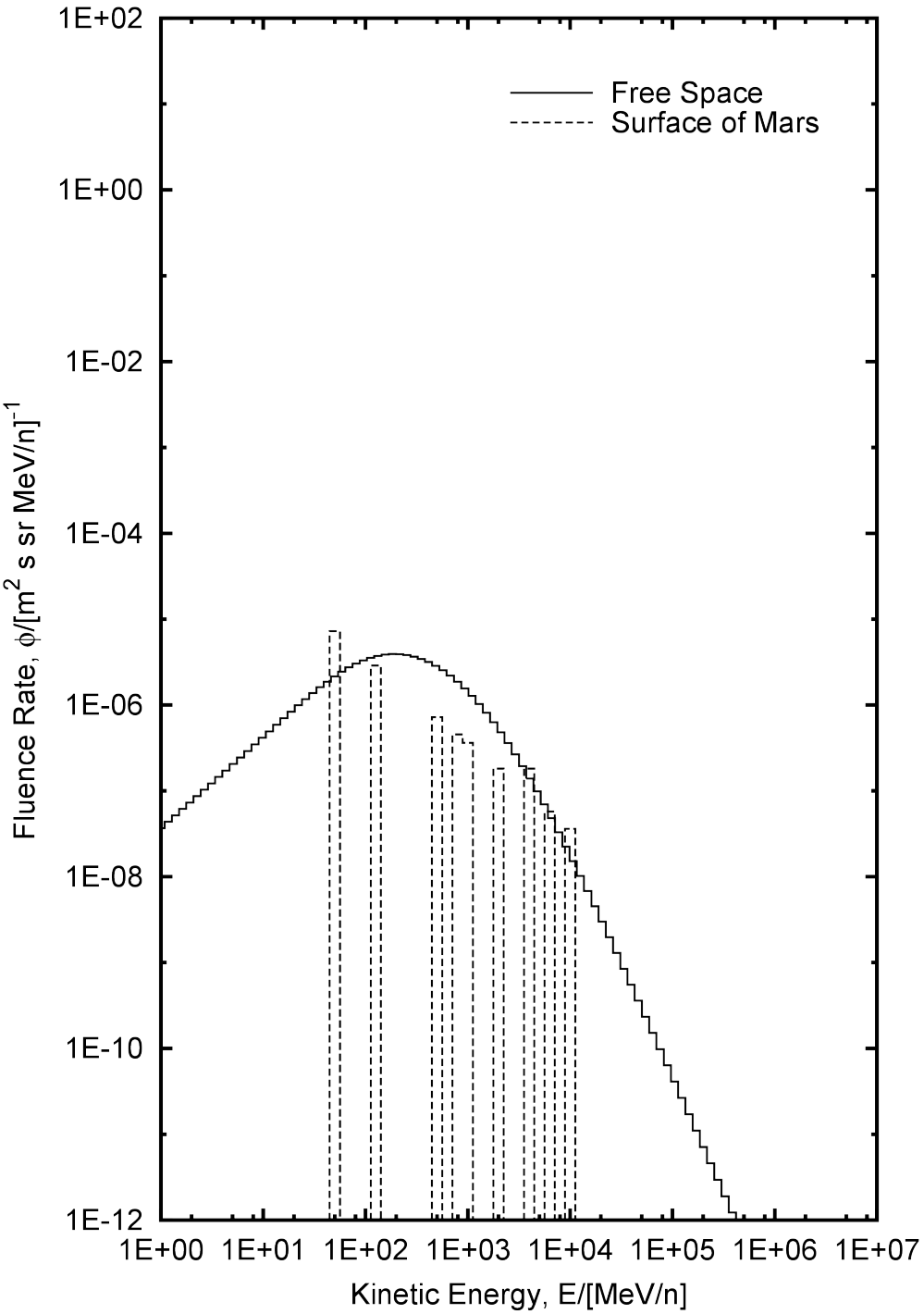

Figure F.32. Comparison of free space and surface of Mars differential energy spectra for $z = 27$ (isotopes combined). The "Free Space" curve is from the Badhwar–O'Neill model and the "Surface of Mars" curve was generated from the particle fluence 1 m above the surface, including albedo ions, with the Badhwar–O'Neill model ($z = 1$ to $z = 28$) incident on the top of the Martian atmosphere.

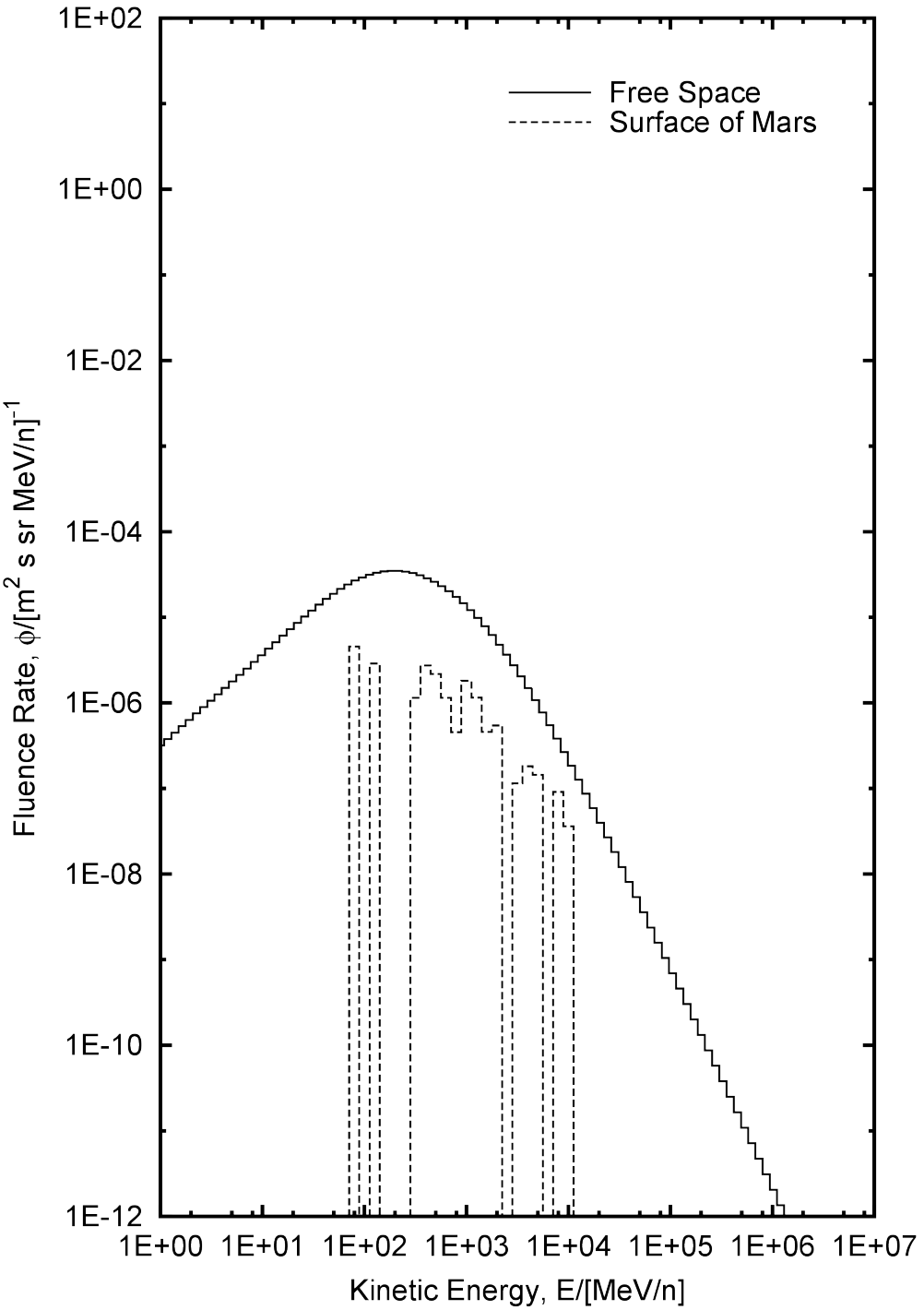

Figure F.33. Comparison of free space and surface of Mars differential energy spectra for $z = 28$ (isotopes combined). The "Free Space" curve is from the Badhwar–O'Neill model and the "Surface of Mars" curve was generated from the particle fluence 1 m above the surface, including albedo ions, with the Badhwar–O'Neill model ($z = 1$ to $z = 28$) incident on the top of the Martian atmosphere.

APPENDIX G

DIFFERENTIAL ENERGY SPECTRA TABULATED DATA

This appendix contains the FLUKA-generated values used to produce the "Surface of Mars" curves in the figures in Appendix F.

The first column E is the kinetic energy of the ion. The second column N is the corresponding number of ions recorded 1 m above the Martian surface in the corresponding energy bin E after simulating 1.0×10^8 histories in FLUKA. The third column ϕ is the fluence rate calculated by setting $N = N_{\text{Surface}}$ in Equation 3.13. The resulting fluence rate has been normalized according to the method described in Section 3.7.2. Finally, the fourth column is a normalized frequency distribution.

$\phi/[\mathrm{m}^2\ \mathrm{s\ sr\ MeV/n}]^{-1}$ as a function of $E/[\mathrm{MeV/n}]$ tabulated data used to generate the "Surface of Mars" differential energy spectrum for H-1:

```
# Using 70 Log Bins
# Min: 1 MeV/n          Max: 1e+07 MeV/n                10 bins/decade
#
# ***Statistics***
# Minimum:        6.7059e-05 MeV/n
# Maximum:        8.6082e+06 MeV/n
# Average:        1.8660e+03 MeV/n
# Frequency Mean: 1.6667e+03 MeV/n (binning-specific)
# Most Probable:  6.3096e+02 MeV/n (binning-specific)
#
# ***Totals***
# N           = 76878882
# FluenceRate = 5.7297e+03 [m^2 s sr]^-1
# Frequency   = 1.00000000
#
# ***Distribution***
#
#
# [MeV/n]                     [m^2 s sr MeV/n]^-1
# Energy        N             FluenceRate                   Frequency
1.0000e+00      1644          1.2253e-01                    0.00002138
1.2589e+00      2495          7.1816e-01                    0.00003245
1.5849e+00      3527          8.0642e-01                    0.00004588
1.9953e+00      5025          9.1262e-01                    0.00006536
2.5119e+00      7544          1.0883e+00                    0.00009813
3.1623e+00      11183         1.2815e+00                    0.00014546
3.9811e+00      16167         1.4716e+00                    0.00021029
5.0119e+00      23795         1.7204e+00                    0.00030951
6.3096e+00      34745         1.9955e+00                    0.00045194
7.9433e+00      50456         2.3018e+00                    0.00065631
1.0000e+01      73540         2.6649e+00                    0.00095657
1.2589e+01      106810        3.0744e+00                    0.00138933
1.5849e+01      153715        3.5145e+00                    0.00199944
1.9953e+01      221273        4.0187e+00                    0.00287820
2.5119e+01      313859        4.5278e+00                    0.00408251
3.1623e+01      444874        5.0979e+00                    0.00578669
3.9811e+01      621754        5.6594e+00                    0.00808745
5.0119e+01      858497        6.2071e+00                    0.01116688
6.3096e+01      1161785       6.6724e+00                    0.01511189
7.9433e+01      1536350       7.0088e+00                    0.01998403
1.0000e+02      1985638       7.1954e+00                    0.02582813
1.2589e+02      2493247       7.1766e+00                    0.03243084
1.5849e+02      3024771       6.9159e+00                    0.03934463
1.9953e+02      3553846       6.4543e+00                    0.04622656
2.5119e+02      4058111       5.8543e+00                    0.05278577
3.1623e+02      4507296       5.1650e+00                    0.05862853
```

3.9811e+02	4895200	4.4558e+00	0.06367418
5.0119e+02	5222496	3.7760e+00	0.06793148
6.3096e+02	5428926	3.1179e+00	0.07061661
7.9433e+02	5387889	2.4579e+00	0.07008282
1.0000e+03	5161272	1.8703e+00	0.06713511
1.2589e+03	4834690	1.3916e+00	0.06288710
1.5849e+03	4267323	9.7568e-01	0.05550709
1.9953e+03	3684516	6.6917e-01	0.04792624
2.5119e+03	3129176	4.5142e-01	0.04070267
3.1623e+03	2460444	2.8195e-01	0.03200416
3.9811e+03	1982657	1.8047e-01	0.02578936
5.0119e+03	1418282	1.0255e-01	0.01844827
6.3096e+03	1050662	6.0342e-02	0.01366646
7.9433e+03	802837	3.6625e-02	0.01044288
1.0000e+04	551174	1.9973e-02	0.00716938
1.2589e+04	409568	1.1789e-02	0.00532744
1.5849e+04	285286	6.5228e-03	0.00371085
1.9953e+04	198048	3.5969e-03	0.00257610
2.5119e+04	142402	2.0543e-03	0.00185229
3.1623e+04	92313	1.0578e-03	0.00120076
3.9811e+04	66467	6.0501e-04	0.00086457
5.0119e+04	43781	3.1655e-04	0.00056948
6.3096e+04	29742	1.7081e-04	0.00038687
7.9433e+04	20680	9.4342e-05	0.00026899
1.0000e+05	13373	4.8460e-05	0.00017395
1.2589e+05	9164	2.6378e-05	0.00011920
1.5849e+05	5960	1.3627e-05	0.00007752
1.9953e+05	4179	7.5897e-06	0.00005436
2.5119e+05	2767	3.9917e-06	0.00003599
3.1623e+05	1841	2.1096e-06	0.00002395
3.9811e+05	1292	1.1760e-06	0.00001681
5.0119e+05	798	5.7697e-07	0.00001038
6.3096e+05	572	3.2851e-07	0.00000744
7.9433e+05	387	1.7655e-07	0.00000503
1.0000e+06	264	9.5666e-08	0.00000343
1.2589e+06	188	5.4114e-08	0.00000245
1.5849e+06	112	2.5608e-08	0.00000146
1.9953e+06	82	1.4892e-08	0.00000107
2.5119e+06	49	7.0689e-09	0.00000064
3.1623e+06	29	3.3232e-09	0.00000038
3.9811e+06	25	2.2756e-09	0.00000033
5.0119e+06	12	8.6763e-10	0.00000016
6.3096e+06	8	4.5946e-10	0.00000010
7.9433e+06	2	9.1240e-11	0.00000003
1.0000e+07	0	0.0000e+00	0.00000000

$\phi/[\mathrm{m}^2\ \mathrm{s\ sr\ MeV/n}]^{-1}$ as a function of $E/[\mathrm{MeV/n}]$ tabulated data used to generate the "Surface of Mars" differential energy spectrum for H-2:

```
# Using 70 Log Bins
# Min: 1 MeV/n          Max: 1e+07 MeV/n                10 bins/decade
#
# ***Statistics***
# Minimum:        1.8542e-03 MeV/n
# Maximum:        3.8339e+06 MeV/n
# Average:        2.3362e+03 MeV/n
# Frequency Mean: 2.0866e+03 MeV/n (binning-specific)
# Most Probable:  6.3096e+02 MeV/n (binning-specific)
#
# ***Totals***
# N           = 429676
# FluenceRate = 3.2024e+01 [m^2 s sr]^-1
# Frequency   = 1.00000000
#
# ***Distribution***
#
#
# [MeV/n]                     [m^2 s sr MeV/n]^-1
# Energy        N             FluenceRate                   Frequency
1.0000e+00      302           2.2508e-02                    0.00070286
1.2589e+00      444           1.2780e-01                    0.00103334
1.5849e+00      573           1.3101e-01                    0.00133356
1.9953e+00      739           1.3421e-01                    0.00171990
2.5119e+00      1023          1.4758e-01                    0.00238086
3.1623e+00      1342          1.5378e-01                    0.00312328
3.9811e+00      1771          1.6120e-01                    0.00412171
5.0119e+00      2200          1.5907e-01                    0.00512014
6.3096e+00      2744          1.5759e-01                    0.00638621
7.9433e+00      3244          1.4799e-01                    0.00754987
1.0000e+01      3629          1.3150e-01                    0.00844590
1.2589e+01      3828          1.1019e-01                    0.00890904
1.5849e+01      3946          9.0222e-02                    0.00918366
1.9953e+01      3734          6.7815e-02                    0.00869027
2.5119e+01      3519          5.0766e-02                    0.00818989
3.1623e+01      3123          3.5787e-02                    0.00726827
3.9811e+01      3241          2.9501e-02                    0.00754289
5.0119e+01      3316          2.3976e-02                    0.00771744
6.3096e+01      3967          2.2783e-02                    0.00923254
7.9433e+01      5054          2.3056e-02                    0.01176235
1.0000e+02      6727          2.4377e-02                    0.01565598
1.2589e+02      8601          2.4757e-02                    0.02001741
1.5849e+02      11222         2.5658e-02                    0.02611735
1.9953e+02      14344         2.6051e-02                    0.03338329
2.5119e+02      18018         2.5993e-02                    0.04193392
3.1623e+02      22077         2.5298e-02                    0.05138058
```

3.9811e+02	25198	2.2936e-02	0.05864419
5.0119e+02	27378	1.9795e-02	0.06371778
6.3096e+02	28927	1.6613e-02	0.06732282
7.9433e+02	28846	1.3159e-02	0.06713431
1.0000e+03	27732	1.0049e-02	0.06454165
1.2589e+03	25817	7.4312e-03	0.06008481
1.5849e+03	22737	5.1986e-03	0.05291662
1.9953e+03	19440	3.5306e-03	0.04524339
2.5119e+03	15820	2.2822e-03	0.03681844
3.1623e+03	12565	1.4398e-03	0.02924296
3.9811e+03	12118	1.1030e-03	0.02820265
5.0119e+03	14745	1.0661e-03	0.03431655
6.3096e+03	10995	6.3146e-04	0.02558905
7.9433e+03	7944	3.6240e-04	0.01848835
1.0000e+04	5493	1.9905e-04	0.01278405
1.2589e+04	3851	1.1085e-04	0.00896257
1.5849e+04	2521	5.7640e-05	0.00586721
1.9953e+04	1598	2.9022e-05	0.00371908
2.5119e+04	1128	1.6273e-05	0.00262523
3.1623e+04	684	7.8381e-06	0.00159190
3.9811e+04	496	4.5148e-06	0.00115436
5.0119e+04	311	2.2486e-06	0.00072380
6.3096e+04	212	1.2176e-06	0.00049340
7.9433e+04	143	6.5236e-07	0.00033281
1.0000e+05	77	2.7903e-07	0.00017920
1.2589e+05	56	1.6119e-07	0.00013033
1.5849e+05	42	9.6029e-08	0.00009775
1.9953e+05	24	4.3588e-08	0.00005586
2.5119e+05	13	1.8754e-08	0.00003026
3.1623e+05	14	1.6043e-08	0.00003258
3.9811e+05	3	2.7307e-09	0.00000698
5.0119e+05	6	4.3382e-09	0.00001396
6.3096e+05	1	5.7432e-10	0.00000233
7.9433e+05	3	1.3686e-09	0.00000698
1.0000e+06	1	3.6237e-10	0.00000233
1.2589e+06	5	1.4392e-09	0.00001164
1.5849e+06	2	4.5728e-10	0.00000465
1.9953e+06	0	0.0000e+00	0.00000000
2.5119e+06	0	0.0000e+00	0.00000000
3.1623e+06	2	2.2918e-10	0.00000465
3.9811e+06	0	0.0000e+00	0.00000000
5.0119e+06	0	0.0000e+00	0.00000000
6.3096e+06	0	0.0000e+00	0.00000000
7.9433e+06	0	0.0000e+00	0.00000000
1.0000e+07	0	0.0000e+00	0.00000000

$\phi/[\mathrm{m}^2\ \mathrm{s\ sr\ MeV/n}]^{-1}$ as a function of $E/[\mathrm{MeV/n}]$ tabulated data used to generate the "Surface of Mars" differential energy spectrum for H-3:

```
# Using 70 Log Bins
# Min: 1 MeV/n          Max: 1e+07 MeV/n                10 bins/decade
#
# ***Statistics***
# Minimum:        2.3951e-03 MeV/n
# Maximum:        1.1983e+06 MeV/n
# Average:        1.6376e+03 MeV/n
# Frequency Mean: 1.4625e+03 MeV/n (binning-specific)
# Most Probable:  6.3096e+02 MeV/n (binning-specific)
#
# ***Totals***
# N           = 389782
# FluenceRate = 2.9050e+01 [m^2 s sr]^-1
# Frequency   = 1.00000000
#
# ***Distribution***
#
#
# [MeV/n]                     [m^2 s sr MeV/n]^-1
# Energy        N             FluenceRate                   Frequency
1.0000e+00      177           1.3192e-02                    0.00045410
1.2589e+00      232           6.6779e-02                    0.00059520
1.5849e+00      362           8.2768e-02                    0.00092872
1.9953e+00      453           8.2272e-02                    0.00116219
2.5119e+00      580           8.3672e-02                    0.00148801
3.1623e+00      740           8.4798e-02                    0.00189850
3.9811e+00      906           8.2467e-02                    0.00232438
5.0119e+00      1031          7.4544e-02                    0.00264507
6.3096e+00      1202          6.9033e-02                    0.00308378
7.9433e+00      1347          6.1450e-02                    0.00345578
1.0000e+01      1370          4.9645e-02                    0.00351479
1.2589e+01      1347          3.8772e-02                    0.00345578
1.5849e+01      1495          3.4182e-02                    0.00383548
1.9953e+01      1598          2.9022e-02                    0.00409973
2.5119e+01      1779          2.5664e-02                    0.00456409
3.1623e+01      2280          2.6127e-02                    0.00584942
3.9811e+01      3083          2.8063e-02                    0.00790955
5.0119e+01      4228          3.0570e-02                    0.01084709
6.3096e+01      5818          3.3414e-02                    0.01492629
7.9433e+01      7486          3.4151e-02                    0.01920561
1.0000e+02      8617          3.1226e-02                    0.02210723
1.2589e+02      9958          2.8663e-02                    0.02554761
1.5849e+02      12381         2.8308e-02                    0.03176391
1.9953e+02      15655         2.8432e-02                    0.04016348
2.5119e+02      19660         2.8362e-02                    0.05043845
3.1623e+02      23251         2.6644e-02                    0.05965129
```

3.9811e+02	26422	2.4050e-02	0.06778661
5.0119e+02	28190	2.0382e-02	0.07232248
6.3096e+02	28860	1.6575e-02	0.07404139
7.9433e+02	28450	1.2979e-02	0.07298952
1.0000e+03	26929	9.7583e-03	0.06908734
1.2589e+03	24548	7.0659e-03	0.06297879
1.5849e+03	21551	4.9274e-03	0.05528988
1.9953e+03	18165	3.2990e-03	0.04660297
2.5119e+03	14792	2.1339e-03	0.03794942
3.1623e+03	11558	1.3245e-03	0.02965247
3.9811e+03	9594	8.7328e-04	0.02461376
5.0119e+03	7433	5.3742e-04	0.01906963
6.3096e+03	5231	3.0043e-04	0.01342032
7.9433e+03	3673	1.6756e-04	0.00942322
1.0000e+04	2480	8.9868e-05	0.00636253
1.2589e+04	1738	5.0027e-05	0.00445890
1.5849e+04	1117	2.5539e-05	0.00286570
1.9953e+04	682	1.2386e-05	0.00174970
2.5119e+04	458	6.6072e-06	0.00117502
3.1623e+04	281	3.2200e-06	0.00072092
3.9811e+04	216	1.9661e-06	0.00055416
5.0119e+04	132	9.5439e-07	0.00033865
6.3096e+04	73	4.1925e-07	0.00018728
7.9433e+04	54	2.4635e-07	0.00013854
1.0000e+05	36	1.3045e-07	0.00009236
1.2589e+05	34	9.7866e-08	0.00008723
1.5849e+05	16	3.6583e-08	0.00004105
1.9953e+05	13	2.3610e-08	0.00003335
2.5119e+05	4	5.7705e-09	0.00001026
3.1623e+05	8	9.1673e-09	0.00002052
3.9811e+05	3	2.7307e-09	0.00000770
5.0119e+05	2	1.4461e-09	0.00000513
6.3096e+05	0	0.0000e+00	0.00000000
7.9433e+05	1	4.5620e-10	0.00000257
1.0000e+06	2	7.2474e-10	0.00000513
1.2589e+06	0	0.0000e+00	0.00000000
1.5849e+06	0	0.0000e+00	0.00000000
1.9953e+06	0	0.0000e+00	0.00000000
2.5119e+06	0	0.0000e+00	0.00000000
3.1623e+06	0	0.0000e+00	0.00000000
3.9811e+06	0	0.0000e+00	0.00000000
5.0119e+06	0	0.0000e+00	0.00000000
6.3096e+06	0	0.0000e+00	0.00000000
7.9433e+06	0	0.0000e+00	0.00000000
1.0000e+07	0	0.0000e+00	0.00000000

$\phi/[\mathrm{m}^2\ \mathrm{s\ sr\ MeV/n}]^{-1}$ as a function of $E/[\mathrm{MeV/n}]$ tabulated data used to generate the "Surface of Mars" differential energy spectrum for $z = 1$ (isotopes combined):

```
# Using 70 Log Bins
# Min: 1 MeV/n          Max: 1e+07 MeV/n                10 bins/decade
#
# ***Statistics***
# Minimum:        6.7059e-05 MeV/n
# Maximum:        8.6082e+06 MeV/n
# Average:        1.7970e+03 MeV/n
# Frequency Mean: 1.6051e+03 MeV/n (binning-specific)
# Most Probable:  6.3096e+02 MeV/n (binning-specific)
#
# ***Totals***
# N           = 81030480
# FluenceRate = 6.0392e+03 [m^2 s sr]^-1
# Frequency   = 1.00000000
#
# ***Distribution***
#
#
# [MeV/n]                     [m^2 s sr MeV/n]^-1
# Energy        N             FluenceRate                   Frequency
1.0000e+00      3890          2.8992e-01                    0.00004801
1.2589e+00      5783          1.6646e+00                    0.00007137
1.5849e+00      8270          1.8909e+00                    0.00010206
1.9953e+00      11462         2.0817e+00                    0.00014145
2.5119e+00      16237         2.3424e+00                    0.00020038
3.1623e+00      23027         2.6387e+00                    0.00028418
3.9811e+00      31736         2.8887e+00                    0.00039166
5.0119e+00      44171         3.1937e+00                    0.00054512
6.3096e+00      61432         3.5282e+00                    0.00075813
7.9433e+00      85294         3.8911e+00                    0.00105262
1.0000e+01      118176        4.2824e+00                    0.00145841
1.2589e+01      164709        4.7410e+00                    0.00203268
1.5849e+01      227917        5.2111e+00                    0.00281273
1.9953e+01      316751        5.7527e+00                    0.00390904
2.5119e+01      436463        6.2965e+00                    0.00538641
3.1623e+01      601844        6.8966e+00                    0.00742738
3.9811e+01      820559        7.4690e+00                    0.01012655
5.0119e+01      1102533       7.9716e+00                    0.01360640
6.3096e+01      1450709       8.3317e+00                    0.01790325
7.9433e+01      1862106       8.4949e+00                    0.02298032
1.0000e+02      2330630       8.4455e+00                    0.02876239
1.2589e+02      2830500       8.1474e+00                    0.03493130
1.5849e+02      3329302       7.6121e+00                    0.04108703
1.9953e+02      3811456       6.9222e+00                    0.04703731
2.5119e+02      4265363       6.1533e+00                    0.05263899
3.1623e+02      4673910       5.3559e+00                    0.05768089
```

3.9811e+02	5030057	4.5785e+00	0.06207611
5.0119e+02	5333867	3.8565e+00	0.06582544
6.3096e+02	5523798	3.1724e+00	0.06816939
7.9433e+02	5468497	2.4947e+00	0.06748691
1.0000e+03	5229862	1.8952e+00	0.06454191
1.2589e+03	4893128	1.4084e+00	0.06038626
1.5849e+03	4315880	9.8679e-01	0.05326243
1.9953e+03	3724315	6.7639e-01	0.04596190
2.5119e+03	3160800	4.5598e-01	0.03900754
3.1623e+03	2485015	2.8476e-01	0.03066766
3.9811e+03	2004546	1.8246e-01	0.02473817
5.0119e+03	1440508	1.0415e-01	0.01777736
6.3096e+03	1066910	6.1275e-02	0.01316677
7.9433e+03	814461	3.7156e-02	0.01005129
1.0000e+04	559149	2.0262e-02	0.00690048
1.2589e+04	415157	1.1950e-02	0.00512347
1.5849e+04	288926	6.6060e-03	0.00356565
1.9953e+04	200329	3.6383e-03	0.00247227
2.5119e+04	143988	2.0772e-03	0.00177696
3.1623e+04	93278	1.0689e-03	0.00115115
3.9811e+04	67179	6.1149e-04	0.00082906
5.0119e+04	44224	3.1975e-04	0.00054577
6.3096e+04	30027	1.7245e-04	0.00037056
7.9433e+04	20877	9.5240e-05	0.00025764
1.0000e+05	13486	4.8869e-05	0.00016643
1.2589e+05	9254	2.6637e-05	0.00011420
1.5849e+05	6018	1.3760e-05	0.00007427
1.9953e+05	4216	7.6569e-06	0.00005203
2.5119e+05	2784	4.0163e-06	0.00003436
3.1623e+05	1863	2.1348e-06	0.00002299
3.9811e+05	1298	1.1815e-06	0.00001602
5.0119e+05	806	5.8276e-07	0.00000995
6.3096e+05	573	3.2908e-07	0.00000707
7.9433e+05	391	1.7837e-07	0.00000483
1.0000e+06	267	9.6753e-08	0.00000330
1.2589e+06	193	5.5553e-08	0.00000238
1.5849e+06	114	2.6065e-08	0.00000141
1.9953e+06	82	1.4892e-08	0.00000101
2.5119e+06	49	7.0689e-09	0.00000060
3.1623e+06	31	3.5523e-09	0.00000038
3.9811e+06	25	2.2756e-09	0.00000031
5.0119e+06	12	8.6763e-10	0.00000015
6.3096e+06	8	4.5946e-10	0.00000010
7.9433e+06	2	9.1240e-11	0.00000002
1.0000e+07	0	0.0000e+00	0.00000000

$\phi/[\mathrm{m}^2\ \mathrm{s\ sr\ MeV/n}]^{-1}$ as a function of $E/[\mathrm{MeV/n}]$ tabulated data used to generate the "Surface of Mars" differential energy spectrum for He-3:

```
# Using 70 Log Bins
# Min: 1 MeV/n          Max: 1e+07 MeV/n                10 bins/decade
#
# ***Statistics***
# Minimum:        5.0189e-03 MeV/n
# Maximum:        4.3263e+06 MeV/n
# Average:        1.7940e+03 MeV/n
# Frequency Mean: 1.6040e+03 MeV/n (binning-specific)
# Most Probable:  6.3096e+02 MeV/n (binning-specific)
#
# ***Totals***
# N           = 350554
# FluenceRate = 2.6127e+01 [m^2 s sr]^-1
# Frequency   = 1.00000000
#
# ***Distribution***
#
#
# [MeV/n]                     [m^2 s sr MeV/n]^-1
# Energy        N             FluenceRate                   Frequency
1.0000e+00      66            4.9189e-03                    0.00018827
1.2589e+00      84            2.4179e-02                    0.00023962
1.5849e+00      97            2.2178e-02                    0.00027670
1.9953e+00      137           2.4881e-02                    0.00039081
2.5119e+00      188           2.7121e-02                    0.00053629
3.1623e+00      243           2.7846e-02                    0.00069319
3.9811e+00      273           2.4849e-02                    0.00077877
5.0119e+00      348           2.5161e-02                    0.00099271
6.3096e+00      356           2.0446e-02                    0.00101554
7.9433e+00      388           1.7700e-02                    0.00110682
1.0000e+01      406           1.4712e-02                    0.00115817
1.2589e+01      480           1.3816e-02                    0.00136926
1.5849e+01      534           1.2209e-02                    0.00152330
1.9953e+01      663           1.2041e-02                    0.00189129
2.5119e+01      829           1.1959e-02                    0.00236483
3.1623e+01      1069          1.2250e-02                    0.00304946
3.9811e+01      1672          1.5219e-02                    0.00476959
5.0119e+01      2266          1.6384e-02                    0.00646405
6.3096e+01      3175          1.8235e-02                    0.00905709
7.9433e+01      4422          2.0173e-02                    0.01261432
1.0000e+02      5942          2.1532e-02                    0.01695031
1.2589e+02      7994          2.3010e-02                    0.02280390
1.5849e+02      10518         2.4048e-02                    0.03000394
1.9953e+02      13794         2.5052e-02                    0.03934914
2.5119e+02      17258         2.4897e-02                    0.04923065
3.1623e+02      20924         2.3977e-02                    0.05968838
```

3.9811e+02	24356	2.2170e-02	0.06947860
5.0119e+02	26869	1.9427e-02	0.07664725
6.3096e+02	28258	1.6229e-02	0.08060955
7.9433e+02	27663	1.2620e-02	0.07891224
1.0000e+03	26790	9.7079e-03	0.07642189
1.2589e+03	24811	7.1416e-03	0.07077654
1.5849e+03	21356	4.8828e-03	0.06092071
1.9953e+03	18557	3.3702e-03	0.05293621
2.5119e+03	14906	2.1504e-03	0.04252127
3.1623e+03	11661	1.3363e-03	0.03326449
3.9811e+03	9686	8.8165e-04	0.02763055
5.0119e+03	6670	4.8226e-04	0.01902703
6.3096e+03	4641	2.6654e-04	0.01323904
7.9433e+03	3410	1.5556e-04	0.00972746
1.0000e+04	2251	8.1570e-05	0.00642126
1.2589e+04	1485	4.2744e-05	0.00423615
1.5849e+04	1033	2.3619e-05	0.00294676
1.9953e+04	645	1.1714e-05	0.00183994
2.5119e+04	441	6.3620e-06	0.00125801
3.1623e+04	314	3.5982e-06	0.00089573
3.9811e+04	210	1.9115e-06	0.00059905
5.0119e+04	136	9.8331e-07	0.00038796
6.3096e+04	98	5.6283e-07	0.00027956
7.9433e+04	61	2.7828e-07	0.00017401
1.0000e+05	40	1.4495e-07	0.00011411
1.2589e+05	26	7.4839e-08	0.00007417
1.5849e+05	18	4.1155e-08	0.00005135
1.9953e+05	6	1.0897e-08	0.00001712
2.5119e+05	7	1.0098e-08	0.00001997
3.1623e+05	7	8.0214e-09	0.00001997
3.9811e+05	5	4.5512e-09	0.00001426
5.0119e+05	1	7.2303e-10	0.00000285
6.3096e+05	4	2.2973e-09	0.00001141
7.9433e+05	2	9.1240e-10	0.00000571
1.0000e+06	0	0.0000e+00	0.00000000
1.2589e+06	1	2.8784e-10	0.00000285
1.5849e+06	0	0.0000e+00	0.00000000
1.9953e+06	1	1.8162e-10	0.00000285
2.5119e+06	0	0.0000e+00	0.00000000
3.1623e+06	1	1.1459e-10	0.00000285
3.9811e+06	1	9.1023e-11	0.00000285
5.0119e+06	0	0.0000e+00	0.00000000
6.3096e+06	0	0.0000e+00	0.00000000
7.9433e+06	0	0.0000e+00	0.00000000
1.0000e+07	0	0.0000e+00	0.00000000

$\phi/[\mathrm{m}^2\ \mathrm{s\ sr\ MeV/n}]^{-1}$ as a function of $E/[\mathrm{MeV/n}]$ tabulated data used to generate the "Surface of Mars" differential energy spectrum for He-4:

```
# Using 70 Log Bins
# Min: 1 MeV/n          Max: 1e+07 MeV/n                10 bins/decade
#
# ***Statistics***
# Minimum:        1.0519e-04 MeV/n
# Maximum:        6.0268e+06 MeV/n
# Average:        1.5974e+03 MeV/n
# Frequency Mean: 1.4262e+03 MeV/n (binning-specific)
# Most Probable:  5.0119e+02 MeV/n (binning-specific)
#
# ***Totals***
# N           = 3083616
# FluenceRate = 2.2982e+02 [m^2 s sr]^-1
# Frequency   = 1.00000000
#
# ***Distribution***
#
#
# [MeV/n]                     [m^2 s sr MeV/n]^-1
# Energy        N             FluenceRate                   Frequency
1.0000e+00      481           3.5849e-02                    0.00015599
1.2589e+00      611           1.7587e-01                    0.00019814
1.5849e+00      723           1.6531e-01                    0.00023446
1.9953e+00      819           1.4874e-01                    0.00026560
2.5119e+00      846           1.2205e-01                    0.00027435
3.1623e+00      924           1.0588e-01                    0.00029965
3.9811e+00      990           9.0113e-02                    0.00032105
5.0119e+00      946           6.8398e-02                    0.00030678
6.3096e+00      1029          5.9097e-02                    0.00033370
7.9433e+00      1134          5.1733e-02                    0.00036775
1.0000e+01      1345          4.8739e-02                    0.00043618
1.2589e+01      1805          5.1955e-02                    0.00058535
1.5849e+01      2618          5.9858e-02                    0.00084900
1.9953e+01      3859          7.0086e-02                    0.00125145
2.5119e+01      5930          8.5548e-02                    0.00192307
3.1623e+01      8841          1.0131e-01                    0.00286709
3.9811e+01      13171         1.1989e-01                    0.00427128
5.0119e+01      19436         1.4053e-01                    0.00630299
6.3096e+01      29346         1.6854e-01                    0.00951675
7.9433e+01      43058         1.9643e-01                    0.01396348
1.0000e+02      61976         2.2458e-01                    0.02009848
1.2589e+02      86965         2.5032e-01                    0.02820228
1.5849e+02      118582        2.7113e-01                    0.03845550
1.9953e+02      154378        2.8037e-01                    0.05006395
2.5119e+02      190623        2.7500e-01                    0.06181801
3.1623e+02      221602        2.5394e-01                    0.07186433
```

3.9811e+02	243386	2.2154e-01	0.07892876
5.0119e+02	253289	1.8313e-01	0.08214025
6.3096e+02	251013	1.4416e-01	0.08140216
7.9433e+02	232267	1.0596e-01	0.07532293
1.0000e+03	212525	7.7013e-02	0.06892071
1.2589e+03	191851	5.5223e-02	0.06221624
1.5849e+03	160416	3.6678e-02	0.05202204
1.9953e+03	136031	2.4705e-02	0.04411412
2.5119e+03	111426	1.6075e-02	0.03613485
3.1623e+03	83056	9.5175e-03	0.02693461
3.9811e+03	66349	6.0393e-03	0.02151662
5.0119e+03	50424	3.6458e-03	0.01635223
6.3096e+03	36856	2.1167e-03	0.01195220
7.9433e+03	26816	1.2233e-03	0.00869628
1.0000e+04	17616	6.3835e-04	0.00571277
1.2589e+04	12967	3.7324e-04	0.00420513
1.5849e+04	8323	1.9030e-04	0.00269910
1.9953e+04	5667	1.0292e-04	0.00183778
2.5119e+04	3833	5.5296e-05	0.00124302
3.1623e+04	2550	2.9221e-05	0.00082695
3.9811e+04	1749	1.5920e-05	0.00056719
5.0119e+04	1031	7.4544e-06	0.00033435
6.3096e+04	745	4.2787e-06	0.00024160
7.9433e+04	483	2.2034e-06	0.00015663
1.0000e+05	311	1.1270e-06	0.00010086
1.2589e+05	222	6.3901e-07	0.00007199
1.5849e+05	97	2.2178e-07	0.00003146
1.9953e+05	103	1.8706e-07	0.00003340
2.5119e+05	50	7.2131e-08	0.00001621
3.1623e+05	43	4.9274e-08	0.00001394
3.9811e+05	33	3.0038e-08	0.00001070
5.0119e+05	15	1.0845e-08	0.00000486
6.3096e+05	11	6.3175e-09	0.00000357
7.9433e+05	5	2.2810e-09	0.00000162
1.0000e+06	8	2.8990e-09	0.00000259
1.2589e+06	4	1.1514e-09	0.00000130
1.5849e+06	1	2.2864e-10	0.00000032
1.9953e+06	1	1.8162e-10	0.00000032
2.5119e+06	2	2.8852e-10	0.00000065
3.1623e+06	1	1.1459e-10	0.00000032
3.9811e+06	1	9.1023e-11	0.00000032
5.0119e+06	1	7.2303e-11	0.00000032
6.3096e+06	0	0.0000e+00	0.00000000
7.9433e+06	0	0.0000e+00	0.00000000
1.0000e+07	0	0.0000e+00	0.00000000

$\phi/[\mathrm{m}^2\ \mathrm{s\ sr\ MeV/n}]^{-1}$ as a function of $E/[\mathrm{MeV/n}]$ tabulated data used to generate the "Surface of Mars" differential energy spectrum for $z = 2$ (isotopes combined):

```
# Using 70 Log Bins
# Min: 1 MeV/n          Max: 1e+07 MeV/n                10 bins/decade
#
# ***Statistics***
# Minimum:        1.0519e-04 MeV/n
# Maximum:        6.0268e+06 MeV/n
# Average:        1.6150e+03 MeV/n
# Frequency Mean: 1.4422e+03 MeV/n (binning-specific)
# Most Probable:  5.0119e+02 MeV/n (binning-specific)
#
# ***Totals***
# N           = 3441694
# FluenceRate = 2.5651e+02 [m^2 s sr]^-1
# Frequency   = 1.00000000
#
# ***Distribution***
#
#
# [MeV/n]                     [m^2 s sr MeV/n]^-1
# Energy        N             FluenceRate                   Frequency
1.0000e+00      1049          7.8181e-02                    0.00030479
1.2589e+00      1298          3.7362e-01                    0.00037714
1.5849e+00      1474          3.3702e-01                    0.00042828
1.9953e+00      1584          2.8768e-01                    0.00046024
2.5119e+00      1680          2.4236e-01                    0.00048813
3.1623e+00      1794          2.0558e-01                    0.00052125
3.9811e+00      1805          1.6430e-01                    0.00052445
5.0119e+00      1704          1.2320e-01                    0.00049511
6.3096e+00      1718          9.8668e-02                    0.00049917
7.9433e+00      1773          8.0884e-02                    0.00051515
1.0000e+01      1920          6.9575e-02                    0.00055786
1.2589e+01      2384          6.8621e-02                    0.00069268
1.5849e+01      3214          7.3485e-02                    0.00093384
1.9953e+01      4555          8.2726e-02                    0.00132348
2.5119e+01      6789          9.7940e-02                    0.00197258
3.1623e+01      9921          1.1369e-01                    0.00288259
3.9811e+01      14858         1.3524e-01                    0.00431706
5.0119e+01      21714         1.5700e-01                    0.00630910
6.3096e+01      32538         1.8687e-01                    0.00945407
7.9433e+01      47499         2.1669e-01                    0.01380105
1.0000e+02      67950         2.4623e-01                    0.01974318
1.2589e+02      95011         2.7348e-01                    0.02760588
1.5849e+02      129147        2.9528e-01                    0.03752425
1.9953e+02      168246        3.0556e-01                    0.04888465
2.5119e+02      207975        3.0003e-01                    0.06042809
3.1623e+02      242625        2.7803e-01                    0.07049581
```

3.9811e+02	267888	2.4384e-01	0.07783609
5.0119e+02	280296	2.0266e-01	0.08144129
6.3096e+02	279426	1.6048e-01	0.08118851
7.9433e+02	260100	1.1866e-01	0.07557325
1.0000e+03	239459	8.6773e-02	0.06957591
1.2589e+03	216792	6.2402e-02	0.06298991
1.5849e+03	181902	4.1590e-02	0.05285246
1.9953e+03	154694	2.8095e-02	0.04494705
2.5119e+03	126403	1.8235e-02	0.03672697
3.1623e+03	94770	1.0860e-02	0.02753586
3.9811e+03	76084	6.9254e-03	0.02210656
5.0119e+03	57146	4.1318e-03	0.01660403
6.3096e+03	41541	2.3858e-03	0.01206993
7.9433e+03	30255	1.3802e-03	0.00879073
1.0000e+04	19884	7.2054e-04	0.00577739
1.2589e+04	14464	4.1633e-04	0.00420258
1.5849e+04	9360	2.1401e-04	0.00271959
1.9953e+04	6318	1.1474e-04	0.00183572
2.5119e+04	4278	6.1715e-05	0.00124299
3.1623e+04	2865	3.2831e-05	0.00083244
3.9811e+04	1960	1.7841e-05	0.00056949
5.0119e+04	1168	8.4449e-06	0.00033937
6.3096e+04	843	4.8415e-06	0.00024494
7.9433e+04	544	2.4817e-06	0.00015806
1.0000e+05	351	1.2719e-06	0.00010198
1.2589e+05	248	7.1385e-07	0.00007206
1.5849e+05	115	2.6294e-07	0.00003341
1.9953e+05	109	1.9796e-07	0.00003167
2.5119e+05	57	8.2230e-08	0.00001656
3.1623e+05	50	5.7296e-08	0.00001453
3.9811e+05	38	3.4589e-08	0.00001104
5.0119e+05	16	1.1568e-08	0.00000465
6.3096e+05	15	8.6148e-09	0.00000436
7.9433e+05	7	3.1934e-09	0.00000203
1.0000e+06	8	2.8990e-09	0.00000232
1.2589e+06	5	1.4392e-09	0.00000145
1.5849e+06	1	2.2864e-10	0.00000029
1.9953e+06	2	3.6323e-10	0.00000058
2.5119e+06	2	2.8852e-10	0.00000058
3.1623e+06	2	2.2918e-10	0.00000058
3.9811e+06	2	1.8205e-10	0.00000058
5.0119e+06	1	7.2303e-11	0.00000029
6.3096e+06	0	0.0000e+00	0.00000000
7.9433e+06	0	0.0000e+00	0.00000000
1.0000e+07	0	0.0000e+00	0.00000000

$\phi/[\mathrm{m}^2\ \mathrm{s\ sr\ MeV/n}]^{-1}$ as a function of $E/[\mathrm{MeV/n}]$ tabulated data used to generate the "Surface of Mars" differential energy spectrum for $z = 3$ (isotopes combined):

```
# Using 70 Log Bins
# Min: 1 MeV/n          Max: 1e+07 MeV/n                10 bins/decade
#
# ***Statistics***
# Minimum:        2.6369e-02 MeV/n
# Maximum:        4.1712e+05 MeV/n
# Average:        2.0535e+03 MeV/n
# Frequency Mean: 1.8350e+03 MeV/n (binning-specific)
# Most Probable:  6.3096e+02 MeV/n (binning-specific)
#
# ***Totals***
# N           = 24981
# FluenceRate = 1.8618e+00 [m^2 s sr]^-1
# Frequency   = 1.00000000
#
# ***Distribution***
#
#
# [MeV/n]                     [m^2 s sr MeV/n]^-1
# Energy        N             FluenceRate                   Frequency
1.0000e+00      8             5.9624e-04                    0.00032024
1.2589e+00      13            3.7419e-03                    0.00052040
1.5849e+00      12            2.7437e-03                    0.00048037
1.9953e+00      13            2.3610e-03                    0.00052040
2.5119e+00      7             1.0098e-03                    0.00028021
3.1623e+00      15            1.7189e-03                    0.00060046
3.9811e+00      9             8.1921e-04                    0.00036027
5.0119e+00      8             5.7842e-04                    0.00032024
6.3096e+00      7             4.0202e-04                    0.00028021
7.9433e+00      15            6.8430e-04                    0.00060046
1.0000e+01      10            3.6237e-04                    0.00040030
1.2589e+01      13            3.7419e-04                    0.00052040
1.5849e+01      23            5.2587e-04                    0.00092070
1.9953e+01      33            5.9933e-04                    0.00132100
2.5119e+01      39            5.6262e-04                    0.00156119
3.1623e+01      48            5.5004e-04                    0.00192146
3.9811e+01      71            6.4627e-04                    0.00284216
5.0119e+01      129           9.3270e-04                    0.00516392
6.3096e+01      189           1.0855e-03                    0.00756575
7.9433e+01      241           1.0994e-03                    0.00964733
1.0000e+02      397           1.4386e-03                    0.01589208
1.2589e+02      528           1.5198e-03                    0.02113606
1.5849e+02      725           1.6576e-03                    0.02902206
1.9953e+02      994           1.8053e-03                    0.03979024
2.5119e+02      1303          1.8797e-03                    0.05215964
3.1623e+02      1521          1.7429e-03                    0.06088627
```

3.9811e+02	1705	1.5520e-03	0.06825187
5.0119e+02	1890	1.3665e-03	0.07565750
6.3096e+02	1973	1.1331e-03	0.07898002
7.9433e+02	1973	9.0008e-04	0.07898002
1.0000e+03	1859	6.7365e-04	0.07441656
1.2589e+03	1657	4.7695e-04	0.06633041
1.5849e+03	1486	3.3976e-04	0.05948521
1.9953e+03	1204	2.1867e-04	0.04819663
2.5119e+03	1010	1.4571e-04	0.04043073
3.1623e+03	778	8.9152e-05	0.03114367
3.9811e+03	734	6.6811e-05	0.02938233
5.0119e+03	713	5.1552e-05	0.02854169
6.3096e+03	542	3.1128e-05	0.02169649
7.9433e+03	348	1.5876e-05	0.01393059
1.0000e+04	254	9.2042e-06	0.01016773
1.2589e+04	179	5.1524e-06	0.00716545
1.5849e+04	113	2.5836e-06	0.00452344
1.9953e+04	63	1.1442e-06	0.00252192
2.5119e+04	38	5.4820e-07	0.00152116
3.1623e+04	28	3.2086e-07	0.00112085
3.9811e+04	29	2.6397e-07	0.00116088
5.0119e+04	16	1.1568e-07	0.00064049
6.3096e+04	3	1.7230e-08	0.00012009
7.9433e+04	5	2.2810e-08	0.00020015
1.0000e+05	3	1.0871e-08	0.00012009
1.2589e+05	5	1.4392e-08	0.00020015
1.5849e+05	0	0.0000e+00	0.00000000
1.9953e+05	1	1.8162e-09	0.00004003
2.5119e+05	0	0.0000e+00	0.00000000
3.1623e+05	0	0.0000e+00	0.00000000
3.9811e+05	1	9.1023e-10	0.00004003
5.0119e+05	0	0.0000e+00	0.00000000
6.3096e+05	0	0.0000e+00	0.00000000
7.9433e+05	0	0.0000e+00	0.00000000
1.0000e+06	0	0.0000e+00	0.00000000
1.2589e+06	0	0.0000e+00	0.00000000
1.5849e+06	0	0.0000e+00	0.00000000
1.9953e+06	0	0.0000e+00	0.00000000
2.5119e+06	0	0.0000e+00	0.00000000
3.1623e+06	0	0.0000e+00	0.00000000
3.9811e+06	0	0.0000e+00	0.00000000
5.0119e+06	0	0.0000e+00	0.00000000
6.3096e+06	0	0.0000e+00	0.00000000
7.9433e+06	0	0.0000e+00	0.00000000
1.0000e+07	0	0.0000e+00	0.00000000

$\phi/[\mathrm{m}^2\ \mathrm{s\ sr\ MeV/n}]^{-1}$ as a function of $E/[\mathrm{MeV/n}]$ tabulated data used to generate the "Surface of Mars" differential energy spectrum for $z = 4$ (isotopes combined):

```
# Using 70 Log Bins
# Min: 1 MeV/n          Max: 1e+07 MeV/n                10 bins/decade
#
# ***Statistics***
# Minimum:        1.4575e-02 MeV/n
# Maximum:        3.5339e+05 MeV/n
# Average:        2.0841e+03 MeV/n
# Frequency Mean: 1.8586e+03 MeV/n (binning-specific)
# Most Probable:  6.3096e+02 MeV/n (binning-specific)
#
# ***Totals***
# N           = 13281
# FluenceRate = 9.8983e-01 [m^2 s sr]^-1
# Frequency   = 1.00000000
#
# ***Distribution***
#
#
# [MeV/n]                     [m^2 s sr MeV/n]^-1
# Energy        N             FluenceRate                   Frequency
1.0000e+00      2             1.4906e-04                    0.00015059
1.2589e+00      0             0.0000e+00                    0.00000000
1.5849e+00      1             2.2864e-04                    0.00007530
1.9953e+00      4             7.2646e-04                    0.00030118
2.5119e+00      1             1.4426e-04                    0.00007530
3.1623e+00      3             3.4378e-04                    0.00022589
3.9811e+00      5             4.5512e-04                    0.00037648
5.0119e+00      1             7.2303e-05                    0.00007530
6.3096e+00      0             0.0000e+00                    0.00000000
7.9433e+00      1             4.5620e-05                    0.00007530
1.0000e+01      4             1.4495e-04                    0.00030118
1.2589e+01      7             2.0149e-04                    0.00052707
1.5849e+01      6             1.3718e-04                    0.00045177
1.9953e+01      11            1.9978e-04                    0.00082825
2.5119e+01      25            3.6066e-04                    0.00188239
3.1623e+01      26            2.9794e-04                    0.00195768
3.9811e+01      35            3.1858e-04                    0.00263534
5.0119e+01      63            4.5551e-04                    0.00474362
6.3096e+01      112           6.4324e-04                    0.00843310
7.9433e+01      128           5.8393e-04                    0.00963783
1.0000e+02      198           7.1749e-04                    0.01490852
1.2589e+02      282           8.1171e-04                    0.02123334
1.5849e+02      343           7.8424e-04                    0.02582637
1.9953e+02      497           9.0263e-04                    0.03742188
2.5119e+02      627           9.0453e-04                    0.04721030
3.1623e+02      771           8.8350e-04                    0.05805286
```

3.9811e+02	848	7.7188e-04	0.06385061
5.0119e+02	1070	7.7364e-04	0.08056622
6.3096e+02	1103	6.3347e-04	0.08305098
7.9433e+02	1054	4.8083e-04	0.07936149
1.0000e+03	1059	3.8375e-04	0.07973797
1.2589e+03	970	2.7921e-04	0.07303667
1.5849e+03	830	1.8977e-04	0.06249529
1.9953e+03	746	1.3549e-04	0.05617047
2.5119e+03	568	8.1941e-05	0.04276786
3.1623e+03	395	4.5264e-05	0.02974174
3.9811e+03	361	3.2859e-05	0.02718169
5.0119e+03	318	2.2992e-05	0.02394398
6.3096e+03	254	1.4588e-05	0.01912507
7.9433e+03	187	8.5309e-06	0.01408027
1.0000e+04	121	4.3847e-06	0.00911076
1.2589e+04	85	2.4467e-06	0.00640012
1.5849e+04	50	1.1432e-06	0.00376478
1.9953e+04	35	6.3565e-07	0.00263534
2.5119e+04	20	2.8852e-07	0.00150591
3.1623e+04	12	1.3751e-07	0.00090355
3.9811e+04	17	1.5474e-07	0.00128002
5.0119e+04	5	3.6151e-08	0.00037648
6.3096e+04	6	3.4459e-08	0.00045177
7.9433e+04	8	3.6496e-08	0.00060236
1.0000e+05	1	3.6237e-09	0.00007530
1.2589e+05	2	5.7568e-09	0.00015059
1.5849e+05	0	0.0000e+00	0.00000000
1.9953e+05	0	0.0000e+00	0.00000000
2.5119e+05	2	2.8852e-09	0.00015059
3.1623e+05	1	1.1459e-09	0.00007530
3.9811e+05	0	0.0000e+00	0.00000000
5.0119e+05	0	0.0000e+00	0.00000000
6.3096e+05	0	0.0000e+00	0.00000000
7.9433e+05	0	0.0000e+00	0.00000000
1.0000e+06	0	0.0000e+00	0.00000000
1.2589e+06	0	0.0000e+00	0.00000000
1.5849e+06	0	0.0000e+00	0.00000000
1.9953e+06	0	0.0000e+00	0.00000000
2.5119e+06	0	0.0000e+00	0.00000000
3.1623e+06	0	0.0000e+00	0.00000000
3.9811e+06	0	0.0000e+00	0.00000000
5.0119e+06	0	0.0000e+00	0.00000000
6.3096e+06	0	0.0000e+00	0.00000000
7.9433e+06	0	0.0000e+00	0.00000000
1.0000e+07	0	0.0000e+00	0.00000000

$\phi/[\mathrm{m}^2\ \mathrm{s\ sr\ MeV/n}]^{-1}$ as a function of $E/[\mathrm{MeV/n}]$ tabulated data used to generate the "Surface of Mars" differential energy spectrum for $z = 5$ (isotopes combined):

```
# Using 70 Log Bins
# Min: 1 MeV/n          Max: 1e+07 MeV/n                10 bins/decade
#
# ***Statistics***
# Minimum:        2.0258e-02 MeV/n
# Maximum:        1.7340e+05 MeV/n
# Average:        1.7160e+03 MeV/n
# Frequency Mean: 1.5307e+03 MeV/n (binning-specific)
# Most Probable:  7.9433e+02 MeV/n (binning-specific)
#
# ***Totals***
# N           = 22209
# FluenceRate = 1.6552e+00 [m^2 s sr]^-1
# Frequency   = 1.00000000
#
# ***Distribution***
#
#
# [MeV/n]                     [m^2 s sr MeV/n]^-1
# Energy        N             FluenceRate                   Frequency
1.0000e+00      0             0.0000e+00                    0.00000000
1.2589e+00      0             0.0000e+00                    0.00000000
1.5849e+00      1             2.2864e-04                    0.00004503
1.9953e+00      1             1.8162e-04                    0.00004503
2.5119e+00      0             0.0000e+00                    0.00000000
3.1623e+00      1             1.1459e-04                    0.00004503
3.9811e+00      1             9.1023e-05                    0.00004503
5.0119e+00      2             1.4461e-04                    0.00009005
6.3096e+00      4             2.2973e-04                    0.00018011
7.9433e+00      4             1.8248e-04                    0.00018011
1.0000e+01      6             2.1742e-04                    0.00027016
1.2589e+01      6             1.7270e-04                    0.00027016
1.5849e+01      17            3.8869e-04                    0.00076546
1.9953e+01      20            3.6323e-04                    0.00090054
2.5119e+01      23            3.3180e-04                    0.00103562
3.1623e+01      41            4.6983e-04                    0.00184610
3.9811e+01      85            7.7370e-04                    0.00382728
5.0119e+01      106           7.6641e-04                    0.00477284
6.3096e+01      168           9.6486e-04                    0.00756450
7.9433e+01      217           9.8995e-04                    0.00977081
1.0000e+02      332           1.2031e-03                    0.01494889
1.2589e+02      480           1.3816e-03                    0.02161286
1.5849e+02      642           1.4679e-03                    0.02890720
1.9953e+02      899           1.6327e-03                    0.04047909
2.5119e+02      1111          1.6028e-03                    0.05002476
3.1623e+02      1423          1.6306e-03                    0.06407312
```

3.9811e+02	1589	1.4464e-03	0.07154757
5.0119e+02	1764	1.2754e-03	0.07942726
6.3096e+02	1846	1.0602e-03	0.08311946
7.9433e+02	1857	8.4716e-04	0.08361475
1.0000e+03	1728	6.2618e-04	0.07780629
1.2589e+03	1583	4.5565e-04	0.07127741
1.5849e+03	1407	3.2170e-04	0.06335269
1.9953e+03	1176	2.1358e-04	0.05295151
2.5119e+03	955	1.3777e-04	0.04300059
3.1623e+03	749	8.5829e-05	0.03372507
3.9811e+03	575	5.2338e-05	0.02589040
5.0119e+03	409	2.9572e-05	0.01841596
6.3096e+03	308	1.7689e-05	0.01386825
7.9433e+03	241	1.0994e-05	0.01085146
1.0000e+04	151	5.4718e-06	0.00679905
1.2589e+04	121	3.4829e-06	0.00544824
1.5849e+04	60	1.3718e-06	0.00270161
1.9953e+04	31	5.6301e-07	0.00139583
2.5119e+04	23	3.3180e-07	0.00103562
3.1623e+04	20	2.2918e-07	0.00090054
3.9811e+04	10	9.1023e-08	0.00045027
5.0119e+04	4	2.8921e-08	0.00018011
6.3096e+04	6	3.4459e-08	0.00027016
7.9433e+04	2	9.1240e-09	0.00009005
1.0000e+05	2	7.2474e-09	0.00009005
1.2589e+05	1	2.8784e-09	0.00004503
1.5849e+05	1	2.2864e-09	0.00004503
1.9953e+05	0	0.0000e+00	0.00000000
2.5119e+05	0	0.0000e+00	0.00000000
3.1623e+05	0	0.0000e+00	0.00000000
3.9811e+05	0	0.0000e+00	0.00000000
5.0119e+05	0	0.0000e+00	0.00000000
6.3096e+05	0	0.0000e+00	0.00000000
7.9433e+05	0	0.0000e+00	0.00000000
1.0000e+06	0	0.0000e+00	0.00000000
1.2589e+06	0	0.0000e+00	0.00000000
1.5849e+06	0	0.0000e+00	0.00000000
1.9953e+06	0	0.0000e+00	0.00000000
2.5119e+06	0	0.0000e+00	0.00000000
3.1623e+06	0	0.0000e+00	0.00000000
3.9811e+06	0	0.0000e+00	0.00000000
5.0119e+06	0	0.0000e+00	0.00000000
6.3096e+06	0	0.0000e+00	0.00000000
7.9433e+06	0	0.0000e+00	0.00000000
1.0000e+07	0	0.0000e+00	0.00000000

$\phi/[\mathrm{m}^2\ \mathrm{s\ sr\ MeV/n}]^{-1}$ as a function of $E/[\mathrm{MeV/n}]$ tabulated data used to generate the "Surface of Mars" differential energy spectrum for $z = 6$ (isotopes combined):

```
# Using 70 Log Bins
# Min: 1 MeV/n          Max: 1e+07 MeV/n                10 bins/decade
#
# ***Statistics***
# Minimum:        5.0621e-04 MeV/n
# Maximum:        5.3280e+05 MeV/n
# Average:        2.0689e+03 MeV/n
# Frequency Mean: 1.8469e+03 MeV/n (binning-specific)
# Most Probable:  7.9433e+02 MeV/n (binning-specific)
#
# ***Totals***
# N           = 50357
# FluenceRate = 3.7531e+00 [m^2 s sr]^-1
# Frequency   = 1.00000000
#
# ***Distribution***
#
#
# [MeV/n]                     [m^2 s sr MeV/n]^-1
# Energy        N             FluenceRate                   Frequency
1.0000e+00      2             1.4906e-04                    0.00003972
1.2589e+00      1             2.8784e-04                    0.00001986
1.5849e+00      0             0.0000e+00                    0.00000000
1.9953e+00      1             1.8162e-04                    0.00001986
2.5119e+00      1             1.4426e-04                    0.00001986
3.1623e+00      0             0.0000e+00                    0.00000000
3.9811e+00      2             1.8205e-04                    0.00003972
5.0119e+00      3             2.1691e-04                    0.00005957
6.3096e+00      4             2.2973e-04                    0.00007943
7.9433e+00      6             2.7372e-04                    0.00011915
1.0000e+01      10            3.6237e-04                    0.00019858
1.2589e+01      18            5.1811e-04                    0.00035745
1.5849e+01      30            6.8592e-04                    0.00059575
1.9953e+01      39            7.0830e-04                    0.00077447
2.5119e+01      66            9.5213e-04                    0.00131064
3.1623e+01      86            9.8549e-04                    0.00170781
3.9811e+01      133           1.2106e-03                    0.00264114
5.0119e+01      195           1.4099e-03                    0.00387235
6.3096e+01      303           1.7402e-03                    0.00601704
7.9433e+01      441           2.0118e-03                    0.00875747
1.0000e+02      682           2.4714e-03                    0.01354330
1.2589e+02      951           2.7374e-03                    0.01888516
1.5849e+02      1395          3.1895e-03                    0.02770221
1.9953e+02      1862          3.3817e-03                    0.03697599
2.5119e+02      2360          3.4046e-03                    0.04686538
3.1623e+02      3003          3.4412e-03                    0.05963421
```

3.9811e+02	3452	3.1421e-03	0.06855055
5.0119e+02	3775	2.7294e-03	0.07496475
6.3096e+02	3962	2.2755e-03	0.07867824
7.9433e+02	4137	1.8873e-03	0.08215342
1.0000e+03	3925	1.4223e-03	0.07794348
1.2589e+03	3529	1.0158e-03	0.07007963
1.5849e+03	3286	7.5131e-04	0.06525409
1.9953e+03	2916	5.2959e-04	0.05790655
2.5119e+03	2321	3.3483e-04	0.04609091
3.1623e+03	1868	2.1406e-04	0.03709514
3.9811e+03	1492	1.3581e-04	0.02962845
5.0119e+03	1185	8.5678e-05	0.02353198
6.3096e+03	835	4.7956e-05	0.01658161
7.9433e+03	687	3.1341e-05	0.01364259
1.0000e+04	420	1.5220e-05	0.00834045
1.2589e+04	326	9.3836e-06	0.00647378
1.5849e+04	201	4.5957e-06	0.00399150
1.9953e+04	147	2.6698e-06	0.00291916
2.5119e+04	115	1.6590e-06	0.00228369
3.1623e+04	64	7.3339e-07	0.00127093
3.9811e+04	44	4.0050e-07	0.00087376
5.0119e+04	22	1.5907e-07	0.00043688
6.3096e+04	21	1.2061e-07	0.00041702
7.9433e+04	16	7.2992e-08	0.00031773
1.0000e+05	6	2.1742e-08	0.00011915
1.2589e+05	4	1.1514e-08	0.00007943
1.5849e+05	1	2.2864e-09	0.00001986
1.9953e+05	1	1.8162e-09	0.00001986
2.5119e+05	3	4.3279e-09	0.00005957
3.1623e+05	1	1.1459e-09	0.00001986
3.9811e+05	0	0.0000e+00	0.00000000
5.0119e+05	1	7.2303e-10	0.00001986
6.3096e+05	0	0.0000e+00	0.00000000
7.9433e+05	0	0.0000e+00	0.00000000
1.0000e+06	0	0.0000e+00	0.00000000
1.2589e+06	0	0.0000e+00	0.00000000
1.5849e+06	0	0.0000e+00	0.00000000
1.9953e+06	0	0.0000e+00	0.00000000
2.5119e+06	0	0.0000e+00	0.00000000
3.1623e+06	0	0.0000e+00	0.00000000
3.9811e+06	0	0.0000e+00	0.00000000
5.0119e+06	0	0.0000e+00	0.00000000
6.3096e+06	0	0.0000e+00	0.00000000
7.9433e+06	0	0.0000e+00	0.00000000
1.0000e+07	0	0.0000e+00	0.00000000

$\phi/[\mathrm{m}^2\ \mathrm{s\ sr\ MeV/n}]^{-1}$ as a function of $E/[\mathrm{MeV/n}]$ tabulated data used to generate the "Surface of Mars" differential energy spectrum for $z = 7$ (isotopes combined):

```
# Using 70 Log Bins
# Min: 1 MeV/n          Max: 1e+07 MeV/n                10 bins/decade
#
# ***Statistics***
# Minimum:        2.4138e-04 MeV/n
# Maximum:        1.2200e+05 MeV/n
# Average:        1.8137e+03 MeV/n
# Frequency Mean: 1.6171e+03 MeV/n (binning-specific)
# Most Probable:  7.9433e+02 MeV/n (binning-specific)
#
# ***Totals***
# N           = 15660
# FluenceRate = 1.1671e+00 [m^2 s sr]^-1
# Frequency   = 1.00000000
#
# ***Distribution***
#
#
# [MeV/n]                     [m^2 s sr MeV/n]^-1
# Energy        N             FluenceRate                   Frequency
1.0000e+00      0             0.0000e+00                    0.00000000
1.2589e+00      1             2.8784e-04                    0.00006386
1.5849e+00      2             4.5728e-04                    0.00012771
1.9953e+00      0             0.0000e+00                    0.00000000
2.5119e+00      0             0.0000e+00                    0.00000000
3.1623e+00      0             0.0000e+00                    0.00000000
3.9811e+00      0             0.0000e+00                    0.00000000
5.0119e+00      2             1.4461e-04                    0.00012771
6.3096e+00      1             5.7432e-05                    0.00006386
7.9433e+00      1             4.5620e-05                    0.00006386
1.0000e+01      5             1.8119e-04                    0.00031928
1.2589e+01      11            3.1663e-04                    0.00070243
1.5849e+01      4             9.1456e-05                    0.00025543
1.9953e+01      14            2.5426e-04                    0.00089400
2.5119e+01      16            2.3082e-04                    0.00102171
3.1623e+01      20            2.2918e-04                    0.00127714
3.9811e+01      36            3.2768e-04                    0.00229885
5.0119e+01      60            4.3382e-04                    0.00383142
6.3096e+01      106           6.0878e-04                    0.00676884
7.9433e+01      146           6.6605e-04                    0.00932312
1.0000e+02      221           8.0084e-04                    0.01411239
1.2589e+02      272           7.8293e-04                    0.01736909
1.5849e+02      388           8.8713e-04                    0.02477650
1.9953e+02      493           8.9537e-04                    0.03148148
2.5119e+02      750           1.0820e-03                    0.04789272
3.1623e+02      947           1.0852e-03                    0.06047254
```

3.9811e+02	1055	9.6030e-04	0.06736909
5.0119e+02	1224	8.8498e-04	0.07816092
6.3096e+02	1302	7.4776e-04	0.08314176
7.9433e+02	1326	6.0492e-04	0.08467433
1.0000e+03	1297	4.7000e-04	0.08282248
1.2589e+03	1129	3.2497e-04	0.07209451
1.5849e+03	1079	2.4670e-04	0.06890166
1.9953e+03	877	1.5928e-04	0.05600255
2.5119e+03	692	9.9830e-05	0.04418902
3.1623e+03	609	6.9786e-05	0.03888889
3.9811e+03	488	4.4419e-05	0.03116220
5.0119e+03	336	2.4294e-05	0.02145594
6.3096e+03	269	1.5449e-05	0.01717752
7.9433e+03	175	7.9835e-06	0.01117497
1.0000e+04	110	3.9861e-06	0.00702427
1.2589e+04	69	1.9861e-06	0.00440613
1.5849e+04	51	1.1661e-06	0.00325670
1.9953e+04	25	4.5404e-07	0.00159642
2.5119e+04	20	2.8852e-07	0.00127714
3.1623e+04	15	1.7189e-07	0.00095785
3.9811e+04	5	4.5512e-08	0.00031928
5.0119e+04	4	2.8921e-08	0.00025543
6.3096e+04	6	3.4459e-08	0.00038314
7.9433e+04	0	0.0000e+00	0.00000000
1.0000e+05	1	3.6237e-09	0.00006386
1.2589e+05	0	0.0000e+00	0.00000000
1.5849e+05	0	0.0000e+00	0.00000000
1.9953e+05	0	0.0000e+00	0.00000000
2.5119e+05	0	0.0000e+00	0.00000000
3.1623e+05	0	0.0000e+00	0.00000000
3.9811e+05	0	0.0000e+00	0.00000000
5.0119e+05	0	0.0000e+00	0.00000000
6.3096e+05	0	0.0000e+00	0.00000000
7.9433e+05	0	0.0000e+00	0.00000000
1.0000e+06	0	0.0000e+00	0.00000000
1.2589e+06	0	0.0000e+00	0.00000000
1.5849e+06	0	0.0000e+00	0.00000000
1.9953e+06	0	0.0000e+00	0.00000000
2.5119e+06	0	0.0000e+00	0.00000000
3.1623e+06	0	0.0000e+00	0.00000000
3.9811e+06	0	0.0000e+00	0.00000000
5.0119e+06	0	0.0000e+00	0.00000000
6.3096e+06	0	0.0000e+00	0.00000000
7.9433e+06	0	0.0000e+00	0.00000000
1.0000e+07	0	0.0000e+00	0.00000000

$\phi/[\mathrm{m}^2\ \mathrm{s\ sr\ MeV/n}]^{-1}$ as a function of $E/[\mathrm{MeV/n}]$ tabulated data used to generate the "Surface of Mars" differential energy spectrum for $z = 8$ (isotopes combined):

```
# Using 70 Log Bins
# Min: 1 MeV/n          Max: 1e+07 MeV/n                10 bins/decade
#
# ***Statistics***
# Minimum:        4.1542e-04 MeV/n
# Maximum:        1.0100e+06 MeV/n
# Average:        2.2864e+03 MeV/n
# Frequency Mean: 2.0460e+03 MeV/n (binning-specific)
# Most Probable:  7.9433e+02 MeV/n (binning-specific)
#
# ***Totals***
# N           = 31457
# FluenceRate = 2.3445e+00 [m^2 s sr]^-1
# Frequency   = 1.00000000
#
# ***Distribution***
#
#
# [MeV/n]                     [m^2 s sr MeV/n]^-1
# Energy        N             FluenceRate                   Frequency
1.0000e+00      1             7.4529e-05                    0.00003179
1.2589e+00      0             0.0000e+00                    0.00000000
1.5849e+00      0             0.0000e+00                    0.00000000
1.9953e+00      3             5.4485e-04                    0.00009537
2.5119e+00      1             1.4426e-04                    0.00003179
3.1623e+00      0             0.0000e+00                    0.00000000
3.9811e+00      3             2.7307e-04                    0.00009537
5.0119e+00      1             7.2303e-05                    0.00003179
6.3096e+00      3             1.7230e-04                    0.00009537
7.9433e+00      5             2.2810e-04                    0.00015895
1.0000e+01      6             2.1742e-04                    0.00019074
1.2589e+01      11            3.1663e-04                    0.00034968
1.5849e+01      12            2.7437e-04                    0.00038147
1.9953e+01      25            4.5404e-04                    0.00079474
2.5119e+01      35            5.0492e-04                    0.00111263
3.1623e+01      60            6.8755e-04                    0.00190737
3.9811e+01      78            7.0998e-04                    0.00247958
5.0119e+01      137           9.9054e-04                    0.00435515
6.3096e+01      175           1.0051e-03                    0.00556315
7.9433e+01      247           1.1268e-03                    0.00785199
1.0000e+02      397           1.4386e-03                    0.01262040
1.2589e+02      584           1.6810e-03                    0.01856503
1.5849e+02      804           1.8383e-03                    0.02555870
1.9953e+02      1054          1.9142e-03                    0.03350606
2.5119e+02      1358          1.9591e-03                    0.04317004
3.1623e+02      1748          2.0031e-03                    0.05556792
```

3.9811e+02	2093	1.9051e-03	0.06653527
5.0119e+02	2291	1.6565e-03	0.07282958
6.3096e+02	2429	1.3950e-03	0.07721652
7.9433e+02	2470	1.1268e-03	0.07851988
1.0000e+03	2410	8.7331e-04	0.07661252
1.2589e+03	2293	6.6002e-04	0.07289316
1.5849e+03	2118	4.8426e-04	0.06733001
1.9953e+03	1898	3.4471e-04	0.06033633
2.5119e+03	1608	2.3197e-04	0.05111740
3.1623e+03	1287	1.4748e-04	0.04091299
3.9811e+03	1022	9.3026e-05	0.03248879
5.0119e+03	785	5.6757e-05	0.02495470
6.3096e+03	610	3.5033e-05	0.01939155
7.9433e+03	420	1.9160e-05	0.01335156
1.0000e+04	282	1.0219e-05	0.00896462
1.2589e+04	232	6.6779e-06	0.00737515
1.5849e+04	147	3.3610e-06	0.00467305
1.9953e+04	94	1.7072e-06	0.00298821
2.5119e+04	75	1.0820e-06	0.00238421
3.1623e+04	47	5.3858e-07	0.00149410
3.9811e+04	26	2.3666e-07	0.00082653
5.0119e+04	29	2.0968e-07	0.00092189
6.3096e+04	20	1.1486e-07	0.00063579
7.9433e+04	5	2.2810e-08	0.00015895
1.0000e+05	8	2.8990e-08	0.00025432
1.2589e+05	3	8.6352e-09	0.00009537
1.5849e+05	1	2.2864e-09	0.00003179
1.9953e+05	1	1.8162e-09	0.00003179
2.5119e+05	1	1.4426e-09	0.00003179
3.1623e+05	1	1.1459e-09	0.00003179
3.9811e+05	1	9.1023e-10	0.00003179
5.0119e+05	0	0.0000e+00	0.00000000
6.3096e+05	0	0.0000e+00	0.00000000
7.9433e+05	1	4.5620e-10	0.00003179
1.0000e+06	1	3.6237e-10	0.00003179
1.2589e+06	0	0.0000e+00	0.00000000
1.5849e+06	0	0.0000e+00	0.00000000
1.9953e+06	0	0.0000e+00	0.00000000
2.5119e+06	0	0.0000e+00	0.00000000
3.1623e+06	0	0.0000e+00	0.00000000
3.9811e+06	0	0.0000e+00	0.00000000
5.0119e+06	0	0.0000e+00	0.00000000
6.3096e+06	0	0.0000e+00	0.00000000
7.9433e+06	0	0.0000e+00	0.00000000
1.0000e+07	0	0.0000e+00	0.00000000

$\phi/[\mathrm{m}^2\ \mathrm{s\ sr\ MeV/n}]^{-1}$ as a function of $E/[\mathrm{MeV/n}]$ tabulated data used to generate the "Surface of Mars" differential energy spectrum for $z = 9$ (isotopes combined):

```
# Using 70 Log Bins
# Min: 1 MeV/n          Max: 1e+07 MeV/n                10 bins/decade
#
# ***Statistics***
# Minimum:        1.0406e+01 MeV/n
# Maximum:        2.1677e+05 MeV/n
# Average:        2.3310e+03 MeV/n
# Frequency Mean: 2.0782e+03 MeV/n (binning-specific)
# Most Probable:  1.2589e+03 MeV/n (binning-specific)
#
# ***Totals***
# N           = 1774
# FluenceRate = 1.3222e-01 [m^2 s sr]^-1
# Frequency   = 1.00000000
#
# ***Distribution***
#
#
# [MeV/n]                     [m^2 s sr MeV/n]^-1
# Energy        N             FluenceRate                   Frequency
1.0000e+00      0             0.0000e+00                    0.00000000
1.2589e+00      0             0.0000e+00                    0.00000000
1.5849e+00      0             0.0000e+00                    0.00000000
1.9953e+00      0             0.0000e+00                    0.00000000
2.5119e+00      0             0.0000e+00                    0.00000000
3.1623e+00      0             0.0000e+00                    0.00000000
3.9811e+00      0             0.0000e+00                    0.00000000
5.0119e+00      0             0.0000e+00                    0.00000000
6.3096e+00      0             0.0000e+00                    0.00000000
7.9433e+00      0             0.0000e+00                    0.00000000
1.0000e+01      1             3.6237e-05                    0.00056370
1.2589e+01      1             2.8784e-05                    0.00056370
1.5849e+01      0             0.0000e+00                    0.00000000
1.9953e+01      1             1.8162e-05                    0.00056370
2.5119e+01      2             2.8852e-05                    0.00112740
3.1623e+01      4             4.5837e-05                    0.00225479
3.9811e+01      5             4.5512e-05                    0.00281849
5.0119e+01      10            7.2303e-05                    0.00563698
6.3096e+01      6             3.4459e-05                    0.00338219
7.9433e+01      10            4.5620e-05                    0.00563698
1.0000e+02      21            7.6098e-05                    0.01183766
1.2589e+02      26            7.4839e-05                    0.01465614
1.5849e+02      46            1.0517e-04                    0.02593010
1.9953e+02      62            1.1260e-04                    0.03494927
2.5119e+02      77            1.1108e-04                    0.04340474
3.1623e+02      89            1.0199e-04                    0.05016911
```

3.9811e+02	115	1.0468e-04	0.06482525
5.0119e+02	123	8.8932e-05	0.06933484
6.3096e+02	126	7.2364e-05	0.07102593
7.9433e+02	134	6.1131e-05	0.07553551
1.0000e+03	114	4.1310e-05	0.06426156
1.2589e+03	148	4.2601e-05	0.08342728
1.5849e+03	129	2.9495e-05	0.07271702
1.9953e+03	118	2.1431e-05	0.06651635
2.5119e+03	82	1.1830e-05	0.04622322
3.1623e+03	80	9.1673e-06	0.04509583
3.9811e+03	50	4.5512e-06	0.02818489
5.0119e+03	67	4.8443e-06	0.03776776
6.3096e+03	43	2.4696e-06	0.02423901
7.9433e+03	26	1.1861e-06	0.01465614
1.0000e+04	25	9.0593e-07	0.01409245
1.2589e+04	12	3.4541e-07	0.00676437
1.5849e+04	8	1.8291e-07	0.00450958
1.9953e+04	4	7.2646e-08	0.00225479
2.5119e+04	5	7.2131e-08	0.00281849
3.1623e+04	1	1.1459e-08	0.00056370
3.9811e+04	0	0.0000e+00	0.00000000
5.0119e+04	0	0.0000e+00	0.00000000
6.3096e+04	1	5.7432e-09	0.00056370
7.9433e+04	1	4.5620e-09	0.00056370
1.0000e+05	0	0.0000e+00	0.00000000
1.2589e+05	0	0.0000e+00	0.00000000
1.5849e+05	0	0.0000e+00	0.00000000
1.9953e+05	1	1.8162e-09	0.00056370
2.5119e+05	0	0.0000e+00	0.00000000
3.1623e+05	0	0.0000e+00	0.00000000
3.9811e+05	0	0.0000e+00	0.00000000
5.0119e+05	0	0.0000e+00	0.00000000
6.3096e+05	0	0.0000e+00	0.00000000
7.9433e+05	0	0.0000e+00	0.00000000
1.0000e+06	0	0.0000e+00	0.00000000
1.2589e+06	0	0.0000e+00	0.00000000
1.5849e+06	0	0.0000e+00	0.00000000
1.9953e+06	0	0.0000e+00	0.00000000
2.5119e+06	0	0.0000e+00	0.00000000
3.1623e+06	0	0.0000e+00	0.00000000
3.9811e+06	0	0.0000e+00	0.00000000
5.0119e+06	0	0.0000e+00	0.00000000
6.3096e+06	0	0.0000e+00	0.00000000
7.9433e+06	0	0.0000e+00	0.00000000
1.0000e+07	0	0.0000e+00	0.00000000

$\phi/[\mathrm{m}^2\ \mathrm{s\ sr\ MeV/n}]^{-1}$ as a function of $E/[\mathrm{MeV/n}]$ tabulated data used to generate the "Surface of Mars" differential energy spectrum for $z = 10$ (isotopes combined):

```
# Using 70 Log Bins
# Min: 1 MeV/n          Max: 1e+07 MeV/n                10 bins/decade
#
# ***Statistics***
# Minimum:        2.0943e+00 MeV/n
# Maximum:        6.1781e+05 MeV/n
# Average:        2.3945e+03 MeV/n
# Frequency Mean: 2.1284e+03 MeV/n (binning-specific)
# Most Probable:  6.3096e+02 MeV/n (binning-specific)
#
# ***Totals***
# N           = 5299
# FluenceRate = 3.9493e-01 [m^2 s sr]^-1
# Frequency   = 1.00000000
#
# ***Distribution***
#
#
# [MeV/n]                     [m^2 s sr MeV/n]^-1
# Energy        N             FluenceRate                   Frequency
1.0000e+00      0             0.0000e+00                    0.00000000
1.2589e+00      0             0.0000e+00                    0.00000000
1.5849e+00      0             0.0000e+00                    0.00000000
1.9953e+00      1             1.8162e-04                    0.00018871
2.5119e+00      1             1.4426e-04                    0.00018871
3.1623e+00      0             0.0000e+00                    0.00000000
3.9811e+00      0             0.0000e+00                    0.00000000
5.0119e+00      1             7.2303e-05                    0.00018871
6.3096e+00      0             0.0000e+00                    0.00000000
7.9433e+00      0             0.0000e+00                    0.00000000
1.0000e+01      0             0.0000e+00                    0.00000000
1.2589e+01      1             2.8784e-05                    0.00018871
1.5849e+01      1             2.2864e-05                    0.00018871
1.9953e+01      8             1.4529e-04                    0.00150972
2.5119e+01      5             7.2131e-05                    0.00094357
3.1623e+01      8             9.1673e-05                    0.00150972
3.9811e+01      12            1.0923e-04                    0.00226458
5.0119e+01      18            1.3014e-04                    0.00339687
6.3096e+01      33            1.8953e-04                    0.00622759
7.9433e+01      42            1.9160e-04                    0.00792602
1.0000e+02      65            2.3554e-04                    0.01226647
1.2589e+02      64            1.8422e-04                    0.01207775
1.5849e+02      131           2.9952e-04                    0.02472165
1.9953e+02      161           2.9240e-04                    0.03038309
2.5119e+02      221           3.1882e-04                    0.04170598
3.1623e+02      288           3.3002e-04                    0.05434988
```

3.9811e+02	341	3.1039e-04	0.06435176
5.0119e+02	384	2.7764e-04	0.07246650
6.3096e+02	430	2.4696e-04	0.08114739
7.9433e+02	415	1.8932e-04	0.07831666
1.0000e+03	400	1.4495e-04	0.07548594
1.2589e+03	419	1.2061e-04	0.07907152
1.5849e+03	365	8.3454e-05	0.06888092
1.9953e+03	307	5.5756e-05	0.05793546
2.5119e+03	257	3.7075e-05	0.04849972
3.1623e+03	204	2.3377e-05	0.03849783
3.9811e+03	193	1.7568e-05	0.03642197
5.0119e+03	148	1.0701e-05	0.02792980
6.3096e+03	106	6.0878e-06	0.02000377
7.9433e+03	94	4.2883e-06	0.01773920
1.0000e+04	61	2.2105e-06	0.01151161
1.2589e+04	35	1.0074e-06	0.00660502
1.5849e+04	25	5.7160e-07	0.00471787
1.9953e+04	21	3.8139e-07	0.00396301
2.5119e+04	8	1.1541e-07	0.00150972
3.1623e+04	9	1.0313e-07	0.00169843
3.9811e+04	8	7.2819e-08	0.00150972
5.0119e+04	2	1.4461e-08	0.00037743
6.3096e+04	1	5.7432e-09	0.00018871
7.9433e+04	0	0.0000e+00	0.00000000
1.0000e+05	3	1.0871e-08	0.00056614
1.2589e+05	0	0.0000e+00	0.00000000
1.5849e+05	1	2.2864e-09	0.00018871
1.9953e+05	0	0.0000e+00	0.00000000
2.5119e+05	0	0.0000e+00	0.00000000
3.1623e+05	0	0.0000e+00	0.00000000
3.9811e+05	0	0.0000e+00	0.00000000
5.0119e+05	1	7.2303e-10	0.00018871
6.3096e+05	0	0.0000e+00	0.00000000
7.9433e+05	0	0.0000e+00	0.00000000
1.0000e+06	0	0.0000e+00	0.00000000
1.2589e+06	0	0.0000e+00	0.00000000
1.5849e+06	0	0.0000e+00	0.00000000
1.9953e+06	0	0.0000e+00	0.00000000
2.5119e+06	0	0.0000e+00	0.00000000
3.1623e+06	0	0.0000e+00	0.00000000
3.9811e+06	0	0.0000e+00	0.00000000
5.0119e+06	0	0.0000e+00	0.00000000
6.3096e+06	0	0.0000e+00	0.00000000
7.9433e+06	0	0.0000e+00	0.00000000
1.0000e+07	0	0.0000e+00	0.00000000

$\phi/[\mathrm{m}^2\ \mathrm{s\ sr\ MeV/n}]^{-1}$ as a function of $E/[\mathrm{MeV/n}]$ tabulated data used to generate the "Surface of Mars" differential energy spectrum for $z = 11$ (isotopes combined):

```
# Using 70 Log Bins
# Min: 1 MeV/n          Max: 1e+07 MeV/n                10 bins/decade
#
# ***Statistics***
# Minimum:        2.2047e+01 MeV/n
# Maximum:        1.5924e+05 MeV/n
# Average:        2.2402e+03 MeV/n
# Frequency Mean: 2.0081e+03 MeV/n (binning-specific)
# Most Probable:  7.9433e+02 MeV/n (binning-specific)
#
# ***Totals***
# N           = 1974
# FluenceRate = 1.4712e-01 [m^2 s sr]^-1
# Frequency   = 1.00000000
#
# ***Distribution***
#
#
# [MeV/n]                     [m^2 s sr MeV/n]^-1
# Energy        N             FluenceRate                   Frequency
1.0000e+00      0             0.0000e+00                    0.00000000
1.2589e+00      0             0.0000e+00                    0.00000000
1.5849e+00      0             0.0000e+00                    0.00000000
1.9953e+00      0             0.0000e+00                    0.00000000
2.5119e+00      0             0.0000e+00                    0.00000000
3.1623e+00      0             0.0000e+00                    0.00000000
3.9811e+00      0             0.0000e+00                    0.00000000
5.0119e+00      0             0.0000e+00                    0.00000000
6.3096e+00      0             0.0000e+00                    0.00000000
7.9433e+00      0             0.0000e+00                    0.00000000
1.0000e+01      0             0.0000e+00                    0.00000000
1.2589e+01      0             0.0000e+00                    0.00000000
1.5849e+01      0             0.0000e+00                    0.00000000
1.9953e+01      3             5.4485e-05                    0.00151976
2.5119e+01      2             2.8852e-05                    0.00101317
3.1623e+01      3             3.4378e-05                    0.00151976
3.9811e+01      5             4.5512e-05                    0.00253293
5.0119e+01      6             4.3382e-05                    0.00303951
6.3096e+01      7             4.0202e-05                    0.00354610
7.9433e+01      14            6.3868e-05                    0.00709220
1.0000e+02      22            7.9722e-05                    0.01114488
1.2589e+02      23            6.6204e-05                    0.01165147
1.5849e+02      51            1.1661e-04                    0.02583587
1.9953e+02      52            9.4440e-05                    0.02634245
2.5119e+02      72            1.0387e-04                    0.03647416
3.1623e+02      105           1.2032e-04                    0.05319149
```

3.9811e+02	135	1.2288e-04	0.06838906
5.0119e+02	157	1.1351e-04	0.07953394
6.3096e+02	146	8.3851e-05	0.07396150
7.9433e+02	167	7.6185e-05	0.08459980
1.0000e+03	148	5.3631e-05	0.07497467
1.2589e+03	147	4.2313e-05	0.07446809
1.5849e+03	135	3.0866e-05	0.06838906
1.9953e+03	139	2.5245e-05	0.07041540
2.5119e+03	87	1.2551e-05	0.04407295
3.1623e+03	88	1.0084e-05	0.04457953
3.9811e+03	75	6.8268e-06	0.03799392
5.0119e+03	53	3.8320e-06	0.02684904
6.3096e+03	54	3.1013e-06	0.02735562
7.9433e+03	19	8.6678e-07	0.00962513
1.0000e+04	23	8.3345e-07	0.01165147
1.2589e+04	12	3.4541e-07	0.00607903
1.5849e+04	7	1.6005e-07	0.00354610
1.9953e+04	9	1.6345e-07	0.00455927
2.5119e+04	0	0.0000e+00	0.00000000
3.1623e+04	2	2.2918e-08	0.00101317
3.9811e+04	4	3.6409e-08	0.00202634
5.0119e+04	0	0.0000e+00	0.00000000
6.3096e+04	0	0.0000e+00	0.00000000
7.9433e+04	0	0.0000e+00	0.00000000
1.0000e+05	1	3.6237e-09	0.00050659
1.2589e+05	0	0.0000e+00	0.00000000
1.5849e+05	1	2.2864e-09	0.00050659
1.9953e+05	0	0.0000e+00	0.00000000
2.5119e+05	0	0.0000e+00	0.00000000
3.1623e+05	0	0.0000e+00	0.00000000
3.9811e+05	0	0.0000e+00	0.00000000
5.0119e+05	0	0.0000e+00	0.00000000
6.3096e+05	0	0.0000e+00	0.00000000
7.9433e+05	0	0.0000e+00	0.00000000
1.0000e+06	0	0.0000e+00	0.00000000
1.2589e+06	0	0.0000e+00	0.00000000
1.5849e+06	0	0.0000e+00	0.00000000
1.9953e+06	0	0.0000e+00	0.00000000
2.5119e+06	0	0.0000e+00	0.00000000
3.1623e+06	0	0.0000e+00	0.00000000
3.9811e+06	0	0.0000e+00	0.00000000
5.0119e+06	0	0.0000e+00	0.00000000
6.3096e+06	0	0.0000e+00	0.00000000
7.9433e+06	0	0.0000e+00	0.00000000
1.0000e+07	0	0.0000e+00	0.00000000

$\phi/[\mathrm{m}^2\ \mathrm{s\ sr\ MeV/n}]^{-1}$ as a function of $E/[\mathrm{MeV/n}]$ tabulated data used to generate the "Surface of Mars" differential energy spectrum for $z = 12$ (isotopes combined):

```
# Using 70 Log Bins
# Min: 1 MeV/n          Max: 1e+07 MeV/n                10 bins/decade
#
# ***Statistics***
# Minimum:        2.4734e+00 MeV/n
# Maximum:        6.6603e+05 MeV/n
# Average:        2.7482e+03 MeV/n
# Frequency Mean: 2.4564e+03 MeV/n (binning-specific)
# Most Probable:  7.9433e+02 MeV/n (binning-specific)
#
# ***Totals***
# N           = 4806
# FluenceRate = 3.5819e-01 [m^2 s sr]^-1
# Frequency   = 1.00000000
#
# ***Distribution***
#
#
# [MeV/n]                     [m^2 s sr MeV/n]^-1
# Energy        N             FluenceRate                   Frequency
1.0000e+00      0             0.0000e+00                    0.00000000
1.2589e+00      0             0.0000e+00                    0.00000000
1.5849e+00      0             0.0000e+00                    0.00000000
1.9953e+00      1             1.8162e-04                    0.00020807
2.5119e+00      0             0.0000e+00                    0.00000000
3.1623e+00      0             0.0000e+00                    0.00000000
3.9811e+00      1             9.1023e-05                    0.00020807
5.0119e+00      1             7.2303e-05                    0.00020807
6.3096e+00      1             5.7432e-05                    0.00020807
7.9433e+00      1             4.5620e-05                    0.00020807
1.0000e+01      0             0.0000e+00                    0.00000000
1.2589e+01      1             2.8784e-05                    0.00020807
1.5849e+01      4             9.1456e-05                    0.00083229
1.9953e+01      1             1.8162e-05                    0.00020807
2.5119e+01      4             5.7705e-05                    0.00083229
3.1623e+01      6             6.8755e-05                    0.00124844
3.9811e+01      7             6.3716e-05                    0.00145651
5.0119e+01      17            1.2291e-04                    0.00353725
6.3096e+01      28            1.6081e-04                    0.00582605
7.9433e+01      37            1.6879e-04                    0.00769871
1.0000e+02      48            1.7394e-04                    0.00998752
1.2589e+02      73            2.1012e-04                    0.01518935
1.5849e+02      103           2.3550e-04                    0.02143154
1.9953e+02      143           2.5971e-04                    0.02975447
2.5119e+02      182           2.6256e-04                    0.03786933
3.1623e+02      244           2.7960e-04                    0.05076987
```

3.9811e+02	293	2.6670e-04	0.06096546
5.0119e+02	321	2.3209e-04	0.06679151
6.3096e+02	364	2.0905e-04	0.07573866
7.9433e+02	397	1.8111e-04	0.08260508
1.0000e+03	367	1.3299e-04	0.07636288
1.2589e+03	356	1.0247e-04	0.07407407
1.5849e+03	362	8.2768e-05	0.07532251
1.9953e+03	280	5.0852e-05	0.05826051
2.5119e+03	273	3.9384e-05	0.05680400
3.1623e+03	187	2.1429e-05	0.03890970
3.9811e+03	169	1.5383e-05	0.03516438
5.0119e+03	147	1.0628e-05	0.03058677
6.3096e+03	130	7.4662e-06	0.02704952
7.9433e+03	76	3.4671e-06	0.01581357
1.0000e+04	59	2.1380e-06	0.01227632
1.2589e+04	38	1.0938e-06	0.00790678
1.5849e+04	24	5.4874e-07	0.00499376
1.9953e+04	20	3.6323e-07	0.00416146
2.5119e+04	16	2.3082e-07	0.00332917
3.1623e+04	6	6.8755e-08	0.00124844
3.9811e+04	3	2.7307e-08	0.00062422
5.0119e+04	5	3.6151e-08	0.00104037
6.3096e+04	2	1.1486e-08	0.00041615
7.9433e+04	1	4.5620e-09	0.00020807
1.0000e+05	3	1.0871e-08	0.00062422
1.2589e+05	0	0.0000e+00	0.00000000
1.5849e+05	1	2.2864e-09	0.00020807
1.9953e+05	0	0.0000e+00	0.00000000
2.5119e+05	0	0.0000e+00	0.00000000
3.1623e+05	2	2.2918e-09	0.00041615
3.9811e+05	0	0.0000e+00	0.00000000
5.0119e+05	0	0.0000e+00	0.00000000
6.3096e+05	1	5.7432e-10	0.00020807
7.9433e+05	0	0.0000e+00	0.00000000
1.0000e+06	0	0.0000e+00	0.00000000
1.2589e+06	0	0.0000e+00	0.00000000
1.5849e+06	0	0.0000e+00	0.00000000
1.9953e+06	0	0.0000e+00	0.00000000
2.5119e+06	0	0.0000e+00	0.00000000
3.1623e+06	0	0.0000e+00	0.00000000
3.9811e+06	0	0.0000e+00	0.00000000
5.0119e+06	0	0.0000e+00	0.00000000
6.3096e+06	0	0.0000e+00	0.00000000
7.9433e+06	0	0.0000e+00	0.00000000
1.0000e+07	0	0.0000e+00	0.00000000

$\phi/[\mathrm{m}^2\ \mathrm{s\ sr\ MeV/n}]^{-1}$ as a function of $E/[\mathrm{MeV/n}]$ tabulated data used to generate the "Surface of Mars" differential energy spectrum for $z = 13$ (isotopes combined):

```
# Using 70 Log Bins
# Min: 1 MeV/n          Max: 1e+07 MeV/n                10 bins/decade
#
# ***Statistics***
# Minimum:        1.4291e+01 MeV/n
# Maximum:        4.1969e+04 MeV/n
# Average:        2.2545e+03 MeV/n
# Frequency Mean: 2.0077e+03 MeV/n (binning-specific)
# Most Probable:  7.9433e+02 MeV/n (binning-specific)
#
# ***Totals***
# N           = 1324
# FluenceRate = 9.8677e-02 [m^2 s sr]^-1
# Frequency   = 1.00000000
#
# ***Distribution***
#
#
# [MeV/n]                     [m^2 s sr MeV/n]^-1
# Energy        N             FluenceRate                   Frequency
1.0000e+00      0             0.0000e+00                    0.00000000
1.2589e+00      0             0.0000e+00                    0.00000000
1.5849e+00      0             0.0000e+00                    0.00000000
1.9953e+00      0             0.0000e+00                    0.00000000
2.5119e+00      0             0.0000e+00                    0.00000000
3.1623e+00      0             0.0000e+00                    0.00000000
3.9811e+00      0             0.0000e+00                    0.00000000
5.0119e+00      0             0.0000e+00                    0.00000000
6.3096e+00      0             0.0000e+00                    0.00000000
7.9433e+00      0             0.0000e+00                    0.00000000
1.0000e+01      0             0.0000e+00                    0.00000000
1.2589e+01      1             2.8784e-05                    0.00075529
1.5849e+01      1             2.2864e-05                    0.00075529
1.9953e+01      0             0.0000e+00                    0.00000000
2.5119e+01      2             2.8852e-05                    0.00151057
3.1623e+01      1             1.1459e-05                    0.00075529
3.9811e+01      3             2.7307e-05                    0.00226586
5.0119e+01      3             2.1691e-05                    0.00226586
6.3096e+01      2             1.1486e-05                    0.00151057
7.9433e+01      9             4.1058e-05                    0.00679758
1.0000e+02      14            5.0732e-05                    0.01057402
1.2589e+02      21            6.0447e-05                    0.01586103
1.5849e+02      31            7.0879e-05                    0.02341390
1.9953e+02      35            6.3565e-05                    0.02643505
2.5119e+02      50            7.2131e-05                    0.03776435
3.1623e+02      67            7.6776e-05                    0.05060423
```

3.9811e+02	76	6.9178e-05	0.05740181
5.0119e+02	79	5.7119e-05	0.05966767
6.3096e+02	86	4.9391e-05	0.06495468
7.9433e+02	120	5.4744e-05	0.09063444
1.0000e+03	115	4.1673e-05	0.08685801
1.2589e+03	118	3.3965e-05	0.08912387
1.5849e+03	99	2.2635e-05	0.07477341
1.9953e+03	82	1.4892e-05	0.06193353
2.5119e+03	70	1.0098e-05	0.05287009
3.1623e+03	63	7.2193e-06	0.04758308
3.9811e+03	46	4.1871e-06	0.03474320
5.0119e+03	40	2.8921e-06	0.03021148
6.3096e+03	28	1.6081e-06	0.02114804
7.9433e+03	17	7.7554e-07	0.01283988
1.0000e+04	13	4.7108e-07	0.00981873
1.2589e+04	10	2.8784e-07	0.00755287
1.5849e+04	9	2.0578e-07	0.00679758
1.9953e+04	5	9.0808e-08	0.00377644
2.5119e+04	4	5.7705e-08	0.00302115
3.1623e+04	3	3.4378e-08	0.00226586
3.9811e+04	1	9.1023e-09	0.00075529
5.0119e+04	0	0.0000e+00	0.00000000
6.3096e+04	0	0.0000e+00	0.00000000
7.9433e+04	0	0.0000e+00	0.00000000
1.0000e+05	0	0.0000e+00	0.00000000
1.2589e+05	0	0.0000e+00	0.00000000
1.5849e+05	0	0.0000e+00	0.00000000
1.9953e+05	0	0.0000e+00	0.00000000
2.5119e+05	0	0.0000e+00	0.00000000
3.1623e+05	0	0.0000e+00	0.00000000
3.9811e+05	0	0.0000e+00	0.00000000
5.0119e+05	0	0.0000e+00	0.00000000
6.3096e+05	0	0.0000e+00	0.00000000
7.9433e+05	0	0.0000e+00	0.00000000
1.0000e+06	0	0.0000e+00	0.00000000
1.2589e+06	0	0.0000e+00	0.00000000
1.5849e+06	0	0.0000e+00	0.00000000
1.9953e+06	0	0.0000e+00	0.00000000
2.5119e+06	0	0.0000e+00	0.00000000
3.1623e+06	0	0.0000e+00	0.00000000
3.9811e+06	0	0.0000e+00	0.00000000
5.0119e+06	0	0.0000e+00	0.00000000
6.3096e+06	0	0.0000e+00	0.00000000
7.9433e+06	0	0.0000e+00	0.00000000
1.0000e+07	0	0.0000e+00	0.00000000

$\phi/[\mathrm{m}^2\ \mathrm{s\ sr\ MeV/n}]^{-1}$ as a function of $E/[\mathrm{MeV/n}]$ tabulated data used to generate the "Surface of Mars" differential energy spectrum for $z = 14$ (isotopes combined):

```
# Using 70 Log Bins
# Min: 1 MeV/n          Max: 1e+07 MeV/n                10 bins/decade
#
# ***Statistics***
# Minimum:        2.7130e+00 MeV/n
# Maximum:        2.3041e+05 MeV/n
# Average:        2.9257e+03 MeV/n
# Frequency Mean: 2.6079e+03 MeV/n (binning-specific)
# Most Probable:  1.0000e+03 MeV/n (binning-specific)
#
# ***Totals***
# N           = 2884
# FluenceRate = 2.1494e-01 [m^2 s sr]^-1
# Frequency   = 1.00000000
#
# ***Distribution***
#
#
# [MeV/n]                     [m^2 s sr MeV/n]^-1
# Energy        N             FluenceRate                   Frequency
1.0000e+00      0             0.0000e+00                    0.00000000
1.2589e+00      0             0.0000e+00                    0.00000000
1.5849e+00      0             0.0000e+00                    0.00000000
1.9953e+00      0             0.0000e+00                    0.00000000
2.5119e+00      1             1.4426e-04                    0.00034674
3.1623e+00      0             0.0000e+00                    0.00000000
3.9811e+00      0             0.0000e+00                    0.00000000
5.0119e+00      0             0.0000e+00                    0.00000000
6.3096e+00      0             0.0000e+00                    0.00000000
7.9433e+00      0             0.0000e+00                    0.00000000
1.0000e+01      0             0.0000e+00                    0.00000000
1.2589e+01      0             0.0000e+00                    0.00000000
1.5849e+01      0             0.0000e+00                    0.00000000
1.9953e+01      1             1.8162e-05                    0.00034674
2.5119e+01      5             7.2131e-05                    0.00173370
3.1623e+01      6             6.8755e-05                    0.00208044
3.9811e+01      8             7.2819e-05                    0.00277393
5.0119e+01      9             6.5072e-05                    0.00312067
6.3096e+01      14            8.0405e-05                    0.00485437
7.9433e+01      18            8.2116e-05                    0.00624133
1.0000e+02      41            1.4857e-04                    0.01421637
1.2589e+02      31            8.9231e-05                    0.01074896
1.5849e+02      72            1.6462e-04                    0.02496533
1.9953e+02      75            1.3621e-04                    0.02600555
2.5119e+02      89            1.2839e-04                    0.03085992
3.1623e+02      116           1.3293e-04                    0.04022191
```

3.9811e+02	171	1.5565e-04	0.05929265
5.0119e+02	193	1.3954e-04	0.06692094
6.3096e+02	188	1.0797e-04	0.06518724
7.9433e+02	212	9.6714e-05	0.07350902
1.0000e+03	242	8.7694e-05	0.08391123
1.2589e+03	240	6.9082e-05	0.08321775
1.5849e+03	194	4.4356e-05	0.06726768
1.9953e+03	205	3.7231e-05	0.07108183
2.5119e+03	146	2.1062e-05	0.05062413
3.1623e+03	130	1.4897e-05	0.04507628
3.9811e+03	113	1.0286e-05	0.03918169
5.0119e+03	98	7.0856e-06	0.03398058
6.3096e+03	75	4.3074e-06	0.02600555
7.9433e+03	45	2.0529e-06	0.01560333
1.0000e+04	48	1.7394e-06	0.01664355
1.2589e+04	36	1.0362e-06	0.01248266
1.5849e+04	21	4.8015e-07	0.00728155
1.9953e+04	9	1.6345e-07	0.00312067
2.5119e+04	8	1.1541e-07	0.00277393
3.1623e+04	7	8.0214e-08	0.00242718
3.9811e+04	5	4.5512e-08	0.00173370
5.0119e+04	2	1.4461e-08	0.00069348
6.3096e+04	4	2.2973e-08	0.00138696
7.9433e+04	2	9.1240e-09	0.00069348
1.0000e+05	1	3.6237e-09	0.00034674
1.2589e+05	1	2.8784e-09	0.00034674
1.5849e+05	1	2.2864e-09	0.00034674
1.9953e+05	1	1.8162e-09	0.00034674
2.5119e+05	0	0.0000e+00	0.00000000
3.1623e+05	0	0.0000e+00	0.00000000
3.9811e+05	0	0.0000e+00	0.00000000
5.0119e+05	0	0.0000e+00	0.00000000
6.3096e+05	0	0.0000e+00	0.00000000
7.9433e+05	0	0.0000e+00	0.00000000
1.0000e+06	0	0.0000e+00	0.00000000
1.2589e+06	0	0.0000e+00	0.00000000
1.5849e+06	0	0.0000e+00	0.00000000
1.9953e+06	0	0.0000e+00	0.00000000
2.5119e+06	0	0.0000e+00	0.00000000
3.1623e+06	0	0.0000e+00	0.00000000
3.9811e+06	0	0.0000e+00	0.00000000
5.0119e+06	0	0.0000e+00	0.00000000
6.3096e+06	0	0.0000e+00	0.00000000
7.9433e+06	0	0.0000e+00	0.00000000
1.0000e+07	0	0.0000e+00	0.00000000

$\phi/[\mathrm{m}^2\ \mathrm{s\ sr\ MeV/n}]^{-1}$ as a function of $E/[\mathrm{MeV/n}]$ tabulated data used to generate the "Surface of Mars" differential energy spectrum for $z = 15$ (isotopes combined):

```
# Using 70 Log Bins
# Min: 1 MeV/n          Max: 1e+07 MeV/n                10 bins/decade
#
# ***Statistics***
# Minimum:        3.6732e+01 MeV/n
# Maximum:        9.6993e+04 MeV/n
# Average:        2.9888e+03 MeV/n
# Frequency Mean: 2.6848e+03 MeV/n (binning-specific)
# Most Probable:  6.3096e+02 MeV/n (binning-specific)
#
# ***Totals***
# N           = 454
# FluenceRate = 3.3836e-02 [m^2 s sr]^-1
# Frequency   = 1.00000000
#
# ***Distribution***
#
#
# [MeV/n]                     [m^2 s sr MeV/n]^-1
# Energy        N             FluenceRate                   Frequency
1.0000e+00      0             0.0000e+00                    0.00000000
1.2589e+00      0             0.0000e+00                    0.00000000
1.5849e+00      0             0.0000e+00                    0.00000000
1.9953e+00      0             0.0000e+00                    0.00000000
2.5119e+00      0             0.0000e+00                    0.00000000
3.1623e+00      0             0.0000e+00                    0.00000000
3.9811e+00      0             0.0000e+00                    0.00000000
5.0119e+00      0             0.0000e+00                    0.00000000
6.3096e+00      0             0.0000e+00                    0.00000000
7.9433e+00      0             0.0000e+00                    0.00000000
1.0000e+01      0             0.0000e+00                    0.00000000
1.2589e+01      0             0.0000e+00                    0.00000000
1.5849e+01      0             0.0000e+00                    0.00000000
1.9953e+01      0             0.0000e+00                    0.00000000
2.5119e+01      0             0.0000e+00                    0.00000000
3.1623e+01      2             2.2918e-05                    0.00440529
3.9811e+01      1             9.1023e-06                    0.00220264
5.0119e+01      3             2.1691e-05                    0.00660793
6.3096e+01      1             5.7432e-06                    0.00220264
7.9433e+01      1             4.5620e-06                    0.00220264
1.0000e+02      6             2.1742e-05                    0.01321586
1.2589e+02      9             2.5906e-05                    0.01982379
1.5849e+02      5             1.1432e-05                    0.01101322
1.9953e+02      13            2.3610e-05                    0.02863436
2.5119e+02      16            2.3082e-05                    0.03524229
3.1623e+02      17            1.9481e-05                    0.03744493
```

3.9811e+02	22	2.0025e-05	0.04845815
5.0119e+02	29	2.0968e-05	0.06387665
6.3096e+02	36	2.0675e-05	0.07929515
7.9433e+02	31	1.4142e-05	0.06828194
1.0000e+03	36	1.3045e-05	0.07929515
1.2589e+03	36	1.0362e-05	0.07929515
1.5849e+03	35	8.0024e-06	0.07709251
1.9953e+03	26	4.7220e-06	0.05726872
2.5119e+03	18	2.5967e-06	0.03964758
3.1623e+03	22	2.5210e-06	0.04845815
3.9811e+03	13	1.1833e-06	0.02863436
5.0119e+03	17	1.2291e-06	0.03744493
6.3096e+03	22	1.2635e-06	0.04845815
7.9433e+03	13	5.9306e-07	0.02863436
1.0000e+04	11	3.9861e-07	0.02422907
1.2589e+04	5	1.4392e-07	0.01101322
1.5849e+04	3	6.8592e-08	0.00660793
1.9953e+04	2	3.6323e-08	0.00440529
2.5119e+04	0	0.0000e+00	0.00000000
3.1623e+04	1	1.1459e-08	0.00220264
3.9811e+04	0	0.0000e+00	0.00000000
5.0119e+04	0	0.0000e+00	0.00000000
6.3096e+04	0	0.0000e+00	0.00000000
7.9433e+04	2	9.1240e-09	0.00440529
1.0000e+05	0	0.0000e+00	0.00000000
1.2589e+05	0	0.0000e+00	0.00000000
1.5849e+05	0	0.0000e+00	0.00000000
1.9953e+05	0	0.0000e+00	0.00000000
2.5119e+05	0	0.0000e+00	0.00000000
3.1623e+05	0	0.0000e+00	0.00000000
3.9811e+05	0	0.0000e+00	0.00000000
5.0119e+05	0	0.0000e+00	0.00000000
6.3096e+05	0	0.0000e+00	0.00000000
7.9433e+05	0	0.0000e+00	0.00000000
1.0000e+06	0	0.0000e+00	0.00000000
1.2589e+06	0	0.0000e+00	0.00000000
1.5849e+06	0	0.0000e+00	0.00000000
1.9953e+06	0	0.0000e+00	0.00000000
2.5119e+06	0	0.0000e+00	0.00000000
3.1623e+06	0	0.0000e+00	0.00000000
3.9811e+06	0	0.0000e+00	0.00000000
5.0119e+06	0	0.0000e+00	0.00000000
6.3096e+06	0	0.0000e+00	0.00000000
7.9433e+06	0	0.0000e+00	0.00000000
1.0000e+07	0	0.0000e+00	0.00000000

$\phi/[\mathrm{m}^2\ \mathrm{s\ sr\ MeV/n}]^{-1}$ as a function of $E/[\mathrm{MeV/n}]$ tabulated data used to generate the "Surface of Mars" differential energy spectrum for $z = 16$ (isotopes combined):

```
# Using 70 Log Bins
# Min: 1 MeV/n          Max: 1e+07 MeV/n                10 bins/decade
#
# ***Statistics***
# Minimum:        5.5131e+00 MeV/n
# Maximum:        4.1680e+04 MeV/n
# Average:        2.7210e+03 MeV/n
# Frequency Mean: 2.4334e+03 MeV/n (binning-specific)
# Most Probable:  1.0000e+03 MeV/n (binning-specific)
#
# ***Totals***
# N           = 737
# FluenceRate = 5.4928e-02 [m^2 s sr]^-1
# Frequency   = 1.00000000
#
# ***Distribution***
#
#
# [MeV/n]                     [m^2 s sr MeV/n]^-1
# Energy        N             FluenceRate                   Frequency
1.0000e+00      0             0.0000e+00                    0.00000000
1.2589e+00      0             0.0000e+00                    0.00000000
1.5849e+00      0             0.0000e+00                    0.00000000
1.9953e+00      0             0.0000e+00                    0.00000000
2.5119e+00      0             0.0000e+00                    0.00000000
3.1623e+00      0             0.0000e+00                    0.00000000
3.9811e+00      0             0.0000e+00                    0.00000000
5.0119e+00      1             7.2303e-05                    0.00135685
6.3096e+00      0             0.0000e+00                    0.00000000
7.9433e+00      0             0.0000e+00                    0.00000000
1.0000e+01      0             0.0000e+00                    0.00000000
1.2589e+01      0             0.0000e+00                    0.00000000
1.5849e+01      1             2.2864e-05                    0.00135685
1.9953e+01      1             1.8162e-05                    0.00135685
2.5119e+01      1             1.4426e-05                    0.00135685
3.1623e+01      0             0.0000e+00                    0.00000000
3.9811e+01      4             3.6409e-05                    0.00542741
5.0119e+01      0             0.0000e+00                    0.00000000
6.3096e+01      3             1.7230e-05                    0.00407056
7.9433e+01      7             3.1934e-05                    0.00949796
1.0000e+02      5             1.8119e-05                    0.00678426
1.2589e+02      8             2.3027e-05                    0.01085482
1.5849e+02      14            3.2010e-05                    0.01899593
1.9953e+02      8             1.4529e-05                    0.01085482
2.5119e+02      31            4.4721e-05                    0.04206242
3.1623e+02      25            2.8648e-05                    0.03392130
```

3.9811e+02	37	3.3679e-05	0.05020353
5.0119e+02	44	3.1813e-05	0.05970149
6.3096e+02	58	3.3311e-05	0.07869742
7.9433e+02	61	2.7828e-05	0.08276798
1.0000e+03	64	2.3192e-05	0.08683853
1.2589e+03	50	1.4392e-05	0.06784261
1.5849e+03	49	1.1203e-05	0.06648575
1.9953e+03	50	9.0808e-06	0.06784261
2.5119e+03	51	7.3574e-06	0.06919946
3.1623e+03	35	4.0107e-06	0.04748982
3.9811e+03	28	2.5487e-06	0.03799186
5.0119e+03	33	2.3860e-06	0.04477612
6.3096e+03	19	1.0912e-06	0.02578019
7.9433e+03	13	5.9306e-07	0.01763908
1.0000e+04	14	5.0732e-07	0.01899593
1.2589e+04	5	1.4392e-07	0.00678426
1.5849e+04	4	9.1456e-08	0.00542741
1.9953e+04	4	7.2646e-08	0.00542741
2.5119e+04	5	7.2131e-08	0.00678426
3.1623e+04	3	3.4378e-08	0.00407056
3.9811e+04	1	9.1023e-09	0.00135685
5.0119e+04	0	0.0000e+00	0.00000000
6.3096e+04	0	0.0000e+00	0.00000000
7.9433e+04	0	0.0000e+00	0.00000000
1.0000e+05	0	0.0000e+00	0.00000000
1.2589e+05	0	0.0000e+00	0.00000000
1.5849e+05	0	0.0000e+00	0.00000000
1.9953e+05	0	0.0000e+00	0.00000000
2.5119e+05	0	0.0000e+00	0.00000000
3.1623e+05	0	0.0000e+00	0.00000000
3.9811e+05	0	0.0000e+00	0.00000000
5.0119e+05	0	0.0000e+00	0.00000000
6.3096e+05	0	0.0000e+00	0.00000000
7.9433e+05	0	0.0000e+00	0.00000000
1.0000e+06	0	0.0000e+00	0.00000000
1.2589e+06	0	0.0000e+00	0.00000000
1.5849e+06	0	0.0000e+00	0.00000000
1.9953e+06	0	0.0000e+00	0.00000000
2.5119e+06	0	0.0000e+00	0.00000000
3.1623e+06	0	0.0000e+00	0.00000000
3.9811e+06	0	0.0000e+00	0.00000000
5.0119e+06	0	0.0000e+00	0.00000000
6.3096e+06	0	0.0000e+00	0.00000000
7.9433e+06	0	0.0000e+00	0.00000000
1.0000e+07	0	0.0000e+00	0.00000000

$\phi/[\mathrm{m}^2\ \mathrm{s\ sr\ MeV/n}]^{-1}$ as a function of $E/[\mathrm{MeV/n}]$ tabulated data used to generate the "Surface of Mars" differential energy spectrum for $z = 17$ (isotopes combined):

```
# Using 70 Log Bins
# Min: 1 MeV/n          Max: 1e+07 MeV/n                10 bins/decade
#
# ***Statistics***
# Minimum:        2.7424e+01 MeV/n
# Maximum:        4.3616e+04 MeV/n
# Average:        2.5675e+03 MeV/n
# Frequency Mean: 2.2908e+03 MeV/n (binning-specific)
# Most Probable:  6.3096e+02 MeV/n (binning-specific)
#
# ***Totals***
# N           = 341
# FluenceRate = 2.5415e-02 [m^2 s sr]^-1
# Frequency   = 1.00000000
#
# ***Distribution***
#
#
# [MeV/n]                     [m^2 s sr MeV/n]^-1
# Energy        N             FluenceRate                   Frequency
1.0000e+00      0             0.0000e+00                    0.00000000
1.2589e+00      0             0.0000e+00                    0.00000000
1.5849e+00      0             0.0000e+00                    0.00000000
1.9953e+00      0             0.0000e+00                    0.00000000
2.5119e+00      0             0.0000e+00                    0.00000000
3.1623e+00      0             0.0000e+00                    0.00000000
3.9811e+00      0             0.0000e+00                    0.00000000
5.0119e+00      0             0.0000e+00                    0.00000000
6.3096e+00      0             0.0000e+00                    0.00000000
7.9433e+00      0             0.0000e+00                    0.00000000
1.0000e+01      0             0.0000e+00                    0.00000000
1.2589e+01      0             0.0000e+00                    0.00000000
1.5849e+01      0             0.0000e+00                    0.00000000
1.9953e+01      0             0.0000e+00                    0.00000000
2.5119e+01      1             1.4426e-05                    0.00293255
3.1623e+01      0             0.0000e+00                    0.00000000
3.9811e+01      0             0.0000e+00                    0.00000000
5.0119e+01      1             7.2303e-06                    0.00293255
6.3096e+01      1             5.7432e-06                    0.00293255
7.9433e+01      3             1.3686e-05                    0.00879765
1.0000e+02      2             7.2474e-06                    0.00586510
1.2589e+02      3             8.6352e-06                    0.00879765
1.5849e+02      6             1.3718e-05                    0.01759531
1.9953e+02      11            1.9978e-05                    0.03225806
2.5119e+02      14            2.0197e-05                    0.04105572
3.1623e+02      13            1.4897e-05                    0.03812317
```

3.9811e+02	16	1.4564e-05	0.04692082
5.0119e+02	16	1.1568e-05	0.04692082
6.3096e+02	30	1.7230e-05	0.08797654
7.9433e+02	22	1.0036e-05	0.06451613
1.0000e+03	27	9.7840e-06	0.07917889
1.2589e+03	30	8.6352e-06	0.08797654
1.5849e+03	23	5.2587e-06	0.06744868
1.9953e+03	20	3.6323e-06	0.05865103
2.5119e+03	20	2.8852e-06	0.05865103
3.1623e+03	15	1.7189e-06	0.04398827
3.9811e+03	21	1.9115e-06	0.06158358
5.0119e+03	18	1.3014e-06	0.05278592
6.3096e+03	7	4.0202e-07	0.02052786
7.9433e+03	10	4.5620e-07	0.02932551
1.0000e+04	5	1.8119e-07	0.01466276
1.2589e+04	0	0.0000e+00	0.00000000
1.5849e+04	3	6.8592e-08	0.00879765
1.9953e+04	1	1.8162e-08	0.00293255
2.5119e+04	1	1.4426e-08	0.00293255
3.1623e+04	0	0.0000e+00	0.00000000
3.9811e+04	1	9.1023e-09	0.00293255
5.0119e+04	0	0.0000e+00	0.00000000
6.3096e+04	0	0.0000e+00	0.00000000
7.9433e+04	0	0.0000e+00	0.00000000
1.0000e+05	0	0.0000e+00	0.00000000
1.2589e+05	0	0.0000e+00	0.00000000
1.5849e+05	0	0.0000e+00	0.00000000
1.9953e+05	0	0.0000e+00	0.00000000
2.5119e+05	0	0.0000e+00	0.00000000
3.1623e+05	0	0.0000e+00	0.00000000
3.9811e+05	0	0.0000e+00	0.00000000
5.0119e+05	0	0.0000e+00	0.00000000
6.3096e+05	0	0.0000e+00	0.00000000
7.9433e+05	0	0.0000e+00	0.00000000
1.0000e+06	0	0.0000e+00	0.00000000
1.2589e+06	0	0.0000e+00	0.00000000
1.5849e+06	0	0.0000e+00	0.00000000
1.9953e+06	0	0.0000e+00	0.00000000
2.5119e+06	0	0.0000e+00	0.00000000
3.1623e+06	0	0.0000e+00	0.00000000
3.9811e+06	0	0.0000e+00	0.00000000
5.0119e+06	0	0.0000e+00	0.00000000
6.3096e+06	0	0.0000e+00	0.00000000
7.9433e+06	0	0.0000e+00	0.00000000
1.0000e+07	0	0.0000e+00	0.00000000

$\phi/[\mathrm{m}^2\ \mathrm{s\ sr\ MeV/n}]^{-1}$ as a function of $E/[\mathrm{MeV/n}]$ tabulated data used to generate the "Surface of Mars" differential energy spectrum for $z = 18$ (isotopes combined):

```
# Using 70 Log Bins
# Min: 1 MeV/n          Max: 1e+07 MeV/n                10 bins/decade
#
# ***Statistics***
# Minimum:        6.2779e+00 MeV/n
# Maximum:        4.9500e+04 MeV/n
# Average:        2.8638e+03 MeV/n
# Frequency Mean: 2.5310e+03 MeV/n (binning-specific)
# Most Probable:  1.0000e+03 MeV/n (binning-specific)
#
# ***Totals***
# N           = 382
# FluenceRate = 2.8470e-02 [m^2 s sr]^-1
# Frequency   = 1.00000000
#
# ***Distribution***
#
#
# [MeV/n]                     [m^2 s sr MeV/n]^-1
# Energy        N             FluenceRate                   Frequency
1.0000e+00      0             0.0000e+00                    0.00000000
1.2589e+00      0             0.0000e+00                    0.00000000
1.5849e+00      0             0.0000e+00                    0.00000000
1.9953e+00      0             0.0000e+00                    0.00000000
2.5119e+00      0             0.0000e+00                    0.00000000
3.1623e+00      0             0.0000e+00                    0.00000000
3.9811e+00      0             0.0000e+00                    0.00000000
5.0119e+00      1             7.2303e-05                    0.00261780
6.3096e+00      0             0.0000e+00                    0.00000000
7.9433e+00      0             0.0000e+00                    0.00000000
1.0000e+01      0             0.0000e+00                    0.00000000
1.2589e+01      1             2.8784e-05                    0.00261780
1.5849e+01      0             0.0000e+00                    0.00000000
1.9953e+01      0             0.0000e+00                    0.00000000
2.5119e+01      1             1.4426e-05                    0.00261780
3.1623e+01      0             0.0000e+00                    0.00000000
3.9811e+01      0             0.0000e+00                    0.00000000
5.0119e+01      0             0.0000e+00                    0.00000000
6.3096e+01      1             5.7432e-06                    0.00261780
7.9433e+01      3             1.3686e-05                    0.00785340
1.0000e+02      4             1.4495e-05                    0.01047120
1.2589e+02      4             1.1514e-05                    0.01047120
1.5849e+02      9             2.0578e-05                    0.02356021
1.9953e+02      9             1.6345e-05                    0.02356021
2.5119e+02      15            2.1639e-05                    0.03926702
3.1623e+02      20            2.2918e-05                    0.05235602
```

3.9811e+02	24	2.1846e-05	0.06282723
5.0119e+02	22	1.5907e-05	0.05759162
6.3096e+02	28	1.6081e-05	0.07329843
7.9433e+02	28	1.2774e-05	0.07329843
1.0000e+03	29	1.0509e-05	0.07591623
1.2589e+03	21	6.0447e-06	0.05497382
1.5849e+03	26	5.9447e-06	0.06806283
1.9953e+03	23	4.1772e-06	0.06020942
2.5119e+03	21	3.0295e-06	0.05497382
3.1623e+03	15	1.7189e-06	0.03926702
3.9811e+03	11	1.0013e-06	0.02879581
5.0119e+03	20	1.4461e-06	0.05235602
6.3096e+03	16	9.1891e-07	0.04188482
7.9433e+03	8	3.6496e-07	0.02094241
1.0000e+04	9	3.2613e-07	0.02356021
1.2589e+04	6	1.7270e-07	0.01570681
1.5849e+04	0	0.0000e+00	0.00000000
1.9953e+04	3	5.4485e-08	0.00785340
2.5119e+04	3	4.3279e-08	0.00785340
3.1623e+04	0	0.0000e+00	0.00000000
3.9811e+04	1	9.1023e-09	0.00261780
5.0119e+04	0	0.0000e+00	0.00000000
6.3096e+04	0	0.0000e+00	0.00000000
7.9433e+04	0	0.0000e+00	0.00000000
1.0000e+05	0	0.0000e+00	0.00000000
1.2589e+05	0	0.0000e+00	0.00000000
1.5849e+05	0	0.0000e+00	0.00000000
1.9953e+05	0	0.0000e+00	0.00000000
2.5119e+05	0	0.0000e+00	0.00000000
3.1623e+05	0	0.0000e+00	0.00000000
3.9811e+05	0	0.0000e+00	0.00000000
5.0119e+05	0	0.0000e+00	0.00000000
6.3096e+05	0	0.0000e+00	0.00000000
7.9433e+05	0	0.0000e+00	0.00000000
1.0000e+06	0	0.0000e+00	0.00000000
1.2589e+06	0	0.0000e+00	0.00000000
1.5849e+06	0	0.0000e+00	0.00000000
1.9953e+06	0	0.0000e+00	0.00000000
2.5119e+06	0	0.0000e+00	0.00000000
3.1623e+06	0	0.0000e+00	0.00000000
3.9811e+06	0	0.0000e+00	0.00000000
5.0119e+06	0	0.0000e+00	0.00000000
6.3096e+06	0	0.0000e+00	0.00000000
7.9433e+06	0	0.0000e+00	0.00000000
1.0000e+07	0	0.0000e+00	0.00000000

$\phi/[\mathrm{m}^2\ \mathrm{s\ sr\ MeV/n}]^{-1}$ as a function of $E/[\mathrm{MeV/n}]$ tabulated data used to generate the "Surface of Mars" differential energy spectrum for $z = 19$ (isotopes combined):

```
# Using 70 Log Bins
# Min: 1 MeV/n          Max: 1e+07 MeV/n                10 bins/decade
#
# ***Statistics***
# Minimum:        1.5848e+01 MeV/n
# Maximum:        5.5603e+04 MeV/n
# Average:        3.0537e+03 MeV/n
# Frequency Mean: 2.7241e+03 MeV/n (binning-specific)
# Most Probable:  1.5849e+03 MeV/n (binning-specific)
#
# ***Totals***
# N           = 292
# FluenceRate = 2.1763e-02 [m^2 s sr]^-1
# Frequency   = 1.00000000
#
# ***Distribution***
#
#
# [MeV/n]                     [m^2 s sr MeV/n]^-1
# Energy        N             FluenceRate                   Frequency
1.0000e+00      0             0.0000e+00                    0.00000000
1.2589e+00      0             0.0000e+00                    0.00000000
1.5849e+00      0             0.0000e+00                    0.00000000
1.9953e+00      0             0.0000e+00                    0.00000000
2.5119e+00      0             0.0000e+00                    0.00000000
3.1623e+00      0             0.0000e+00                    0.00000000
3.9811e+00      0             0.0000e+00                    0.00000000
5.0119e+00      0             0.0000e+00                    0.00000000
6.3096e+00      0             0.0000e+00                    0.00000000
7.9433e+00      0             0.0000e+00                    0.00000000
1.0000e+01      0             0.0000e+00                    0.00000000
1.2589e+01      1             2.8784e-05                    0.00342466
1.5849e+01      0             0.0000e+00                    0.00000000
1.9953e+01      1             1.8162e-05                    0.00342466
2.5119e+01      0             0.0000e+00                    0.00000000
3.1623e+01      0             0.0000e+00                    0.00000000
3.9811e+01      0             0.0000e+00                    0.00000000
5.0119e+01      0             0.0000e+00                    0.00000000
6.3096e+01      2             1.1486e-05                    0.00684932
7.9433e+01      0             0.0000e+00                    0.00000000
1.0000e+02      1             3.6237e-06                    0.00342466
1.2589e+02      4             1.1514e-05                    0.01369863
1.5849e+02      6             1.3718e-05                    0.02054795
1.9953e+02      14            2.5426e-05                    0.04794521
2.5119e+02      7             1.0098e-05                    0.02397260
3.1623e+02      12            1.3751e-05                    0.04109589
```

3.9811e+02	12	1.0923e-05	0.04109589
5.0119e+02	17	1.2291e-05	0.05821918
6.3096e+02	14	8.0405e-06	0.04794521
7.9433e+02	22	1.0036e-05	0.07534247
1.0000e+03	11	3.9861e-06	0.03767123
1.2589e+03	25	7.1960e-06	0.08561644
1.5849e+03	26	5.9447e-06	0.08904110
1.9953e+03	23	4.1772e-06	0.07876712
2.5119e+03	19	2.7410e-06	0.06506849
3.1623e+03	13	1.4897e-06	0.04452055
3.9811e+03	13	1.1833e-06	0.04452055
5.0119e+03	17	1.2291e-06	0.05821918
6.3096e+03	8	4.5946e-07	0.02739726
7.9433e+03	10	4.5620e-07	0.03424658
1.0000e+04	7	2.5366e-07	0.02397260
1.2589e+04	0	0.0000e+00	0.00000000
1.5849e+04	0	0.0000e+00	0.00000000
1.9953e+04	2	3.6323e-08	0.00684932
2.5119e+04	4	5.7705e-08	0.01369863
3.1623e+04	0	0.0000e+00	0.00000000
3.9811e+04	0	0.0000e+00	0.00000000
5.0119e+04	1	7.2303e-09	0.00342466
6.3096e+04	0	0.0000e+00	0.00000000
7.9433e+04	0	0.0000e+00	0.00000000
1.0000e+05	0	0.0000e+00	0.00000000
1.2589e+05	0	0.0000e+00	0.00000000
1.5849e+05	0	0.0000e+00	0.00000000
1.9953e+05	0	0.0000e+00	0.00000000
2.5119e+05	0	0.0000e+00	0.00000000
3.1623e+05	0	0.0000e+00	0.00000000
3.9811e+05	0	0.0000e+00	0.00000000
5.0119e+05	0	0.0000e+00	0.00000000
6.3096e+05	0	0.0000e+00	0.00000000
7.9433e+05	0	0.0000e+00	0.00000000
1.0000e+06	0	0.0000e+00	0.00000000
1.2589e+06	0	0.0000e+00	0.00000000
1.5849e+06	0	0.0000e+00	0.00000000
1.9953e+06	0	0.0000e+00	0.00000000
2.5119e+06	0	0.0000e+00	0.00000000
3.1623e+06	0	0.0000e+00	0.00000000
3.9811e+06	0	0.0000e+00	0.00000000
5.0119e+06	0	0.0000e+00	0.00000000
6.3096e+06	0	0.0000e+00	0.00000000
7.9433e+06	0	0.0000e+00	0.00000000
1.0000e+07	0	0.0000e+00	0.00000000

$\phi/[\mathrm{m}^2\ \mathrm{s\ sr\ MeV/n}]^{-1}$ as a function of $E/[\mathrm{MeV/n}]$ tabulated data used to generate the "Surface of Mars" differential energy spectrum for $z = 20$ (isotopes combined):

```
# Using 70 Log Bins
# Min: 1 MeV/n          Max: 1e+07 MeV/n                10 bins/decade
#
# ***Statistics***
# Minimum:        5.8393e+01 MeV/n
# Maximum:        3.0809e+04 MeV/n
# Average:        2.5066e+03 MeV/n
# Frequency Mean: 2.2267e+03 MeV/n (binning-specific)
# Most Probable:  1.2589e+03 MeV/n (binning-specific)
#
# ***Totals***
# N           = 435
# FluenceRate = 3.2420e-02 [m^2 s sr]^-1
# Frequency   = 1.00000000
#
# ***Distribution***
#
#
# [MeV/n]                     [m^2 s sr MeV/n]^-1
# Energy        N             FluenceRate                   Frequency
1.0000e+00      0             0.0000e+00                    0.00000000
1.2589e+00      0             0.0000e+00                    0.00000000
1.5849e+00      0             0.0000e+00                    0.00000000
1.9953e+00      0             0.0000e+00                    0.00000000
2.5119e+00      0             0.0000e+00                    0.00000000
3.1623e+00      0             0.0000e+00                    0.00000000
3.9811e+00      0             0.0000e+00                    0.00000000
5.0119e+00      0             0.0000e+00                    0.00000000
6.3096e+00      0             0.0000e+00                    0.00000000
7.9433e+00      0             0.0000e+00                    0.00000000
1.0000e+01      0             0.0000e+00                    0.00000000
1.2589e+01      0             0.0000e+00                    0.00000000
1.5849e+01      0             0.0000e+00                    0.00000000
1.9953e+01      0             0.0000e+00                    0.00000000
2.5119e+01      0             0.0000e+00                    0.00000000
3.1623e+01      0             0.0000e+00                    0.00000000
3.9811e+01      0             0.0000e+00                    0.00000000
5.0119e+01      1             7.2303e-06                    0.00229885
6.3096e+01      2             1.1486e-05                    0.00459770
7.9433e+01      2             9.1240e-06                    0.00459770
1.0000e+02      5             1.8119e-05                    0.01149425
1.2589e+02      2             5.7568e-06                    0.00459770
1.5849e+02      11            2.5150e-05                    0.02528736
1.9953e+02      11            1.9978e-05                    0.02528736
2.5119e+02      13            1.8754e-05                    0.02988506
3.1623e+02      20            2.2918e-05                    0.04597701
```

3.9811e+02	29	2.6397e-05	0.06666667
5.0119e+02	27	1.9522e-05	0.06206897
6.3096e+02	32	1.8378e-05	0.07356322
7.9433e+02	30	1.3686e-05	0.06896552
1.0000e+03	34	1.2321e-05	0.07816092
1.2589e+03	38	1.0938e-05	0.08735632
1.5849e+03	32	7.3165e-06	0.07356322
1.9953e+03	20	3.6323e-06	0.04597701
2.5119e+03	26	3.7508e-06	0.05977011
3.1623e+03	14	1.6043e-06	0.03218391
3.9811e+03	24	2.1846e-06	0.05517241
5.0119e+03	22	1.5907e-06	0.05057471
6.3096e+03	14	8.0405e-07	0.03218391
7.9433e+03	13	5.9306e-07	0.02988506
1.0000e+04	3	1.0871e-07	0.00689655
1.2589e+04	3	8.6352e-08	0.00689655
1.5849e+04	3	6.8592e-08	0.00689655
1.9953e+04	2	3.6323e-08	0.00459770
2.5119e+04	2	2.8852e-08	0.00459770
3.1623e+04	0	0.0000e+00	0.00000000
3.9811e+04	0	0.0000e+00	0.00000000
5.0119e+04	0	0.0000e+00	0.00000000
6.3096e+04	0	0.0000e+00	0.00000000
7.9433e+04	0	0.0000e+00	0.00000000
1.0000e+05	0	0.0000e+00	0.00000000
1.2589e+05	0	0.0000e+00	0.00000000
1.5849e+05	0	0.0000e+00	0.00000000
1.9953e+05	0	0.0000e+00	0.00000000
2.5119e+05	0	0.0000e+00	0.00000000
3.1623e+05	0	0.0000e+00	0.00000000
3.9811e+05	0	0.0000e+00	0.00000000
5.0119e+05	0	0.0000e+00	0.00000000
6.3096e+05	0	0.0000e+00	0.00000000
7.9433e+05	0	0.0000e+00	0.00000000
1.0000e+06	0	0.0000e+00	0.00000000
1.2589e+06	0	0.0000e+00	0.00000000
1.5849e+06	0	0.0000e+00	0.00000000
1.9953e+06	0	0.0000e+00	0.00000000
2.5119e+06	0	0.0000e+00	0.00000000
3.1623e+06	0	0.0000e+00	0.00000000
3.9811e+06	0	0.0000e+00	0.00000000
5.0119e+06	0	0.0000e+00	0.00000000
6.3096e+06	0	0.0000e+00	0.00000000
7.9433e+06	0	0.0000e+00	0.00000000
1.0000e+07	0	0.0000e+00	0.00000000

$\phi/[\mathrm{m}^2\ \mathrm{s\ sr\ MeV/n}]^{-1}$ as a function of $E/[\mathrm{MeV/n}]$ tabulated data used to generate the "Surface of Mars" differential energy spectrum for $z = 21$ (isotopes combined):

```
# Using 70 Log Bins
# Min: 1 MeV/n          Max: 1e+07 MeV/n                10 bins/decade
#
# ***Statistics***
# Minimum:        3.0863e+01 MeV/n
# Maximum:        4.8417e+04 MeV/n
# Average:        2.7464e+03 MeV/n
# Frequency Mean: 2.4565e+03 MeV/n (binning-specific)
# Most Probable:  1.0000e+03 MeV/n (binning-specific)
#
# ***Totals***
# N           = 175
# FluenceRate = 1.3043e-02 [m^2 s sr]^-1
# Frequency   = 1.00000000
#
# ***Distribution***
#
#
# [MeV/n]                     [m^2 s sr MeV/n]^-1
# Energy        N             FluenceRate                   Frequency
1.0000e+00      0             0.0000e+00                    0.00000000
1.2589e+00      0             0.0000e+00                    0.00000000
1.5849e+00      0             0.0000e+00                    0.00000000
1.9953e+00      0             0.0000e+00                    0.00000000
2.5119e+00      0             0.0000e+00                    0.00000000
3.1623e+00      0             0.0000e+00                    0.00000000
3.9811e+00      0             0.0000e+00                    0.00000000
5.0119e+00      0             0.0000e+00                    0.00000000
6.3096e+00      0             0.0000e+00                    0.00000000
7.9433e+00      0             0.0000e+00                    0.00000000
1.0000e+01      0             0.0000e+00                    0.00000000
1.2589e+01      0             0.0000e+00                    0.00000000
1.5849e+01      0             0.0000e+00                    0.00000000
1.9953e+01      0             0.0000e+00                    0.00000000
2.5119e+01      1             1.4426e-05                    0.00571429
3.1623e+01      0             0.0000e+00                    0.00000000
3.9811e+01      0             0.0000e+00                    0.00000000
5.0119e+01      0             0.0000e+00                    0.00000000
6.3096e+01      0             0.0000e+00                    0.00000000
7.9433e+01      2             9.1240e-06                    0.01142857
1.0000e+02      3             1.0871e-05                    0.01714286
1.2589e+02      1             2.8784e-06                    0.00571429
1.5849e+02      2             4.5728e-06                    0.01142857
1.9953e+02      0             0.0000e+00                    0.00000000
2.5119e+02      8             1.1541e-05                    0.04571429
3.1623e+02      7             8.0214e-06                    0.04000000
```

3.9811e+02	11	1.0013e-05	0.06285714
5.0119e+02	13	9.3993e-06	0.07428571
6.3096e+02	13	7.4662e-06	0.07428571
7.9433e+02	14	6.3868e-06	0.08000000
1.0000e+03	23	8.3345e-06	0.13142857
1.2589e+03	13	3.7419e-06	0.07428571
1.5849e+03	12	2.7437e-06	0.06857143
1.9953e+03	5	9.0808e-07	0.02857143
2.5119e+03	9	1.2984e-06	0.05142857
3.1623e+03	6	6.8755e-07	0.03428571
3.9811e+03	7	6.3716e-07	0.04000000
5.0119e+03	7	5.0612e-07	0.04000000
6.3096e+03	5	2.8716e-07	0.02857143
7.9433e+03	6	2.7372e-07	0.03428571
1.0000e+04	1	3.6237e-08	0.00571429
1.2589e+04	2	5.7568e-08	0.01142857
1.5849e+04	1	2.2864e-08	0.00571429
1.9953e+04	1	1.8162e-08	0.00571429
2.5119e+04	0	0.0000e+00	0.00000000
3.1623e+04	1	1.1459e-08	0.00571429
3.9811e+04	1	9.1023e-09	0.00571429
5.0119e+04	0	0.0000e+00	0.00000000
6.3096e+04	0	0.0000e+00	0.00000000
7.9433e+04	0	0.0000e+00	0.00000000
1.0000e+05	0	0.0000e+00	0.00000000
1.2589e+05	0	0.0000e+00	0.00000000
1.5849e+05	0	0.0000e+00	0.00000000
1.9953e+05	0	0.0000e+00	0.00000000
2.5119e+05	0	0.0000e+00	0.00000000
3.1623e+05	0	0.0000e+00	0.00000000
3.9811e+05	0	0.0000e+00	0.00000000
5.0119e+05	0	0.0000e+00	0.00000000
6.3096e+05	0	0.0000e+00	0.00000000
7.9433e+05	0	0.0000e+00	0.00000000
1.0000e+06	0	0.0000e+00	0.00000000
1.2589e+06	0	0.0000e+00	0.00000000
1.5849e+06	0	0.0000e+00	0.00000000
1.9953e+06	0	0.0000e+00	0.00000000
2.5119e+06	0	0.0000e+00	0.00000000
3.1623e+06	0	0.0000e+00	0.00000000
3.9811e+06	0	0.0000e+00	0.00000000
5.0119e+06	0	0.0000e+00	0.00000000
6.3096e+06	0	0.0000e+00	0.00000000
7.9433e+06	0	0.0000e+00	0.00000000
1.0000e+07	0	0.0000e+00	0.00000000

$\phi/[\mathrm{m}^2\ \mathrm{s\ sr\ MeV/n}]^{-1}$ as a function of $E/[\mathrm{MeV/n}]$ tabulated data used to generate the "Surface of Mars" differential energy spectrum for $z = 22$ (isotopes combined):

```
# Using 70 Log Bins
# Min: 1 MeV/n          Max: 1e+07 MeV/n                10 bins/decade
#
# ***Statistics***
# Minimum:        1.3390e+01 MeV/n
# Maximum:        4.5192e+04 MeV/n
# Average:        2.6084e+03 MeV/n
# Frequency Mean: 2.3367e+03 MeV/n (binning-specific)
# Most Probable:  1.2589e+03 MeV/n (binning-specific)
#
# ***Totals***
# N           = 327
# FluenceRate = 2.4371e-02 [m^2 s sr]^-1
# Frequency   = 1.00000000
#
# ***Distribution***
#
#
# [MeV/n]                     [m^2 s sr MeV/n]^-1
# Energy        N             FluenceRate                   Frequency
1.0000e+00      0             0.0000e+00                    0.00000000
1.2589e+00      0             0.0000e+00                    0.00000000
1.5849e+00      0             0.0000e+00                    0.00000000
1.9953e+00      0             0.0000e+00                    0.00000000
2.5119e+00      0             0.0000e+00                    0.00000000
3.1623e+00      0             0.0000e+00                    0.00000000
3.9811e+00      0             0.0000e+00                    0.00000000
5.0119e+00      0             0.0000e+00                    0.00000000
6.3096e+00      0             0.0000e+00                    0.00000000
7.9433e+00      0             0.0000e+00                    0.00000000
1.0000e+01      0             0.0000e+00                    0.00000000
1.2589e+01      1             2.8784e-05                    0.00305810
1.5849e+01      0             0.0000e+00                    0.00000000
1.9953e+01      0             0.0000e+00                    0.00000000
2.5119e+01      0             0.0000e+00                    0.00000000
3.1623e+01      0             0.0000e+00                    0.00000000
3.9811e+01      2             1.8205e-05                    0.00611621
5.0119e+01      0             0.0000e+00                    0.00000000
6.3096e+01      2             1.1486e-05                    0.00611621
7.9433e+01      0             0.0000e+00                    0.00000000
1.0000e+02      1             3.6237e-06                    0.00305810
1.2589e+02      4             1.1514e-05                    0.01223242
1.5849e+02      7             1.6005e-05                    0.02140673
1.9953e+02      7             1.2713e-05                    0.02140673
2.5119e+02      11            1.5869e-05                    0.03363914
3.1623e+02      16            1.8335e-05                    0.04892966
```

3.9811e+02	17	1.5474e-05	0.05198777
5.0119e+02	17	1.2291e-05	0.05198777
6.3096e+02	25	1.4358e-05	0.07645260
7.9433e+02	23	1.0493e-05	0.07033639
1.0000e+03	22	7.9722e-06	0.06727829
1.2589e+03	32	9.2109e-06	0.09785933
1.5849e+03	21	4.8015e-06	0.06422018
1.9953e+03	26	4.7220e-06	0.07951070
2.5119e+03	15	2.1639e-06	0.04587156
3.1623e+03	14	1.6043e-06	0.04281346
3.9811e+03	13	1.1833e-06	0.03975535
5.0119e+03	19	1.3737e-06	0.05810398
6.3096e+03	10	5.7432e-07	0.03058104
7.9433e+03	9	4.1058e-07	0.02752294
1.0000e+04	5	1.8119e-07	0.01529052
1.2589e+04	5	1.4392e-07	0.01529052
1.5849e+04	0	0.0000e+00	0.00000000
1.9953e+04	2	3.6323e-08	0.00611621
2.5119e+04	0	0.0000e+00	0.00000000
3.1623e+04	0	0.0000e+00	0.00000000
3.9811e+04	1	9.1023e-09	0.00305810
5.0119e+04	0	0.0000e+00	0.00000000
6.3096e+04	0	0.0000e+00	0.00000000
7.9433e+04	0	0.0000e+00	0.00000000
1.0000e+05	0	0.0000e+00	0.00000000
1.2589e+05	0	0.0000e+00	0.00000000
1.5849e+05	0	0.0000e+00	0.00000000
1.9953e+05	0	0.0000e+00	0.00000000
2.5119e+05	0	0.0000e+00	0.00000000
3.1623e+05	0	0.0000e+00	0.00000000
3.9811e+05	0	0.0000e+00	0.00000000
5.0119e+05	0	0.0000e+00	0.00000000
6.3096e+05	0	0.0000e+00	0.00000000
7.9433e+05	0	0.0000e+00	0.00000000
1.0000e+06	0	0.0000e+00	0.00000000
1.2589e+06	0	0.0000e+00	0.00000000
1.5849e+06	0	0.0000e+00	0.00000000
1.9953e+06	0	0.0000e+00	0.00000000
2.5119e+06	0	0.0000e+00	0.00000000
3.1623e+06	0	0.0000e+00	0.00000000
3.9811e+06	0	0.0000e+00	0.00000000
5.0119e+06	0	0.0000e+00	0.00000000
6.3096e+06	0	0.0000e+00	0.00000000
7.9433e+06	0	0.0000e+00	0.00000000
1.0000e+07	0	0.0000e+00	0.00000000

$\phi/[\mathrm{m}^2\ \mathrm{s\ sr\ MeV/n}]^{-1}$ as a function of $E/[\mathrm{MeV/n}]$ tabulated data used to generate the "Surface of Mars" differential energy spectrum for $z = 23$ (isotopes combined):

```
# Using 70 Log Bins
# Min: 1 MeV/n          Max: 1e+07 MeV/n                10 bins/decade
#
# ***Statistics***
# Minimum:        9.9992e+00 MeV/n
# Maximum:        2.0926e+04 MeV/n
# Average:        2.9948e+03 MeV/n
# Frequency Mean: 2.6774e+03 MeV/n (binning-specific)
# Most Probable:  1.0000e+03 MeV/n (binning-specific)
#
# ***Totals***
# N           = 200
# FluenceRate = 1.4906e-02 [m^2 s sr]^-1
# Frequency   = 1.00000000
#
# ***Distribution***
#
#
# [MeV/n]                     [m^2 s sr MeV/n]^-1
# Energy        N             FluenceRate                   Frequency
1.0000e+00      0             0.0000e+00                    0.00000000
1.2589e+00      0             0.0000e+00                    0.00000000
1.5849e+00      0             0.0000e+00                    0.00000000
1.9953e+00      0             0.0000e+00                    0.00000000
2.5119e+00      0             0.0000e+00                    0.00000000
3.1623e+00      0             0.0000e+00                    0.00000000
3.9811e+00      0             0.0000e+00                    0.00000000
5.0119e+00      0             0.0000e+00                    0.00000000
6.3096e+00      0             0.0000e+00                    0.00000000
7.9433e+00      1             4.5620e-05                    0.00500000
1.0000e+01      0             0.0000e+00                    0.00000000
1.2589e+01      0             0.0000e+00                    0.00000000
1.5849e+01      0             0.0000e+00                    0.00000000
1.9953e+01      0             0.0000e+00                    0.00000000
2.5119e+01      0             0.0000e+00                    0.00000000
3.1623e+01      0             0.0000e+00                    0.00000000
3.9811e+01      1             9.1023e-06                    0.00500000
5.0119e+01      0             0.0000e+00                    0.00000000
6.3096e+01      0             0.0000e+00                    0.00000000
7.9433e+01      1             4.5620e-06                    0.00500000
1.0000e+02      5             1.8119e-05                    0.02500000
1.2589e+02      1             2.8784e-06                    0.00500000
1.5849e+02      2             4.5728e-06                    0.01000000
1.9953e+02      5             9.0808e-06                    0.02500000
2.5119e+02      4             5.7705e-06                    0.02000000
3.1623e+02      5             5.7296e-06                    0.02500000
```

3.9811e+02	10	9.1023e-06	0.05000000
5.0119e+02	8	5.7842e-06	0.04000000
6.3096e+02	8	4.5946e-06	0.04000000
7.9433e+02	13	5.9306e-06	0.06500000
1.0000e+03	23	8.3345e-06	0.11500000
1.2589e+03	19	5.4690e-06	0.09500000
1.5849e+03	19	4.3442e-06	0.09500000
1.9953e+03	7	1.2713e-06	0.03500000
2.5119e+03	10	1.4426e-06	0.05000000
3.1623e+03	7	8.0214e-07	0.03500000
3.9811e+03	7	6.3716e-07	0.03500000
5.0119e+03	16	1.1568e-06	0.08000000
6.3096e+03	10	5.7432e-07	0.05000000
7.9433e+03	5	2.2810e-07	0.02500000
1.0000e+04	9	3.2613e-07	0.04500000
1.2589e+04	1	2.8784e-08	0.00500000
1.5849e+04	1	2.2864e-08	0.00500000
1.9953e+04	2	3.6323e-08	0.01000000
2.5119e+04	0	0.0000e+00	0.00000000
3.1623e+04	0	0.0000e+00	0.00000000
3.9811e+04	0	0.0000e+00	0.00000000
5.0119e+04	0	0.0000e+00	0.00000000
6.3096e+04	0	0.0000e+00	0.00000000
7.9433e+04	0	0.0000e+00	0.00000000
1.0000e+05	0	0.0000e+00	0.00000000
1.2589e+05	0	0.0000e+00	0.00000000
1.5849e+05	0	0.0000e+00	0.00000000
1.9953e+05	0	0.0000e+00	0.00000000
2.5119e+05	0	0.0000e+00	0.00000000
3.1623e+05	0	0.0000e+00	0.00000000
3.9811e+05	0	0.0000e+00	0.00000000
5.0119e+05	0	0.0000e+00	0.00000000
6.3096e+05	0	0.0000e+00	0.00000000
7.9433e+05	0	0.0000e+00	0.00000000
1.0000e+06	0	0.0000e+00	0.00000000
1.2589e+06	0	0.0000e+00	0.00000000
1.5849e+06	0	0.0000e+00	0.00000000
1.9953e+06	0	0.0000e+00	0.00000000
2.5119e+06	0	0.0000e+00	0.00000000
3.1623e+06	0	0.0000e+00	0.00000000
3.9811e+06	0	0.0000e+00	0.00000000
5.0119e+06	0	0.0000e+00	0.00000000
6.3096e+06	0	0.0000e+00	0.00000000
7.9433e+06	0	0.0000e+00	0.00000000
1.0000e+07	0	0.0000e+00	0.00000000

$\phi/[\mathrm{m}^2\ \mathrm{s\ sr\ MeV/n}]^{-1}$ as a function of $E/[\mathrm{MeV/n}]$ tabulated data used to generate the "Surface of Mars" differential energy spectrum for $z = 24$ (isotopes combined):

```
# Using 70 Log Bins
# Min: 1 MeV/n          Max: 1e+07 MeV/n                10 bins/decade
#
# ***Statistics***
# Minimum:        1.5474e+01 MeV/n
# Maximum:        1.3742e+05 MeV/n
# Average:        3.8245e+03 MeV/n
# Frequency Mean: 3.4563e+03 MeV/n (binning-specific)
# Most Probable:  3.9811e+03 MeV/n (binning-specific)
#
# ***Totals***
# N           = 273
# FluenceRate = 2.0347e-02 [m^2 s sr]^-1
# Frequency   = 1.00000000
#
# ***Distribution***
#
#
# [MeV/n]                     [m^2 s sr MeV/n]^-1
# Energy        N             FluenceRate                   Frequency
1.0000e+00      0             0.0000e+00                    0.00000000
1.2589e+00      0             0.0000e+00                    0.00000000
1.5849e+00      0             0.0000e+00                    0.00000000
1.9953e+00      0             0.0000e+00                    0.00000000
2.5119e+00      0             0.0000e+00                    0.00000000
3.1623e+00      0             0.0000e+00                    0.00000000
3.9811e+00      0             0.0000e+00                    0.00000000
5.0119e+00      0             0.0000e+00                    0.00000000
6.3096e+00      0             0.0000e+00                    0.00000000
7.9433e+00      0             0.0000e+00                    0.00000000
1.0000e+01      0             0.0000e+00                    0.00000000
1.2589e+01      1             2.8784e-05                    0.00366300
1.5849e+01      0             0.0000e+00                    0.00000000
1.9953e+01      0             0.0000e+00                    0.00000000
2.5119e+01      0             0.0000e+00                    0.00000000
3.1623e+01      0             0.0000e+00                    0.00000000
3.9811e+01      0             0.0000e+00                    0.00000000
5.0119e+01      0             0.0000e+00                    0.00000000
6.3096e+01      2             1.1486e-05                    0.00732601
7.9433e+01      2             9.1240e-06                    0.00732601
1.0000e+02      2             7.2474e-06                    0.00732601
1.2589e+02      4             1.1514e-05                    0.01465201
1.5849e+02      2             4.5728e-06                    0.00732601
1.9953e+02      8             1.4529e-05                    0.02930403
2.5119e+02      7             1.0098e-05                    0.02564103
3.1623e+02      13            1.4897e-05                    0.04761905
```

3.9811e+02	18	1.6384e-05	0.06593407
5.0119e+02	11	7.9533e-06	0.04029304
6.3096e+02	20	1.1486e-05	0.07326007
7.9433e+02	18	8.2116e-06	0.06593407
1.0000e+03	14	5.0732e-06	0.05128205
1.2589e+03	20	5.7568e-06	0.07326007
1.5849e+03	17	3.8869e-06	0.06227106
1.9953e+03	18	3.2691e-06	0.06593407
2.5119e+03	17	2.4525e-06	0.06227106
3.1623e+03	17	1.9481e-06	0.06227106
3.9811e+03	21	1.9115e-06	0.07692308
5.0119e+03	17	1.2291e-06	0.06227106
6.3096e+03	6	3.4459e-07	0.02197802
7.9433e+03	4	1.8248e-07	0.01465201
1.0000e+04	4	1.4495e-07	0.01465201
1.2589e+04	1	2.8784e-08	0.00366300
1.5849e+04	2	4.5728e-08	0.00732601
1.9953e+04	3	5.4485e-08	0.01098901
2.5119e+04	1	1.4426e-08	0.00366300
3.1623e+04	0	0.0000e+00	0.00000000
3.9811e+04	0	0.0000e+00	0.00000000
5.0119e+04	0	0.0000e+00	0.00000000
6.3096e+04	1	5.7432e-09	0.00366300
7.9433e+04	0	0.0000e+00	0.00000000
1.0000e+05	1	3.6237e-09	0.00366300
1.2589e+05	1	2.8784e-09	0.00366300
1.5849e+05	0	0.0000e+00	0.00000000
1.9953e+05	0	0.0000e+00	0.00000000
2.5119e+05	0	0.0000e+00	0.00000000
3.1623e+05	0	0.0000e+00	0.00000000
3.9811e+05	0	0.0000e+00	0.00000000
5.0119e+05	0	0.0000e+00	0.00000000
6.3096e+05	0	0.0000e+00	0.00000000
7.9433e+05	0	0.0000e+00	0.00000000
1.0000e+06	0	0.0000e+00	0.00000000
1.2589e+06	0	0.0000e+00	0.00000000
1.5849e+06	0	0.0000e+00	0.00000000
1.9953e+06	0	0.0000e+00	0.00000000
2.5119e+06	0	0.0000e+00	0.00000000
3.1623e+06	0	0.0000e+00	0.00000000
3.9811e+06	0	0.0000e+00	0.00000000
5.0119e+06	0	0.0000e+00	0.00000000
6.3096e+06	0	0.0000e+00	0.00000000
7.9433e+06	0	0.0000e+00	0.00000000
1.0000e+07	0	0.0000e+00	0.00000000

$\phi/[\mathrm{m}^2\ \mathrm{s\ sr\ MeV/n}]^{-1}$ as a function of $E/[\mathrm{MeV/n}]$ tabulated data used to generate the "Surface of Mars" differential energy spectrum for $z = 25$ (isotopes combined):

```
# Using 70 Log Bins
# Min: 1 MeV/n          Max: 1e+07 MeV/n                10 bins/decade
#
# ***Statistics***
# Minimum:        2.9097e+01 MeV/n
# Maximum:        1.3388e+05 MeV/n
# Average:        3.4741e+03 MeV/n
# Frequency Mean: 3.1428e+03 MeV/n (binning-specific)
# Most Probable:  6.3096e+02 MeV/n (binning-specific)
#
# ***Totals***
# N           = 219
# FluenceRate = 1.6322e-02 [m^2 s sr]^-1
# Frequency   = 1.00000000
#
# ***Distribution***
#
#
# [MeV/n]                     [m^2 s sr MeV/n]^-1
# Energy        N             FluenceRate                   Frequency
1.0000e+00      0             0.0000e+00                    0.00000000
1.2589e+00      0             0.0000e+00                    0.00000000
1.5849e+00      0             0.0000e+00                    0.00000000
1.9953e+00      0             0.0000e+00                    0.00000000
2.5119e+00      0             0.0000e+00                    0.00000000
3.1623e+00      0             0.0000e+00                    0.00000000
3.9811e+00      0             0.0000e+00                    0.00000000
5.0119e+00      0             0.0000e+00                    0.00000000
6.3096e+00      0             0.0000e+00                    0.00000000
7.9433e+00      0             0.0000e+00                    0.00000000
1.0000e+01      0             0.0000e+00                    0.00000000
1.2589e+01      0             0.0000e+00                    0.00000000
1.5849e+01      0             0.0000e+00                    0.00000000
1.9953e+01      0             0.0000e+00                    0.00000000
2.5119e+01      1             1.4426e-05                    0.00456621
3.1623e+01      1             1.1459e-05                    0.00456621
3.9811e+01      1             9.1023e-06                    0.00456621
5.0119e+01      1             7.2303e-06                    0.00456621
6.3096e+01      0             0.0000e+00                    0.00000000
7.9433e+01      1             4.5620e-06                    0.00456621
1.0000e+02      3             1.0871e-05                    0.01369863
1.2589e+02      0             0.0000e+00                    0.00000000
1.5849e+02      3             6.8592e-06                    0.01369863
1.9953e+02      5             9.0808e-06                    0.02283105
2.5119e+02      7             1.0098e-05                    0.03196347
3.1623e+02      7             8.0214e-06                    0.03196347
```

3.9811e+02	10	9.1023e-06	0.04566210
5.0119e+02	13	9.3993e-06	0.05936073
6.3096e+02	21	1.2061e-05	0.09589041
7.9433e+02	21	9.5802e-06	0.09589041
1.0000e+03	14	5.0732e-06	0.06392694
1.2589e+03	19	5.4690e-06	0.08675799
1.5849e+03	10	2.2864e-06	0.04566210
1.9953e+03	16	2.9059e-06	0.07305936
2.5119e+03	14	2.0197e-06	0.06392694
3.1623e+03	10	1.1459e-06	0.04566210
3.9811e+03	10	9.1023e-07	0.04566210
5.0119e+03	8	5.7842e-07	0.03652968
6.3096e+03	6	3.4459e-07	0.02739726
7.9433e+03	1	4.5620e-08	0.00456621
1.0000e+04	4	1.4495e-07	0.01826484
1.2589e+04	5	1.4392e-07	0.02283105
1.5849e+04	2	4.5728e-08	0.00913242
1.9953e+04	2	3.6323e-08	0.00913242
2.5119e+04	0	0.0000e+00	0.00000000
3.1623e+04	2	2.2918e-08	0.00913242
3.9811e+04	0	0.0000e+00	0.00000000
5.0119e+04	0	0.0000e+00	0.00000000
6.3096e+04	0	0.0000e+00	0.00000000
7.9433e+04	0	0.0000e+00	0.00000000
1.0000e+05	0	0.0000e+00	0.00000000
1.2589e+05	1	2.8784e-09	0.00456621
1.5849e+05	0	0.0000e+00	0.00000000
1.9953e+05	0	0.0000e+00	0.00000000
2.5119e+05	0	0.0000e+00	0.00000000
3.1623e+05	0	0.0000e+00	0.00000000
3.9811e+05	0	0.0000e+00	0.00000000
5.0119e+05	0	0.0000e+00	0.00000000
6.3096e+05	0	0.0000e+00	0.00000000
7.9433e+05	0	0.0000e+00	0.00000000
1.0000e+06	0	0.0000e+00	0.00000000
1.2589e+06	0	0.0000e+00	0.00000000
1.5849e+06	0	0.0000e+00	0.00000000
1.9953e+06	0	0.0000e+00	0.00000000
2.5119e+06	0	0.0000e+00	0.00000000
3.1623e+06	0	0.0000e+00	0.00000000
3.9811e+06	0	0.0000e+00	0.00000000
5.0119e+06	0	0.0000e+00	0.00000000
6.3096e+06	0	0.0000e+00	0.00000000
7.9433e+06	0	0.0000e+00	0.00000000
1.0000e+07	0	0.0000e+00	0.00000000

$\phi/[\mathrm{m}^2\ \mathrm{s\ sr\ MeV/n}]^{-1}$ as a function of $E/[\mathrm{MeV/n}]$ tabulated data used to generate the "Surface of Mars" differential energy spectrum for $z = 26$ (isotopes combined):

```
# Using 70 Log Bins
# Min: 1 MeV/n          Max: 1e+07 MeV/n                10 bins/decade
#
# ***Statistics***
# Minimum:        3.8718e+01 MeV/n
# Maximum:        1.1190e+05 MeV/n
# Average:        3.3181e+03 MeV/n
# Frequency Mean: 2.9945e+03 MeV/n (binning-specific)
# Most Probable:  7.9433e+02 MeV/n (binning-specific)
#
# ***Totals***
# N           = 616
# FluenceRate = 4.5910e-02 [m^2 s sr]^-1
# Frequency   = 1.00000000
#
# ***Distribution***
#
#
# [MeV/n]                     [m^2 s sr MeV/n]^-1
# Energy        N             FluenceRate                   Frequency
1.0000e+00      0             0.0000e+00                    0.00000000
1.2589e+00      0             0.0000e+00                    0.00000000
1.5849e+00      0             0.0000e+00                    0.00000000
1.9953e+00      0             0.0000e+00                    0.00000000
2.5119e+00      0             0.0000e+00                    0.00000000
3.1623e+00      0             0.0000e+00                    0.00000000
3.9811e+00      0             0.0000e+00                    0.00000000
5.0119e+00      0             0.0000e+00                    0.00000000
6.3096e+00      0             0.0000e+00                    0.00000000
7.9433e+00      0             0.0000e+00                    0.00000000
1.0000e+01      0             0.0000e+00                    0.00000000
1.2589e+01      0             0.0000e+00                    0.00000000
1.5849e+01      0             0.0000e+00                    0.00000000
1.9953e+01      0             0.0000e+00                    0.00000000
2.5119e+01      0             0.0000e+00                    0.00000000
3.1623e+01      1             1.1459e-05                    0.00162338
3.9811e+01      1             9.1023e-06                    0.00162338
5.0119e+01      2             1.4461e-05                    0.00324675
6.3096e+01      3             1.7230e-05                    0.00487013
7.9433e+01      5             2.2810e-05                    0.00811688
1.0000e+02      6             2.1742e-05                    0.00974026
1.2589e+02      5             1.4392e-05                    0.00811688
1.5849e+02      14            3.2010e-05                    0.02272727
1.9953e+02      12            2.1794e-05                    0.01948052
2.5119e+02      20            2.8852e-05                    0.03246753
3.1623e+02      18            2.0627e-05                    0.02922078
```

3.9811e+02	29	2.6397e-05	0.04707792
5.0119e+02	41	2.9644e-05	0.06655844
6.3096e+02	45	2.5844e-05	0.07305195
7.9433e+02	52	2.3722e-05	0.08441558
1.0000e+03	46	1.6669e-05	0.07467532
1.2589e+03	44	1.2665e-05	0.07142857
1.5849e+03	43	9.8315e-06	0.06980519
1.9953e+03	42	7.6279e-06	0.06818182
2.5119e+03	36	5.1934e-06	0.05844156
3.1623e+03	36	4.1253e-06	0.05844156
3.9811e+03	28	2.5487e-06	0.04545455
5.0119e+03	26	1.8799e-06	0.04220779
6.3096e+03	12	6.8918e-07	0.01948052
7.9433e+03	10	4.5620e-07	0.01623377
1.0000e+04	10	3.6237e-07	0.01623377
1.2589e+04	9	2.5906e-07	0.01461039
1.5849e+04	5	1.1432e-07	0.00811688
1.9953e+04	3	5.4485e-08	0.00487013
2.5119e+04	5	7.2131e-08	0.00811688
3.1623e+04	2	2.2918e-08	0.00324675
3.9811e+04	2	1.8205e-08	0.00324675
5.0119e+04	1	7.2303e-09	0.00162338
6.3096e+04	0	0.0000e+00	0.00000000
7.9433e+04	0	0.0000e+00	0.00000000
1.0000e+05	2	7.2474e-09	0.00324675
1.2589e+05	0	0.0000e+00	0.00000000
1.5849e+05	0	0.0000e+00	0.00000000
1.9953e+05	0	0.0000e+00	0.00000000
2.5119e+05	0	0.0000e+00	0.00000000
3.1623e+05	0	0.0000e+00	0.00000000
3.9811e+05	0	0.0000e+00	0.00000000
5.0119e+05	0	0.0000e+00	0.00000000
6.3096e+05	0	0.0000e+00	0.00000000
7.9433e+05	0	0.0000e+00	0.00000000
1.0000e+06	0	0.0000e+00	0.00000000
1.2589e+06	0	0.0000e+00	0.00000000
1.5849e+06	0	0.0000e+00	0.00000000
1.9953e+06	0	0.0000e+00	0.00000000
2.5119e+06	0	0.0000e+00	0.00000000
3.1623e+06	0	0.0000e+00	0.00000000
3.9811e+06	0	0.0000e+00	0.00000000
5.0119e+06	0	0.0000e+00	0.00000000
6.3096e+06	0	0.0000e+00	0.00000000
7.9433e+06	0	0.0000e+00	0.00000000
1.0000e+07	0	0.0000e+00	0.00000000

$\phi/[\mathrm{m}^2\ \mathrm{s\ sr\ MeV/n}]^{-1}$ as a function of $E/[\mathrm{MeV/n}]$ tabulated data used to generate the "Surface of Mars" differential energy spectrum for $z = 27$ (isotopes combined):

```
# Using 70 Log Bins
# Min: 1 MeV/n          Max: 1e+07 MeV/n                10 bins/decade
#
# ***Statistics***
# Minimum:        5.9821e+01 MeV/n
# Maximum:        1.2264e+04 MeV/n
# Average:        3.2873e+03 MeV/n
# Frequency Mean: 2.8739e+03 MeV/n (binning-specific)
# Most Probable:  3.9811e+03 MeV/n (binning-specific)
#
# ***Totals***
# N           = 10
# FluenceRate = 7.4529e-04 [m^2 s sr]^-1
# Frequency   = 1.00000000
#
# ***Distribution***
#
#
# [MeV/n]                     [m^2 s sr MeV/n]^-1
# Energy        N             FluenceRate                   Frequency
1.0000e+00      0             0.0000e+00                    0.00000000
1.2589e+00      0             0.0000e+00                    0.00000000
1.5849e+00      0             0.0000e+00                    0.00000000
1.9953e+00      0             0.0000e+00                    0.00000000
2.5119e+00      0             0.0000e+00                    0.00000000
3.1623e+00      0             0.0000e+00                    0.00000000
3.9811e+00      0             0.0000e+00                    0.00000000
5.0119e+00      0             0.0000e+00                    0.00000000
6.3096e+00      0             0.0000e+00                    0.00000000
7.9433e+00      0             0.0000e+00                    0.00000000
1.0000e+01      0             0.0000e+00                    0.00000000
1.2589e+01      0             0.0000e+00                    0.00000000
1.5849e+01      0             0.0000e+00                    0.00000000
1.9953e+01      0             0.0000e+00                    0.00000000
2.5119e+01      0             0.0000e+00                    0.00000000
3.1623e+01      0             0.0000e+00                    0.00000000
3.9811e+01      0             0.0000e+00                    0.00000000
5.0119e+01      1             7.2303e-06                    0.10000000
6.3096e+01      0             0.0000e+00                    0.00000000
7.9433e+01      0             0.0000e+00                    0.00000000
1.0000e+02      0             0.0000e+00                    0.00000000
1.2589e+02      1             2.8784e-06                    0.10000000
1.5849e+02      0             0.0000e+00                    0.00000000
1.9953e+02      0             0.0000e+00                    0.00000000
2.5119e+02      0             0.0000e+00                    0.00000000
3.1623e+02      0             0.0000e+00                    0.00000000
```

3.9811e+02	0	0.0000e+00	0.00000000
5.0119e+02	1	7.2303e-07	0.10000000
6.3096e+02	0	0.0000e+00	0.00000000
7.9433e+02	1	4.5620e-07	0.10000000
1.0000e+03	1	3.6237e-07	0.10000000
1.2589e+03	0	0.0000e+00	0.00000000
1.5849e+03	0	0.0000e+00	0.00000000
1.9953e+03	1	1.8162e-07	0.10000000
2.5119e+03	0	0.0000e+00	0.00000000
3.1623e+03	0	0.0000e+00	0.00000000
3.9811e+03	2	1.8205e-07	0.20000000
5.0119e+03	0	0.0000e+00	0.00000000
6.3096e+03	1	5.7432e-08	0.10000000
7.9433e+03	0	0.0000e+00	0.00000000
1.0000e+04	1	3.6237e-08	0.10000000
1.2589e+04	0	0.0000e+00	0.00000000
1.5849e+04	0	0.0000e+00	0.00000000
1.9953e+04	0	0.0000e+00	0.00000000
2.5119e+04	0	0.0000e+00	0.00000000
3.1623e+04	0	0.0000e+00	0.00000000
3.9811e+04	0	0.0000e+00	0.00000000
5.0119e+04	0	0.0000e+00	0.00000000
6.3096e+04	0	0.0000e+00	0.00000000
7.9433e+04	0	0.0000e+00	0.00000000
1.0000e+05	0	0.0000e+00	0.00000000
1.2589e+05	0	0.0000e+00	0.00000000
1.5849e+05	0	0.0000e+00	0.00000000
1.9953e+05	0	0.0000e+00	0.00000000
2.5119e+05	0	0.0000e+00	0.00000000
3.1623e+05	0	0.0000e+00	0.00000000
3.9811e+05	0	0.0000e+00	0.00000000
5.0119e+05	0	0.0000e+00	0.00000000
6.3096e+05	0	0.0000e+00	0.00000000
7.9433e+05	0	0.0000e+00	0.00000000
1.0000e+06	0	0.0000e+00	0.00000000
1.2589e+06	0	0.0000e+00	0.00000000
1.5849e+06	0	0.0000e+00	0.00000000
1.9953e+06	0	0.0000e+00	0.00000000
2.5119e+06	0	0.0000e+00	0.00000000
3.1623e+06	0	0.0000e+00	0.00000000
3.9811e+06	0	0.0000e+00	0.00000000
5.0119e+06	0	0.0000e+00	0.00000000
6.3096e+06	0	0.0000e+00	0.00000000
7.9433e+06	0	0.0000e+00	0.00000000
1.0000e+07	0	0.0000e+00	0.00000000

$\phi/[\mathrm{m}^2\ \mathrm{s\ sr\ MeV/n}]^{-1}$ as a function of $E/[\mathrm{MeV/n}]$ tabulated data used to generate the "Surface of Mars" differential energy spectrum for $z = 28$ (isotopes combined):

```
# Using 70 Log Bins
# Min: 1 MeV/n          Max: 1e+07 MeV/n                10 bins/decade
#
# ***Statistics***
# Minimum:        9.6855e+01 MeV/n
# Maximum:        1.0439e+04 MeV/n
# Average:        2.2762e+03 MeV/n
# Frequency Mean: 2.1030e+03 MeV/n (binning-specific)
# Most Probable:  1.0000e+03 MeV/n (binning-specific)
#
# ***Totals***
# N           = 34
# FluenceRate = 2.5340e-03 [m^2 s sr]^-1
# Frequency   = 1.00000000
#
# ***Distribution***
#
#
# [MeV/n]                     [m^2 s sr MeV/n]^-1
# Energy        N             FluenceRate                   Frequency
1.0000e+00      0             0.0000e+00                    0.00000000
1.2589e+00      0             0.0000e+00                    0.00000000
1.5849e+00      0             0.0000e+00                    0.00000000
1.9953e+00      0             0.0000e+00                    0.00000000
2.5119e+00      0             0.0000e+00                    0.00000000
3.1623e+00      0             0.0000e+00                    0.00000000
3.9811e+00      0             0.0000e+00                    0.00000000
5.0119e+00      0             0.0000e+00                    0.00000000
6.3096e+00      0             0.0000e+00                    0.00000000
7.9433e+00      0             0.0000e+00                    0.00000000
1.0000e+01      0             0.0000e+00                    0.00000000
1.2589e+01      0             0.0000e+00                    0.00000000
1.5849e+01      0             0.0000e+00                    0.00000000
1.9953e+01      0             0.0000e+00                    0.00000000
2.5119e+01      0             0.0000e+00                    0.00000000
3.1623e+01      0             0.0000e+00                    0.00000000
3.9811e+01      0             0.0000e+00                    0.00000000
5.0119e+01      0             0.0000e+00                    0.00000000
6.3096e+01      0             0.0000e+00                    0.00000000
7.9433e+01      1             4.5620e-06                    0.02941176
1.0000e+02      0             0.0000e+00                    0.00000000
1.2589e+02      1             2.8784e-06                    0.02941176
1.5849e+02      0             0.0000e+00                    0.00000000
1.9953e+02      0             0.0000e+00                    0.00000000
2.5119e+02      0             0.0000e+00                    0.00000000
3.1623e+02      1             1.1459e-06                    0.02941176
```

3.9811e+02	3	2.7307e-06	0.08823529
5.0119e+02	3	2.1691e-06	0.08823529
6.3096e+02	2	1.1486e-06	0.05882353
7.9433e+02	1	4.5620e-07	0.02941176
1.0000e+03	5	1.8119e-06	0.14705882
1.2589e+03	4	1.1514e-06	0.11764706
1.5849e+03	2	4.5728e-07	0.05882353
1.9953e+03	3	5.4485e-07	0.08823529
2.5119e+03	0	0.0000e+00	0.00000000
3.1623e+03	1	1.1459e-07	0.02941176
3.9811e+03	2	1.8205e-07	0.05882353
5.0119e+03	2	1.4461e-07	0.05882353
6.3096e+03	0	0.0000e+00	0.00000000
7.9433e+03	2	9.1240e-08	0.05882353
1.0000e+04	1	3.6237e-08	0.02941176
1.2589e+04	0	0.0000e+00	0.00000000
1.5849e+04	0	0.0000e+00	0.00000000
1.9953e+04	0	0.0000e+00	0.00000000
2.5119e+04	0	0.0000e+00	0.00000000
3.1623e+04	0	0.0000e+00	0.00000000
3.9811e+04	0	0.0000e+00	0.00000000
5.0119e+04	0	0.0000e+00	0.00000000
6.3096e+04	0	0.0000e+00	0.00000000
7.9433e+04	0	0.0000e+00	0.00000000
1.0000e+05	0	0.0000e+00	0.00000000
1.2589e+05	0	0.0000e+00	0.00000000
1.5849e+05	0	0.0000e+00	0.00000000
1.9953e+05	0	0.0000e+00	0.00000000
2.5119e+05	0	0.0000e+00	0.00000000
3.1623e+05	0	0.0000e+00	0.00000000
3.9811e+05	0	0.0000e+00	0.00000000
5.0119e+05	0	0.0000e+00	0.00000000
6.3096e+05	0	0.0000e+00	0.00000000
7.9433e+05	0	0.0000e+00	0.00000000
1.0000e+06	0	0.0000e+00	0.00000000
1.2589e+06	0	0.0000e+00	0.00000000
1.5849e+06	0	0.0000e+00	0.00000000
1.9953e+06	0	0.0000e+00	0.00000000
2.5119e+06	0	0.0000e+00	0.00000000
3.1623e+06	0	0.0000e+00	0.00000000
3.9811e+06	0	0.0000e+00	0.00000000
5.0119e+06	0	0.0000e+00	0.00000000
6.3096e+06	0	0.0000e+00	0.00000000
7.9433e+06	0	0.0000e+00	0.00000000
1.0000e+07	0	0.0000e+00	0.00000000

APPENDIX H
DOWNWARD AND ALBEDO NEUTRON SPECTRA

This appendix contains the differential energy spectra for downward and albedo neutrons 1 m above the surface of Mars. These data were generated from 1.0×10^8 FLUKA histories which corresponds to a simulated counting time of 0.545 y.

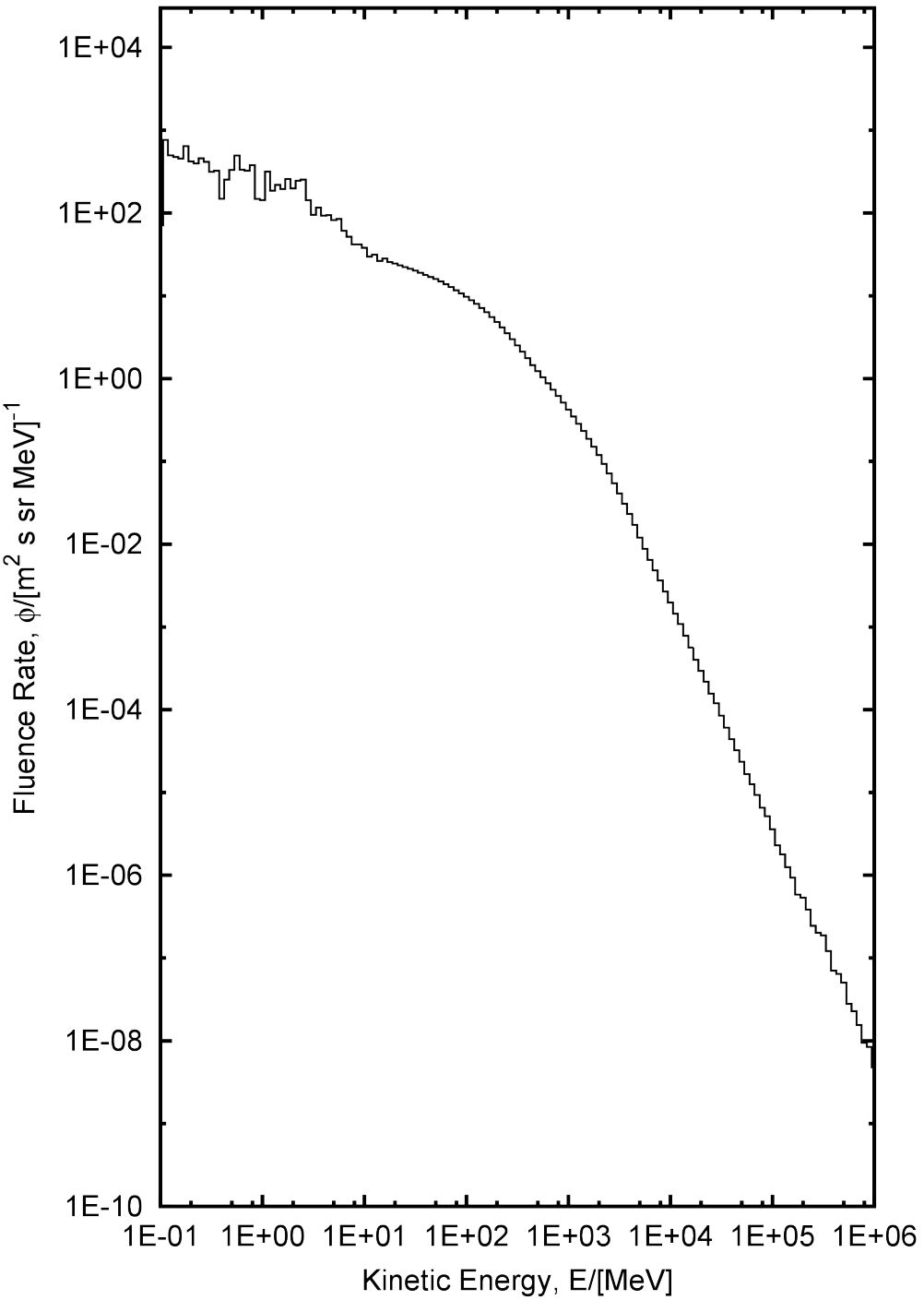

Figure H.1. Surface of Mars downward neutron differential energy spectrum. These data were generated from the particle fluence 1 m above the surface with the Badhwar–O'Neill model ($z = 1$ to $z = 28$) incident on the top of the Martian atmosphere.

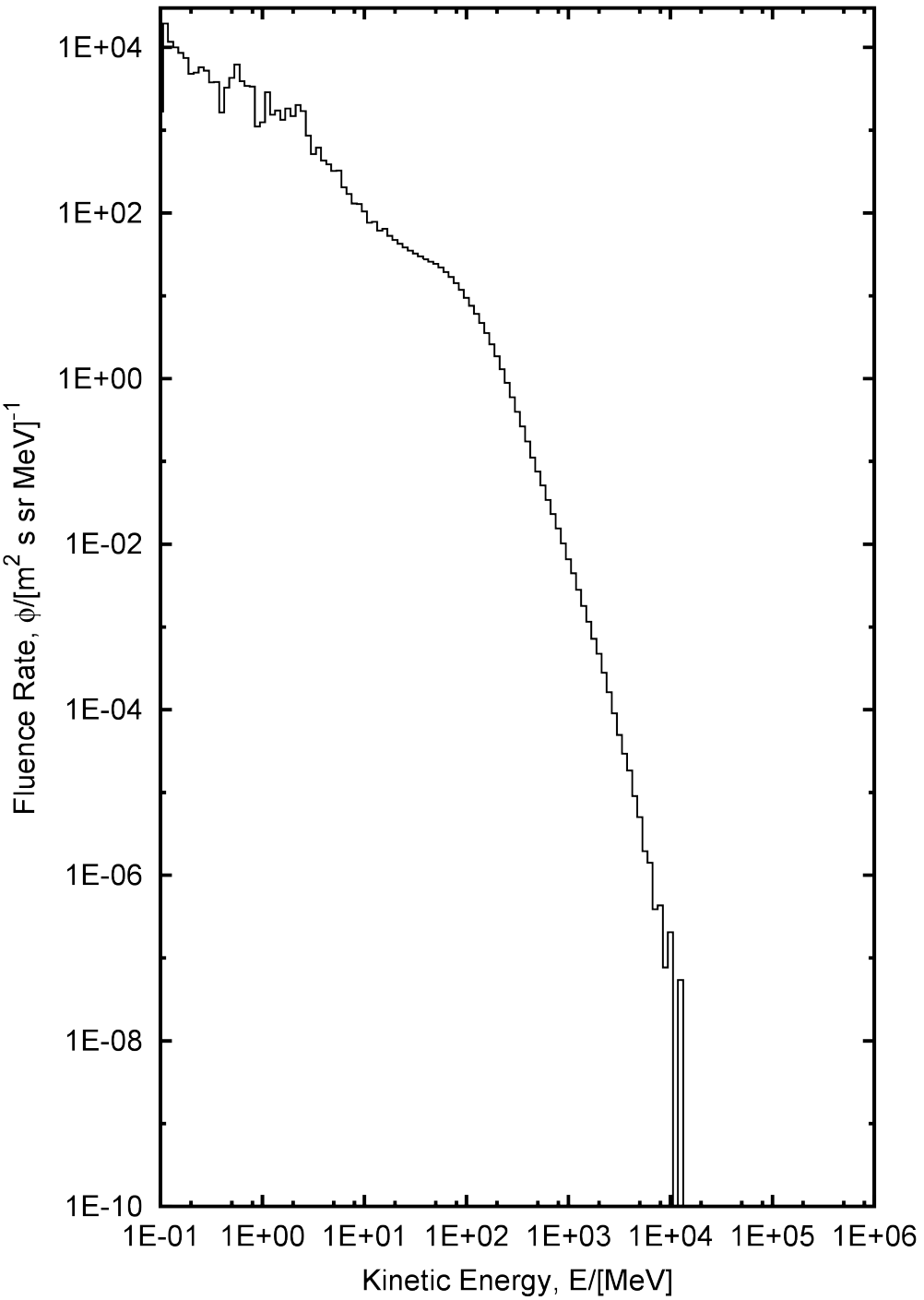

Figure H.2. Surface of Mars albedo neutron differential energy spectrum. These data were generated from the particle fluence 1 m above the surface with the Badhwar–O'Neill model ($z = 1$ to $z = 28$) incident on the top of the Martian atmosphere.

$\phi/[\mathrm{m}^2\ \mathrm{s\ sr\ MeV}]^{-1}$ as a function of $E/[\mathrm{MeV}]$ tabulated data used to generate the differential energy spectrum for downward neutrons:

```
# Using 160 Log Bins
# Min: 0.1 MeV/n                Max: 1e+07 MeV/n                20 bins/decade
#
# ***Statistics***
# Minimum:        3.5830e-09 MeV/n
# Maximum:        7.7355e+06 MeV/n
# Average:        3.8901e+02 MeV/n
# Frequency Mean: 3.6746e+02 MeV/n (binning-specific)
# Most Probable:  1.4125e+02 MeV/n (binning-specific)
#
# ***Totals***
# N           = 61458218
# FluenceRate = 4.5804e+03 [m^2 s sr]^-1
# Frequency   = 1.00000000
#
# ***Distribution***
#
#
# [MeV/n]                     [m^2 s sr MeV/n]^-1
# Energy        N             FluenceRate                     Frequency
1.0000e-01      95203         7.0954e+01                      0.00154907
1.1220e-01      124935        7.6311e+02                      0.00203284
1.2589e-01      91452         4.9785e+02                      0.00148804
1.4125e-01      97588         4.7348e+02                      0.00158788
1.5849e-01      105525        4.5631e+02                      0.00171702
1.7783e-01      166774        6.4273e+02                      0.00271362
1.9953e-01      122080        4.1932e+02                      0.00198639
2.2387e-01      129257        3.9569e+02                      0.00210317
2.5119e-01      167952        4.5823e+02                      0.00273278
2.8184e-01      171007        4.1583e+02                      0.00278249
3.1623e-01      144650        3.1349e+02                      0.00235363
3.5481e-01      167725        3.2397e+02                      0.00272909
3.9811e-01      86294         1.4855e+02                      0.00140411
4.4668e-01      165091        2.5329e+02                      0.00268623
5.0119e-01      241838        3.3069e+02                      0.00393500
5.6234e-01      406351        4.9523e+02                      0.00661183
6.3096e-01      307843        3.3437e+02                      0.00500898
7.0795e-01      334592        3.2391e+02                      0.00544422
7.9433e-01      437554        3.7752e+02                      0.00711954
8.9125e-01      192666        1.4815e+02                      0.00313491
1.0000e+00      209440        1.4354e+02                      0.00340784
1.1220e+00      517468        3.1607e+02                      0.00841983
1.2589e+00      341770        1.8605e+02                      0.00556101
1.4125e+00      450896        2.1877e+02                      0.00733663
1.5849e+00      450948        1.9500e+02                      0.00733747
1.7783e+00      668715        2.5772e+02                      0.01088081
```

1.9953e+00	575808	1.9778e+02	0.00936910
2.2387e+00	805271	2.4652e+02	0.01310274
2.5119e+00	928339	2.5328e+02	0.01510521
2.8184e+00	586841	1.4270e+02	0.00954862
3.1623e+00	438419	9.5015e+01	0.00713361
3.5481e+00	603309	1.1653e+02	0.00981657
3.9811e+00	540989	9.3130e+01	0.00880255
4.4668e+00	614668	9.4307e+01	0.01000140
5.0119e+00	599917	8.2034e+01	0.00976138
5.6234e+00	692459	8.4391e+01	0.01126715
6.3096e+00	560086	6.0836e+01	0.00911328
7.0795e+00	532878	5.1586e+01	0.00867057
7.9433e+00	485213	4.1863e+01	0.00789501
8.9125e+00	544453	4.1866e+01	0.00885891
1.0000e+01	554509	3.8002e+01	0.00902254
1.1220e+01	485985	2.9684e+01	0.00790757
1.2589e+01	577090	3.1416e+01	0.00938996
1.4125e+01	543592	2.6374e+01	0.00884490
1.5849e+01	653258	2.8248e+01	0.01062930
1.7783e+01	662093	2.5517e+01	0.01077306
1.9953e+01	714674	2.4548e+01	0.01162862
2.2387e+01	761197	2.3302e+01	0.01238560
2.5119e+01	812896	2.2179e+01	0.01322681
2.8184e+01	868323	2.1115e+01	0.01412867
3.1623e+01	927852	2.0109e+01	0.01509728
3.5481e+01	982971	1.8986e+01	0.01599413
3.9811e+01	1037788	1.7865e+01	0.01688607
4.4668e+01	1098755	1.6858e+01	0.01787808
5.0119e+01	1165051	1.5931e+01	0.01895680
5.6234e+01	1223179	1.4907e+01	0.01990261
6.3096e+01	1271508	1.3811e+01	0.02068898
7.0795e+01	1315285	1.2733e+01	0.02140129
7.9433e+01	1354382	1.1685e+01	0.02203744
8.9125e+01	1387168	1.0667e+01	0.02257091
1.0000e+02	1419364	9.7274e+00	0.02309478
1.1220e+02	1445241	8.8276e+00	0.02351583
1.2589e+02	1462736	7.9628e+00	0.02380049
1.4125e+02	1467192	7.1185e+00	0.02387300
1.5849e+02	1462313	6.3233e+00	0.02379361
1.7783e+02	1440083	5.5500e+00	0.02343190
1.9953e+02	1402978	4.8190e+00	0.02282816
2.2387e+02	1355108	4.1484e+00	0.02204926
2.5119e+02	1295137	3.5336e+00	0.02107346
2.8184e+02	1232741	2.9976e+00	0.02005820
3.1623e+02	1162377	2.5191e+00	0.01891329
3.5481e+02	1093680	2.1125e+00	0.01779550
3.9811e+02	1026690	1.7674e+00	0.01670550
4.4668e+02	947790	1.4542e+00	0.01542170
5.0119e+02	898266	1.2283e+00	0.01461588
5.6234e+02	851562	1.0378e+00	0.01385595
6.3096e+02	807505	8.7710e-01	0.01313909

7.0795e+02	759566	7.3531e-01	0.01235906
7.9433e+02	713778	6.1584e-01	0.01161404
8.9125e+02	664697	5.1112e-01	0.01081543
1.0000e+03	616063	4.2221e-01	0.01002409
1.1220e+03	569761	3.4801e-01	0.00927070
1.2589e+03	522042	2.8419e-01	0.00849426
1.4125e+03	478390	2.3211e-01	0.00778399
1.5849e+03	433909	1.8763e-01	0.00706023
1.7783e+03	390197	1.5038e-01	0.00634898
1.9953e+03	347958	1.1952e-01	0.00566170
2.2387e+03	304013	9.3067e-02	0.00494666
2.5119e+03	261562	7.1364e-02	0.00425593
2.8184e+03	223009	5.4228e-02	0.00362863
3.1623e+03	189398	4.1047e-02	0.00308174
3.5481e+03	159158	3.0742e-02	0.00258969
3.9811e+03	134406	2.3138e-02	0.00218695
4.4668e+03	111619	1.7125e-02	0.00181618
5.0119e+03	88053	1.2041e-02	0.00143273
5.6234e+03	72304	8.8118e-03	0.00117647
6.3096e+03	59502	6.4630e-03	0.00096817
7.0795e+03	49826	4.8235e-03	0.00081073
7.9433e+03	42185	3.6397e-03	0.00068640
8.9125e+03	34797	2.6757e-03	0.00056619
1.0000e+04	28881	1.9793e-03	0.00046993
1.1220e+04	23659	1.4451e-03	0.00038496
1.2589e+04	19857	1.0810e-03	0.00032310
1.4125e+04	16163	7.8420e-04	0.00026299
1.5849e+04	13043	5.6400e-04	0.00021223
1.7783e+04	10402	4.0088e-04	0.00016925
1.9953e+04	8572	2.9443e-04	0.00013948
2.2387e+04	7146	2.1876e-04	0.00011627
2.5119e+04	5728	1.5628e-04	0.00009320
2.8184e+04	4896	1.1905e-04	0.00007966
3.1623e+04	3910	8.4738e-05	0.00006362
3.5481e+04	3149	6.0824e-05	0.00005124
3.9811e+04	2552	4.3932e-05	0.00004152
4.4668e+04	2114	3.2435e-05	0.00003440
5.0119e+04	1719	2.3506e-05	0.00002797
5.6234e+04	1368	1.6672e-05	0.00002226
6.3096e+04	1157	1.2567e-05	0.00001883
7.0795e+04	965	9.3418e-06	0.00001570
7.9433e+04	761	6.5658e-06	0.00001238
8.9125e+04	675	5.1905e-06	0.00001098
1.0000e+05	525	3.5980e-06	0.00000854
1.1220e+05	377	2.3027e-06	0.00000613
1.2589e+05	328	1.7856e-06	0.00000534
1.4125e+05	259	1.2566e-06	0.00000421
1.5849e+05	217	9.3834e-07	0.00000353
1.7783e+05	152	5.8580e-07	0.00000247
1.9953e+05	156	5.3583e-07	0.00000254
2.2387e+05	126	3.8572e-07	0.00000205

2.5119e+05	90	2.4555e-07	0.00000146
2.8184e+05	83	2.0183e-07	0.00000135
3.1623e+05	87	1.8855e-07	0.00000142
3.5481e+05	63	1.2169e-07	0.00000103
3.9811e+05	41	7.0581e-08	0.00000067
4.4668e+05	42	6.4439e-08	0.00000068
5.0119e+05	37	5.0595e-08	0.00000060
5.6234e+05	23	2.8030e-08	0.00000037
6.3096e+05	21	2.2810e-08	0.00000034
7.0795e+05	16	1.5489e-08	0.00000026
7.9433e+05	11	9.4906e-09	0.00000018
8.9125e+05	11	8.4585e-09	0.00000018
1.0000e+06	7	4.7973e-09	0.00000011
1.1220e+06	10	6.1080e-09	0.00000016
1.2589e+06	8	4.3550e-09	0.00000013
1.4125e+06	0	0.0000e+00	0.00000000
1.5849e+06	9	3.8918e-09	0.00000015
1.7783e+06	6	2.3124e-09	0.00000010
1.9953e+06	3	1.0304e-09	0.00000005
2.2387e+06	2	6.1226e-10	0.00000003
2.5119e+06	1	2.7284e-10	0.00000002
2.8184e+06	1	2.4317e-10	0.00000002
3.1623e+06	5	1.0836e-09	0.00000008
3.5481e+06	3	5.7946e-10	0.00000005
3.9811e+06	0	0.0000e+00	0.00000000
4.4668e+06	2	3.0685e-10	0.00000003
5.0119e+06	0	0.0000e+00	0.00000000
5.6234e+06	0	0.0000e+00	0.00000000
6.3096e+06	1	1.0862e-10	0.00000002
7.0795e+06	2	1.9361e-10	0.00000003
7.9433e+06	0	0.0000e+00	0.00000000
8.9125e+06	0	0.0000e+00	0.00000000
1.0000e+07	0	0.0000e+00	0.00000000

$\phi/[\mathrm{m}^2\ \mathrm{s\ sr\ MeV}]^{-1}$ as a function of $E/[\mathrm{MeV}]$ tabulated data used to generate the differential energy spectrum for albedo neutrons:

```
# Using 160 Log Bins
# Min: 0.1 MeV/n                Max: 1e+07 MeV/n                20 bins/decade
#
# ***Statistics***
# Minimum:        1.1990e-10 MeV/n
# Maximum:        1.3116e+04 MeV/n
# Average:        2.0282e+01 MeV/n
# Frequency Mean: 1.9151e+01 MeV/n (binning-specific)
# Most Probable:  2.2387e+00 MeV/n (binning-specific)
#
# ***Totals***
# N           = 151235691
# FluenceRate = 1.1272e+04 [m^2 s sr]^-1
# Frequency   = 1.00000000
#
# ***Distribution***
#
#
# [MeV/n]                     [m^2 s sr MeV/n]^-1
# Energy        N             FluenceRate                   Frequency
1.0000e-01      2265454       1.6884e+03                    0.01497963
1.1220e-01      3174982       1.9393e+04                    0.02099360
1.2589e-01      2138180       1.1640e+04                    0.01413806
1.4125e-01      2056767       9.9790e+03                    0.01359975
1.5849e-01      1986193       8.5886e+03                    0.01313310
1.7783e-01      1936199       7.4620e+03                    0.01280253
1.9953e-01      1399291       4.8063e+03                    0.00925239
2.2387e-01      1623986       4.9715e+03                    0.01073811
2.5119e-01      2112762       5.7644e+03                    0.01397000
2.8184e-01      2155015       5.2403e+03                    0.01424938
3.1623e-01      1736241       3.7628e+03                    0.01148037
3.5481e-01      1986219       3.8365e+03                    0.01313327
3.9811e-01      953007        1.6406e+03                    0.00630147
4.4668e-01      2125668       3.2614e+03                    0.01405533
5.0119e-01      3130566       4.2808e+03                    0.02069992
5.6234e-01      5104756       6.2212e+03                    0.03375365
6.3096e-01      3592346       3.9019e+03                    0.02375330
7.0795e-01      3543507       3.4303e+03                    0.02343036
7.9433e-01      3902705       3.3672e+03                    0.02580545
8.9125e-01      1435558       1.1039e+03                    0.00949219
1.0000e+00      1813632       1.2429e+03                    0.01199209
1.1220e+00      4713572       2.8791e+03                    0.03116706
1.2589e+00      2829233       1.5402e+03                    0.01870744
1.4125e+00      3571189       1.7327e+03                    0.02361340
1.5849e+00      3101152       1.3410e+03                    0.02050542
1.7783e+00      4735476       1.8250e+03                    0.03131189
```

1.9953e+00	4317282	1.4829e+03	0.02854671
2.2387e+00	6578805	2.0140e+03	0.04350035
2.5119e+00	6232748	1.7005e+03	0.04121215
2.8184e+00	3535276	8.5966e+02	0.02337594
3.1623e+00	2378966	5.1557e+02	0.01573019
3.5481e+00	3190038	6.1617e+02	0.02109316
3.9811e+00	2503336	4.3094e+02	0.01655255
4.4668e+00	2518984	3.8648e+02	0.01665602
5.0119e+00	2354656	3.2198e+02	0.01556945
5.6234e+00	2674554	3.2595e+02	0.01768467
6.3096e+00	1880548	2.0426e+02	0.01243455
7.0795e+00	1746089	1.6903e+02	0.01154548
7.9433e+00	1511089	1.3037e+02	0.00999162
8.9125e+00	1662921	1.2787e+02	0.01099556
1.0000e+01	1525114	1.0452e+02	0.01008435
1.1220e+01	1250633	7.6389e+01	0.00826943
1.2589e+01	1439835	7.8382e+01	0.00952047
1.4125e+01	1260344	6.1149e+01	0.00833364
1.5849e+01	1492422	6.4535e+01	0.00986819
1.7783e+01	1376200	5.3038e+01	0.00909970
1.9953e+01	1368850	4.7017e+01	0.00905110
2.2387e+01	1387452	4.2474e+01	0.00917410
2.5119e+01	1408651	3.8433e+01	0.00931428
2.8184e+01	1446357	3.5170e+01	0.00956360
3.1623e+01	1496985	3.2443e+01	0.00989836
3.5481e+01	1551947	2.9976e+01	0.01026178
3.9811e+01	1607661	2.7676e+01	0.01063017
4.4668e+01	1682724	2.5818e+01	0.01112650
5.0119e+01	1772589	2.4239e+01	0.01172071
5.6234e+01	1804053	2.1986e+01	0.01192875
6.3096e+01	1788475	1.9426e+01	0.01182575
7.0795e+01	1743555	1.6879e+01	0.01152873
7.9433e+01	1653356	1.4265e+01	0.01093231
8.9125e+01	1529307	1.1760e+01	0.01011208
1.0000e+02	1377610	9.4412e+00	0.00910903
1.1220e+02	1239967	7.5738e+00	0.00819890
1.2589e+02	1112573	6.0566e+00	0.00735655
1.4125e+02	970373	4.7081e+00	0.00641630
1.5849e+02	821434	3.5520e+00	0.00543148
1.7783e+02	673958	2.5974e+00	0.00445634
1.9953e+02	540709	1.8572e+00	0.00357527
2.2387e+02	423697	1.2971e+00	0.00280157
2.5119e+02	324470	8.8527e-01	0.00214546
2.8184e+02	244860	5.9542e-01	0.00161906
3.1623e+02	183026	3.9666e-01	0.00121020
3.5481e+02	136588	2.6382e-01	0.00090315
3.9811e+02	101150	1.7413e-01	0.00066882
4.4668e+02	72159	1.1071e-01	0.00047713
5.0119e+02	54941	7.5128e-02	0.00036328
5.6234e+02	41973	5.1153e-02	0.00027753
6.3096e+02	31582	3.4304e-02	0.00020883

7.0795e+02	23796	2.3036e-02	0.00015734
7.9433e+02	17946	1.5484e-02	0.00011866
8.9125e+02	13275	1.0208e-02	0.00008778
1.0000e+03	9581	6.5662e-03	0.00006335
1.1220e+03	7265	4.4375e-03	0.00004804
1.2589e+03	5179	2.8193e-03	0.00003424
1.4125e+03	3688	1.7893e-03	0.00002439
1.5849e+03	2680	1.1589e-03	0.00001772
1.7783e+03	1868	7.1991e-04	0.00001235
1.9953e+03	1379	4.7366e-04	0.00000912
2.2387e+03	912	2.7919e-04	0.00000603
2.5119e+03	595	1.6234e-04	0.00000393
2.8184e+03	371	9.0215e-05	0.00000245
3.1623e+03	229	4.9629e-05	0.00000151
3.5481e+03	153	2.9552e-05	0.00000101
3.9811e+03	107	1.8420e-05	0.00000071
4.4668e+03	59	9.0522e-06	0.00000039
5.0119e+03	37	5.0595e-06	0.00000024
5.6234e+03	16	1.9499e-06	0.00000011
6.3096e+03	13	1.4120e-06	0.00000009
7.0795e+03	4	3.8722e-07	0.00000003
7.9433e+03	5	4.3139e-07	0.00000003
8.9125e+03	1	7.6896e-08	0.00000001
1.0000e+04	3	2.0560e-07	0.00000002
1.1220e+04	0	0.0000e+00	0.00000000
1.2589e+04	1	5.4438e-08	0.00000001
1.4125e+04	0	0.0000e+00	0.00000000
1.5849e+04	0	0.0000e+00	0.00000000
1.7783e+04	0	0.0000e+00	0.00000000
1.9953e+04	0	0.0000e+00	0.00000000
2.2387e+04	0	0.0000e+00	0.00000000
2.5119e+04	0	0.0000e+00	0.00000000
2.8184e+04	0	0.0000e+00	0.00000000
3.1623e+04	0	0.0000e+00	0.00000000
3.5481e+04	0	0.0000e+00	0.00000000
3.9811e+04	0	0.0000e+00	0.00000000
4.4668e+04	0	0.0000e+00	0.00000000
5.0119e+04	0	0.0000e+00	0.00000000
5.6234e+04	0	0.0000e+00	0.00000000
6.3096e+04	0	0.0000e+00	0.00000000
7.0795e+04	0	0.0000e+00	0.00000000
7.9433e+04	0	0.0000e+00	0.00000000
8.9125e+04	0	0.0000e+00	0.00000000
1.0000e+05	0	0.0000e+00	0.00000000
1.1220e+05	0	0.0000e+00	0.00000000
1.2589e+05	0	0.0000e+00	0.00000000
1.4125e+05	0	0.0000e+00	0.00000000
1.5849e+05	0	0.0000e+00	0.00000000
1.7783e+05	0	0.0000e+00	0.00000000
1.9953e+05	0	0.0000e+00	0.00000000
2.2387e+05	0	0.0000e+00	0.00000000

2.5119e+05	0	0.0000e+00	0.00000000
2.8184e+05	0	0.0000e+00	0.00000000
3.1623e+05	0	0.0000e+00	0.00000000
3.5481e+05	0	0.0000e+00	0.00000000
3.9811e+05	0	0.0000e+00	0.00000000
4.4668e+05	0	0.0000e+00	0.00000000
5.0119e+05	0	0.0000e+00	0.00000000
5.6234e+05	0	0.0000e+00	0.00000000
6.3096e+05	0	0.0000e+00	0.00000000
7.0795e+05	0	0.0000e+00	0.00000000
7.9433e+05	0	0.0000e+00	0.00000000
8.9125e+05	0	0.0000e+00	0.00000000
1.0000e+06	0	0.0000e+00	0.00000000
1.1220e+06	0	0.0000e+00	0.00000000
1.2589e+06	0	0.0000e+00	0.00000000
1.4125e+06	0	0.0000e+00	0.00000000
1.5849e+06	0	0.0000e+00	0.00000000
1.7783e+06	0	0.0000e+00	0.00000000
1.9953e+06	0	0.0000e+00	0.00000000
2.2387e+06	0	0.0000e+00	0.00000000
2.5119e+06	0	0.0000e+00	0.00000000
2.8184e+06	0	0.0000e+00	0.00000000
3.1623e+06	0	0.0000e+00	0.00000000
3.5481e+06	0	0.0000e+00	0.00000000
3.9811e+06	0	0.0000e+00	0.00000000
4.4668e+06	0	0.0000e+00	0.00000000
5.0119e+06	0	0.0000e+00	0.00000000
5.6234e+06	0	0.0000e+00	0.00000000
6.3096e+06	0	0.0000e+00	0.00000000
7.0795e+06	0	0.0000e+00	0.00000000
7.9433e+06	0	0.0000e+00	0.00000000
8.9125e+06	0	0.0000e+00	0.00000000
1.0000e+07	0	0.0000e+00	0.00000000